

“Rethinking High-Grade Serous Carcinoma: Development of new tools for deep tissue profiling”



Shamundeeswari Anandan

Thesis for the degree of Philosophiae Doctor (PhD)
University of Bergen, Norway
2021

UNIVERSITY OF BERGEN



“Rethinking High-Grade Serous Carcinoma: Development of new tools for deep tissue profiling”

Shamundeeswari Anandan



Thesis for the degree of Philosophiae Doctor (PhD)
at the University of Bergen

Date of defense: 03.09.2021

© Copyright Shamundeeswari Anandan

The material in this publication is covered by the provisions of the Copyright Act.

Year: 2021

Title: “Rethinking High-Grade Serous Carcinoma: Development of new tools for deep tissue profiling”

Name: Shamundeeswari Anandan

Print: Skipnes Kommunikasjon / University of Bergen

Scientific environment

This work was conducted under the auspices of the Innovative Novel Ovarian cancer treatment Approaches (INOVA) Group, a part of the Precision Oncology Group at the Department of Clinical Science, University of Bergen. The group is part of the Norwegian Centre for excellence, called the Centre for Cancer Biomarkers (CCBIO), at the University of Bergen. The research focuses of the group are cancer biomarkers, preclinical models and clinical trials.

Professor Line Bjørge, Professor Emmet McCormack and Researcher Liv Cecilie Vestrheim Thomsen served as the supervisors of this project. The work was conducted in collaboration with the Department of Obstetrics and Gynaecology, Haukeland University Hospital, Bergen, Norway, and the Faculty of Electrical Engineering, Mathematics and Computer Science Intelligent Systems, TU Delft, Netherlands.

The candidate is employed by Helse Bergen HF. The thesis work was part of the Image-Guided Surgery and Personalised Postoperative Immunotherapy to Improving Cancer Outcome (ISPIC) EU consortium, and received economic support from Helse Vest RHF, Helse Bergen HF, the Norwegian Cancer Society, NFR/CCBIO and the Marie Skłodowska-Curie actions, supported by and carried out within the H2020-MSCA-ITN 2015 (project acronym ISPIC).



Acknowledgements

This PhD is a dream come true for me and my family, so on that note of gratitude I would like to thank the following individuals.

First and foremost, my primary supervisor, Line Bjørge, for constantly inspiring and motivating me with her guidance and dedication, for recognising my inner talents and above all for giving me this wonderful opportunity. I wish to thank Emmet McCormack, my co-supervisor and an expert in his field, for his innovative ideas and thoughts. I will forever be thankful to have had such focused supervisors: They have been instrumental in every step of this journey towards my PhD and have made me a better professional.

My mentor, Liv Cecilie Vestrheim Thomsen, for always being patient with me and my curiosity, and for participating in discussions with thought-provoking comments, sceptical questions and valuable contributions to my cytometry by time-of-flight (CyTOF) experiments. She has always been a good friend and a well-wisher. Stein-Erik Gullaksen, for teaching me the very basics of titration and for sharing his expertise in the field of single-cell mass CyTOF. Mihaela Lucia Popa, for mentoring me on the basics of animal handling and surgical techniques. Jørn Skavland and Geir Bredholt for their valuable contributions to the CyTOF panel design.

Katrin Kleinmanns, my colleague and ‘partner in crime’, for always being very supportive right from Day 1 as we started together. She has always been a great source of motivation for me, with her hard work and the healthy competitive environment she has fostered.

My co-authors (in alphabetical order): Bjørn Tore Gjertsen, Emmet McCormack, Geir Bredholt, Grete Alrek Iversen, Jørn Skavland, Katrin Kleinmanns, Lars Andreas Akslen, Line Bjørge, Liv Cecilie Vestrheim Thomsen, Stein-Erik Gullaksen and Tamim Abdelaal.

All the technicians at McCormack and KK Labs for all their support with the ordering, animal work and collection of patient samples. All my colleagues at McCormack Lab,

who have always been like a family, for creating such a great environment to work around, for all the interesting discussions and lunch breaks.

My special thanks to the INOVa team, for all the brainstorming discussions and endless Friday afternoon meetings, preparing for the weekend. I am happy to have been part of such a dynamic group. I would like to thank the people at the CyTOF – Friday group meetings for all the fruitful conversations and being a great platform to exchange ideas.

My co-author Tamim Abdelaal, from TU Delft, Netherlands, has also been my colleague for a short time at the University of Bergen. I am thankful for his contribution to the analysis of the CyTOF data, for patiently taking part in interesting discussions about his data analysis algorithms and providing explanations.

The Department of Clinical Science (K2) for their administrative assistance and for the course work. The Department of Gynaecology and Obstetrics, particularly Helse Vest, for the funding.

All the patients who have consented to contribute for this project without any direct reward or benefit. Special thanks are due to them for being instrumental in this translational research.

My family and friends have always been my greatest strength, and I am blessed to have such lovely people around: to start with my parents, who let me dream high and did all they could to help me to make those dreams come true; my husband, for his unconditional love and support, for always motivating me to fly even higher, for participating in all the scientific discussions and for always considering my PhD as our first baby, as I have. Above all our baby boy, who has been the greatest source of inspiration in life, especially through this journey of my PhD.

Last but not the least, I thank the Almighty for this wonderful life!

Bergen, May 2021

Shamundeeswari Anandan

Abbreviations

ACT: Adoptive cell transfer

ALDH: Aldehyde dehydrogenase

APC: Antigen-presenting cells

α SMA: Alpha-smooth muscle actin

ATM: Ataxia-telangiectasia mutated

ATP: Adenosine triphosphate

ATR: ATM- and Rad3-related

BRCA: BReast CAncer genes

CA-125: Cancer antigen 125

CAF: Cancer-associated fibroblasts

CAR: Chimeric antigen receptor

CCL: Chemokine ligand

CD: Cluster of differentiation

CEA: Carcinoembryonic antigen

CSC: Cancer stem cells

CT: Computed tomography

CTA: Cancer/testis antigens

CTC: Circulating tumour cells

CTLA4: Cytotoxic T-lymphocyte protein 4

CyTOF: Single-cell cytometry by time-of-flight

DAMP: Danger-associated molecular patterns

DC: Dendritic cells

DDR: DNA damage response

DNA-PKcs: DNA-dependent protein kinase catalytic subunit kinases

DSB: Double-strand breaks

ECM: Extracellular matrix

EMA: European Medicines Agency

EMT: Epithelial-to-mesenchymal transition

EOC: Epithelial ovarian cancer

EpCAM: Epithelial cell adhesion molecule

FAP α : Fibroblast activation protein alpha

FDA: Food and Drug Administration

FFPE: Formalin-fixed paraffin-embedded

FGF: Fibroblast growth factor

FIGO: International Federation of Gynaecology and Obstetrics

FIGS: Fluorescent image-guided surgery

FITC: Fluorescein isothiocyanate

FOLR1: Folate receptor alpha

Foxp3: Forkhead box protein P3

FTE: Fallopian tube epithelium

GM-CSF: Granulocyte macrophage-colony stimulating factor

HE4: Human epididymis protein 4

HGSOC: High-grade serous ovarian cancer

HLA-DR: Human Leukocyte Antigen – DR isotype

HRD: Homologous recombination deficiency

HRR: Homologous recombination repair

HSNE: Hierarchical stochastic neighbour embedding

IFN γ : Interferon gamma

IHC: Immunohistochemistry

IL: Interleukin

IMC: Imaging mass cytometry

LAG-3: Lymphocyte-activation gene 3

LOH: Loss of heterozygosity

LST: Large-scale transition

MAPK: Mitogen-activated protein kinase

MDSC: Myeloid-derived suppressor cells

MET: Mesenchymal-to-epithelial transition

MIBI-TOF: Multiplexed ion beam imaging by time-of-flight

MMPs: Matrix metalloproteinases

MRI: Magnetic resonance imaging

MST: Minimum spanning tree

NACT: Neoadjuvant chemotherapy

NGS: Next-generation sequencing

NK: Natural killer

OS: Overall survival

OSE: Ovarian surface epithelium

OXPPOS: Oxidative phosphorylation

PARPi: Poly-ADP-ribose-polymerase inhibitors

PBMC: Peripheral blood nuclear cells

PD-1: Programmed cell death protein

PDGF: Platelet-derived growth factor

PDGFRb: Platelet-derived growth factor receptor beta polypeptide

PDL1: Programmed cell death protein ligand

PET: Positron-emissions tomography

PFS: Progression-free survival

PI3K: Phosphoinositide-3-kinase

PLD: Pegylated liposomal doxorubicin

QoL: Quality of life

ROS: Reactive oxygen species

RRSO: Risk reducing salpingo-oophorectomy

SCOUT: So-called secretory cell outgrowth

scRNA-seq: Single-cell RNA sequencing

SPADE: Spanning-tree progression analysis of density-normalised events

SSB: Single-strand breaks

STIC: Serous tubal intraepithelial carcinoma

TAA: Tumour-associated antigens

TAG72: Tumour-associated glycoprotein 72

TAI: Telomeric allelic imbalance

TAM: Tumour-associated macrophages

TGF: Transforming growth factor

TIL: Tumour-infiltrating lymphocyte

TIM3: T-cell immunoglobulin and mucin-domain containing-3

TME: Tumour microenvironment

TNF α : Tumour necrosis factor alpha

Tregs: Regulatory T cells

tSNE: t-distributed stochastic neighbour embedding

UMAP: Uniform manifold approximation and projection

VEGF: Vascular endothelial growth factor

Abstract

Background: High-grade serous ovarian cancer (HGSOC) is the most frequently occurring and most fatal epithelial ovarian cancer (EOC) subtype. The reciprocal interplay of the different components encompassed within the tumour microenvironment (TME) are fundamental for tumour growth, advancement, and therapy response. It is therefore important to be able to deeply characterize the complex and diverse TME with multidimensional approaches.

Aims: The main aim of this project was to establish novel multiparametric mass cytometry panels and thoroughly characterise the HGSOC TME.

Methods: We first developed a novel 35-marker ovarian TME-based Cytometry by time-of-flight (CyTOF) panel (pan-tumour panel) and utilized it to examine the effects of six different tissue dissociation methods on cell surface antigen expression profiles in HGSOC tumour samples (**Paper I**). We further established a unique immune panel (pan-immune) for the detailed immunophenotyping of chemo-naïve HGSOC patients. The individual tumour immune microenvironments were characterized with tailored computational analysis (**Paper II**). With the use of an established merging algorithm—CyTOFmerge—the pan-tumour and pan-immune datasets were merged for a more in-depth immune delineation of the ten ovarian chemo-naïve TME profiles in addition to tumour and stromal cell phenotyping (**Paper III**).

Results: We have established a novel ovarian TME-based CyTOF panel for HGSOC that is capable of delineating the immune, tumour, and stromal cells of the TME. Utilizing this panel, we demonstrated that, although the six tissue dissociation methods have a certain level of influence on the TME antigen expression profiles, inter-patient differences between the tumour samples are still clear. In addition, we identified a previously undescribed stem-like cell subset (**Paper I**). We have developed a unique 34-marker immune panel and have provided a detailed characterization of the ovarian tumour immune microenvironment of chemo-naïve patients. We identified a high degree of interpatient immune cell heterogeneity and discovered an abundance of conventional dendritic cells (DC), natural killer (NK) cells, and unassigned

hematopoietic cells. Certain monocyte and dendritic cell (DC) clusters have shown prognostic relevance within the ovarian TME (**Paper II**). The merged dataset analysis revealed a new level of complexity with a more in-depth immune (myeloid cells) delineation in addition to tumour and stromal (fibroblast subsets) cell phenotypes. We identified an even higher degree of interpatient TME heterogeneity and a novel tumour cell metacluster, CD45⁻CD56⁻(EpCAM⁺FOLR1⁻CD24⁻). As a benefit of integrating the datasets, we identified even higher clinical associations (from 12 [pan-tumour dataset] to 20 [merged dataset]). Furthermore, most of these observed associations were majorly between PFS, OS, and infiltrating immune cell subsets (**Paper III**).

Conclusions and consequences: (Paper I) In conclusion, the panel represents a promising profiling tool for the in-depth phenotyping of the HGSOC TME cell subsets. Although the tissue dissociation methods have influence on the TME antigen expression profiles, inter-patient differences are still clear. (**Paper II**) Our findings revealed a high degree of heterogeneity and identified phenotypic profiles that can be explored for use in HGSOC phenotypic profiling. (**Paper III**) Together, the merged sketching illustrates that comprehensive individual TME mapping for HGSOC patients can contribute to a better understanding each patient's unique micromilieu given the need for more personalized treatment approaches.

List of Publications

- I. **Anandan, S.***; Thomsen, L.C.V. *; Gullaksen, S.-E.; Abdelaal, T.; Kleinmanns, K.; Skavland, J.; Bredholt, G.; Gjertsen, B.T.; McCormack, E.; Bjørge, L. “Phenotypic characterization by mass cytometry of the microenvironment in ovarian cancer and impact of tumour dissociation methods”. *Cancers* 2021, *13*, 755.

- II. **Anandan, S.**; Kleinmanns, K.; Gullaksen, S.-E.; Iversen, G.A.; Akslen, L.A.; McCormack, E.; Bjørge, L, Thomsen, L.C.V. “The use of high-dimensional single-cell analysis discloses emerging insight to the complexity of the immune tumour microenvironment in treatment naïve high-grade serous ovarian carcinomas”. *Manuscript*

- III. **Anandan, S.**; Thomsen, L.C.V.; Kleinmanns, K.; Abdelaal, T.; Gullaksen, S.-E.; Iversen, G.A.; Akslen, L.A.; McCormack, E.; Bjørge, L. “Integration of mass cytometry data with CyTOFmerge reveals the heterogeneous and complex tumour milieu in high-grade serous ovarian carcinomas” *Manuscript*

* Authors contributed equally

The published paper is reprinted with permission from Cancers. All rights reserved.

Contents

SCIENTIFIC ENVIRONMENT.....	3
ACKNOWLEDGEMENTS.....	4
ABBREVIATIONS.....	6
ABSTRACT.....	10
LIST OF PUBLICATIONS.....	12
CONTENTS.....	13
1. INTRODUCTION.....	15
1.1 HIGH-GRADE SEROUS OVARIAN CANCER.....	15
1.1.1 Epidemiology.....	15
1.1.2 Pathogenesis.....	18
1.1.3 Aetiology and risk factors.....	22
1.1.4 Symptoms, diagnostics and staging.....	24
1.1.5 Current treatment modalities and challenges.....	25
1.1.6 Biomarkers.....	34
1.2 TUMOR MICROENVIRONMENT.....	34
1.2.1 Constituents of the HGSOC TME.....	36
1.2.2 The uniqueness and plasticity of HGSOC TME.....	47
1.2.3 HGSOC TME heterogeneity at the multiscale level and its clinical impact.....	51
1.2.4 Targeting the ovarian TME.....	52
1.3 ADVANCEMENT OF TME CHARACTERISATION TOOLS WITH EMPHASIS ON EOC..	53
1.3.1 Advances in single-cell protein measurements.....	54
1.3.2 The ‘-omic’ techniques.....	56
1.3.3 Spatial profiling of patient TMEs: The Future?.....	58
2. AIMS OF THE PROJECT.....	61
2.1 BACKGROUND.....	61
2.2 GENERAL AIM.....	61
2.3 SPECIFIC AIMS.....	62
3. MATERIALS AND METHODS.....	63
3.1 MATERIALS.....	63
3.2 METHODOLOGICAL CONSIDERATIONS.....	64

4. SUMMARY OF RESULTS.....	74
5. DISCUSSION.....	76
6. CONCLUSIONS.....	95
7. FUTURE PERSPECTIVES.....	97
8. REFERENCES.....	99

1. Introduction

High-grade serous ovarian carcinoma (HGSOC) is the most common and most lethal epithelial ovarian cancer (EOC) subtype. It is characterised by ubiquitous mutations in the *TP53* gene, coupled with homologous recombination repair machinery deficiency (HRR) including dysfunction in the Breast CAncer (BRCA) genes, as well as chromosomal instability (1). The tumours are heterogeneous, characterised by different microenvironmental features (2). As our understanding of the molecular background grows, molecular (BRCA mutations, HRR deficiencies) and phenotypic profiling (platinum sensitivity, degree of debulking) are beginning to be integrated into clinical practice and trials. It is believed that the introduction of poly-ADP-ribose-polymerase (PARP) inhibitors in frontline treatment is producing an overall survival (OS) benefit (3). Further improvements will require rethinking, and a roadmap for research priorities has been outlined (4). A more comprehensive profile and understanding of the tumour microenvironment is currently considered to be a leading research priority, in the hope that it will enable the development of better strategies for managing this disease (5).

1.1 High-Grade Serous Ovarian Cancer

1.1.1 Epidemiology

EOC is the sixth most common malignant neoplasm and the leading cause of death from gynaecological malignancies in the Western world. Due to the intra-abdominal location of these tumours and the number of unspecific symptoms, the majority of women all over the world are diagnosed at advanced stages (6). Together with a rapid development of chemotherapy resistance and the evasion of immunological surveillance, this explains at least in part, these patients' dismal prognoses (4). According to the Cancer Registry of Norway, the ovarian cancer mortality rate is high but has improved in recent years (2013–2019) (Fig. 1). In 2019, 306 patients died from the disease in Norway (7).

The lifetime risk for a woman in Norway to develop ovarian cancer is estimated to be

around 1 in 77; the age-adjusted incidence rate (new cases per 100 000 people per year) was 18.6 for Norway in 2019, and 528 new cases were reported in 2019 (Fig. 1) (7). Although the incidence rates in developed countries in North America and elsewhere in Europe are the highest in the world, Norway's rate is not far behind.

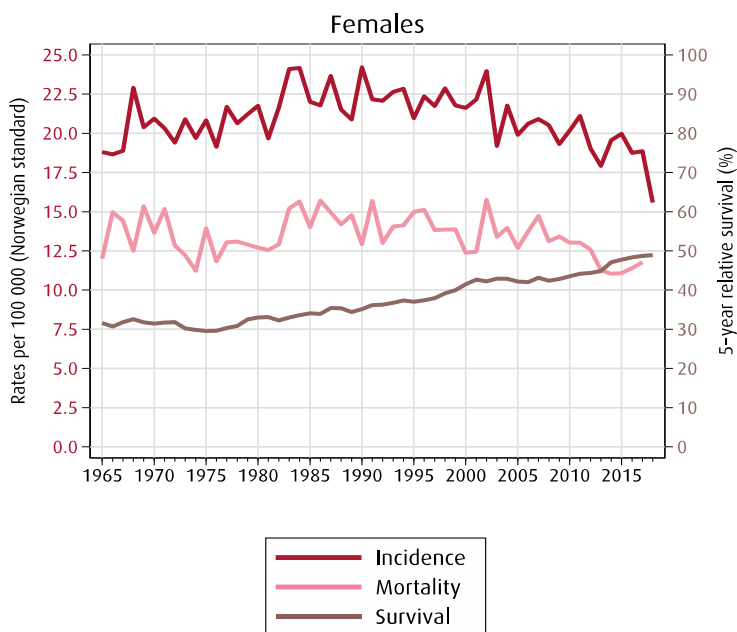


Figure 1. Norwegian epidemiological data of ovarian cancer (graph adapted from Cancer Registry 2019 (7)).

The incidence rates are lowest in developing countries such as those of Africa and Asia. According to the National Cancer Registry Programme (NCRP, Bangalore, India), there were around 4818 ovarian cancer cases registered in the various cancer registries in India during the period 2012–2014: The number of cases differed from 15 cases in Nagaland to 688 cases in Delhi (Table 1) (8).

Table 1. Age adjusted rate (AAR), % of total cases and rank of ovarian cancer in different registries of India (2012–2014) (table adapted from Takiar et al. (8)).

Cancer Registry	Number of Cases	AAR	% of total cases	Rank
Delhi	688	10.0	7.2	4.0
Kamrup	131	8.7	5.5	5.0
Bhopal	136	8.4	7.8	3.0
Chennai	409	8.2	6.6	3.0
Mumbai	468	8.1	6.9	3.0
Pasighat	12	8.1	7.6	4.0
Kolkata	203	8.0	7.8	3.0
Thiruvananthapuram	468	7.0	5.9	4.0
Naharlagun	48	6.7	6.8	6.0
Dibrugarh	120	6.5	8.9	4.0
Bangalore	240	6.5	5.3	3.0
Pune	273	6.3	7.4	3.0
Nagpur	152	6.0	6.3	3.0
Patiala	155	5.5	4.9	4.0
Kolam	292	5.4	5.3	4.0
Sikkim	40	4.9	5.9	6.0
Aurangabad	69	4.7	6.2	3.0
Wardha	94	4.4	6.6	3.0
Cachar	106	4.1	5.1	5.0
Ahmedabad	220	4.0	5.3	3.0
Mizoram	56	3.7	2.7	7.0
Manipur	146	3.5	5.7	5.0
Tripura	164	3.2	6.1	4.0
Barshi-Rural	22	2.9	4.6	3.0
Barshi-Exp	52	2.3	4.6	3.0
Meghalaya	39	2.1	2.4	8.0
Nagaland	15	1.7	2.8	10.0

Ovarian cancer is predominant among postmenopausal women, with patients' median age range being 61 years in Norway and 63 years in the United States (7, 9). In India, approximately 50% of the total cases affect women between 45–65 years of age (median age: 53 years) (8). The 5-year survival rate is still below 50%, although combined international efforts over the last three decades have led to meaningful improvements in survival parameters. This improvement, however, is due for the most part to the increased number of chemotherapy lines given—not to the improvement of frontline treatment (4). How the introduction of PARP inhibitors in the frontline setting will make a difference is currently unclear, but we have reason to believe that it will be

beneficial (3, 10).

1.1.2 Pathogenesis

The origin and pathogenesis of EOC have been mysterious for decades, with different concepts being introduced, but traditionally it was regarded as a single disease entity, irrespective of the histopathologic subtype (11). Today, EOC is subdivided primarily into at least five different histological subtypes with different aetiologies, genetic backgrounds, phenotypic characteristics and clinical features (Table 2) (12). The frequency of the subtypes differs as well, with HGSC being the most common and lethal subtype (70%) and low-grade serous carcinoma (<5%) being the rarest.

Table 2. Clinical and molecular features of the five most common ovarian cancer types (table adapted from Prat et al. (12)).

	HGSC	LGSC	MC	EC	CCC
Risk factors	<i>BRCA1/2</i>	?	?	HNPC ^a	?
Precursor lesions	Tubal intraepithelial carcinoma	Serous borderline tumor	Cystadenoma/borderline tumor?	Atypical endometriosis	Atypical endometriosis
Pattern of spread	Very early transcoelomic spread	Transcoelomic spread	Usually confined to ovary	Usually confined to pelvis	Usually confined to pelvis
Molecular abnormalities	<i>BRCA, p53</i>	<i>BRAF, KRAS</i>	<i>KRAS, HER2</i>	<i>PTEN, ARID1A</i>	<i>HNFI, ARID1A</i>
Chemosensitivity	High	Intermediate	Low	High	Low
Prognosis	Poor	Intermediate	Favorable	Favorable	Intermediate

HGSC, high-grade serous carcinoma; LGSC, low-grade serous carcinoma; MC, mucinous carcinoma; EC, endometrioid carcinoma; CCC, clear-cell carcinoma.
^aHereditary nonpolyposis colorectal carcinoma.

Initiation

In light of the novel findings produced by large clinicopathologic and molecular genetic studies over the past decade, it is now accepted that the majority of HGSCs arise from an extraovarian site, the epithelium in the fimbriated distal part of the fallopian tubes (Fig. 2). Why the epithelium in the tubes is susceptible remains unknown (13), but there is reason to believe that inflammation plays a role, as it does in many types of cancer. Associations with both peritoneal (endometriosis, talc and infections) and ovulation-induced inflammation processes have been reported (14). More recently, Nené et al. showed that an aberrant cervico-vaginal microbiome may also be a contributing factor, especially in *BRCA* mutation carriers (15).

How these cells transform and disseminate remain unclear, but several inflammation-inducing factors originating from the fallopian tubes, follicular fluid or the peritoneum may be part of the cause (13). Epithelial cells are exposed to elevated levels of inflammatory mediators (such as cytokines, prostaglandins, reactive oxygen species (ROS)) and growth factors which promote a chronic inflammatory microenvironment (14). Precursor lesions in the tubes with distinct 'p53 signatures', evolving into so-called secretory cell outgrowths (SCOUTs) and serous tubal intraepithelial carcinomas (STICs) can be established. STICs are described as the immediate precursor to invasive HGSOC and the earliest histologically recognisable lesion in the pathogenesis of high-grade serous carcinoma (16). STICs are the most accepted preneoplastic lesion, as they share the same morphological gene mutation of *TP53*, with positive p53 and γ H2AX stainings and missing expression of Ki-67, as has also been observed in HGSOC tumours (17). Nevertheless, Lohmussar et al. recently reported results supporting the dual origin hypothesis of HGSOC, highlighting both the ovarian surface epithelium (OSE) and STICs as potential candidate tissues of origin in an organoid-based tumour progression model (18).

Activin A, a component of follicular fluid, may stimulate STIC cells to migrate to the ovary, where they develop further into a primary tumour upon mesenchymal-to-epithelial transition (MET) (19). Another possible pathogenesis mechanism is the implantation of the normal fimbria epithelium on the denuded ovarian surface at the site of rupture when ovulation occurs, following tumour development in the inclusion cysts (20). Once the tumour is established, the proinflammatory microenvironment will promote further dissemination and establishment of metastasis, ascitic fluid production and development of chemoresistance (14).

HGSOC is often susceptible to widespread carcinomatosis, with micrometastases all over the abdominal cavity. It usually metastasises through the transcoelomic route, in contrast to other carcinomas which spread via the haematogenous route (21). This may result from the shedding of small clusters of malignant cells directly from the ovary or fallopian tube into the surrounding tissue, such as the peritoneal lining. The release of vascular endothelial growth factors (VEGF) and blocked lymph vessels from malignant

cell clusters cause leaky vessels, resulting in the formation of ascites fluid (22). Characteristically, the malignant cells remain confined in the peritoneal cavity, in direct contact with intraperitoneal fluid both as peritoneal implants and solid tumour masses, as well as free-floating tumour cells and cell aggregates (spheroids) (23).

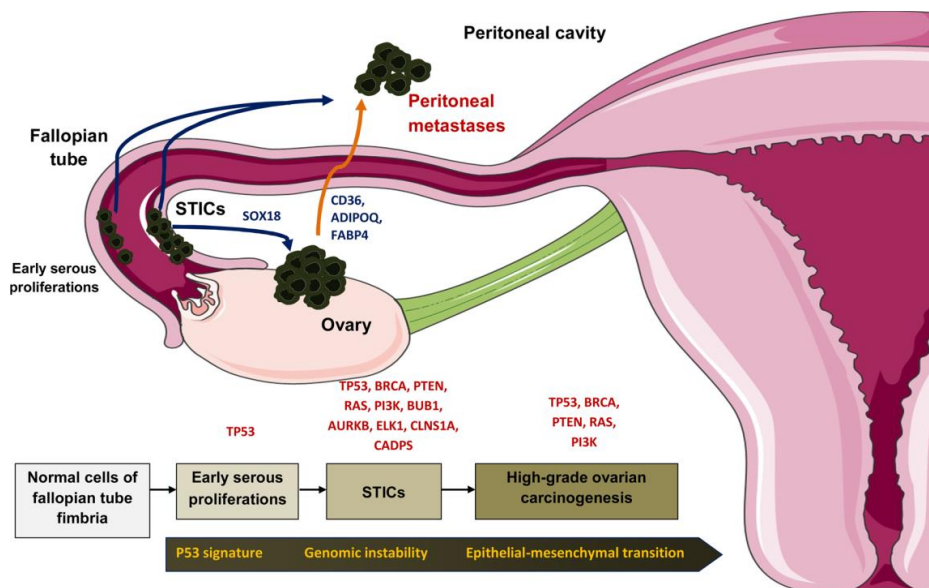


Figure 2. Cells of origin for HGSOC (image adapted from Khalid et al. (24)).

Genetics

In recent years, notable progress has been made in understanding the different steps of pathogenesis in HGSOC. With the exception of their presence in *TP53* and *BRCA1/BRCA2*, point mutations in tumour suppressors are relatively uncommon (25). Instead, HGSOC is characterised by genomic structural variations and DNA copy number changes, making it chromosomally unstable. These are drivers of molecular subtype specifications (Fig. 3) and lead to global changes in gene expression (4).

The Cancer Genome Atlas (TCGA) study of HGSOC revealed *BRCA1* and *BRCA2* mutations in 22% and *TP53* mutation in 96% of cases, with only nine more additional mutations identified in *CSMD3*, *NF1*, *CDK12*, *FAT3*, *GABRA6* and *RB1* genes. A smaller group of HR DNA-repair-associated mutations can be found in *RAD51C*, *BRIP1*, *RAD51D*, *PTEN* (6% loss of function), *ATM* and *ATR* genes (4, 25).

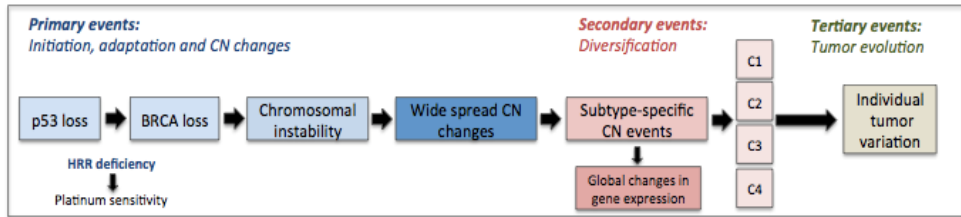


Figure 3. Pathogenesis of high-grade serous carcinomas (image adapted from Bowtell et al. (4)).

Based on transcriptional data, HGSOc can be stratified into four promoter methylation subtypes (immunoreactive, differentiated, proliferative and mesenchymal clusters) and seven copy number signatures, all of which are associated with different tumour microenvironmental features and clinical outcomes (25, 26).

Around half of HGSOcs display defects in the homologous recombination repair (HRR) and homologous recombination deficiency (HRD) pathways, which mainly arise from germline and somatic mutations or from epigenetic changes in the *BRCA1/2* genes, and, to a relatively lesser extent, from mutations in other molecules in the HRR pathways (4, 26). The gene products of *BRCA1/2* are involved in the maintenance of genomic stability and DNA damage repair, as well as apoptosis and transcriptional regulation. HRR is a key determinant of platinum and poly (ADP-ribose) polymerase inhibitors (PARPi) sensitivity (27). Some tumours without HRR defects have amplification of the *CCNE1* gene, which is associated with acquired chemoresistance and poor prognosis (4, 25). Together with the tumour cell's plasticity, these molecular alterations result in the establishment of a highly heterogeneous disease (see also Section 1.2.1) (28). Molecular traits for most other HGSOcs with no apparent HRR defects are poorly defined. The only genetics information currently used in clinical practice is *TP53* mutations for diagnostics and *BRCA1/BRCA2* mutations for identification of hereditary and selection of treatment (4). Although HRD testing is used more and more, in Norway so far it has only applied for patients participating in clinical trials (29).

Gene expression profiles have been identified which are associated with debulking status, OS and response to platinum therapy (30). To date, at least 15 ovarian cancer genome-wide association studies have been performed, most of which have evaluated susceptibility loci along with clinical outcomes (31). The TCGA study indicated that the immunoreactive molecular subtype was associated with superior OS and the mesenchymal subtype with the worst OS (32). These findings were in line with an earlier classification, published by Tothill et al. in 2008, which were based on unsupervised hierarchically clustered gene expression data from 285 high-grade advanced tumours (33). Although these data were refined and validated independently, the use of gene expression biomarkers in clinical settings is still challenging due to important shortcomings, including lack of identification of robust gene signatures in larger cohort samples with strong statistical interference. However, Millstein et al. recently identified a high-confidence HGSOC prognostic signature which has proven useful for stratifying patients in a treatment-specific manner. When tested with gene set enrichment analysis, the developed signature demonstrated promising results, highlighting the role of the immune system in OS of ovarian cancer (34). Hence, supporting the potential use and need for further investigation of immune therapy and targeted treatments for HGSOC.

1.1.3 Aetiology and risk factors

There are many genetic and phenotypic risk factors which contribute to an individual's risk of developing cancer. Approximately 85–90% of ovarian cancers are believed to be sporadic, while 10–15% are hereditary (6). Substantial variation exists on the basis of ethnicity and geography—e.g. the age-adjusted incidence rate (new cases per 100 000) in Norway was 15.6 (2018) (25) and 5.3 in India (based on data from 2012–2014) (8).

Germline *BRCA1* mutation carriers face a 39–46% risk of developing ovarian carcinoma by the age of 70, whereas only 10–27% of women with inherited *BRCA2* mutation are at risk of developing ovarian cancer (35). The cancers occurring in these women are usually HGSOCs and manifest at an earlier age than the sporadic cases. Low-penetrance mutations in genes such as *BRIP1*, *RAD1C*, *RAD1D*, *BARD1*, *CHEK2*,

MER11A, *RAD50*, *PALB2* and *ATM*, all important for HRR, are vital (36-38). Mismatch repair genes (*MSH2* and *MLH1*), which predisposed for hereditary nonpolyposis colorectal cancer (HNPCC or Lynch syndrome) (39) can also increase the susceptibility. These women develop the disorder about 10 years earlier than women with a non-hereditary form.

EOC are seldom diagnosed in pre-menopausal women (<45 years old); as with other epithelial cancers, the disease tends to be diagnosed more frequently with increasing age. Identification of non-genetic risk factors are based primarily on epidemiological findings. In their review paper from 2012, Hunn and Rodriguez tried to separate them into different groups (reproductive, hormonal, inflammatory, dietary and surgical), some being distinct while others were overlapping (40). Many of the risk factors are associated with the absolute number of ovulations a woman experiences throughout the course of her life, and positive associations with both early menarche and late menopause have been recognised. Use of oral contraceptives (length-of-use dependent), pregnancies (number dependent) and breastfeeding reduce the risk (41). Infertility, polycystic ovarian syndrome and obesity are independent risk factors, while the risk associated with use of drugs used for assisted reproduction is still unclear (42, 43). The positive correlation between chronic inflammation such as endometrioses and the development of clear cell and endometrioid cancers are clear. Environmental factors such as pelvic inflammatory disease, smoking and talc can also be triggers (14). The role dysbiosis plays in the microbiome must be further evaluated (15).

In high-risk groups, 80–95% risk reduction is reported with traditional prophylactic bilateral risk-reducing salpingo-oophorectomy. Based on recent findings on fallopian tubal precursor lesions, supported by ongoing studies such as the Preventing Ovarian Cancer through early Excision of Tubes and late Ovarian Removal (PROTECTOR) and Women Choosing Surgical Prevention (WISP) trials, it has been suggested that removing the fallopian tubes might be sufficient, allowing for removal of ovaries to be delayed or even for the ovaries to be retained.

1.1.4 Symptoms, diagnostics and staging

EOC symptoms are not explicit and consist of abdominal or pelvic discomfort, gastrointestinal problems, unexplainable weight loss and/or vaginal bleeding, and they can at least in part be explained by intra-abdominal localisation of tumour tissues, indicating advanced disease stage. Typically, they may manifest themselves months before diagnosis. Late diagnosis is one of the most serious challenges with this disorder, and as already mentioned in EOC almost 75% of patients have advanced disease by the time of diagnosis (44, 45).

As the patients have different problems, it is difficult to establish a recommended diagnostic algorithm. Predominant symptoms are thus used to determine the survey of methodologies used. Through examinations for the abdomen and genitalia with ultrasound, parameters such as the presence of ascites and tumour characteristics are measured. Imaging modalities alone or combined, such as computed tomography (CT), magnetic resonance imaging (MRI), positron-emissions tomography (PET)-CT, as well as serum biomarkers such as cancer antigen 125 (CA125/MUC16) and carcinoembryonic antigen (CEA), are also applied. CA125 is an EOC-associated serum biomarker often found in elevated levels in women with EOC. To avoid misclassifications with gastrointestinal cancers, CEA is included in the standard clinical diagnostic algorithms (46-48). On the other hand, the use of human epididymis protein 4 (HE4), another EOC associated tumour biomarker, has not yet been implemented in Norway. Sometimes upfront laparoscopic- or ultrasound-guided biopsies are needed for clinical decision-making.

Staging is the description of the size and location of the cancer. EOC is staged according to the 2014 International Federation of Gynaecology and Obstetrics (FIGO) staging system (which was updated in 2018). The stage is determined based on perioperative judgements in combination with histopathological evaluation. The four disease stages (I–IV) are defined in Table 3 (49) below.

Table 3. FIGO Ovarian Cancer Staging (2014) (table adapted from Mutch et al. (49)).

I	Tumor confined to ovaries or fallopian tube(s)
IA	Tumor limited to one ovary (capsule intact) or fallopian tube, No tumor on ovarian or fallopian tube surface No malignant cells in the ascites or peritoneal washings
IB	Tumor limited to both ovaries (capsules intact) or fallopian tubes No tumor on ovarian or fallopian tube surface No malignant cells in the ascites or peritoneal washings
IC	Tumor limited to one or both ovaries or fallopian tubes, with any of the following: IC1 Surgical spill intraoperatively IC2 Capsule ruptured before surgery or tumor on ovarian or fallopian tube surface IC3 Malignant cells present in the ascites or peritoneal washings
II	Tumor involves one or both ovaries or fallopian tubes with pelvic extension (below pelvic brim) or peritoneal cancer (Tp)
IIA	Extension and/or implants on the uterus and/or fallopian tubes/and/or ovaries
IIB	Extension to other pelvic intraperitoneal tissues
III	Tumor involves one or both ovaries, or fallopian tubes, or primary peritoneal cancer, with cytologically or histologically confirmed spread to the peritoneum outside the pelvis and/or metastasis to the retroperitoneal lymph nodes
IIIA	Metastasis to the retroperitoneal lymph nodes with or without microscopic peritoneal involvement beyond the pelvis
IIIA1	Positive retroperitoneal lymph nodes only (cytologically or histologically proven)
IIIA1(i)	Metastasis \leq 10 mm in greatest dimension (note this is tumor dimension and not lymph node dimension)
IIIA1(ii)	Metastasis > 10 mm in greatest dimension
IIIA 2	Microscopic extrapelvic (above the pelvic brim) peritoneal involvement with or without positive retroperitoneal lymph nodes
IIIB	Macroscopic peritoneal metastases beyond the pelvic brim \leq 2 cm in greatest dimension, with or without metastasis to the retroperitoneal lymph nodes
IIIC	Macroscopic peritoneal metastases beyond the pelvic brim > 2 cm in greatest dimension, with or without metastases to the retroperitoneal nodes (Note 1)
IV	Distant metastasis excluding peritoneal metastases Stage IV A: Pleural effusion with positive cytology Stage IV B: Metastases to extra-abdominal organs (including inguinal lymph nodes and lymph nodes outside of abdominal cavity) (Note 2) (Note 1: includes extension of tumor to capsule of liver and spleen without parenchymal involvement of either organ) (Note 2: Parenchymal metastases are Stage IV B)

Notes:

1. Includes extension of tumor to capsule of liver and spleen without parenchymal involvement of either organ.
2. Parenchymal metastases are Stage IV B.

1.1.5 Current treatment modalities and challenges

EOC prognoses have remained poor for years (50). Current prognostic factors include age, FIGO stage (5-year survival of Stage IV is 5%, compared to 92% for Stage I), degree of debulking surgery, performance status and histological subtype (51, 52). Despite this diversity, most patients receive the same standard treatment, which includes cytoreductive surgery in combination with platinum-based chemotherapy (53). Alternatively, advanced-stage (IIIC and IV) patients could receive three cycles of neoadjuvant therapy (NACT) followed by interval debulking surgery (54). The addition of anti-angiogenetic agents and PARP inhibitors as maintenance therapy is based on phenotypic selection criteria (ICON7) and the presence of mutations in the BRCA1 and BRCA2 genes (SOLO1), respectively (55-57). There are also several ongoing randomised clinical trials searching for new treatment approaches on the basis of histotype and molecular subgroup stratification.

Upon recurrence, which is common, patients still receive multiple therapeutics (primarily chemotherapy and/or targeted drugs but sometimes also surgery) (Fig. 4), but their treatment changes from cure to palliation. New treatment strategies are needed to extend chemotherapy-free intervals, as interval periods between successful lines of chemotherapeutics become shorter with recurrence (58).

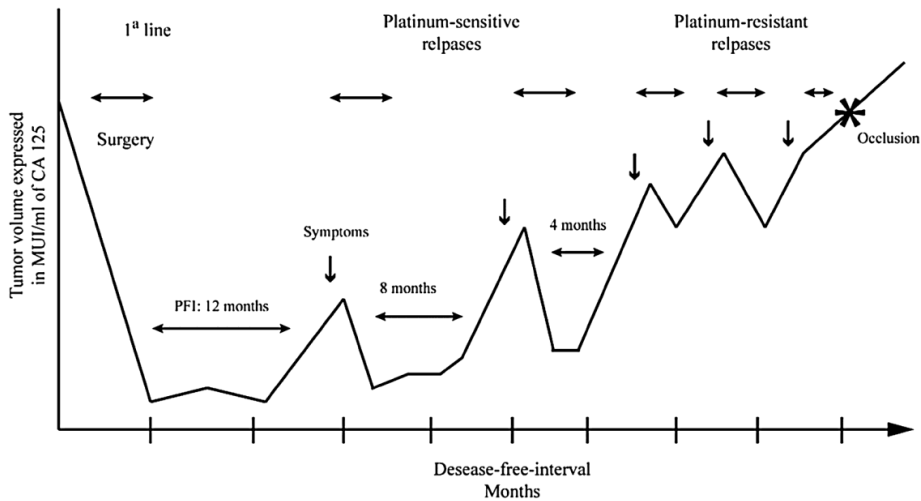


Figure 4. HGSOc progression (graph adapted from Giornelli et al. (58)).

Cytoreductive surgery

The goal of cytoreductive surgery, the most important intervention in treatment of EOC, is complete tumour resection (meaning residual disease less than 1 cm³) (59). Furthermore, the words “debulking” and “cytoreductive surgery” are interchangeably utilized in the literature to describe the surgery for the treatment of ovarian cancer patients. However, the word “debulking” is considered to mean “reduction of tumor mass” relative to the word “cytoreductive” which intends to mean “complete resection of the tumor” (60). Initial staging of patients is as mentioned (paragraph 1.1.4) evaluated during the primary cytoreductive surgery and thereafter finalised based on the conclusive results from the histopathological examinations (Table 3). Macroscopic visible residual disease has been shown to be the single most important independent negative prognostic factor (51, 61). The extent of debulking is influenced both by the

aggressiveness of the surgical approach and the inherent tumour biological characteristics and disease stage (62). It remains unknown whether a suboptimal disease outcome after surgery is only due to surgical skills or can be explained by the intrinsic biology of the tumour itself and residual tumour result in cancer-sustaining cell clones. Therefore, in addition to the imaging modalities used (see Section 1.1.4), stratification of patients on the basis of tumour biology and the laparoscopic scoring algorithm, predictive biomarkers could aid in the identification of patients with the benefit of complete tumour debulking (63, 64). Currently, the benefits of radical upfront debulking surgery are being addressed in a large international Trial of Radical Upfront Surgical Therapy (TRUST) trial (65). On the other hand, systematic pelvic and paraaortic lymphadenectomy after complete debulking surgery was investigated in the LION trial and was reported to have no benefits for PFS and OS in patients (66). These findings have already been implemented in the treatment guidelines.

The aggressive surgical approaches for metastatic EOC are unique; no other cancers have shown a similar advantage once the disease has spread. Surgical training and sufficient experience with advanced surgical procedures and handling of complications are a prerequisite for treating patients with EOC. Together with centralisation to specialised gynaeco-oncologic centres, improved outcome is the result (62, 67). Alternatively, for patients for whom optimal tumour resection is not an option either because of coexisting illnesses, age and performance status or the spread of the disease, NACT followed by interval debulking surgery can be offered (68). This management strategy has been shown to increase the rate of complete cytoreduction and to reduce morbidity.

Fluorescent image-guided surgery (FIGS), a recently emerging surgical strategy, has been used to improve optimal tumour debulking intraoperatively (69). The first in-human study was performed by van Dam et al., with folate conjugated to fluorescein isothiocyanate (FITC) as the tracer (70). The use of different fluorescent dye conjugated mAbs directed against different tumour-associated antigens is being tested (71).

Secondary debulking will probably be used more often in the future, as the randomised phase III multicentre studies DESKTOP III and SOC-1 have shown a substantial increase in PFS in properly selected patients for whom platinum still is an option (72–74). The OS data from DESKTOP III was presented at ASCO2020 and they are also favourable (73). The effect of further debulking attempts is still experimental and should only be offered to selective patients (75). Studies conducted in the late 1990s showed that surgery for platinum-resistant disease is usually not recommended (65). Palliative surgery is considered an option only when surgical intervention could aid in resolving gastrointestinal obstructions caused by ovarian cancer metastasis (76).

Chemotherapy

Except for patients with low-risk FIGO stage IA tumours, frontline adjuvant chemotherapy after debulking surgery with platinum-taxane regimens is offered and yields a response rate of > 80% with 40–60% complete responses. This finding is also supported by the results of clinical trials with improved OS and PFS rates (77). Based on the toxicity profile, since the mid-1980s the standard treatment regimen in Norway has included six cycles of paclitaxel (175 mg/m²) combined with carboplatin (AUC, 5 or 6) every third week (53). On the other hand, NACT, which is offered primarily to inoperable patients, usually comprises 3 cycles of the same chemotherapy regimen followed by 3 treatment rounds after interval debulking surgery (78).

Bevacizumab was introduced in the frontline setting more than 10 years ago for selected groups of patients. In Norway, its use is approved by the authorities for so-called ‘high-risk’ patients for 18 months (7.5 mg/m²); complete tumour resection is not possible during PDS (residual disease > 1cm), in patients with stage IV disease and in patients receiving NACT. Indications for use and the dosage administered differ in different parts of Europe (56, 79).

PARPi is a relatively new group of drugs. Data from the SOLO-1 study evaluating the effect of the PARPi olaparib as a consolidation therapy as part of frontline therapy was impressive, showing an increase in PFS > 3 years when the treatment groups were compared (57), and as already mentioned the OS data is also promising (3). Based on

data presented in 2018 (57) the drug was approved for use in Norway, and BRCA carriers and women with somatic BRCA mutation are currently offered olaparib as a consolidation therapy for 2 years if they are responding to platinum as part of the first line treatment regimen. At present patients qualifying for both olaparib and bevacizumab are offered only olaparib, as the data from the PAOLA-1 study did not clearly show which patient group would benefit from the combination (80).

Despite the various efforts to improve frontline and maintenance treatment, recurrence is common in HGSOE patients (80–90%). The traditional classification of relapsed patients has changed to women experiencing progression of disease within ≤ 6 months (previously referred to as ‘platinum-resistant relapse’), or who fail to respond at all to frontline treatment or relapse within 4–6 weeks (previously classified as ‘platinum-refractory’) after completing a platinum-based regimen. As understanding of the disease is constantly improving, there exists today less rigid paradigm for recurrent ovarian cancer treatment than only a couple of years back. Patients who still have platinum as an option regularly receive carboplatin combined with pegylated liposomal doxorubicin (PLD), paclitaxel or gemcitabine, whereas those for whom platinum is not an option often receive one of the three combination drugs as a single agent therapy (58). Nevertheless, there is considerable emphasis on the categorisation of patients based on their clinical characteristics for better treatment outcomes. Mirza et al. and Glajzer et al. recently highlighted the importance of identifying treatment algorithms for improved patient selection with treatment benefit (81, 82). Targeted therapeutics in a recurrent set up has been shown to prolong PFS2 in both platinum-sensitive disease (PARPi: ARIEL3, SOLO-2; bevacizumab: OCEANS, GOG213) and platinum-resistant disease (bevacizumab: AURELIA) (83-87). In Norway, bevacizumab is approved for use in patients experiencing recurrent disease and symptomatic large volumes of ascites and/or pleural effusions. Furthermore, PARPi are approved for use as consolidation therapy in patients with recurrence treated with a platinum-containing regimen who have responded to platinum until progression. Olaparib is approved for BRCA mutated patients (SOLO-2) as well as BRCA wild-type patients while niraparib is only approved for BRCA wild-type patients (NOVA trial)(85, 88).

In addition to extending chemotherapy-free intervals between successive lines of treatment in relapsed patients, there is a greater need to support conventional chemotherapy regimens with more new selective targeted therapies with lower cytotoxic profiles.

Targeted therapy in use for HGSOC

Since Hanahan and Weinberg's landmark definition of the biological characteristics which enable tumour growth and metastatic dissemination as the 'hallmarks of cancer', in addition to a repertoire of recruited, apparently normal cells that contribute to the acquisition of hallmark traits by creating the "tumor microenvironment", there have been increased efforts to identify a more selective treatment approach and therapeutic target identification (Fig. 5) (89, 90).

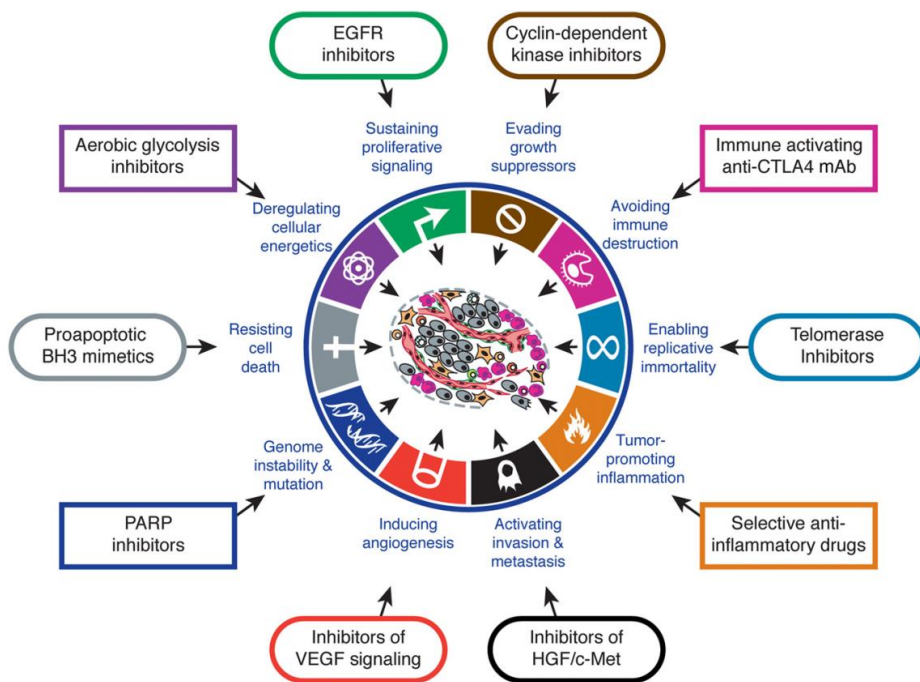


Figure 5. Therapeutic targeting of the hallmarks of cancer (image adapted from Hanahan and Weinberg (89)).

Only drugs targeting the two hallmarks, angiogenesis (the VEGF-inhibitor bevacizumab) and genomic instability (the PARPi – olaparib, niraparib, rucaparib), are approved by the Food and Drug Administration (FDA) and/or the European Medicines Agency (EMA) for treating patients with EOC.

Inhibition of angiogenesis

Very often hypoxia-driven proangiogenic pathways are activated in HGSOE, with increased production of VEGF and other proangiogenic factors which promote formation of new blood vessels. Tumour angiogenesis is induced early in the process of tumour progression. The activated angiogenic switch then leads to neovascularisation, often giving rise to leaky vessels which provides access for the tumor cells to penetrate and metastasize to other parts of the body apart from supplying nutrients and oxygen to the tumours. This results in deprived tumour perfusion, reduced drug diffusion and the formation of effusions (89). Given the central importance of angiogenesis to the development of ovarian cancer, it was natural that this biological system was chosen as the point of attack for more targeted treatment of this disease (91).

Bevacizumab (a humanised monoclonal antibody) was the first EMA-approved angiogenesis inhibitor (2011) for high-risk patients (Stage IIIC–IV) in frontline settings (GOG218 and ICON7); a year later it was approved for recurrent, platinum-sensitive disease (GOG213 and OCEANS) (79, 83, 84, 92). It was also specifically assessed in combination with weekly paclitaxel in recurrent platinum-resistant disease and was shown to have improved PFS but without prolonged OS (AURELIA) (86). As mentioned above, the use of bevacizumab in advanced-stage high-risk patients in the frontline setting and recurrent disease with large volumes of ascites and/or pleural effusions is the standard treatment in many countries, including Norway, due to its improvement of PFS and patients' QoL (56, 79, 86). Despite these advantages, both the FDA and the EMA have approved the use of bevacizumab only once, either in the frontline or the recurrent setting. Based on the data from GOG218 trial, CD31 is suggested to be a predictive biomarker for bevacizumab therapy response (58, 93).

Interestingly, high concentrations of CD31+ vessels show a positive association with increased tumour infiltration of effector T cells (94). Several other anti-angiogenic agents, including thrombospondin, receptor tyrosine kinases (cediranib, pazopanib, nintedanib and angiopoietin) and trebananib have been developed and studied but have not shown relevant clinical efficacy (95-97).

PARPi

Approximately 50% of HGSOc patients have underlying HRR deficiencies. HRR deficiencies mainly arise following somatic or germline mutations in BRCA1 and BRCA2 genes, which are involved in maintenance of genomic stability and DNA damage repair (98). Loss of heterozygosity (LOH) due to *BRCA1* hypermethylation and functional loss or gain of other genes (*RAD51C*, *RAD51D*, *BRIP1*, *PTEN*, *ATM* and *ATR*) involved in HRR are also reasons for HRR defects (99, 100). The proteins PARP1 and PARP2 are involved in single-strand breaks (SSB), which help to avoid double-strand breaks (DSB) during DNA replication. Inhibition of PARP1 leads to SSB repair failure, which in and of itself does not affect DSB repair; however, repeated SSBs have been shown to collapse replication forks, resulting in DSBs. Hence, if both PARP1 and BRCA proteins are deficient in the same cell, this combined effect results in chromosomal instability and even death, also known as ‘synthetic lethality’ (101). This favourable prognostic genomic instability is the foundation of the effectiveness of PARPi. PARP1 is the best-characterised PARP protein: Basically, PARPi traps PARP1, making HRR-deficient cells accumulate SSBs, which collapses replication forks, as mentioned above, resulting in DSBs and finally cell apoptosis. This ability to ‘trap’ the PARP-DNA complex explains the different magnitudes of cytotoxicity exerted by the PARPi; of the five PARPi to date, talazoparib appears to be the most potent PARP trapper studied so far, although it is still not approved by either the FDA or the EMA for clinical use (102).

Due to the exceptional effects shown in studies, both in the frontline and the recurrent setting in platinum-sensitive disease, in the last few years the EMA and the FDA have approved the use of many different PARP inhibitors. Olaparib was the first EMA- and

FDA-approved PARP-inhibitor for newly diagnosed EOC in BRCA mutation patients with advanced disease as maintenance therapy after finishing chemotherapy, based on the results from SOLO-1 (57). Different PARPis (olaparib, niraparib and rucaparib) have been approved to treat recurrent platinum-sensitive disease, based on data from promising studies (the SOLO-2, NOVA and ARIEL3 studies, respectively) (85, 88, 103), and today more and more countries are allowing use of PARPi for the whole patient population with platinum-sensitive disease. In most studies, the gain in PFS for BRCA mutation patients, the gain in PFS for HRD patients and the gain in PFS for wild-type are comparable, but the drugs differ in their panels of side effects. Data from trials combining targeted therapies like the AVANOVA (bevacizumab + niraparib) and ICON9 (cediranib + olaparib) trials were encouraging, (104, 105). It is the hope that the increased in the platinum-free intervals will avoid development of platinum resistance in platinum-sensitive relapsed disease. More studies examining effects in patients for whom platinum is not an option are however necessary.

The DNA damage response (DDR) constitutes a network of proteins which coordinate the cell-cycle progression with DNA repair to avoid DNA damage being passed permanently to daughter cells (106). Apart from ataxia-telangiectasia mutated (ATM), ATM- & Rad3-related (ATR) and DNA-dependent protein kinase catalytic subunit kinases (DNA-PKcs), are the key proteins that signal DNA damage to DNA repair pathways and cell-cycle checkpoints. There are around 450 genes coding for proteins involved in DDR (107-111). Currently, in addition to PARPi, the improvement in our understanding of DDR biology is enabling the exploitation of more DDR-targeting molecules (112).

However, the microenvironment of the tumour cells, which is genetically more stable than the tumour cells themselves, is attractive as a point of attack for therapeutic intervention and is gaining momentum (see Section 1.1.5), which will allow more cancer hallmarks to be targeted (Fig. 5).

1.1.6 Biomarkers

The Biomarkers Definitions Working Group defines a biomarker as ‘a characteristic that is objectively measured and evaluated as an indicator of normal biological processes, pathogenic processes, or pharmacologic responses to a therapeutic intervention’ (113). As mentioned earlier, the hallmarks of cancer not only aid in understanding the complexity of the tumours but also give meaningful insights into identifying such characteristic biomarkers of the disease (89, 90). Biomarkers play a vital role in the diagnosis, prognosis and predictiveness of EOC. CA125, p53 and HE4 are used as diagnostic biomarkers, respectively, to identify and assess the disease and its progression in EOC (114). Of the several predictive biomarkers, such as BRCAness, platinum sensitivity (response to PARPi) (100, 115), absence of CCNE1 amplification, immune status and age (chemotherapy response) (116), tumour T-cell infiltration, mutational burden and PD-L1 expression (117, 118), only a few are used in clinical settings. Prognostic biomarkers such as FIGO stage, tumour grade, degree of debulking surgery, performance status, and BRCA1/2 mutational status help avoiding overtreatment in patients. In addition to germline BRCA status, mutational signatures, including alterations in *CHEK1/2*, *PALB2*, *RAD51C* and other genes in the HRR pathway, have also proven to be sensitive biomarkers to PARPi (100, 115). The future awaits more defined panels of tumour biomarkers, including individualised molecular tumour profiling using techniques such as CyTOF and liquid biopsies with blood-borne cancer-related cell-free DNA and/or tumour-associated proteins as well as circulating tumour cells (CTC).

1.2 Tumour microenvironment (TME)

Current investigations of the 10 different traits which together comprise the hallmarks of cancer have demonstrated compelling evidence that these functional traits gained by the tumour cells (tumour cells, cancer stem cells) involve other cellular (mesothelial cells, adipocytes, stromal cells such as cancer-associated fibroblasts, pericytes, endothelial cells and immune cells) and non-cellular components (extracellular matrix components, growth factors, chemokines and cytokines) of their immediate

surroundings termed as the tumour microenvironment (TME) (Fig. 6) (89). Within this milieu, tumour-driven stimuli prompt cells to reprogram themselves into tumour-supporting phenotypes, thereby creating a tumour-permissive environment; this plays a pivotal role in tumour formation and the progression and regulation of ascites production (119). Though, there is an ongoing discussion if tumor cells themselves are part of the TME, we have considered to include them as well.

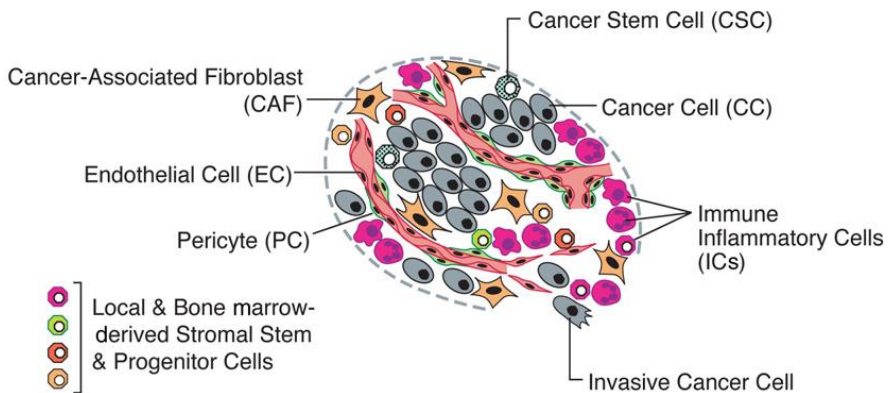


Figure 6. The tumour microenvironment (image adapted from Hanahan & Weinberg (89))

Similar to other solid tumours, there is an escalating appreciation of the critical role that TME plays in promoting and sustaining HGSOc growth, response to therapies, chemoresistance, recurrence and metastasis (2, 5, 120). Characteristics such as intra-abdominal localisation, metastatic tropism, cellular plasticity, presence of a cancer stem cell niche (for further details, see Section 1.2.2) and genetic instability (see Section 1.1.2), govern the interplay between the different cellular compartments in the TME, which facilitates the inter- and intratumour molecular and phenotypic heterogeneity that characterise HGSOc (13, 28, 120-125). Signalling within the TME is achieved through cell-to-cell contact or the release of soluble factors such as cytokines and exosomes (120).

1.2.1 Constituents of the HGSOC TME

HGSOC spreads primarily by transcoelomic dissemination through direct migration of ovarian cancer cells to the peritoneal cavity and omentum via the peritoneal fluid (126). However, recent studies indicate that the hematogenous route may also play a role (127). The disease remains confined most often to the abdominal cavity. Together, this results in an intra-abdominal milieu consisting of both the primary tumour, peritoneal implants, omental metastasis and ascitic fluid (a non-solid component). Cancer progression is majorly driven by this intra-abdominal tumour environment rather than the properties of the tumour itself and contributes predominantly to prognosis (128).

Cellular decomposition of the HGSOC TME

Ovarian TME comprises three major cellular compartments: (1) tumour cells (cancer cells, cancer stem cells); (2) stromal cells (cancer-associated fibroblasts, pericytes, endothelial cells); and (3) immune cells (T cells, MDSCs, dendritic cells, TAMs) and other non-cellular components (extracellular matrix components, growth factors, cytokines and chemokines) (Fig. 7). The different constituents have characteristic as well as overlapping functions (129).

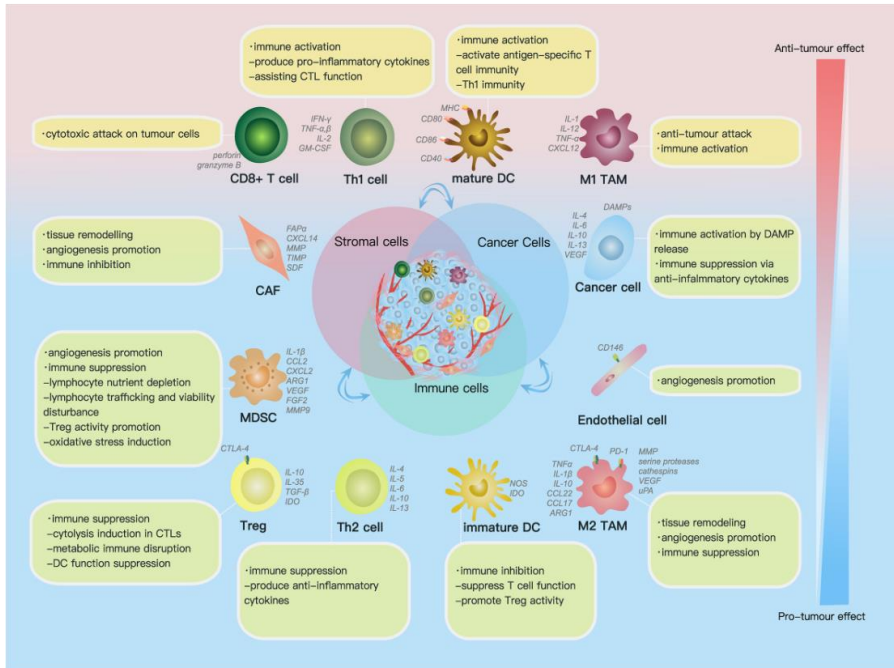


Figure 7. Ovarian TME components and its characteristic functions (image adapted from Yang et al. (129)).

1. Tumour cell compartment

(a). Cancer cells

HGSOC cancer cells lack genomic stability due to the presence of *TP53* mutation, along with HRD in 50% tumours (see Section 1.1.2) (4, 26). It is the *TP53* mutation that allows cancer cells to tolerate DNA repair deficiencies, copy number abnormalities and multiple large chromosomal structural variants without undergoing cell cycle arrest or apoptosis (130). The inherent plasticity of tumour cells which allow them to switch between epithelial and mesenchymal characteristics, combined with the unstable genetic status, as mentioned above, creates an overwhelming intra-tumoral heterogeneity which represents a distinct therapeutic challenge. The proinflammatory microenvironment not only helps these tumour cells to transform upon MET and further disseminate to form a primary tumour in the ovarian site, but also promotes

metastasis through EMT transition, along with the production of ascitic fluid and the development of chemoresistance (28, 120). Known cell surface markers expressed on the ovarian cancer cells include EpCAM, TAG72 and FOLR1 (131-133).

(b). Cancer stem cells

HGSOC is a stem cell-driven tumour type (134). However, the exact cell of origin remains elusive (135). It is widely believed that cancer cells and cancer stem cells (CSCs) maintain a dynamic equilibrium regulated by a cascade of signalling pathways which, when disturbed, facilitate the cancer cells gaining stem-like properties (136). CSCs are highly plastic, flexible and dynamic, with the ability to self-renew and differentiate into various cell types based on the cues of the TME. CSCs are potentially able to develop into an entire tumour from a single cell. These CSCs hold increased capacity to resist unfavourable biological conditions such as a low proliferation rate, upregulation of efflux pumps and detoxifying enzymes (134). Emerging evidence suggests that CSCs are responsible for tumour recurrence and drug-resistance (134, 136, 137).

According to the more recent described cellular plasticity model, tumour cells can switch between stem-cell like and differentiated states so that some differentiated non-tumorigenic malignant cells can dedifferentiate into CSCs (also mentioned in section 1.2.2 – The ovarian cancer stem cell niche) (138, 139). Considerable effort has been made to define and characterise these cells, as reviewed by Hatina et al. and Chaffer & Weinberg (134, 139). Known cell surface markers expressed on tumour-initiating cancer stem cells (CSCs) include CD44, CD133, CD24, CD144, CD117, EpCAM and ALDH1A1 (137).

CD44⁺ cells possess a distinctive genetic profile in relation to chemoresistance and tumorigenicity and are actively involved in NFκB activity, with the potential to promote a pro-inflammatory TME (140). CD133⁺ cells show higher tumorigenic capacity and increased chemoresistance. Through multiple signalling pathways, CD133 can also modulate the stemness and metastatic potential of a tumour (141, 142). Beyond being a putative CSC marker, CD24 is also associated with cell adhesion,

mediating attachment of tumour cells to fibronectin or collagen during metastatic dissemination (71, 143). CD24 has the ability to induce EMT via PI3K/AKT and MAPK pathways, supporting the possibility that it is a significant metastatic progression marker for poor clinical outcome (144, 145).

CD117⁺ cells have self-renewal and differentiation capacity with high heterogeneity (146); they also promote chemoresistance and exhibit tumour-initiation through Wnt/ β -catenin-ATP-binding cassette G2 signalling (147). From a clinical perspective, high expression of CD117⁺ is correlated with poor PFS rate and possible peritoneal metastasis (148, 149). ALDH⁺ cells exhibit a functioning role in mediating drug resistance with improved DNA repair and increased drug efflux transporters (150, 151). Clinically, a higher percentage of ALDH⁺ cells is associated with poor outcomes (152), so a comprehensive approach to elucidate the complete spectrum of ovarian CSCs and its heterogeneity would be a way forward—an achievement which is potentially around the corner, given the recent advances in single-cell protein measurements (153).

2. Stromal cell compartment

(a). Endothelial cells

Endothelial cells are cells lining blood and lymphatic vessels, representing the interspace for transendothelial migration of inflammatory cells into the surrounding tissue. They are known to express CD34, CD31 (also a predictive biomarker for bevacizumab therapy response), CD105 and CD146 (154-158), and can also function as semi-professional antigen presenting cells (154-158). Blood vessels play a crucial role in oxygen and nutrient supply (155). Angiogenesis is a complicated process involving angiogenic activators such as VEGF, PDGF, FGF-2, TGF α and TGF β , TNF α , interleukin 8 (IL-8) and prostaglandin E2, along with angiogenic inhibitors such as angiopoietin (Angs), thrombospondin 1 (TSP-1), and endostatin (159, 160). Angiogenesis in tumours is a dysregulated process; the vessels are structurally abnormal with junctional defects, tortuous, dilated, hyperpermeable and poorly covered by surrounding cells with blood flow patchy perfusion (89, 155). Expression of VEGF indicates poor clinical outcomes; on the other hand, enhanced Angs

expression is associated with increased relapse and decreased survival rates (161-164). Multiple studies have as mentioned been undertaken targeting angiogenesis. High endothelial venules, together with recruited inflammatory cells from circulation, form the immune aggregates which support an adaptive anti-tumour immune response (129).

(b). Cancer-associated fibroblasts

Fibroblasts within the tumour milieu are known as cancer-associated fibroblasts (CAFs) and hold the ability to transdifferentiate from other cell types such as pericytes, epithelial cells and endothelial cells through exposure to VEGF, PDGF, TGF- β , ROS and MMPs (165-167). CAFs express FAP α and there are several subtypes of CAFs which perform multiple roles in the TME. CAFs can enhance tumour progression with high expression of CXCL14, an important tumour-growth-promoting factor (168). They are also responsible for ECM growth and remodelling, which contributes to desmoplasia and stromal stiffness, factors associated with poor prognosis (169-172). CAFs promote immune inhibition and angiogenesis. Givel et al. found that CAFs increase regulatory T cells' (Tregs) infiltration of the tumour site, thus exerting a tumour suppression effect in the TME (172). They also accelerate recurrence and increase platinum resistance (171). On the whole, CAF and EMT contribute to the invasive and metastatic abilities of HGSOV and are associated with poor prognosis (171, 172).

(c). Pericytes

Pericytes are contractile cells lining microvessels and are known to express α SMA (173). Major functions include regulation of endothelial cell proliferation, differentiation and microvascular permeability through paracrine regulators such as vasoactive agents and TGF- β (173, 174). Pericytes may play a potent pro-tumorigenic/pro-metastatic role in ovarian cancer progression and are associated with highly predictive relapse and mortality (175).

(d). Adipocytes and mesothelial cells

A monolayer of mesothelial cells lining the peritoneum acts as a barrier and maintains peritoneal homeostasis, possessing characteristics of both epithelial and mesenchymal cells (176). Various factors such as fibronectin, ICAM-1, angiogenic and inflammatory mediators secreted into the ovarian TME by mesothelial cells enhance tissue stiffness and cellular adhesion (176, 177). The literature says, 86% of reactive mesothelial cells express N-cadherin and 93% of mesothelial cells express calretinin (178). On the other hand, the omentum is comprised mostly of adipocytes, which can alter lipid metabolism, thus increasing the fuel source for the rapid growth of ovarian tumour cells (for more details please refer to paragraph 1.2.2). In addition, senescent mesothelial cells promote invasion and migration by inducing production of angiogenic factors by ovarian tumour cells, whereas adipocytes foster metastasis via cytokine production (177, 179).

3. Immune cell compartment

(a). Tumour-associated macrophages (TAMs)

Macrophages residing within the tumours are known as 'TAMs' and are the most abundant cell population present in tumour tissues (180). They can be divided prominently into anti-tumour M1 macrophages (CD86 and TNF α) and pro-tumour M2 macrophages (CD163, CD204, CD206) (Fig. 7) (181-185). In EOC, TAMs express a predominantly M2 phenotype and are actively associated with tumour invasion, metastasis, angiogenesis and early recurrence (186-188). Firstly, by producing the chemokine CCL22, M2 macrophages can accelerate the immunosuppression of Treg cell transport to tumours and inhibit the proliferation of T cells (189). Secondly, they express the ligand receptors for PD-1 and CTLA-4 which, upon activation, regulate the cell cycle of T cells and inhibit its cytotoxic function (190). They can also inhibit the activation of T cells via the depletion of L-arginine (191). Apart from immune suppression, M2 macrophages are also involved in tissue repair, angiogenesis and ECM remodelling (192-196). They can reconstruct, regulate and degrade ECM and its components by secreting MMPs, cathepsins and serine proteases, which might aid

cancer cell migration, invasion and metastasis (194). A subtype of M2 macrophages which express TIE2, are known as TIE2 macrophages and recruited by CCL3, CCL5, CCL8 and TIE2-ligand Ang2: They are considered the most important factor in tumour vascularisation, because a deficiency of this phenotype leads to the restriction of the angiogenic switch (197, 198). TAMs have high plasticity and the simple dichotomy phenotyping of M1/M2 macrophages alone cannot explain the complexity of the TAM heterogeneity (199). In addition to inter-tumoral heterogeneity, recent studies have detailed the intra-tumoral heterogeneity of TAMs, wherein different microregions within the same tumour show varied levels of TAM infiltration, along with differential functional status in tumour progression level-dependant manner (200-205). Several ovarian studies have revealed that M1/M2 and M2/TAM ratio are positively associated with PFS and OS, although the overall TAM density has been shown to have no prognostic significance (200, 206, 207).

(b). Granulocytes

Neutrophils are a heterogenous group of cells majorly expressing CD66b, CD11b and CD16. They are majorly classified into two main functional groups, namely, antitumor (N1) and protumor (N2) subtypes (208). Neutrophils have a prime role in the TME, towards tumor initiation through alteration of extracellular matrix via secretion of certain molecules such as MMP-9 (209). In addition, they exhibit antitumor activity either by direct killing of tumor cells or through T-cell recruitment. In a recent EOC study, high neutrophil-to-lymphocyte ratio was associated with poor overall survival in some group of patients (210).

Granulocytes encompasses the eosinophils, basophils and neutrophils. The role of granulocytes within the ovarian TME is not yet fully understood. Basophils influence several cell subsets including fibroblasts, monocytes, macrophages, T and B lymphocytes (211). Besides they indirectly effect the tumor growth with the production of VEGF-A (212). In general, EOC patients have elevated levels of basophils in their ascites compared to their blood level (213). Eosinophils on the other hand, are commonly seen in the TME, and are known to be associated with either poor or better

prognosis as presented in various cancer types (214). They promote T-cell proliferation, DC maturation and furthermore, regulate other granulocyte subsets in addition to mast cells (215, 216).

(c). Dendritic cells

There are two types of dendritic cells (DCs – CD11c⁺HLA-DR⁺). Conventional DCs (cDCs – CD1c⁺ or CD141⁺) which are involved in presenting antigens to CD4⁺ and CD8⁺ T cells via MHC II and MHC I respectively, which subsequently initiate series of T cell activities. Plasmacytoid DCs (pDCs – CD123⁺) produce IFN γ upon antigen stimulation, in addition to activation of lymphocytes and other myeloid cells (217, 218). Apart from T cell activation, DCs play a crucial role in the augmentation of cytotoxic T cells (CD8⁺) in the TME. Upon antigen exposure, DCs mature, characterised by elevated levels of MHC membrane expression and co-stimulatory molecules (CD86, CD80, CD40) (219, 220). Immune modulating molecules in the TME such as IL-6, IL-10, and VEGF, tumour-derived soluble mediators and exosomes might cause DC dysfunction, leading to inhibition of DC maturation (221-223). Immature tolerogenic DCs promote immune tolerance and suppress anti-tumour immunity via several mechanisms, some of which include low-level production of pro-inflammatory cytokines and high levels of immune suppressive cytokines. They also harbour enzymes which negatively influence T cell effector functions, such as nitric oxide synthase (NOS) and IDO, which promote Treg differentiation, tumour angiogenesis and metastasis (224-227). Various studies have concluded that DCs are highly plastic, contributing to either anti-tumour or pro-tumour effects. They are functionally influenced by multiple factors, such as their location and interactions within the tumour, the percentage of tumour-to-stroma ratio and the developmental stage of the tumour (217, 228-230).

(d). Myeloid-derived suppressor cells

Myeloid-derived suppressor cells (MDSCs) co-express myeloid markers GR-1, CD33 and CD11b and are of three phenotypes: PMN-MDSCs, M-MDSCs and a small group of progenitors and precursor cells involved in myeloid colony-forming activity (231,

232). Studies have confirmed that MDSCs promote tumour progression via various mechanisms, including the inhibition of immune cells (mainly T cells). MDSCs are involved in immune suppression via the following mechanisms: (1) acceleration of lymphocyte nutrient depletion; (2) disturbance of lymphocyte viability and trafficking; (3) promotion of Treg activation and expansion; and (4) stimulation to generate oxidative stress (232-237). Apart from immune suppression, MDSCs facilitate neovascularisation through hypoxia and activation of the STAT3 pathway, leading to secretion of factors which in turn stimulate invasion and metastasis by the production of MMPs (238, 239). Though the mechanisms are yet to be clarified, MDSCs exhibit differential functions and varied differentiation states based on the cues of its surrounding TME.

(e). Lymphocytes

Lymphocytes are an important part of the TME, comprising T helper cells ($CD3^+CD4^+$) – Th1 cells (antitumorigenic) and Th2 cells (protumorigenic), cytotoxic T cells ($CD3^+CD4^+CD8^+$) and regulatory T cells ($CD4^+CD25^+Foxp3^+$), NK T cells ($CD3^+CD56^+CD1d^+$) and B cells ($CD20^+$) (240, 241). Upon antigen encounter, naïve T cells are activated and differentiate into specific subtypes based on the cytokine environment: Cytotoxic T cells produce cell lytic molecules such as granzymes, perforin and inflammatory cytokines to destroy pathogen-infected or malignant cells (242-244).

Multiple studies have reported that $CD8^+$ T cell infiltration is linked to increased PFS and OS and disease-specific survival, with the location of the TILs within the tumour being important for this prognostic effect (245-252). CD103 has now become a definite marker for antigen-encountered tissue resident T cells (253). PD-1 and LAG-3 are co-expressed on exhausted T cells, and there is compelling evidence that these checkpoint inhibitors are highly expressed in tissue-resident ($CD103^+CD8^+$) cytotoxic T cells, making them first targets for anti-PD-1 therapy (254, 255). In contrast, Tregs play a crucial role in immune suppression via four mechanisms: (1) secretion of immunosuppressive molecules, including VEGF, IL-10, IL-35 and TGF- β ; (2) Tregs

induce apoptosis of effector T cells with secretion of perforin and granzyme B; (3) Tregs regulate metabolic disruption through multiple mechanisms; and (4) modulation of dendritic cell function and maturation (256, 257). Treg cell infiltration was linked to decreased survival and a high death hazard, also supported by our own previous paper, highlighting the presence and accumulation of activated regulatory T cells in the ovarian TME (258).

B lymphocytes promote tumour progression by regulating the Th1:Th2 ratio and producing protumorigenic cytokines. High expressions of CD20 and CD138 are associated with advanced tumour grade in ovarian patients (259). Regulatory B cells, known to express CD80 and CD86, contribute to immune suppression via IL-10 production, which suppresses IFN γ production of cytotoxic T cells (260). On the other hand, effector B cells present antigens and promote T-cell responses (261). NK cells have multiple functions as they kill targets and trigger inflammation through antigen-independent pathways (262-264). Although the presence of NK cells alone have contrasting prognostic values in EOC, their co-infiltration with cytotoxic CD8⁺ T cells show a strong association with patient survival (253, 265). Jiménez-Sánchez et al recently demonstrated increased NK cell infiltration and expansion of T-cells following neoadjuvant chemotherapy (266). NKT cells share characteristics of both the innate and adaptive arms of the immune system, and are known to express CD161. These cells are substantially present in the thymus, liver, spleen and bone marrow, compared to peripheral blood (267). NK T cells are unlike common NK cells in that they recognise glycolipid antigens and are thus important mediators of antitumour immune responses (268).

Correlation of T lymphocytes and clinical outcomes has long been studied, since Zhang et al. identified a positive association between T-cell infiltration and survival rate (269). Based on the degree of immune infiltration in tumours, primarily based on CD3 and CD8 T cell populations, tumours could be classified in an immune-based context as 'hot' (highly infiltrated), 'altered – immunosuppressed and excluded' (intermediate infiltration) and 'cold' (non-infiltrated) tumours (246, 270). For many tumours, PD-L1 expression (>1%) is an important parameter for response or indicator of immune

checkpoint blockade treatment (271). However, this has not been the case for EOC (JAVELIN trial (272) and IMagyn050/GOG 3015 / ENGOT-0V39 trial (273)). The roles of tumour microsatellite instability have not yet been systematically examined. Still the professional communities, illustrated by the number of ongoing studies, consider EOC as a potential candidate for checkpoint blockade therapy despite its low success rate. The focus is however changing to combination regimens, including both angiogenesis inhibition and / or PARP inhibition (ATENA, Ov-43, FIRST, JAVELIN100 PARP and DUO-O). The biological rationale is clear: Anti-angiogenesis enhances HR deficiency and makes cells more susceptible to PARP inhibition as well as modifying the immunophenotype, while DNA-damaging agents have the potential to enhance the response to immunotherapy by promoting neoantigen release, increase the tumor mutational burden and enhance PD-L1 expression (274).

4. Non-cellular components of the ovarian TME

The extracellular matrix (ECM) is comprised of several biochemically distinct components, including proteins, polysaccharides, proteoglycans and glycoproteins with different biochemical and physical properties (275). Abnormal changes in the composition and amount of ECM significantly alter these properties with malignant transformation, potentiating oncogenic effects on several growth factor signalling pathways (178, 276). For instance, when collagen deposition increases, there is a positive regulation of integrin signalling, thereby promoting cell proliferation and survival (277). Low pH and hypoxia naturally associate TME with the Warburg effect, whereby tumour cells sustain a high rate of aerobic glycolysis. Downregulation of E-cadherin and positive regulation of TWIST1 and β -catenin also facilitates metastatic dissemination via basement membrane with access to neovasculature (276, 278). Several other molecules have also been identified in EOC stroma, such as MMPs, cytokines (the respective roles of which are explained under different cell subtypes above), and hyaluronic acid (279-282). Apart from direct remodelling of the ECM, inflammation associated with EOC also promotes a desmoplastic stromal response (283). There is also significant consensus that endometriosis-associated inflammation and fibrosis in the peritoneum and ovaries increase the risk of EOC (284).

1.2.2 The uniqueness and plasticity of HGSOE TME

In addition, to the two main conventional models (stochastic or hierarchical model) proposed to explain the intra-tumoral heterogeneity of cell subsets, a third model named the plasticity model is conceptualized to present a more flexible understanding of the tumoral stem cell niche (285).

The ovarian cancer stem cell niche

There is available evidence to support the hypothesis that the stem cell niche of ovarian CSCs plays an important role in initiation of the tumour, involving only a few tumour-initiating cells (CSCs) (123). The presence of a cancer-prone stem cell niche in the mesothelium and the oviductal epithelium supports the idea that the fallopian tube epithelium could play a vital role in maintaining the cancer stem cell niche (134, 286-290). So far little is known about the niche in non-metastatic lesions. Though CSCs comprise only a very small proportion of primary tumours, they are enriched in recurrent tumours and are especially chemoresistant, proving their inherent ability to expand even under unfavourable biological conditions (134, 291-293). CSCs are highly dynamic, heterogenous and influenced based on the cues of the surrounding pro-inflammatory ovarian TME (28).

The interaction of the stem cell niche and surrounding TME is known to be bidirectional, as it allows the ovarian CSCs to maintain the stemness of its niche as well while also supporting tumour progression by differentiating the CSCs to other cell types as needed by the TME (294-298). To mediate the self-renewal of the ovarian CSCs, T cells and M2 macrophages secrete IL-17 (299). CAFs influence the self-renewing capacity of ovarian CSCs through FGF, VEGF and IGF secretion (300-302). Other vital cues for tumorigenesis include the production of IL-6 by adipocytes and TGF- β by mesenchymal stem cells (303). Ovarian CSCs CD133⁺ induces its own self-renewal by autocrine activation of IL-23 secretion, whereas CD44⁺ CSCs induces its own differentiation to endothelial cells by CCL5 secretion. Ovarian CSCs initiates differentiation of monocytes to M2 macrophages and initiates tumorigenesis by

secreting CCL5 (CD133⁺) and extracellular vesicles (EVs) (304, 305). The role of microRNAs and EVs in gene regulation and cell communication between ovarian CSC niche and tumour stroma from ongoing studies ensures its important role in the self-renewal of ovarian CSCs (123).

Organoid technology has already been explored as a promising platform for modelling tumorigenesis (306-308). Controlled growth conditions of 3D organoids has greatly benefited our understanding of the crosstalk between a stem cell niche and its factors in regulating stem cell lineage selection and differentiation (309). Eradication of CSCs is increasingly seen to be a potential therapeutic avenue for improving survival rates in EOC patients. Even though CSCs are currently being identified and isolated with several phenotypic markers, their functional and phenotypic heterogeneity needs further dissection to understand their complexity the at intra-tumour level and to eradicate them effectively (310).

Ovarian TME plasticity with disease progression

As Stephan Paget proposed in his ‘seed and soil hypothesis’, the primary tumour and the metastatic pattern of spread is not random; rather, it is an interplay between the ‘seed’ (specific cancer cells) and the ‘soil’ (particular organ microenvironments) (127). Therefore, the crosstalk between the cancer cells and the surrounding TME forms the primary tumour; the dynamic interaction of the stromal cells with the tumour cells within the orchestrated TME via paracrine signalling networks has the ability to promote progression of not only the primary tumour but also the metastasis (28, 129, 294-298).

In general, cancer TME is in many ways consistent with TME formed during normal wound-healing processes but resemble wounds which fail to heal, creating a state of chronic inflammation without any self-limitations or regulations. A similar chronic inflammatory microenvironment is created in ovarian cancer during the ovulation process by repeated secretion of ROS, chemokines, growth factors and cytokines by the ovaries and recruited immune cells (Fig. 8) (14). The cellular and non-cellular components of the inflammatory TME, along with the prevailing cancer stem cell

niche, potentiates the initiation of EOC from a minor fraction of tumour-initiating CSCs featuring characteristics of both epithelial and mesenchymal stem cells (123, 310). During tumour initiation, the critical epithelial marker Pax2 (paired box 2) is repressed in oviductal cells, followed by SCOUTs and finally STIC formation (detailed pathogenesis presented in Section 1.1.2). This whole process is orchestrated by EMT (311-314).

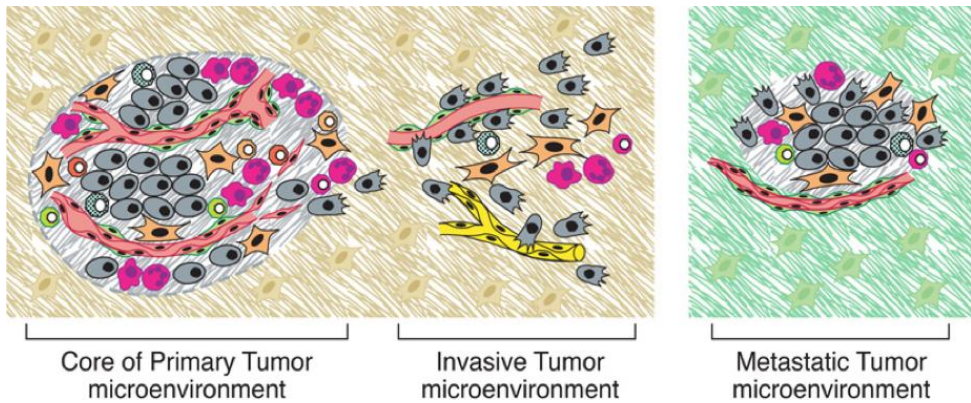


Figure 8. Changes within the TME upon tumour progression (image adapted from Hanahan & Weinberg (89))

Generally speaking, cellular plasticity is the ability of cells to differentiate into a new cell phenotype with other identical characteristics. ‘Cadherin switching’ induces the epithelial cells to undergo EMT, lose E-cadherin-mediated cell-cell interactions and upregulate other cadherins, such as N-cadherin and P-cadherin (19, 315, 316). These cells then gain a more invasive phenotype resembling fibroblasts and proliferate (Fig. 8) (89). The EMT switch allows these tumour cells to survive under crowded hypoxic conditions and to interact with neighbouring stromal cells through mesenchymal signalling. Induction of matrix metalloproteinase (MMP) -9 cleaves the ectodomain of E-cadherin, which loosens the cell-cell adhesion and allows the cells to shed as spheroids or single cells into ascites (22, 23, 317). Proteolytic activity also plays an important role in the initial detachment of the spheroids from the ovarian surface. Secretion of VEGF by EOC cells increases vascular permeability and promotes ascites formation. Malignant ascitic fluid is rich in CSCs, extracellular vesicles, tumour-

promoting soluble factors, cancer-associated immune cells such as T-cells and TAMs, CAFs, myeloid cells and activating mesothelial cells, creating a tumour-promoting microenvironment (317). As mentioned above in Section 1.1.2, ascites is considered a prerequisite for the characteristic ovarian transcoelomic dissemination of primary tumour cells or cell aggregates to the omentum and peritoneum (318).

Before homing to the peritoneum and omentum, the disseminated tumour cells or cell clusters interact primarily with the mesothelial cells covering the basement membrane. The core of the spheroids maintains a mesenchymal phenotype, expressing Sip1, a well-known regulator of E-cadherin and MMP-2. E-cadherin loss leads to transcriptional up-regulation of $\alpha_5\beta_1$ -integrin, receptor of fibronectin, facilitating the adhesion of these cell aggregates to the secondary site. MMP-2 potentiates the fast disaggregation of spheroids on adhesion to mesothelial surface layer (319, 320). The binding of tumour cells is not only coordinated by integrins but also by CD44 (321-324). The omentum, the large fat pad covering the bowel and abdominal cavities, is the preferred site of metastasis in ovarian cancer and represents a central player in creating a unique suitable metastatic niche in the intraperitoneal cavity (325). Successful colonisation of the micro- and macro-metastatic tumour requires the shedding of mesenchymal properties (partially/completely) via MET (Fig. 8) (326-329). Apart from the characteristic transcoelomic spread, tumour cells preferentially home to 'milky spots' in the omentum through haematogenous dissemination, prior to spreading into the 'non-milky spot' areas of the omentum and peritoneal cavity. These milky spots are often highly vascularised regions with aggregates of immune cells and are major reservoirs of intraperitoneal macrophages (330-334).

The omentum harbours a variety of stromal cells, including fibroblasts, myeloid cells, adipocytes and macrophages, which, when malignant tumour cells start to grow, are converted into distinct cancer-associated stromal cells by cancer-derived mediators (294, 335). Ovarian cancer cells polarise TAMs into M2 phenotype, which are involved in the establishment of inflammatory and immunosuppressive TME (336, 337). Omental adipocytes produce chemokines and cytokines such as IL-6, IL-8, MCP-1 and adiponectin, which promotes tumour growth and omental metastases (186). They also

activate p38 and STAT3 pathways in order to create an ideal TME for sustained ovarian cancer cell growth (338). Normal cells rely on the tricarboxylic acid (TCA) cycle and oxidative phosphorylation (OXPHOS) as their major sources of energy. In contrast, tumour cells go on a glycolytic switch due to the Warburg effect, which is mainly promoted by oncogenes, to meet their enhanced energy requirements. Tumour cells adapt to lipid, amino acid, fatty acid (FA) and cholesterol metabolism to create macromolecules biosynthesis for anabolic processes. TME-induced metabolic reprogramming also results in increased OXPHOS with elevated glutamate and fatty acid production (121, 339-341).

1.2.3 HGSOC TME heterogeneity at the multiscale level and its clinical impact

Over the years many researchers have tried to characterise and understand the heterogeneity of HGSOC TME (see Section 1.3). Apart from various cell subtypes, cellular states and interactions, HGSOC is, as already mentioned, characterised by overwhelming inter- and intra-tumour molecular and phenotypic heterogeneity, which are governed by the presence of genetic instability (Section 1.1.2), a cancer stem cell niche and the cellular plasticity of the different cell types within the TME (explained in Sections 1.2.1–2) (28, 123, 129).

Landmark publications exemplifying the ovarian intertumor heterogeneity (between patients) include the TCGA study, which identified four prominent molecular tumour subtypes (immunoreactive, proliferative, differentiated and mesenchymal) based on promotor methylation, and concluded that the mesenchymal molecular subtype was associated with the worst OS and the immunoreactive subtype was positively associated with OS (25). Similar findings have been presented based on unsupervised hierarchically clustered gene expression data by Tothill et al. in 2008 (33). However, as mentioned below in Section 1.3.2, Geistlinger et al. recently concluded that the notion of individual subtypes does not realistically project the genomic complexity and heterogeneity observed in HGSOC, highlighting its ambiguity not just in bulk tumours but even at the cellular level. Instead, they specify that most HGSOC tumours are

polyclonal, where a single tumour consists of a heterogeneous group of distinct cancer genotypes arising from varied subclones. They also proposed a model based on their observations where the differentiated and proliferative subtypes are placed at opposite ends of the tumour development timeline. Subtype-associated DNA alterations tend to occur subclonally, merely attributing the higher ploidy and subclonality of the proliferative subtype tumours rather than supporting the existence of subclones with several well-defined subtypes (122).

The tumor milieu communicates important cues that induces inherent plasticity to the neighbouring cells which gives them the ability to differentiate in a tumour progression level-dependent manner. This feature, coupled with unstable genetic status, creates the overwhelming intratumoural heterogeneity and creates also a therapeutic challenge (28). For example, recent studies have shed light on the intratumour heterogeneity and the infiltrated T cell interactions (Section 1.2.1). One study, highlighted the presence of simultaneous tumour progression and metastases regression comprising T cell infiltration with oligoclonal expansion of certain subtypes (2). Tumours with high tumour heterogeneity increases the probability of selection of subclones which could escape the immune system known as immune cell exclusion. In addition, some cells within a tumour might display metastatic potential by acquiring additional mutations, evolving independently from the primary clone and adapting to the surrounding environment. This demonstrates that a single biopsy might not be representative of the entire tumour and that metastasis may harbour mutations which are not present in the initial tumour, and vice versa (2, 266). Therefore, better understanding of inter- and intra-tumoral phenotypic heterogeneity, along with the driving forces of TME heterogeneity accounting for such variations, are critical aims from basic and clinical perspectives. We hope the focus of this thesis will at least in part fulfil the aim of unravelling the complex heterogeneity of HGSOE to a new level of detail.

1.2.4 Targeting the ovarian TME

The anti-angiogenic agent bevacizumab is the only drug which targets the ovarian TME and has been approved in Europe for EOC (79, 83, 84, 92). Several ovarian TME-

targeting drugs are currently being tested in early phase trials as well as in randomised phase II and III studies (129). We can categorise these drugs into different major therapy groups, such as anti-angiogenesis therapy (342, 343), immunotherapy (adoptive cell transfer, or ACT), chimeric antigen receptor (CARs) cells, oncolytic virotherapies (OVs), DC-based vaccines (344), co-stimulatory mAbs (such as anti-CD137) (345), checkpoint inhibitors mAbs (anti-PDL1 and IDO inhibitors) (346-348) and CAF targeted therapy (349-351). Together with PARP inhibitors (57, 85, 88, 103) and drugs which target DNA repair and DNA damage responses (DDR) (352), TME-targeting drugs will be part of the backbone of future personalized therapy for EOC. This means that drugs which target hallmarks such as tumour-promoting inflammation, avoidance of immune destruction and invasion and metastasis formation (see Section 1.1.5 and Fig. 5) will be introduced.

1.3 Advancement of TME characterisation tools with emphasis on EOC

Given the better understanding of the complex composition of the ovarian cancer TME (see Section 1.2) achieved in recent years, it has become evident that the study of EOC tumours must encompass the dynamic interactions between the constituents of the TME to capture more aspects for successful clinical management of the disease (89). The study of HGSOC is even more complicated given the overwhelming tumour heterogeneity which can occur at different levels, intratumorally, between tumour lesions and across patients (intertumoral), along with the inherent plasticity of the cancer cells themselves (28). Characterisation techniques such as immunohistochemical staining, flow cytometry, ‘-omic’ techniques (genomics, proteomics, transcriptomics), and the newly emerging tools for single-cell profiling, such as single-cell RNA sequencing (scRNA-seq), mass cytometry by time-of-flight (CyTOF) and imaging mass cytometry, are playing a critical role in resolving the above-mentioned complexity, identifying predictive biomarkers and the selection of patients for successful individualised treatment of HGSOC.

1.3.1 Advances in single-cell protein measurements

For decades flow cytometry has been the preferred method of analysing high-throughput protein expression in single cells in ovarian cancer: Fluorescent dyes are used and the fluorescence emission is registered by photomultiplier tubes. This technique has thus been paramount in characterising cell phenotypes, revealing certain subsets which were not explored previously, detecting DNA and RNA content, cell cycle stage, activation of cellular pathways and even isolation of functionally distinct cell subsets to characterise of tumours (353).

Numerous flow cytometric ovarian studies have been carried out in the past decades, ranging from simple to complex multi-colour flow cytometric panels. Lee et al. developed a simple flow cytometric assay which used staining for γ H2AX and MRE11 as surrogate markers in PBMCs to predict the therapy response in ovarian patients for PARPi (354). In another study conducted by our own group, we utilised a complex multi-colour flow cytometry panel, demonstrating an accumulation of Tregs, CD4⁺ and CD8⁺ T cells in ascitic fluid from ovarian patients (258).

Although in general most studies use up to 10 parameters, recent developments in spectral flow cytometry have enabled simultaneous detection of up to 32 channels in one experiment with the ability to measure the full spectra of every cell which are not mixed by the autofluorescence spectrum or the reference spectra of the fluorescent dyes (355). However, designing multiparameter flow cytometry panels is a challenging and laborious task due to the broad emission spectra of the fluorescent dyes. In addition, the number of markers which could be simultaneously assayed was initially limited to around 14 markers, with most studies so far focusing on in-depth analysis of specific cellular lineages instead of a broader system-wide approach.

Nevertheless, with the advent of mass cytometry (CyTOF) in 2009, the limitation of spectral overlap was overcome by the introduction of metal-isotope-conjugated antibodies to detect antigens. The metal isotopes attached to each cell are distinctive by mass and are quantified by a quadrupole time-of-flight spectrometer. Theoretically, up to 100 parameters per cell can be ideally measured, but current chemical methods

limit its use up to 40–50 parameters per cell at one given time (153). Based on the scope of question and intent in study analysis specific computational tools could be selected. Aim of the study dictates parameters measured such as abundance, expression levels, cellular identity and population structure (356). Current single-cell computational tools available for extensive mass cytometry data analysis include: (1) unsupervised clustering-based algorithms such as Phenograph (357), SPADE (358) and FlowSOM (359); (2) non-linear dimensionality reduction-based algorithms such as t-SNE (360); and (3) the recently improved hierarchical approach of the t-SNE dimensionality-reduction-based technique called HSNE (361). Uniform manifold approximation and projection (UMAP) is the most recent single cell analysis-based dimensionality reduction tool introduced (362).

Mass cytometry has expanded the limit of single cell data measurement in an individual experiment, making it highly suitable for system-wide analysis at single cell resolution, such as investigating cellular phenotypes in cancer microenvironments. Several studies have applied mass cytometry in phenotyping immune cell profiles and monitoring their changes upon treatment in peripheral blood and different tissue types from patients with renal cancer (363), breast cancer (364), lung cancer (365-367), glioma (368, 369), melanoma (370-374), liver cancer (375, 376), myeloma (377-380) and colorectal cancer (381-383), among others. Since the advent of mass cytometry, only few studies on ovarian cancer have been published. Gonzalez et al. included a mass cytometry panel of 41 antibodies, of which four antibodies were used to manually gate viable tumour cells (excluding stromal, immune and blood vessel cells), while the rest of the panel was dedicated to interrogate HGSOC tumour biology (384). In the other study, Toker et al. used a 35-marker panel with an exclusive focus on the different subsets of T cells in the ovarian TME (385). Another recent study, was from Kverneland and team, demonstrating the benefit of adoptive cell therapy combined with immune checkpoints in ovarian carcinoma (386). The most recent study, by Casado and colleagues, presented an CyTOF analysis workflow named “*Cyto*” for interactive analysis of large-scale cytometry data. They demonstrated reliable delineation of immune and tumor subpopulations within the two evaluated datasets, which included a HGSOC dataset as well (387).

To date, most mass cytometry studies have focused primarily on surface and intracellular cellular markers, but the technology can also be utilised to evaluate cell signalling processes by analysing protein phosphorylation (388). The number of potential cell phenotypes also increases exponentially with the rise in the number of antibodies being simultaneously measured, resulting from the combination of different markers used, making multidimensional analysis a key possibility in this technique. It thus renders visible the phenotypic heterogeneity of the tumours and optimises therapeutic targeting of selective patient groups in clinical settings. For example, in a recent study on dysproteinaemia patients, a 33-marker CyTOF panel was used to characterise the tumour immune microenvironment (TiME) at diagnosis and after standard frontline therapies. They identified novel subsets unique to the TiME which may play a role in tumour immune escape and immunosurveillance (389). Another study, this one focused on the breast tumour microenvironment, revealed important implications for characterising tumour-infiltrating immune cells (390). However, the data analysis of complex mass cytometry datasets remains challenging, as traditional flow cytometry manual gating strategies are not sufficient to capture the phenotypic differences; more importantly, finding clinically relevant findings in such system-wide analysis datasets is not easy and needs further interdisciplinary expertise in making meaningful interpretations.

1.3.2 The ‘-omic’ techniques

Next-generation sequencing (NGS) of DNA and RNA allows for the reconstruction of ‘average’ genomes and ‘average’ transcriptomes, which can then be resolved using bioinformatic algorithms to determine the composition of tumour microenvironments or to perform clonal evolution analysis. NGS findings have revolutionised cancer biology studies by generating high-throughput data, as the individual DNA and RNA molecules are represented here as sequencing reads, thus allowing the retention of information about phenotypes, genotypes, sub-clonal alterations and cellular states (391-393).

Recent major findings obtained using ‘-omics’ approaches (transcriptomics, proteomics and genomics) have unravelled the complexity and heterogeneity of ovarian tumours (for more details on tumour heterogeneity, see Section 1.2.4), as illustrated in Figure 9 (2, 394-397). The illustration lists important cues for exploring treatment targets and designing novel biomarkers, as well as correlations between therapeutic regimens and ovarian TME profiles, revealing implications for precise patient selection (121, 398-404).

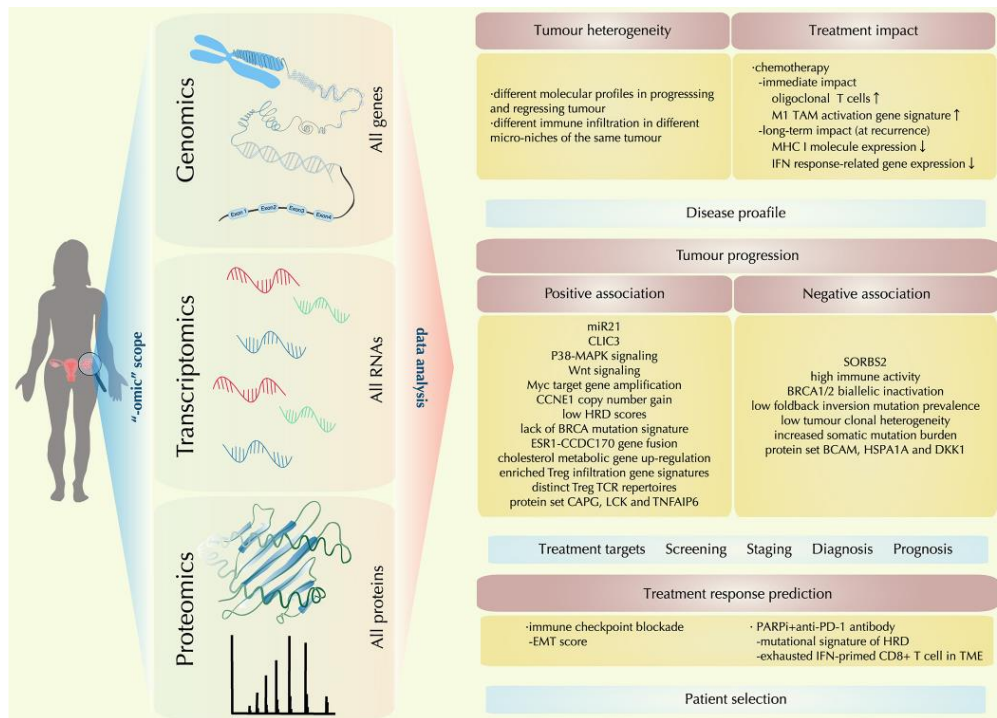


Figure 9. Recent molecular findings of the ovarian TME from the ‘-omics’ techniques (image adapted from Yang et al. (129))

Traditionally, molecular profiling has relied on analysis of bulk cell populations, but single-cell DNA- and RNA-sequencing have recently emerged as powerful tools for a more unbiased and systematic characterisation of cells in ovarian tumours. One good example is the recent publication by Geistlinger et al., who discussed the ambiguity of the discrete subtype classification observed in the landmark TCGA study (122). To

date, most high-throughput studies have focused on DNA, RNA and protein expression, but a number of recent studies focused on the epigenetic regulation of gene expression at the single-cell level, using developing techniques such as ATAC-seq (405), bisulphite sequencing (406), ChIC-sequencing (407) and chromosome conformation capture (3C) (408). Although such detailed genetic decomposition of tumours enables the rationalisation of targeted cancer therapies, there are drawbacks to single-cell sequencing methods, including non-uniform coverage and artefacts introduced during genomic amplification, all of which contribute to a high rate of false positive and false negative findings (409). The throughput is also limited by available sequencing depth, protocol complexity and cost, which can together affect the analysis pipeline downstream and thus the inference of cellular interactions.

1.3.3 Spatial profiling of patient TMEs: The Future?

Immunohistochemical staining (IHC) is the conventional method used to evaluate the morphology of ovarian tissues and localise specific antigens using light microscopy. IHC is a valuable tool for characterising, identifying and visualising ovarian cancer biological processes, and it is thus useful in ovarian tumour biology research and clinical diagnostics (410-416). Zhang et al. produced an important IHC study in ovarian cancer in 2003: They identified as already mentioned a positive association between the infiltration and presence of CD3⁺/CD8⁺ tumour-infiltrating lymphocytes (TILs) and improved clinical outcomes (269).

Most single-cell technologies, such as flow cytometry and mass cytometry, require tissue dissociation in order to measure single cells; however, these dissociation techniques, both mechanical and enzymatic, might cause loss of certain cell surface markers. Furthermore, the cellular dissociation of the sample degrades the spatial resolution of the sample, so traditional IHC- and immunofluorescence-based methods are powerful techniques for obtaining spatial information for the biological samples of interest. However, in immunohistochemistry, a limited number of markers which can be captured on a slide simultaneously is considered to be an important limitation (417).

Recent technological advancements, such as imaging mass cytometry (IMC) (418) and multiplexed ion beam imaging by time-of-flight (MIBI-TOF) (419) have greatly influenced and expanded the number of markers which could be used on a slide at a given time. Both imaging approaches use the traditional IHC workflow, but they also use metal-isotope-conjugated antibodies, which can be detected through a time-of-flight mass spectrometer. Both IMC and MIBI-TOF allow for the characterisation of inter- and intratumoural phenotypic heterogeneity, with spatial resolution at the single-cell level. IMC is now being applied in the study of tumour microenvironment and its heterogeneity in several types of cancer, such as pancreatic cancer (420), breast cancer (421, 422) and colorectal cancer (423). Several computational tools have been developed to analyse the spatially resolved multiplexed tissue arrangements, including ImaCytE (424) and HistoCAT (425). These tools apply cell segmentation masks to extract single-cell data from images using a combination of two computer programs, CellProfiler (426) and Ilastik (427). The extracted single-cell data is further used to assess spatial localisation and cellular interactions with dimensionality reduction tools such as t-SNE.

IMC is a relatively new technique, and we have only been able to identify a few abstracts, including the ones presented recently at the SGO 2021 meeting, and one paper that focused on EOC profiling using IMC (3, 428). More recently, a modified version of our ovarian mass cytometry panel presented in **Paper I** has been transferred to the HyperionTM Imaging System for ovarian tissue section analysis (unpublished results). IMC can be applied to both snap-frozen and FFPE samples, which are conventional methods of tissue storage in clinical repositories. Currently IMC enables simultaneous imaging of up to 40 proteins with a subcellular resolution of 1 μ m. Nevertheless, such high-throughput imaging entails the limitation of a relatively long imaging time of 2 h per field of 1mm² (429). Though IMC resolves certain issues that we encounter with single cell suspension samples however, it raises new challenges in visualising 40 markers simultaneously, and prior knowledge is needed regarding which cell phenotypes could be present and what their physical relationships could be.

The practice of integrating multiple datasets of individual tissue ranging from single-cell decomposition to spatial resolution (367, 382, 383) is growing, which leads us to expect that in the coming years such integrative approaches will improve insights into how the various components of the TME interact in tissues.

2. Aims of the study

2.1 Background

Over the last three decades, the survival parameters and quality of life for patients with HGSOE have improved; however, the five-year survival rate is still low. The severity is due to the high frequency of late-stage diagnoses, the development of chemoresistance, and tumour evasion of host immune responses (50, 55, 430, 431). HGSOE is characterized by a unique intra-abdominal milieu consisting of both the primary tumour, peritoneal implants, omental metastasis, and ascitic fluid, which greatly influences the therapy response rate (119, 432). In line with other cancers, there has been an exponential growth of molecular characteristic HGSOE data recently, and the identification of HRD and replication stress in tumour cells have resulted in the inclusion of PARP inhibitors as consolidation therapy in first line treatment (3). This is believed, as mentioned, to result in improved overall survival. Further progress will necessitate reassessment, and hence a roadmap for research priorities has been outlined (4). Over the last years, it has also become increasingly clear that, in addition to the features of neoplastic cells, the composition of the heterogenous HGSOE TME is important for biology, prognosis, and treatment selection. Further progress in treatment responses and outcome parameters will necessitate a better understanding of the biological complexity within the TME. Multiparametric mass cytometry analysis allows for the simultaneous detection of more than 40 parameters and is highly suitable for such a system-wide analysis (153).

2.2 General aim

Cytometry by time-of-flight (CyTOF) multiplexed imaging, an advanced single-cell proteomics methodology, enables the multi-dimensional phenotypic categorization of single cells and the characterization of the TME composition. The main aim of this PhD project is to develop novel HGSOE mass cytometry panels and, with the application of emerging bioinformatic tools, to excavate the TME and detail its inter-

compartmentalized reciprocity with the aim of identifying biomarker signatures for the biomarker-driven selection of patients to improve therapy response and survival rates.

2.3 Specific objectives

1. To develop a HGSOC mass cytometry panel for in-depth characterisation and to evaluate the influence of tumour dissociation methods on the single-cell profiling results (**Paper I**)
2. To create a HGSOC mass cytometry panel for immunophenotyping the TiME landscape to classify immune cell populations, identify clinically relevant cell subsets, and better understand the underlying biological complexity (**Paper II**)
3. To characterize the HGSOC TME with increased depth by integrating the two mass cytometry panels established using the computational panel merging algorithm, CyTOFmerge (**Paper III**)

3. Materials and methodological considerations

3.1 Materials

3.1.1 Peripheral blood mononuclear cells

Blood samples from healthy donors at the Blood Bank, Department of Immunology and Transfusion Medicine, Haukeland University Hospital, Bergen, Norway, were used. Peripheral blood mononuclear cells were isolated from aliquots before being cryopreserved and stored for further use (**Papers I-III**).

1.1.1 Ovarian tumour samples

HGSOC tumour samples collected during primary cytoreductive surgery following written consent were analysed. All samples were part of the Bergen Gynaecologic Cancer Biobank (GYNCAN), Department of Obstetrics and Gynaecology, Haukeland University Hospital (HUS), Bergen, Norway (**Papers I-III**). Clinicopathological information (age, disease stage at diagnosis, surgical outcome, and survival parameters such as PFS and OS) for each patient was gathered. In **Paper I**, we included four patients. In **Papers II** and **III**, the same ten tumour samples from chemo-naïve HGSOC patients were analysed.

3.1.3 Ovarian cancer cell lines

The human ovarian serous adenocarcinoma cell lines OV-90 (American Type Culture Collection (ATCC), ATCC CRL-11732) and Caov-3 (ATCC HTB-75) were used in **Paper I** for the optimization of the pan-tumour mass cytometry panel. In **Papers II-III**, OV-90 cells were utilized as control samples. Both cell lines, the OV-90 cells (RPMI 1640) and Caov-3 cells (DMEM), were cultured and maintained per the manufacturer's instructions with the respective medium supplemented with 10% foetal calf serum (FCS), 2 mM L-glutamine, and penicillin 100 IU/ml.

3.1.4 CD34⁺ stem cells

The CD34⁺ stem cells were isolated from umbilical cord blood samples collected from presumed healthy singleton pregnancies delivered by caesarean section as part of the Research Biobank for Blood Diseases, HUS, Bergen, Norway, via a standardized process described elsewhere (433). The umbilical blood samples were collected in ACD-A tubes. Lymphoprep™ density gradient centrifugation followed by CD34⁺ magnetic associated cell sorting (MACS) were the procedures used.

3.1.5 Ethical Approval

The biobanks (GYNCAN, Reference ID 2014/1907; the Blood Donor Biobank, Reference ID: 2212/2247; and the Research Biobank for Blood Diseases, Reference ID 2015/1759) as well as the different projects presented in **Papers I-III** (Reference ID: 2017/623) have been approved by the regional ethical committee.

3.2 Methodological considerations

3.2.1 Tumour tissue processing

All the clinical tumour samples (**Papers I-III**) used were immediately processed to obtain single-cell suspensions via different dissociation methods. Resected tumour pieces collected during cytoreductive surgery procedures, cut into small uniform cubes, and dissociated with conventional mechanical dissociation along with five different enzymatic dissociation methods. Prior to enzymatic treatment, tissue pieces were washed with HBSS or PBS and transferred into the respective pre-warmed enzyme mixtures (Table 4 and Figure 12 below; also presented in **Paper I**). All the reactions were conducted with constant shaking at 37 °C. The cells were then strained through a cell strainer, checked for cell viability, centrifuged, and cryopreserved in freezing media. The protocol used are commonly used for the dissociation of solid tumours (434, 435).

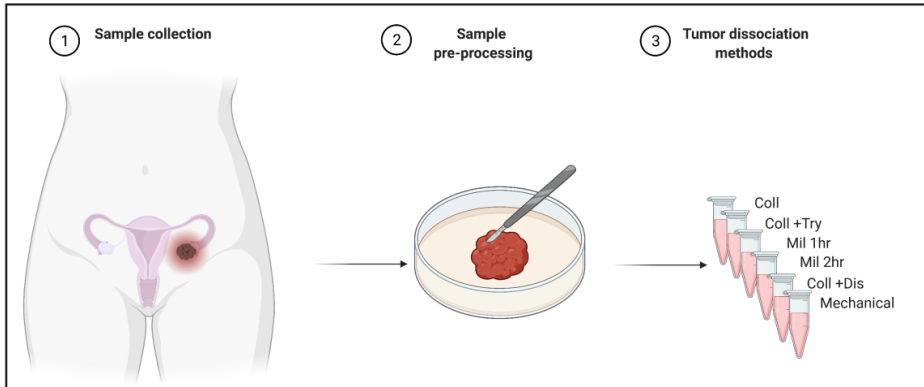


Figure 12. Tumour dissociation

As we were initially unsure about which of the disaggregation techniques would optimally preserve both the viability as well as the phenotypic characteristics of the single cell suspensions produced, we compared the dissociation methods (as presented in **Paper I** and discussed in paragraph 5.1.1)

Table 4. Tumour dissociation conditions (modified from Paper I (435))

Dissociation Conditions	Primary Enzyme	Incubation time	Secondary enzyme	Incubation time
Coll	Collagenase II + CaCl ₂	2 hours		
Coll+Try	Collagenase II + CaCl ₂	2 hours	TrypLE	5 minutes
Mil 1hr	Miltenyi	1 hour		
Mil 2hr	Miltenyi	2 hours		
Coll+Dis	Collagenase II + CaCl ₂	1 hour	Dispase	30 minutes
Mech	Mechanical – no enzyme	-	-	-

3.2.2 Stimulation of PBMC

Peripheral blood mononuclear cells (PBMCs) were isolated from the blood samples of healthy donors via density gradient centrifugation with Lymphoprep® in **Papers I-III**. To enhance the identification of the optimal dilution of certain antibody markers—including markers expressed in activated immune cells only—all markers for immune cells and immune checkpoints were titrated concomitantly on unstimulated and

stimulated PBMCs. The PBMCs were stimulated with 2.5 μ g/ml phytohemagglutinin (PHA) for a period of 48 hours at 37 °C in a humidified atmosphere with 5% CO₂ and used as control samples when the different mass cytometry panels were established (**Papers I and II**).

3.2.3 Mass cytometry

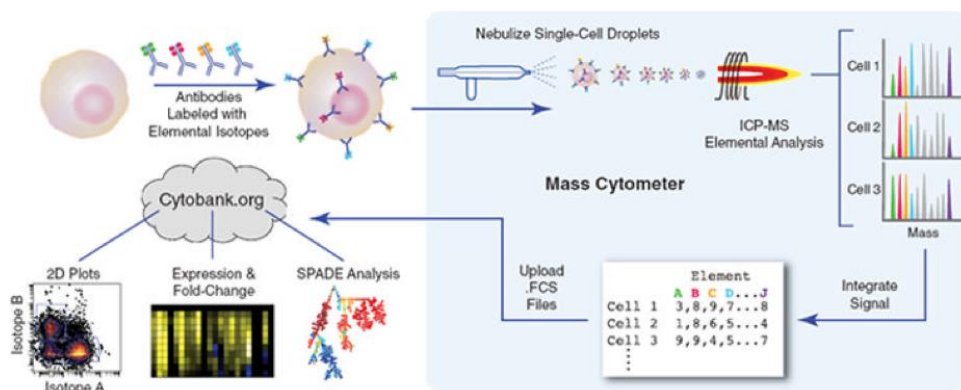


Figure 13. Overview of CyTOF workflow (adapted from Bendall et al. (436))

Cytometry by time-of-flight (CyTOF) is an efficient method that utilizes stable isotopes tagged with monoclonal antibodies as reporters and can detect multiple parameters per cell at one given time (Figure 13). Cells coupled with antibody-isotope conjugates are sprayed as single-cell droplets into an inductively coupled argon plasma, in which each cell is vaporized and ionized into its atomic constituents. These resulting ionic clouds are then sampled by a time-of-flight mass spectrometer, and the corresponding signal from each cell's constituent ions are quantified by the detector. CyTOF is capable of in-depth phenotypic profiling, enabling a global depiction of the constituent cells of the TME.

Panel development

The design of CyTOF panels involves a step-by-step optimization process, starting with the panel design and ending with determining the optimal antibody concentrations and panel validation (Figure 14).



Figure 14. Mass cytometry panel development

During this thesis work, two mass cytometry panels for analysing cells in suspension were established (**Papers I and II**), and the workflow just presented was used. To our surprise, there is only a limited number of published studies focusing on the actual panel development process (437-439), although the quantity of publications using CyTOF as a tool for phenotypic single cell profiling is increasing considerably for a range of dissociated solid cancers (363, 364, 367, 369, 371, 381). This is the case for both custom-made and commercially available panels.

Panel design

The first panel, later called the *pan-tumour panel*, should outline the tumour, stromal, and immune cell subsets that constitute the HGSOC TME (**Paper I**), while the second panel, called the *pan-immune panel*, was generated with the intention to immunophenotype the TiME of HGSOC (**Paper II**). To select the appropriate targets and corresponding antibodies, we used a semi-structured process:

- A literature review to identify potential phenotyping and functional targets of interest
- The selection of the most appropriate and multipurpose markers to minimize the number of markers in the panel. Definitions of the marker types are explained below:
 - Appropriate: Definitive markers of cell subsets and/or functional states that have a proven and longstanding history of being used to identify a certain cell population or cytotoxic state, as well as markers necessary for the identification of a defined cell population.
 - Versatile: Markers that can identify multiple subsets of cells and effectively bring down the number of markers that have to be included in the panel.

- Literature review to determine the expression level of the different markers.
 - This information was a key determinant in the panel design and the positioning of the markers within the panel (either to the ‘high-sensitivity’ or ‘lower-sensitivity’ part of the mass spectrum) to ensure that the markers could still be detected with sufficient sensitivity.

Table 5. An overview of the CyTOF panel markers (as presented in Paper III)

Tag	<i>Pan-tumour panel</i>		<i>Pan-immune panel</i>	
	Human mAb	Clone	Human mAb	Clone
89Y	CD45	HI30	CD45	Hi30
141Pr	EpCAM/CD326	9C4	EpCAM/CD326	9C4
142Nd	CD133*	5-E3 (5E3)	CD303*	201A
143Nd	CD117	104-D2	CD117	104-D2
144Nd			CD33*	WM53
145Nd	CD4	RPAT4	CD4	RPAT4
146Nd	CD8a	RPAT8	CD8a	RPAT8
147Sm	CD20	2H7	CD20	2H7
148Nd	CD34	581	CD16	3G8
149Sm	TAG72*	0.N.561	CD25	2A3
150Nd	LAG-3/CD223	11C3C65		
151Eu	CD103	BER- ACT8	CD123	6H6
152Sm	CD44*	BJ18	CD95/Fas	DX2
153Eu	CD47*	CC2C6	CD7	EH12-2H7
154Sm	TIM-3	F38-2E2	CD163	GHI/61
155Gd	PD1/CD279	EH12. 2H7	PD-1/CD279	2H7
156Gd	PDGFRB/CD140b	18A2	CD86	IT2.2
158Gd	FOLR1*	548908	CD335*	BAB281
159Tb	PD-L1/CD274	29E.2A3	CCR7	Go43H7
160Gd	CD14	M5E2	CD14	M5E2
161Dy	CTLA-4/CD152	14D3	CTLA-4	14D3
162Dy	Foxp3	259D/C7	CD11c	Bu15
163Dy	CD56	NCAM16.2	CD56	NCAM16.2
164Dy	CD45RO	UCHL1	CD45RO	UCHL1
165Ho	OX40/CD134*	Ber- ACT35 (ACT35)	CD127	A019D5
166Er	CD24	ML5	CD34	581
167Er	CD25*	2A3	CD27	O323
168Er	IFN γ	B27		
169Tm	CD19	HIB19	CD19	HIB19
170Er	CD3	UCHT1	CD3	UCHT1
171Yb	AXL*	MM0098- 2N33	CD62L*	DREG-56

172Yb	CD73*	AD2	CD73*	AD2
173Yb			CD141	1A4
174Yb	HLA-DR	L243	HLA-DR	L243
175Lu	aSMA*	1A4		
176Yb	FAPalpha*	F11-24	CD1c*	L161
209Bi	CD11b	ICRF44	CD47	CC2C6

*in-house self-conjugated; out of the 17 overlapping markers, highlighted (in grey) are the 15 overlapping markers between both panels with the same metal tags, excluding CD25 and CD47, which have different metal tags in the separate panels.

In parallel, the composition of the antibody panels was designed with the use of the Maxpar® panel designer from Fluidigm (**Papers I and II**). The panel designer is an interactive web-based application that aids in optimizing the panel performance with an algorithm that selects the optimal metal tag for each target with minimal signal overlap. The use of the panel designer is discussed in more detail in paragraph 5.1.1. For the pan-tumour panel, we ended up with a group of 35 human monoclonal antibodies, identifying tumour cells and distinguishing major stromal cells, including pericytes, endothelial cells, and fibroblasts in addition to common infiltrating immune cells (**Paper I**) (Table 5). The 34 pan-immune panel, was designed to characterise subsets of T cells, DCs, B cells, NK cells, myeloid-derived cells, and macrophages that comprise the HGSOc TiME (**Paper II**) (Table 5). Both panel markers included surface lineage markers (immune, stromal, and tumour—including tumour stem-like cells) and intracellular functional markers (foxp3 and IFN γ) (**Papers I and II**) (Figure 14).

Custom-conjugation

Most of the antibodies from both panels were Maxpar® metal-conjugated antibodies; however, since our panel design involved some customization, some in-house conjugations were necessary. Both the readymade Maxpar® metal-conjugated antibodies and in-house conjugated antibodies were purchased from Fluidigm, BioLegend, or Abcam (**Papers I-III**) for use. Out of the 69 panel antibodies (Table 5), 17 were custom-conjugated (11 mAb from the *pan-tumour panel* and 7 mAb from the *pan-immune panel*) according to the manufacturer's protocol.

Titration of antibodies

In addition to securing the optimal functioning of the reagent, antibody titration is also required to identify the concentration that best separates the positive and negative cell subsets from the background. Since a very high titer might diminish the signal-to-noise ratio due to unspecific binding, titrations are also important and may impact the success of the antibody panel. In mass cytometry, the titration of heavy metal-labelled antibodies is the key to determine optimal staining dilutions, reduce non-specific binding, and validate any contaminations in the corresponding channels (isotopic impurity, M+16, and M+/-1). In our study, the immune antibodies in both panels were titrated first on healthy and stimulated PBMCs, whereas the tumour and stromal antibodies were first titrated on a mixture of ovarian cancer cell lines (**Papers I-III**) followed by titration on an ovarian patient sample mix in order to determine the optimized antibody titer values.

Panel validation

Panel validation is an important step after the titration of the panel antibodies, and running a whole panel test on the actual study samples of interest is essential. In most cases, antibodies are initially titrated on control samples that best represent the final patient sample types of interest, as actual patient samples can be considered too rare and precious for control titration runs. In our study, following the titration of antibodies on appropriate control samples, a final panel validation step was carried out. In this step, the whole panel was validated on a mixture of primary ovarian patient samples (**Paper I-III**).

3.2.4 Sample preparation

It is crucial to follow a clean sample preparation pipeline, starting from the clinical sample collection until the data acquisition and analysis. All samples used in the mass cytometry experiments were prepared carefully under specific conditions (**Paper I-III**).

Cisplatin binds non-specifically to intracellular DNA and stains viable cells; in addition, it enters the disrupted cell membrane of dead cells more easily than that of live cells. Cryopreserved samples were thawed, stained with Cell-ID Cisplatin to assess cell viability, fixated using Stable-Lyse and Stable-Store, and subjected to permeabilization barcoding with palladium isotopes as per the manufacturer's instructions. To increase the efficiency and decrease the technical variability, sample barcoding of the samples is a useful strategy. Exceptionally, for the merged dataset analysis (**Paper III**), two separate sets (2 = 1x pan-tumour panel + 1x pan-immune panel) of equal portions of the barcoded sample mixture pool were prepared. Barcoded samples (**Papers I-III**) were incubated with a FcR blocking reagent, which was followed by antibody staining with predetermined specific panel antibody dilutions; then, they were finally resuspended in a nucleic acid Ir-Intercalator. All samples underwent intermediate washing steps when necessary until they were diluted in Cell Acquisition Solution (CAS) before running on the Helios machine as per the standard protocol (Fluidigm, CA) (**Papers I-III**).

3.2.5 Data analysis

The establishment of the high-dimensional analysis platform that CyTOF represents has necessitated the development of new data managing strategies and tools (356). Although many consider CyTOF an advanced form of flow cytometry, it is important to note that many of the analytic tools used to analyse and visualize mass cytometry data circumvent traditional bivariate plots, as the number of parameter pairs increases exponentially with the number of parameters analysed (356).

(i). Data cleansing and debarcoding

To be able to analyse the data generated, it is important to clean the data. Acquired data was normalized using EQ™ Four Element Calibration Beads with the Fluidigm software (Fluidigm) on the machine. Removal of doublets and debris and the gating out of live singlets were performed using standard tools on the Cytobank platform (v7.2.0 and v7.3.0, Beckman Coulter, Inc., IN) (**Papers I-III**). Barcoding samples helps in running multiple samples simultaneously without any possible sample bias,

which improves the quality of the generated results. In **Paper I**, barcoded files were debarcoded using the Premessa debarcoder GUI package (<https://github.com/ParkerICI/premessa>) in R (version R 3.4.1 GUI 1.70 El Capitan build (7375)) with a 20-plex-debarcoding key (Fluidigm), while, in Paper II, the debarcoding was performed using the Cytobank platform.

ii) Time of flight analysis platforms

Different analytical platforms were used in this project based on the scope of the question and intended analysis (356, 440). In **Paper I**, Arsinh (x/5)-transformed .fcs files from Cytobank were clustered in a density-based clustering method called X-shift (VorteX, Java version 1.0) (441). X-shift finds the local density maxima of data-points (cell event), which becomes the cell cluster centroid in a nearest neighbour graph using the weighted K-nearest-neighbour density estimation in a multidimensional marker space. The K value is automatically selected from the elbow point, also known as the ‘switch point’, via under-clustering or over-fragmenting the dataset with a Mahalanobis distance less than 2.0 (**Paper I**). This algorithm has a high degree of user-defined inputs from data importation until the clustering of the dataset.

In **Papers II and III**, the Astrolabe Cytometry Platform (Astrolabe Diagnostics, Inc., NJ) was selected for a fully automated analysis pipeline that included both unsupervised clustering and statistics. Acquired single-cell data (**Paper II and III**) after initial data cleaning and debarcoding has been clustered using the *FlowSOM* R package (359) and labelled using the Ek’Balam algorithm (442), as per the analysis pipeline. Following the cluster labelling method implementation, differential abundance analysis and visualization were done via the automated Astrolabe Cytometry Platform (**Papers II-III**) (443-447). For a more in-depth delineation of the immune cells, in **Paper III**, both panel (*pan-tumour* and *pan-immune*) datasets—with a total of 17 overlapping markers and 18 unique markers—were imputed together using an established merging algorithm called CyTOFmerge in Matlab 2019a (MathWorks) (**Paper III**). As a quality control step, the panel antibody expression pattern was plotted on Cytobank as t-Distributed Stochastic Neighbour Embedding (t-SNE) plots,

a nonlinear dimensionality reduction algorithm that reduces high-dimensional data down to two dimensions for easy visualization (**Paper I-III**).

(iii). Visualisation

In **Paper I**, to visualize the differences between the differently dissociated tumour samples across the patients, flow pie-charts and stacked bar plots (in a XY table format) were plotted using the clustering data obtained from X-shift using Prism (6.0c version) (GraphPad). In addition, heatmaps were created using the X-shift algorithm to effectively visualize patterns within the clustered mass cytometry data across the dissociated tumour samples. Median expressions (arcsin-transformed dual counts) of functional markers in the panel were investigated using Cox proportional-hazards models (**Paper I**). Histograms were plotted to show and compare the expression distribution of each marker per condition and were plotted using Matlab 2019a (MathWorks) (**Paper I**). In **Papers II-III** following cluster labelling, differential abundance analysis and visualization were done through the automated Astrolabe Cytometry Platform (Astrolabe Diagnostics, Inc., NJ). In addition, heatmaps and bar plots were created using Prism (8.0c version) (GraphPad) to effectively visualize patterns within the clustered mass cytometry data across the patient tumour samples (**Papers II-III**).

4. Main Results

4.1 Paper I

We developed a novel ovarian mass cytometry using a CyTOF panel that enables the simultaneous detection of up to 35 parameters detailing the ovarian TME at the single-cell level. The mass cytometry panel development involved multiple steps, starting with the selection of markers from current literature and ending with panel optimization along with validation. We were able to successfully delineate and distinguish all the major TME cellular phenotypes, including the immune, stromal, and tumour subsets, with the established mass cytometry panel. We further used the panel for detailed evaluation of the effects of six different ovarian tumour dissociation methods to secure the integrity of the cell epitopes from any unwanted technical variabilities caused during the dissociation process. From our evaluation, we identified that, while the tissue dissociation methods have varied levels of impact on the different antigen expression profiles, they still hold the capacity to clearly show the interpatient differences present in the individual TME signatures.

4.2 Paper II

We delineated the tumour immune microenvironment of ten individual chemo-naïve ovarian patients with a newly created 34-marker immune cell-focused panel presenting their myeloid and lymphoid cell phenotypes. We identified 28 main immune cell populations (consisting of a total 184 cell subsets), including 16 lymphoid and 12 myeloid cell populations, from the clustering analysis. Our immune profiling revealed a high degree of interpatient heterogeneity. The four most frequently found cell clusters across the patient samples were conventional dendritic cells (DC), natural killer (NK) cells, and unassigned hematopoietic cells. Several DC and monocyte cell subsets showed associations with clinical features.

4.3 Paper III

We jointly investigated the immune, stromal, and tumour cell phenotypes of the ovarian TME at a greater magnification with the merging of the individual datasets (pan-tumour dataset and pan-immune dataset). We identified a high inter-sample cell phenotypic heterogeneity and a more in-depth immune delineation in addition to tumour and stromal cell phenotypes, including a total of 39 cell clusters (29 immune (three myeloid lineage cells), nine tumour (cancer stem-like cells), and one stromal (fibroblast subsets) cell clusters). In addition, we identified a novel tumour cell metacluster, CD45⁻CD56⁻(EpCAM⁺FOLR1⁺CD24⁻), the most frequently found across all patients. Furthermore, with the merging of the two datasets, we identified even higher clinical associations (from 12 (pan-tumour dataset) to 20 (merged dataset)), with most of these observed associations majorly prevailing between infiltrating immune cell subsets and survival rates (PFS, OS) (**Paper III**).

5. Discussion of results

HGSOC is a heterogenous disease often diagnosed at advanced stages with poor prognosis (50, 430, 431). Although the development of HGSOC, which involves multiple genetic alterations, is becoming well-characterized, the use of reliable molecular markers or profiles for diagnostics, prognosis, the tailoring of therapeutic strategies, and the prediction of therapeutic responses are only at early stages (448-450). The unusual tumour milieu facilitates the development of, as mentioned in paragraph 1.2, the inter- and intratumour molecular and phenotypic heterogeneity that characterise this EOC subtype (2, 119, 432). With the advancement of bioinformatics, harnessing evolving tools, such as CyTOF, and incorporating algorithms employing machine learning generate a seemingly limitless ability to comprehensively map such heterogenous TME (451). CyTOF provides significant possibilities for understanding such a complex framework of interplay between cancer cells and their surrounding non-tumour neighbouring cells. With a better understanding of the molecular processes occurring at the protein level and the identification of the cellular phenotypes involved, it is likely that traditional profiling will be challenged and complemented with genomic profiling at the single-cell level. Together, the molecular markers or profiles will be used to establish more patient-centric stratification strategies for diagnosis, treatment selection, and follow-up, with the aim of improving outcome parameters.

This thesis is based on three subprojects (**Papers I-III**). The first two projects focused on the development and application of panels for the TME profiling of a single-cell suspension of HGSOC tumours with CyTOF. The outlines of the two papers differed, as **Paper I** concentrated on pan-tumour profiling, while **Paper II** emphasised immune cell-focused deep phenotyping. We also explored different tools for clustering, visualizing, and analysing mass cytometry data: the time-of-flight analysis platform Cytobank (**Papers I-III**), X-shift (**Paper I**), Astrolabe Cytometry Platform (**Papers II and III**), and MATLAB (**Paper III**). In **Paper I**, attention was additionally focused on the establishment of a panel on the effects the different dissociation methods used had on the cell subset profiling. In **Paper II**, we further classified immune cell populations and identified clinically relevant clusters. In the last subproject, **Paper III**, the

Careful planning is needed for designing an experimental approach, as different factors and conditions can influence data acquisition, data analysis, and the results generated. These include marker selection, panel design, conjugation, the titration of antibodies, and panel validation, including appropriate sample fixation and storage (Figure 15). Standardizations are of importance to circumvent incorrect interpretations.

Marker selection

For the selection of markers, we followed the semi-structured process presented in paragraph 3.2.3. The focus of the literature review was to identify potential phenotyping and functional targets of interest, understand their expression levels, and select the most appropriate of them to minimize the number of markers in the panel (Table 6). This information was a key determinant in the panel design, as the best combination of the antibody with an appropriate heavy-metal isotope to achieve the best possible signal intensity for detecting targets of interest on the sample is the most vital part of the CyTOF panel design (453).

Table 6. An overview of the CyTOF panel markers

Target	Purpose
CD8a	Cytotoxic T-cells
CD4	T-helper cells
CD3	T-cells
CD45RO	Activated memory T-cells
HLA-DR	B cells, activated T-cells, DC, monocyte/macrophages and non professional-APC
CD20	B-cells
CD25	T-regulatory cells
CD56	Natural killer cells
CD19	B-cells
CD14	Monocytes, Natural killer cells
CD11b	MDSC, monocytes and macrophages
CD45	Common leukocyte antigen
CD103	Infiltrating T-cells
CD34	Endothelial, stem cell marker
CD47	Inhibits phagocytosis; overexpression in EOC cells (EMT)
Foxp3	T-regulatory cells
IFN γ	Expressed by infiltrating T-cells upon recognition of tumor cells
PD1,PD-L1, CTLA-4, LAG-3,OX40, TIM-3	Immune checkpoint
CD303	Plasmacytoid DC
CD33	Myeloid progenitors, monocytes, DC, mast cells and granulocyte
CD16	NK cells, monocytes, macrophages and neutrophils
CD123	DC, mast cells, basophils, macrophages, T and B cells, neutrophils, monocytes and fibroblasts
CD95	Activation marker
CD7	T-cells, NK cells, haematopoietic cells
CD163	Macrophages, monocytes,
CD86	B and T cells, astrocytes, DC, monocytes/macrophages
CD335	NK cells
CCR7	affects interactions between T cells and dendritic cells and their downstream effect
CD11c	Monocytes, macrophages DC, granulocytes and NK cells
CD127	B and T cells
CD27	T, B and NK cells
CD62L	B cells, Monocytes, granulocytes
CD141	DC (Type 1)
CD1c	DC (Type 2)
CD24	Cancer stem cell marker
CD44	Cancer stem cell marker
CD133	Cancer stem cell marker
EpCAM	Cancer stem cell marker
FOLR1	Highly expressed in cancers with epithelial origin
CD73	Cancer stem cell marker
CD117	Cancer stem cell marker
TAG72	Tumor progression marker from benign to malignant
PDGFR β	associated with vasculature in Tumor microenvironment
FAPa	secreted by Cancer associated Fibroblast (CAF)
α SMA	pericytes

In **Paper I**, for the pan-tumour panel, we ended up with a group of 35 human monoclonal antibodies, identifying tumour cells and distinguishing major stromal cells (including pericytes, endothelial cells, and fibroblasts) in addition to common

infiltrating immune cells. In **Paper II**, we selected 34 pan-immune panel antibodies to characterise subsets of T cells, DCs, B cells, NK cells, myeloid-derived cells, and macrophages that comprise the HGSOc TiME. The panel used by Casado et al. for establishing an effective workflow for mass cytometry data is the only panel we identified that, similar to our work (**Papers I and III**), is used for a pan-tumour profiling approach (387). Currently, apart from the paper by Gonzalez et al., in which the focus was to interrogate the HGSOc tumour biology (384), all other papers published (Toker, Kverneland, and Bobisse groups) have developed panels focusing on infiltrating the T-lymphocytes of the TME (385, 386, 454). Each of these studies interrogated specific compartments of the TME in detail, while our panels provide a relatively broader overview of the main populations of either one (immune) or all compartments (immune, stromal, and tumour) of the HGSOc TME (**Papers I-III**). Therefore, it is essential, before the panel is set up, to focus on the aim and strategy of the project as well as to possess an understanding of the phenotypic and/or functional characteristics needed to gain the required biological information. The main aim of **Paper I** was to develop an ovarian TME-based CyTOF panel and use the developed panel for the comprehensive characterisation of all different compartments (tumour, stromal, and immune) of the ovarian TME along with the evaluation of the tumour dissociation effects (435). In an ongoing project, we have experienced that the backbone of the pan-tumour panel is robust, which is used when designing project specific panels, e.g., in the translational research protocol for the NSGO-OV-UMB1/ENGOT-OV-30 trial. The aim of Paper II was to develop an in-depth immune phenotyping CyTOF panel and immunophenotype the ovarian TiME. However, as also mentioned in paragraph 1.3 and in **Papers I-III**, while both our panels (pan-tumour and pan-immune) present a broader overview of the different compartments of the TME, there is less resolution over specific subsets, which are some of the limitations that can be overcome with the use of more focused panels. For instance, given that the role of myeloid cells in the TiME requires a deeper understanding (455), a design that focus more on TAM and MDSC can be a useful approach. Later paragraphs will discuss what can be gained by the use of merged panels (paragraph 5.2).

Panel design

The value of mass cytometry experiments also depends on the quality of the panel composition. The Helios version of mass cytometry is able to detect ion mass tags within a range of 75–209 Da, providing 135 channels; however, only around 50 are currently in use due to limitations with heavy metal isotope availability (439, 456). The first step of panel design involves the classification of markers into primary (highly expressed or well-defined backbone markers such as CD45, CD3, CD4, CD19), secondary (medium expression markers such as CD44, CD62L), or tertiary (low or unknown expression markers such as LAG-3) antigens. In panel design, it is crucial to consider all this information in addition to the three sources of crosstalk among channels, namely isotopic impurity, abundance sensitivity, and the oxidation of metals (also explained in paragraph 3.2.3) (457, 458). Apart from considering these conventions, the use of dedicated software for panel design is highly recommended. Currently, Fluidigm offers preconfigured screening panels in addition to an online panel design tool called Maxpar Panel Designer (<https://dvsscience.com>). This software calculates and predicts signal overlaps based on user inputs, aiding in optimized panel design (458).

Conjugation

Pre-conjugated, metal-labelled antibodies are commercially available; however, they can sometimes be unavailable based on the specific panel design. Hence, this limitation demands the custom conjugation of antibodies with heavy metal-labelled isotopes. One important consideration in custom conjugation includes selecting the right antibody clone; one way to accomplish this would be to use the readily available Maxpar® ready antibodies or known clones of antibodies from prior flow cytometry experiments with similar sample types of interest (458). A detailed protocol for conjugating antibodies with heavy-metal isotopes was published by Han and colleagues (459). Our panels required multiple ($n = 17$) in-house antibody conjugations (**Paper I-II**), similar to the ovarian panel presented by Gonzalez et al., where most of the panel antibodies except for two (CD44 and CD45) were in-house conjugated (384).

Titration of antibodies

Each of the current CyTOF panels described (**Papers I and II**) followed an optimization process tailored for mass cytometry (as also explained in paragraph 3.2.3) similar to the steps demonstrated in the study by Brodie et al. (438). Following marker selection and panel design, the next step was optimal titration of the antibody–metal pairs to reduce the amount of non-specific signal spill over (including signal overlap due to isotope purity, abundance sensitivity in the $M \pm 1$ channel, and oxide formation in the $M + 16$ channel) between the mass channels. Furthermore, it is recommended that the primary antibodies (backbone) of the panel (such as CD45, CD3, CD4, CD19) are titrated first, followed by the secondary (medium expression markers) or tertiary (low or unknown expression markers) antigens (458).

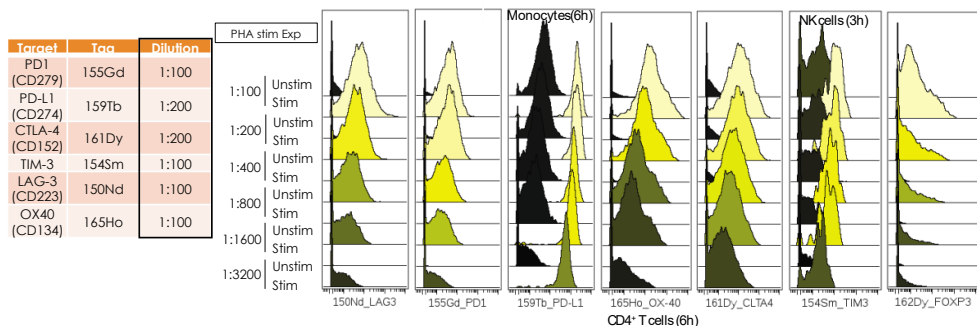


Figure 17. Antibody staining on PHA stimulated PBMC

We first titrated the backbone antibodies and the secondary panel antibodies on a mixture of ovarian cancer cell lines and healthy PBMC samples. The tertiary or more difficult to validate antigens required some extra steps, e.g., the immune checkpoints (LAG-3, TIM3, PD1, PD-L1, OX40, CTLA-4) in the panel needed stimulation of the PBMCs to generate a higher antigen expression for the titration of relevant antibodies (Figure 17). In addition, finding appropriate positive and negative controls for the tumour and stromal antibodies was relatively challenging compared to for the common immune antibodies; hence, these tertiary antigens were titrated on a mixture of ovarian cancer cell lines and PBMC (stimulated and unstimulated) samples known to express or lack the target of interest, thus serving as positive and negative controls. The

knowledge gained from the titration of the pan-tumour panel antibodies (**Paper I**), as mentioned above, aided in designing and optimizing the titration of the pan-immune panel antibodies (**Paper II**).

Fixation

The stabilization of clinical samples in their natural state of occurrence that closely resembles in-vivo conditions is vital and crucial, as small perturbations may affect important characteristics of the cells. We fixed our samples using Stable-Lyse and Stable-Store solution. Recently, Sakkestad et al. illustrated a comparative overview of four different commercially available whole blood preservation kits in terms of leukocyte surface marker detectability in blood samples and presented important considerations for planning these kinds of experiments (460). Specifically, they highlighted that the use of Stable-Lyse and Stable-Store along with the other preservation kits (mentioned in the paper) had an influence on the expression of certain functional antigens (CXCR3, CCR4, CCR6 and CXCR5). However, since all our samples were lysed and fixed with the same preservation kit (Stable-Lyse and Stable-Store), there was no bias between the samples in our set-up. Moreover, none of the above-mentioned markers were part of our panels.

Panel validation

Panel validation in terms of running the whole panel on the actual samples of interest is essential in following panel titration; as in most cases, the titrations are carried out on suitable control samples since clinical samples are limited in availability (458). Thorough evaluation of the three major sources of impurities between mass channels during the panel validation is important, and, if needed, adjustments of the panel are recommended in this step.

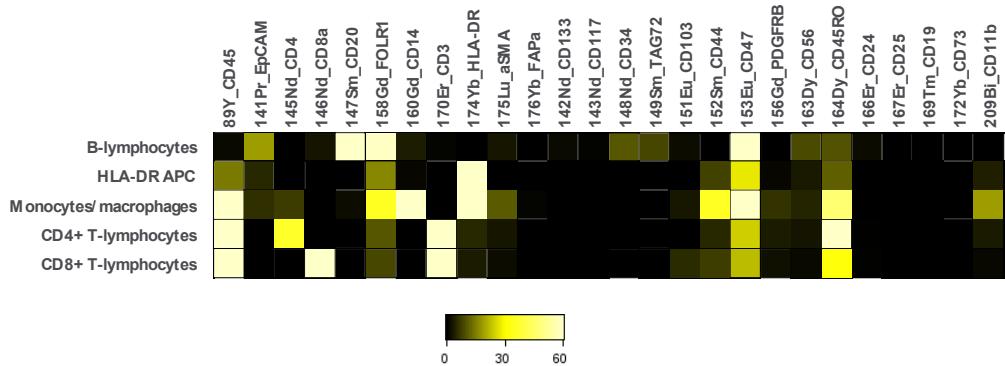


Figure 18. Panel validation

In our study, following the titration of antibodies on appropriate control samples, a final panel validation step was carried out. In this step, the whole panel was validated on a mixture of primary ovarian patient samples (**Paper I-III**). In addition, multiple sample preparation protocols were tested to identify one that would allow for the optimal detection of all parameters from the panel, similar to the approach followed by Brodie et al. (438).

5.1.2 Sample preparation - the influence of different sample dissociation methods

Each of the developed CyTOF panels are optimized for tumour single-cell suspension samples. The primary goal while dissociating tumours is to be preserve cell diversity and viability; however, certain variations are technically induced during this process, which might obscure biological insights (434). Though no earlier studies have been reported on HGSOc, a few similar studies on other cancer types that focus on the cellular effects of disaggregation methods have been published. In **Paper I**, we presented a structured comparison of the influence of six commonly used tumour dissociation methods on all three compartments of the ovarian TME utilizing the ovarian TME-based CyTOF panel (see also Figure 17).

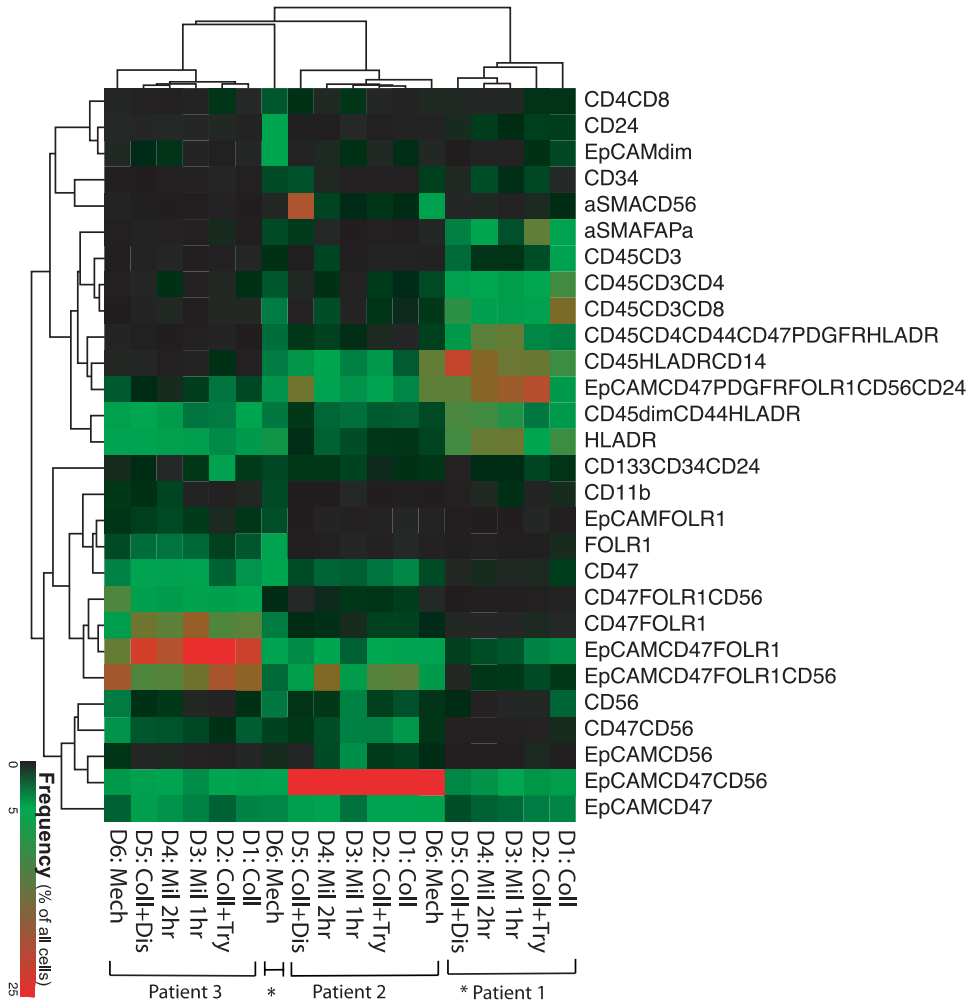


Figure 17. Tumour dissociation effects across patients (adapted from Anandan et al. (71))

From our study, we identified that each of the dissociation techniques influenced the TME cell populations differently. Similar results were published by Leelation et al. in their study on gliomas, tonsils, and melanomas (434). In addition, we reported the effects on certain immune subgroups, as also identified by Poláková et al., who compared the dissociation of tonsillar carcinoma tissues (437). Nevertheless, the interpatient differences observed within these patients were not outweighed by the dissociation effects, as each individual presented a unique combination of TME cell

populations, which was consistent across all the disaggregation methods (**Paper I**). It is also worth mentioning that the dissociation methods used affected some phenotypic markers in the identification of cell subsets while functional marker expressions remained comparable (**Paper I**). This is worth keeping in mind (as just discussed, (paragraph 5.1.1) during the project design.

5.1.3 Selection of CyTOF data-analytical platforms

CytoTOF generates high throughput data and poses a potential challenge towards the efficient interpretation of such high-dimensional data (356, 461). Traditional bivariate plots have been cumbersome and inefficient in CyTOF data analysis; therefore, novel computational analytical tools are being developed (Figure 18). Currently, multiple analytical tools are being introduced, including unsupervised clustering-based algorithms, such as Phenograph, SPADE, FlowSOM, X-shift, and non-linear dimensionality reduction-based algorithms like t-SNE and HSNE (357-361). Nevertheless, new and improved high-dimensional data analytical tools are constantly emerging, including fully automated analysis pipelines.

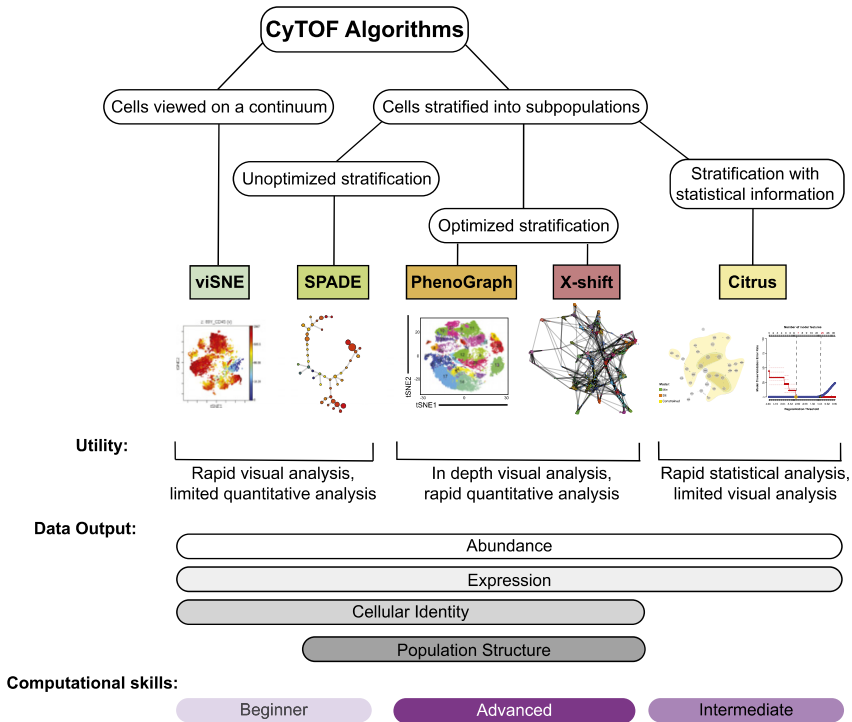


Figure 18. CyTOF analytical platforms (adapted from Kimball et al. (356))

In all the papers (**Papers I-III**), after carefully considering various analytical platforms (SPADE, X-shift, FlowSOM, Astrolabe Cytometry Platform) and their limitations based on the practical application of the dataset on these platforms, we selected those that we judged to suit the goals of the studies the best. This was similar to the approach suggested by Kimball et al. in their paper from 2017, where they compared the benefits and limitations of five different CyTOF analytical platforms (SPADE, viSNE, X-shift, Phenograph, and Citrus) on a single dataset (356).

For the pan-tumour datasets, we applied two approaches for each dataset based on the scope of the question and chose the ones that best benefitted the parameters measured for the specific study. SPADE and X-shift (435) were explored in **Paper I**, as the major focus here was to demonstrate the panel's phenotypic potential in cellular identification along with the detection of tumour dissociation effects. $\text{Arsinh}(x/5)$ transformed data analysed with the use of X-shift from Cytobank is a density-based clustering method. X-shift was selected due to its ability to quantify both the number of cell clusters and

to understand the diverse cell populations within a CyTOF dataset. Apart from the required computational background of the user, X-shift is very sensitive to the input cell number, and any comparison across experimental conditions must be first standardized based on cell numbers (356). When analysing the data set, different attempts to visualize the finding were done, e.g., with the use of SPADE (Figure 19), but, given that the quantification capacity was limited, we then switched to X-shift.

In **Paper I**, we evaluated the influence of six different tumour dissociation methods on single cell suspensions, therefore, as mentioned above, we had to carefully ensure that we included an equal number of cells from each of the dissociation methods from the respective patient samples to enable comparison of the dissociation effects on the single cells. In addition, X-shift has the capacity to delineate cell clusters of indeterminate phenotypes that are lacking the expression of a definitive lineage marker, which enabled us to identify a novel cancer stem-like population (reported in both **Paper I** and **Paper III**), expressing a range of phenotypic markers, such as CD24, EpCAM, CD133, CD34, CD47, CD4, and CD8. Finally, X-shift is not equipped with automated statistical analysis, which was a drawback. The FlowSOM and Astrolabe Cytometry Platform algorithms were applied on the other pan-tumour dataset (**Paper III**), as the aim here was to attain a comprehensive understanding of the heterogenous HGSOc TME landscape and to be able to identify possible clinical associations; hence, automatization of the statistical analyses was preferred. As illustrated and explained in more detail in **Paper III**, a higher number of cell clusters was identified with this clustering platform algorithm compared to the populations presented in **Paper I** (SPADE and X-shift algorithm).

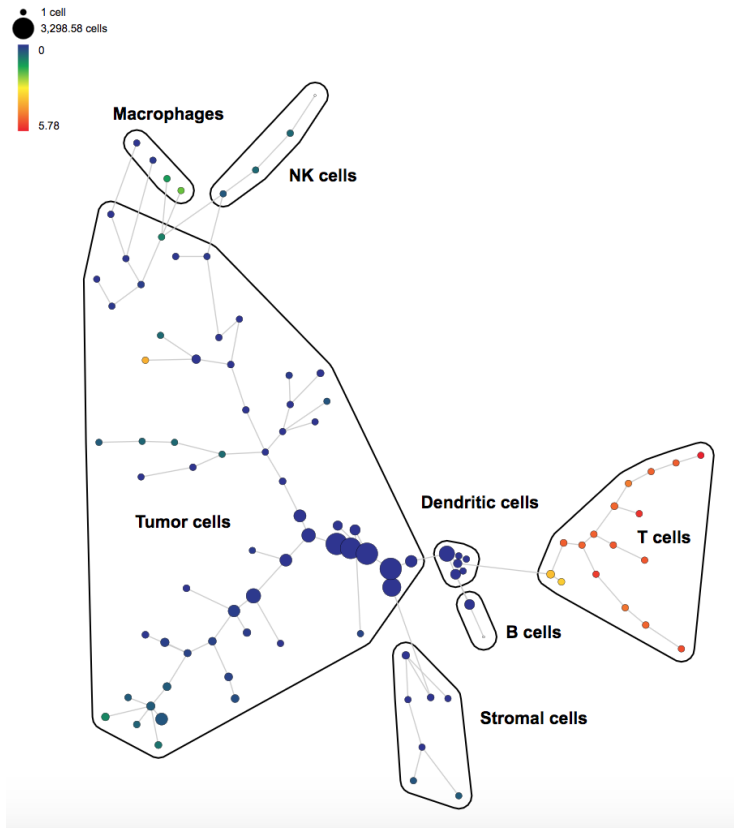


**Figure 18. SPADE illustration of the major cell lineages
(scaled by CD3 expression level)**

Different attempts were made to visualize the data in **Paper I**. Although the SPADE trees were able to provide a good overview of the major cell populations (Figure 19), since the actual experiments (Paper I) needed a much greater quantification capacity and higher characterisation resolution with actual event counts per cluster for evaluating the tumour dissociation effects, X-shift was chosen for the original publication (Paper I) (435).

As the major focus of **Papers II-III** was to gain a broader overview of the heterogenous HGSOC TME landscape and to identify possible clinical associations, Astrolabe Cytometry Platform was selected, as it enables both automated statistical analysis and data visualization tools. Astrolabe Cytometry Platform is, as mentioned, a recently

developed fully automated cloud-based analytics platform. During this work, we determined this is a user-friendly platform and does not require advanced computational skills to use. Cluster labelling, method implementation, statistical analysis, differential abundance analysis, and visualization were done through the automated pipeline. Although utilized in several benchmark publications and clinical trials, Astrolabe has been primarily used for the immunophenotyping of CyTOF data and lacks standardized clustering strategies for tumour or stromal cells (442, 452). However, with the inputs from the X-shift analysis from **Paper I**, we could customize the labelling strategies of the analysis pipeline for these tumour and stromal cell subsets. Although these issues are important to consider, the ability of the Astrolabe Cytometry Platform to more extensively delineate the TME than the X-shift alone provided new insights regarding the cellular complexity and phenotypic diversity of ovarian TME.

5.2 The identification of the HGSOc TME constitution by mass cytometry

As noted in paragraph 1.1.6, few molecular biomarkers have been integrated into clinical practice for HGSOc. Although the TME is not clearly defined and its plasticity is not fully understood, single-cell mass cytometry is a potent technique to reveal intratumour heterogeneity for HGSOc if the standardisation of the factors discussed in paragraph 5.1 are fulfilled. In addition to the establishment of the two mass cytometry panels, one of the main research priorities addressed in this thesis work has been to identify valuable phenotypic cell characteristics to profile single cells and recognize clinically relevant cell clusters.

The single-cell profiling performed with the use of the pan-tumour and pan-immune panels alone or combined and focusing on the abundance of cellular subsets disclosed the heterogeneous composition of the cellular components of the HGSOc TME (**Papers I-III**). Heterogeneity is an inherent feature of HGSOc tumours (paragraphs 1.1.2, 1.2.2 and 1.2.3), has been described at both the genomic and proteomic levels, and is believed to contribute to the poor outcome of this patient group (2, 25, 26, 266, 455). This

diversity is, for the most part, directed by copy number changes, the stem cell niche, and cellular plasticity (462). The interpatient heterogeneity identified through our single-cell analysis reveals new levels of phenotypic complexity in the HGSOC TME that can be added to the features already known. Intratumour heterogeneity also exists (2, 266). Studies including the profiling of multiple segments of the same tumour as well as metastases from different regions are therefore needed to provide additional insights at both the cellular and molecular levels, which is a result of the selective pressure exerted by distinctive cellular interactions within the tumour (402, 463, 464).

To decode the cellular complexity, the high-dimensional analysis platform X-shift and the Astrolabe algorithm were used, as described in paragraph 5.1.3. The cellular markers in both panels identified the main cell subsets through a labelling strategy applied by the Astrolabe platform (**Papers II-III**). Although the use of a pan-tumour profiling panel has its limitations, we were able to, in line with Casado et al., outline all the three main cellular subsets and distinguish the different patients' profiles in **Papers I and III**. Casado et al. showed that their profiling platform was able to recognize alternations in the cell constitution of the TME as the disease progresses (387). As illustrated and described in detail in **Paper III**, the FlowSOM analysis according to Astrolabe Cytometry Platform algorithms were able to detect more cell populations than when the SPADE and X-shift algorithms were used in **Paper I**. This again illustrates the importance of considering the scope of the question and the parameters measured as well as the data output of the study when selecting the analytic tools (356).

The use of more cell subset-dedicated panels has also been suggested to be one solution for increasing the depth of the phenotyping. In **Paper II**, when we used a more immune cell-focused panel, a high degree of interpatient heterogeneity was revealed for both the myeloid and lymphoid cell phenotypes. The HGSOC TiME is a strong determinant of the clinical outcome (465). To date, as mentioned, most studies have focused on the role of T cells, while analyses comprehensively describing different TME-compartments are missing (385, 386, 454). In our study (**Paper II**), cytotoxic CD8⁺ T cells that are able to attack tumour cells were present in three of 10 samples. The most

abundant cell clusters across the patient samples were conventional dendritic cells (DC), natural killer (NK) cells, and unassigned hematopoietic cells. In addition, several DC and monocyte cell subsets demonstrated associations with clinical features. However, the correlations with clinical features must be examined in larger clinical cohorts. With the use of the detailed single-cell profiling of the immune scenery within numerous lineages, it is our hope to obtain a better understanding of the complexity of the HGSOc TiME and, in this way, be able to recognize anti-tumour immune responses and develop novel immunotherapeutic strategies that match each patient's unique immune phenotype (see also paragraph 5.1.1).

Two of the CD56⁺ fibroblast subsets identified are negatively associated with PFS and OS, one of which expresses high levels of EpCAM while the other expresses FOLR1, while neither express α SMA or CD24. CAFs could exhibit both pro-tumorigenic, as in the case of myofibroblasts (α SMA expression), which are involved in wound healing and are linked to EOC progression and anti-tumorigenic effects in the TME (466, 467). To exemplify their anti-tumorigenic effects, inflammation-associated CAFs (FAP α expression) have been illustrated to be associated with immunosuppression in other solid tumour types (467). Similarly, Hornburg et al. recently presented specific compositions of T-cells and fibroblasts within immune-infiltrated and immune-excluded tumours (455). This highlights the importance of profiling the tumour, stromal, and immune (myeloid and lymphoid) lineage cells to understand both the biological complexity as well as the patients' suitability for immunotherapeutics.

The power of CyTOF to reveal the full heterogeneity of a biological specimen sample is restricted by the number of markers in a panel. When we combined different panels with the merging algorithms in **Paper III**, the complexity was extended due to both the increase in the identified cell subsets as well as the quantity and depth of the phenotypic characteristics (Table 7).

Table 7. An overview of the clinical associations

Clinical feature	Immune dataset (profiling level)	P value	FDR value	Associated cell subset			Merged dataset (assignment level)	P value	FDR value
				Tumor dataset (assignment level)	P value	FDR value			
OS	CD1c- CD141- dendritic cell (conventional) CD11clo HLA-DRlo CD163hi	6.98e-05	0.012	NK Cell	0.003355911	0.024610017	NK Cell (CD56+ CD16-)	9.3779E-05	0.00375118
	CD1c- CD141- dendritic cell (conventional) CD11chi HLA-DRlo	0.0002	0.019	CD4+ CD8+ T Cell	0.004734434	0.026039385	NKT Cell	0.00132735	0.01454865
				CD45- CD56- (EpCAM- FOLR1+ CD24+)	0.003219847	0.024610017	CD45- CD56- (EpCAM- FOLR1+ CD24+)	0.00145487	0.01454865
				CD45- CD56- (EpCAM- FOLR1+ CD24-)	0.001515254	0.024610017	Dendritic Cell (Plasmacytoid)	0.00464929	0.03502385
PFS	CD1c- CD141- dendritic cell (conventional) CD11clo HLA-DRlo CD163hi	6.98e-05	0.013	CD45- CD56- (EpCAM- FOLR1+ CD24-)	0.001515254	0.024610017	CD45- CD56- (EpCAM- FOLR1+ CD24+)	0.00145487	0.01454865
	CD1c- CD141- dendritic cell (conventional) CD11chi HLA-DRlo	0.0002	0.019	CD45- CD56- (EpCAM- FOLR1+ CD24+)	0.003219847	0.024610017	CD45- CD56- (EpCAM- FOLR1+ CD24+)	0.00464929	0.03502385
				NK Cell	0.003355911	0.024610017	NK Cell (CD56+ CD16-)	9.3779E-05	0.00375118
				CD4+ CD8+ T Cell	0.004734434	0.026039385	NKT Cell	0.00132735	0.01454865
Recurrence	CD1c- CD141- dendritic cell (conventional) CD11chi HLA-DRlo	7.74e-05	0.014	B Cell	0.006053995	0.133187884	NK Cell (CD56+ CD16-)	0.0017508	0.07003218
	Monocyte (CD14- CD16+) CD45ROlo CD86lo HLA-DRhi	0.0008	0.038				NKT Cell	0.00795685	0.15913701
	Dendritic cell [Type 1 CD141+] no profile	0.0008	0.038						
	Monocyte (CD14- CD16+) CD45ROhi CD86lo HLA-DRhi	0.0008	0.038						
Clinical status	Dendritic cell [Type 1 CD141+] no profile	3.31e-05	0.006				CD45- CD56- (EpCAM- FOLR1+ CD24+)	0.00025004	0.01000173
	CD1c- CD141- dendritic cell (conventional) CD11chi HLA-DRlo	0.0001	0.012				Dendritic Cell (Plasmacytoid)	0.00670012	0.07179445
	Monocyte (CD14- CD16+) CD45ROhi CD86lo HLA-DRhi	0.0007	0.037				NK Cell (CD56+ CD16-)	0.00709202	0.07179445
	Monocyte (CD14- CD16+) CD45ROlo CD86lo HLA-DRhi	0.0009	0.037				CM- unassigned	0.00794603	0.07179445
Tumor stage	CD4+ CD8+ T-cell CD141lo CD7hi CD86lo	0.0010	0.037				CM- HLA-DR+	0.00897431	0.07179445
	CD4+ CD8+ T-cell no profile	0.0015	0.046						
	CD1c- CD141- dendritic cell (conventional) CD11clo HLA-DRlo CD163hi	0.0001	0.024	CD45- CD56- (EpCAM+ FOLR1- CD24-)	0.000218168	0.004799694	CD45- CD56- (EpCAM+ FOLR1- CD24-)	0.00099218	0.03968712
				CD45- CD56- (EpCAM+ FOLR1+ CD24-)	0.001316907	0.014485974			
			CM- unassigned	0.006354754	0.046601531				

The eradication of CSCs is increasingly seen as a potential therapeutic avenue for improving survival rates in EOC patients. With the use of both panels alone and combined, we were able to identify some undescribed cell types CD45⁻CD56⁻(EpCAM⁻FOLR1⁻CD24⁻) and (CD45⁺HLA-DR⁺CD11c⁺CD33⁺) cells. Both the undefined cell types identified (**Papers I and III**) expressed some common markers (CD24, EpCAM, CD133, CD34, CD47). This finding was also in line with the data presented by Gonzalez et al. (384). Whether the specific rare cell phenotypes discovered represent possible targets for therapeutic intervention and/or disease surveillance must be examined further.

We acknowledged that the correlations between cell clusters with clinical features revealed in **Paper II** and **Paper III** are exploratory and should be interpreted with care mainly given the small-scale cohort size. Nevertheless, these observations might be hypothesis-generating.

The complex composition of the cell populations in the TME represents an important challenge to identify molecular makers for prognostication and the selection of therapy and has prevented effective cellular stratification. Similar complexity has been described for both transcriptional data and copy number abbreviations (4, 26, 30, 455). Despite the fact that the different signatures described in paragraph 1.1.2 are correlated

with different TME landscapes and clinical outcomes, this knowledge has still not been implemented into clinical practice (4, 25). Comprehensive high-dimensional profiling has the potential to substitute single-phenotype biomarker strategies and reveal an intricate network ready for therapeutic intervention. Nevertheless, the established panels (alone or combined) need further validation in a larger cohort presenting with more detailed clinical characteristics. Based on T-cell infiltration patterns, tumours are classified as immune infiltrated, excluded, or desert, which influences their response to cancer immunotherapies (119, 432, 468-470). Still, while different patterns for the enrichment of macrophages and fibroblasts have also been described, most studies have focused exclusively on the characterization of tumour-infiltrating T cells (385, 386, 454). Moreover, a systematic single-cell characterization of how other cell types in the TME shape the tumour immune phenotype is lacking (455).

6. Conclusions

The comprehensive molecular profiling of HGSOC has resulted in a more comprehensive understanding of the HGSOC pathogenesis. Although BRCA mutation and HRD testing are being integrated into wider clinical practice, most multi-dimensional efforts have not yet been able to identify biomarkers or profiles that have been translated into clinical strategies and can result in more individualized patient care. Through a translational biomedical research approach, this thesis has resulted in the generation of CyTOF panels for use alone or combined for the classification of cell populations and the identification of clinically relevant clusters as well as better insight into the biological intricacy of the HGSOC TME.

The following conclusions can be drawn:

1. Two novel ovarian TME-based CyTOF panels were established. They can be used for the profiling of all major cellular populations (tumour, stromal, immune) and delineate the lymphoid and myeloid cell lineages in detail, respectively (**Papers I and II**). Both panels are optimized for single-cell suspensions.
2. The use of the CyTOFmerge algorithm resulted in a more in-depth profiling of the cells, enabling us to identify both abundant as well as rare cell populations (**Paper III**).
3. The use of different tissue dissociation methods for generating single-cell suspensions influenced the expression of some lineage markers, while the manifestation of functional markers did not change (**Paper I**). However, the interpatient disparities were more significant than changes identified when different dissociation methods were used. As this represents a potential challenge for data acquisition, the results emphasise the importance of the careful planning of experimental pipelines.
4. Although heterogeneity is a well-known feature of HGSOC, the interpatient heterogeneity revealed by profiling with both panels alone or combined (**Paper I-III**) reveals a new level of complexity for the ovarian TME. This study improves

current understanding of the ovarian TME, rendering a broader characterisation of the immune, stromal, and tumour cells along with unprecedented depth.

5. Myeloid cells along with NK cells were the most abundant immune cells identified within the ovarian TME from the pan-immune panel (**Paper II**).
6. Dendritic cells and monocytes might have prognostic relevance in ovarian cancer (**Paper II**).

7. Future perspectives

HGSOC tumours are highly heterogeneous, and, in order to identify more effective prognostic and therapeutic biomarkers or profiles, a more comprehensive characterization of the TME is urgently required (4). The development of better and more reliable tools for deep-tissue profiling is necessary to both understand the biological complexity and to guide the future treatment of cancer (471). Mass cytometry is a novel proteomic platform for high-dimensional phenotypic and functional analysis of single cells (472). It has the potential to intensely portray the diverse and intricate TME and stratify patients by combining high-plex information with clinical information while forecasting the sensitivity to targeted, personalize treatment (451, 458). The comprehensive approach used in this thesis by analysing single-cell suspensions of HGSOC tumour tissue can be used to identify heterogeneity, phenotypic signatures, and profiles as well as specific cell clusters. The use of single-cell suspensions, which require streamlined standardization, represents a limitation that might be overcome by the introduction of imaging mass cytometry (418). If high-plex data can also be fused with mass cytometry information regarding the check-point inhibitor profile, the applicability can be increased and result in new biomarker-based patient-centric treatment stratification that hopefully will improve the prognosis for HGSOC patients.

As already mentioned, the HGSOC milieu is unique, and profiling the TME in terms of all the tumour elements—including the primary tumour, ascites fluid, and metastases—will be of importance for better understanding intrapatient heterogeneity and clonality as well as the development of therapy resistance (2, 266). Together this would provide a complete overview of the individual patient's TME, a dynamic entity, and the crucial orchestrator of ovarian tumour progression (119, 432).

We are entering a new era of single-cell data generation and other high-throughput omics platforms, such as genomic cytometry (e.g., scRNA-seq), are also being implemented (455). Combined, they will provide a much greater variability of diverse biological entities, with the hope of generating wide-ranging profile atlases and

machine learning algorithms (in software) that can also support clinical decision making for patients with HGSOC.

8. References

1. Lisio M-A, Fu L, Goyeneche A, Gao Z-H, Telleria C. High-Grade Serous Ovarian Cancer: Basic Sciences, Clinical and Therapeutic Standpoints. *International journal of molecular sciences*. 2019;20(4):952.
2. Jiménez-Sánchez A, Memon D, Pourpe S, Veeraraghavan H, Li Y, Vargas HA, et al. Heterogeneous Tumor-Immune Microenvironments among Differentially Growing Metastases in an Ovarian Cancer Patient. *Cell*. 2017;170(5):927-38.e20.
3. Cancer MOYsSaSBiO, SOLO-1 -YF-uo.
4. Bowtell DD, Böhm S, Ahmed AA, Aspuria PJ, Bast RC, Jr., Beral V, et al. Rethinking ovarian cancer II: reducing mortality from high-grade serous ovarian cancer. *Nat Rev Cancer*. 2015;15(11):668-79.
5. Bowtell DD, Böhm S, Ahmed AA, Aspuria P-J, Bast RC, Jr., Beral V, et al. Rethinking ovarian cancer II: reducing mortality from high-grade serous ovarian cancer. *Nature reviews Cancer*. 2015;15(11):668-79.
6. Lisio MA, Fu L, Goyeneche A, Gao ZH, Telleria C. High-Grade Serous Ovarian Cancer: Basic Sciences, Clinical and Therapeutic Standpoints. *Int J Mol Sci*. 2019;20(4).
7. Cancer Registry of Norway. Cancer in Norway 2019 - Cancer incidence m, survival and prevalence in, Norway.
8. Takiar R. Status of Ovarian Cancer in India (2012-14). 2019.
9. Torre LA, Trabert B, DeSantis CE, Miller KD, Samimi G, Runowicz CD, et al. Ovarian cancer statistics, 2018. *CA: A Cancer Journal for Clinicians*. 2018;68(4):284-96.
10. Papa A, Caruso D, Strudel M, Tomao S, Tomao F. Update on Poly-ADP-ribose polymerase inhibition for ovarian cancer treatment. *Journal of translational medicine*. 2016;14(1):267.
11. Kurman RJ, Shih Ie M. The Dualistic Model of Ovarian Carcinogenesis: Revisited, Revised, and Expanded. *Am J Pathol*. 2016;186(4):733-47.
12. Prat J. New insights into ovarian cancer pathology. *Annals of Oncology*. 2012;23:x111-x7.
13. Bergsten TM, Burdette JE, Dean M. Fallopian tube initiation of high grade serous ovarian cancer and ovarian metastasis: Mechanisms and therapeutic implications. *Cancer Letters*. 2020;476:152-60.
14. Savant SS, Sriramkumar S, O'Hagan HM. The role of inflammation and inflammatory mediators in the development, progression, metastasis, and chemoresistance of epithelial ovarian cancer. *Cancers*. 2018;10(8):251.
15. Néné NR, Reisel D, Leimbach A, Franchi D, Jones A, Evans I, et al. Association between the cervicovaginal microbiome, *BRCA1* mutation status, and risk of ovarian cancer: a case-control study. *The Lancet Oncology*. 2019;20(8):1171-82.
16. Loret N, Denys H, Tummers P, Berx G. The Role of Epithelial-to-Mesenchymal Plasticity in Ovarian Cancer Progression and Therapy Resistance. *Cancers (Basel)*. 2019;11(6).
17. Jarboe E, Folkins A, Nucci MR, Kindelberger D, Drapkin R, Miron A, et al. Serous Carcinogenesis in the Fallopian Tube: A Descriptive Classification. *International Journal of Gynecological Pathology*. 2008;27(1):1-9.

18. Löhmußaar K, Kopper O, Korving J, Begthel H, Vreuls CPH, van Es JH, et al. Assessing the origin of high-grade serous ovarian cancer using CRISPR-modification of mouse organoids. *Nat Commun.* 2020;11(1):2660.
19. Dean M, Davis DA, Burdette JE. Activin A stimulates migration of the fallopian tube epithelium, an origin of high-grade serous ovarian cancer, through non-canonical signaling. *Cancer Lett.* 2017;391:114-24.
20. Feeley K, Wells M. Precursor lesions of ovarian epithelial malignancy. *Histopathology.* 2001;38(2):87-95.
21. Tan DS, Agarwal R, Kaye SB. Mechanisms of transcoelomic metastasis in ovarian cancer. *Lancet Oncol.* 2006;7(11):925-34.
22. Ford CE, Werner B, Hacker NF, Warton K. The untapped potential of ascites in ovarian cancer research and treatment. *British Journal of Cancer.* 2020;123(1):9-16.
23. Al Habyan S, Kalos C, Szymborski J, McCaffrey L. Multicellular detachment generates metastatic spheroids during intra-abdominal dissemination in epithelial ovarian cancer. *Oncogene.* 2018;37(37):5127-35.
24. El Bairi K, Al Jarroudi O, Le Page C, Afqir S. Does the “Devil” originate from the fallopian tubes? *Seminars in Cancer Biology.* 2021.
25. Integrated genomic analyses of ovarian carcinoma. *Nature.* 2011;474(7353):609-15.
26. Macintyre G, Goranova TE, De Silva D, Ennis D, Piskorz AM, Eldridge M, et al. Copy number signatures and mutational processes in ovarian carcinoma. *Nat Genet.* 2018;50(9):1262-70.
27. Ledermann J, Harter P, Gourley C, Friedlander M, Vergote I, Rustin G, et al. Olaparib maintenance therapy in platinum-sensitive relapsed ovarian cancer. *N Engl J Med.* 2012;366(15):1382-92.
28. Mukherjee S, Phadte P, Mehrotra M, Ray P. Plasticity in Ovarian Cancer: The Molecular Underpinnings and Phenotypic Heterogeneity. *Journal of the Indian Institute of Science.* 2020;100(3):537-53.
29. Miller RE, Leary A, Scott CL, Serra V, Lord CJ, Bowtell D, et al. ESMO recommendations on predictive biomarker testing for homologous recombination deficiency and PARP inhibitor benefit in ovarian cancer. *Annals of Oncology.* 2020.
30. Verhaak RG, Tamayo P, Yang JY, Hubbard D, Zhang H, Creighton CJ, et al. Prognostically relevant gene signatures of high-grade serous ovarian carcinoma. *J Clin Invest.* 2013;123(1):517-25.
31. Pinto R, Assis J, Nogueira A, Pereira C, Pereira D, Medeiros R. Rethinking ovarian cancer genomics: where genome-wide association studies stand? *Pharmacogenomics.* 2017;18(17):1611-25.
32. Lheureux S, Gourley C, Vergote I, Oza AM. Epithelial ovarian cancer. *The Lancet.* 2019;393(10177):1240-53.
33. Tothill RW, Tinker AV, George J, Brown R, Fox SB, Lade S, et al. Novel molecular subtypes of serous and endometrioid ovarian cancer linked to clinical outcome. *Clin Cancer Res.* 2008;14(16):5198-208.
34. Millstein J, Budden T, Goode EL, Anglesio MS, Talhouk A, Intermaggio MP, et al. Prognostic gene expression signature for high-grade serous ovarian cancer. *Annals of Oncology.* 2020;31(9):1240-50.

35. Lancaster JM, Powell CB, Kauff ND, Cass I, Chen LM, Lu KH, et al. Society of Gynecologic Oncologists Education Committee statement on risk assessment for inherited gynecologic cancer predispositions. *Gynecol Oncol.* 2007;107(2):159-62.
36. Song H, Dicks E, Ramus SJ, Tyrer JP, Intermaggio MP, Hayward J, et al. Contribution of Germline Mutations in the RAD51B, RAD51C, and RAD51D Genes to Ovarian Cancer in the Population. *J Clin Oncol.* 2015;33(26):2901-7.
37. Ramus SJ, Song H, Dicks E, Tyrer JP, Rosenthal AN, Intermaggio MP, et al. Germline Mutations in the BRIP1, BARD1, PALB2, and NBN Genes in Women With Ovarian Cancer. *J Natl Cancer Inst.* 2015;107(11).
38. Norquist BM, Harrell MI, Brady MF, Walsh T, Lee MK, Gulsuner S, et al. Inherited mutations in women with ovarian carcinoma. *JAMA oncology.* 2016;2(4):482-90.
39. Ketabi Z, Bartuma K, Bernstein I, Malander S, Grönberg H, Björck E, et al. Ovarian cancer linked to Lynch syndrome typically presents as early-onset, non-serous epithelial tumors. *Gynecologic oncology.* 2011;121(3):462-5.
40. Hunn J, Rodriguez GC. Ovarian cancer: etiology, risk factors, and epidemiology. *Clin Obstet Gynecol.* 2012;55(1):3-23.
41. Webb PM, Jordan SJ. Epidemiology of epithelial ovarian cancer. *Best Pract Res Clin Obstet Gynaecol.* 2017;41:3-14.
42. Vargas AN. Natural history of ovarian cancer. *Ecancermedalscience.* 2014;8:465.
43. Tomao F, Lo Russo G, Spinelli GP, Stati V, Prete AA, Prinzi N, et al. Fertility drugs, reproductive strategies and ovarian cancer risk. *J Ovarian Res.* 2014;7:51.
44. Goff BA, Mandel LS, Drescher CW, Urban N, Gough S, Schurman KM, et al. Development of an ovarian cancer symptom index: possibilities for earlier detection. *Cancer.* 2007;109(2):221-7.
45. Hoskins WJ. Principles and practice of gynecologic oncology: Lippincott Williams & Wilkins; 2005.
46. Sørensen SS, Mosgaard BJ. Combination of cancer antigen 125 and carcinoembryonic antigen can improve ovarian cancer diagnosis. *Dan Med Bull.* 2011;58(11):A4331.
47. Montagnana M, Benati M, Danese E. Circulating biomarkers in epithelial ovarian cancer diagnosis: from present to future perspective. *Ann Transl Med.* 2017;5(13):276.
48. Zivanovic O, Sima CS, Iasonos A, Bell-McGuinn KM, Sabbatini PJ, Leitao MM, et al. Exploratory analysis of serum CA-125 response to surgery and the risk of relapse in patients with FIGO stage IIIC ovarian cancer. *Gynecol Oncol.* 2009;115(2):209-14.
49. Mutch DG, Prat J. 2014 FIGO staging for ovarian, fallopian tube and peritoneal cancer. *Gynecologic Oncology.* 2014;133(3):401-4.
50. Cancer Registry of Norway. Cancer in Norway 2018 - Cancer incidence, survival and prevalence in, Norway. Oslo: Cancer Registry of Norway.
51. du Bois A, Reuss A, Pujade-Lauraine E, Harter P, Ray-Coquard I, Pfisterer J. Role of surgical outcome as prognostic factor in advanced epithelial ovarian cancer: a combined exploratory analysis of 3 prospectively randomized phase 3 multicenter trials: by the Arbeitsgemeinschaft Gynaekologische Onkologie Studiengruppe

- Ovarialkarzinom (AGO-OVAR) and the Groupe d'Investigateurs Nationaux Pour les Etudes des Cancers de l'Ovaire (GINECO). *Cancer*. 2009;115(6):1234-44.
52. Sundar S, Neal RD, Kehoe S. Diagnosis of ovarian cancer. *BMJ : British Medical Journal*. 2015;351:h4443.
53. du Bois A, Quinn M, Thigpen T, Vermorken J, Avall-Lundqvist E, Bookman M, et al. 2004 consensus statements on the management of ovarian cancer: final document of the 3rd International Gynecologic Cancer Intergroup Ovarian Cancer Consensus Conference (GCIG OCCC 2004). *Ann Oncol*. 2005;16 Suppl 8:viii7-viii12.
54. Vergote I, Tropé CG, Amant F, Kristensen GB, Ehlen T, Johnson N, et al. Neoadjuvant Chemotherapy or Primary Surgery in Stage IIIC or IV Ovarian Cancer. *New England Journal of Medicine*. 2010;363(10):943-53.
55. Vaughan S, Coward JI, Bast RC, Jr., Berchuck A, Berek JS, Brenton JD, et al. Rethinking ovarian cancer: recommendations for improving outcomes. *Nat Rev Cancer*. 2011;11(10):719-25.
56. Perren TJ, Swart AM, Pfisterer J, Ledermann JA, Pujade-Lauraine E, Kristensen G, et al. A Phase 3 Trial of Bevacizumab in Ovarian Cancer. *New England Journal of Medicine*. 2011;365(26):2484-96.
57. Moore K, Colombo N, Scambia G, Kim B-G, Oaknin A, Friedlander M, et al. Maintenance Olaparib in Patients with Newly Diagnosed Advanced Ovarian Cancer. *New England Journal of Medicine*. 2018;379(26):2495-505.
58. Giornelli GH. Management of relapsed ovarian cancer: a review. *Springerplus*. 2016;5(1):1197.
59. Griffiths CT. Surgical resection of tumor bulk in the primary treatment of ovarian carcinoma. *Natl Cancer Inst Monogr*. 1975;42:101-4.
60. Garg PK, Kumar R, Choudhary D. Cytoreductive or debulking surgery in ovarian cancer: The name does matter! *Journal of surgical oncology*. 2021.
61. Harter P, Muallem ZM, Buhrmann C, Lorenz D, Kaub C, Hils R, et al. Impact of a structured quality management program on surgical outcome in primary advanced ovarian cancer. *Gynecol Oncol*. 2011;121(3):615-9.
62. Torres D, Wang C, Kumar A, Bakkum-Gamez JN, Weaver AL, McGree ME, et al. Factors that influence survival in high-grade serous ovarian cancer: A complex relationship between molecular subtype, disease dissemination, and operability. *Gynecologic Oncology*. 2018;150(2):227-32.
63. van Meurs HS, Tajik P, Hof MH, Vergote I, Kenter GG, Mol BW, et al. Which patients benefit most from primary surgery or neoadjuvant chemotherapy in stage IIIC or IV ovarian cancer? An exploratory analysis of the European Organisation for Research and Treatment of Cancer 55971 randomised trial. *Eur J Cancer*. 2013;49(15):3191-201.
64. Gharpure KM, Pradeep S, Sans M, Rupaimoole R, Ivan C, Wu SY, et al. FABP4 as a key determinant of metastatic potential of ovarian cancer. *Nat Commun*. 2018;9(1):2923.
65. Reuss A, du Bois A, Harter P, Fotopoulou C, Sehouli J, Aletti G, et al. TRUST: Trial of Radical Upfront Surgical Therapy in advanced ovarian cancer (ENGOT ov33/AGO-OVAR OP7). *Int J Gynecol Cancer*. 2019;29(8):1327-31.

-
66. Harter P, Sehouli J, Lorusso D, Reuss A, Vergote I, Marth C, et al. A Randomized Trial of Lymphadenectomy in Patients with Advanced Ovarian Neoplasms. *New England Journal of Medicine*. 2019;380(9):822-32.
 67. du Bois A, Rochon J, Pfisterer J, Hoskins WJ. Variations in institutional infrastructure, physician specialization and experience, and outcome in ovarian cancer: a systematic review. *Gynecol Oncol*. 2009;112(2):422-36.
 68. Chiofalo B, Bruni S, Certelli C, Sperduti I, Baiocco E, Vizza E. Primary debulking surgery vs. interval debulking surgery for advanced ovarian cancer: review of the literature and meta-analysis. *Minerva Med*. 2019;110(4):330-40.
 69. Tipirneni KE, Warram JM, Moore LS, Prince AC, de Boer E, Jani AH, et al. Oncologic Procedures Amenable to Fluorescence-guided Surgery. *Ann Surg*. 2017;266(1):36-47.
 70. van Dam GM, Themelis G, Crane LM, Harlaar NJ, Pleijhuis RG, Kelder W, et al. Intraoperative tumor-specific fluorescence imaging in ovarian cancer by folate receptor- α targeting: first in-human results. *Nat Med*. 2011;17(10):1315-9.
 71. Kleinmanns K, Bischof K, Anandan S, Popa M, Akslen LA, Fosse V, et al. CD24-targeted fluorescence imaging in patient-derived xenograft models of high-grade serous ovarian carcinoma. *EBioMedicine*. 2020;56.
 72. Bois AD, Vergote I, Ferron G, Reuss A, Meier W, Greggi S, et al. Randomized controlled phase III study evaluating the impact of secondary cytoreductive surgery in recurrent ovarian cancer: AGO DESKTOP III/ENGOT ov20. *Journal of Clinical Oncology*. 2017;35(15_suppl):5501-.
 73. Bois AD, Sehouli J, Vergote I, Ferron G, Reuss A, Meier W, et al. Randomized phase III study to evaluate the impact of secondary cytoreductive surgery in recurrent ovarian cancer: Final analysis of AGO DESKTOP III/ENGOT-ov20. 2020;38(15_suppl):6000-.
 74. Shi T, Zhu J, Feng Y, Tu D, Zhang Y, Zhang P, et al. Secondary cytoreduction followed by chemotherapy versus chemotherapy alone in platinum-sensitive relapsed ovarian cancer (SOC-1): a multicentre, open-label, randomised, phase 3 trial. *Lancet Oncol*. 2021;22(4):439-49.
 75. Munkarah AR, Coleman RL. Critical evaluation of secondary cytoreduction in recurrent ovarian cancer. *Gynecol Oncol*. 2004;95(2):273-80.
 76. Kucukmetin A, Naik R, Galaal K, Bryant A, Dickinson HO. Palliative surgery versus medical management for bowel obstruction in ovarian cancer. *Cochrane Database Syst Rev*. 2010;2010(7):Cd007792.
 77. Colombo N, Pecorelli S. What have we learned from ICON1 and ACTION? *International Journal of Gynecologic Cancer*. 2003;13(Suppl 2):140-3.
 78. Etemadmoghadam D, deFazio A, Beroukhi R, Mermel C, George J, Getz G, et al. Integrated genome-wide DNA copy number and expression analysis identifies distinct mechanisms of primary chemoresistance in ovarian carcinomas. *Clin Cancer Res*. 2009;15(4):1417-27.
 79. Burger RA, Brady MF, Bookman MA, Fleming GF, Monk BJ, Huang H, et al. Incorporation of Bevacizumab in the Primary Treatment of Ovarian Cancer. *New England Journal of Medicine*. 2011;365(26):2473-83.
 80. Ray-Coquard IL, Harter P, Martin AG, Cropet C, Pignata S, Fujiwara K, et al. PAOLA-1: An ENGOT/GCIG phase III trial of olaparib versus placebo combined with

bevacizumab as maintenance treatment in patients with advanced ovarian cancer following first-line platinum-based chemotherapy plus bevacizumab. *Journal of Clinical Oncology*. 2017;35(15_suppl):TPS5605-TPS.

81. Glajzer J, Grabowski JP, Sehouli J, Pfisterer J. Recurrent Treatment in Ovarian Cancer Patients: What Are the Best Regimens and the Order They Should Be Given? *Curr Treat Options Oncol*. 2020;21(6):49.

82. Mirza MR, Coleman RL, González-Martín A, Moore KN, Colombo N, Ray-Coquard I, et al. The forefront of ovarian cancer therapy: update on PARP inhibitors. *Annals of Oncology*. 2020;31(9):1148-59.

83. Aghajanian C, Blank SV, Goff BA, Judson PL, Teneriello MG, Husain A, et al. OCEANS: a randomized, double-blind, placebo-controlled phase III trial of chemotherapy with or without bevacizumab in patients with platinum-sensitive recurrent epithelial ovarian, primary peritoneal, or fallopian tube cancer. *J Clin Oncol*. 2012;30(17):2039-45.

84. Coleman RL, Brady MF, Herzog TJ, Sabbatini P, Armstrong DK, Walker JL, et al. Bevacizumab and paclitaxel-carboplatin chemotherapy and secondary cytoreduction in recurrent, platinum-sensitive ovarian cancer (NRG Oncology/Gynecologic Oncology Group study GOG-0213): a multicentre, open-label, randomised, phase 3 trial. *Lancet Oncol*. 2017;18(6):779-91.

85. Pujade-Lauraine E, Ledermann JA, Selle F, GebSKI V, Penson RT, Oza AM, et al. Olaparib tablets as maintenance therapy in patients with platinum-sensitive, relapsed ovarian cancer and a BRCA1/2 mutation (SOLO2/ENGOT-Ov21): a double-blind, randomised, placebo-controlled, phase 3 trial. *Lancet Oncol*. 2017;18(9):1274-84.

86. Pujade-Lauraine E, Hilpert F, Weber B, Reuss A, Poveda A, Kristensen G, et al. Bevacizumab combined with chemotherapy for platinum-resistant recurrent ovarian cancer: The AURELIA open-label randomized phase III trial. *J Clin Oncol*. 2014;32(13):1302-8.

87. Ledermann JA, Harter P, Gourley C, Friedlander M, Vergote I, Rustin G, et al. Overall survival in patients with platinum-sensitive recurrent serous ovarian cancer receiving olaparib maintenance monotherapy: an updated analysis from a randomised, placebo-controlled, double-blind, phase 2 trial. *Lancet Oncol*. 2016;17(11):1579-89.

88. Mirza MR, Monk BJ, Herrstedt J, Oza AM, Mahner S, Redondo A, et al. Niraparib Maintenance Therapy in Platinum-Sensitive, Recurrent Ovarian Cancer. *New England Journal of Medicine*. 2016;375(22):2154-64.

89. Hanahan D, Weinberg RA. Hallmarks of cancer: the next generation. *Cell*. 2011;144(5):646-74.

90. Hanahan D, Weinberg RA. The hallmarks of cancer. *Cell*. 2000;100(1):57-70.

91. Graybill W, Sood AK, Monk BJ, Coleman RL. State of the science: Emerging therapeutic strategies for targeting angiogenesis in ovarian cancer. *Gynecol Oncol*. 2015;138(2):223-6.

92. Oza AM, Cook AD, Pfisterer J, Embleton A, Ledermann JA, Pujade-Lauraine E, et al. Standard chemotherapy with or without bevacizumab for women with newly diagnosed ovarian cancer (ICON7): overall survival results of a phase 3 randomised trial. *The Lancet Oncology*. 2015;16(8):928-36.

-
93. Birrer MJ, Choi Y, Brady MF, Mannel RS, Burger RA, WEI W, et al. Retrospective analysis of candidate predictive tumor biomarkers (BMs) for efficacy in the GOG-0218 trial evaluating front-line carboplatin–paclitaxel (CP) ± bevacizumab (BEV) for epithelial ovarian cancer (EOC). *Journal of Clinical Oncology*. 2015;33(15_suppl):5505-.
 94. Ruscito I, Cacsire Castillo-Tong D, Vergote I, Ignat I, Stanske M, Vanderstichele A, et al. Characterisation of tumour microvessel density during progression of high-grade serous ovarian cancer: clinico-pathological impact (an OCTIPS Consortium study). *Br J Cancer*. 2018;119(3):330-8.
 95. Petrillo M, Nero C, Amadio G, Gallo D, Fagotti A, Scambia G. Targeting the hallmarks of ovarian cancer: The big picture. *Gynecol Oncol*. 2016;142(1):176-83.
 96. du Bois A, Kristensen G, Ray-Coquard I, Reuss A, Pignata S, Colombo N, et al. Standard first-line chemotherapy with or without nintedanib for advanced ovarian cancer (AGO-OVAR 12): a randomised, double-blind, placebo-controlled phase 3 trial. *Lancet Oncol*. 2016;17(1):78-89.
 97. Vergote I, Hanker LC, Floquet A, Rau J, Kim J-W, Izquierdo EO, et al. AGO-OVAR 16: A phase III study to evaluate the efficacy and safety of pazopanib (PZ) monotherapy versus placebo in women who have not progressed after first line chemotherapy for epithelial ovarian, fallopian tube, or primary peritoneal cancer—Overall survival (OS) results. 2018;36(15_suppl):5518-.
 98. Pujade-Lauraine E. New treatments in ovarian cancer. *Ann Oncol*. 2017;28(suppl_8):viii57-viii60.
 99. Turner N, Tutt A, Ashworth A. Hallmarks of 'BRCAness' in sporadic cancers. *Nature Reviews Cancer*. 2004;4(10):814-9.
 100. Lord CJ, Ashworth A. BRCAness revisited. *Nat Rev Cancer*. 2016;16(2):110-20.
 101. Franzese E, Centonze S, Diana A, Carlino F, Guerrera LP, Di Napoli M, et al. PARP inhibitors in ovarian cancer. *Cancer Treatment Reviews*. 2019;73:1-9.
 102. Murai J, Huang S-yN, Das BB, Renaud A, Zhang Y, Doroshow JH, et al. Trapping of PARP1 and PARP2 by Clinical PARP Inhibitors. *Cancer Research*. 2012;72(21):5588-99.
 103. Coleman RL, Oza AM, Lorusso D, Aghajanian C, Oaknin A, Dean A, et al. Rucaparib maintenance treatment for recurrent ovarian carcinoma after response to platinum therapy (ARIEL3): a randomised, double-blind, placebo-controlled, phase 3 trial. *The Lancet*. 2017;390(10106):1949-61.
 104. Mirza MR, Ávall Lundqvist E, Birrer MJ, dePont Christensen R, Nyvang GB, Malander S, et al. Niraparib plus bevacizumab versus niraparib alone for platinum-sensitive recurrent ovarian cancer (NSGO-AVANOVA2/ENGOT-ov24): a randomised, phase 2, superiority trial. *Lancet Oncol*. 2019;20(10):1409-19.
 105. Liu JF, Barry WT, Birrer M, Lee JM, Buckanovich RJ, Fleming GF, et al. Overall survival and updated progression-free survival outcomes in a randomized phase II study of combination cediranib and olaparib versus olaparib in relapsed platinum-sensitive ovarian cancer. *Ann Oncol*. 2019;30(4):551-7.
 106. Jackson SP, Bartek J. The DNA-damage response in human biology and disease. *Nature*. 2009;461(7267):1071-8.

107. Maréchal A, Zou L. DNA damage sensing by the ATM and ATR kinases. *Cold Spring Harb Perspect Biol.* 2013;5(9).
108. Pearl LH, Schierz AC, Ward SE, Al-Lazikani B, Pearl FM. Therapeutic opportunities within the DNA damage response. *Nat Rev Cancer.* 2015;15(3):166-80.
109. Corcoran NM, Clarkson MJ, Stuchbery R, Hovens CM. Molecular Pathways: Targeting DNA Repair Pathway Defects Enriched in Metastasis. *Clin Cancer Res.* 2016;22(13):3132-7.
110. Blackford AN, Jackson SP. ATM, ATR, and DNA-PK: The Trinity at the Heart of the DNA Damage Response. *Mol Cell.* 2017;66(6):801-17.
111. Harper JW, Elledge SJ. The DNA damage response: ten years after. *Mol Cell.* 2007;28(5):739-45.
112. Färkkilä A, Gulhan DC, Casado J, Jacobson CA, Nguyen H, Kochupurakkal B, et al. Immunogenomic profiling determines responses to combined PARP and PD-1 inhibition in ovarian cancer. *Nat Commun.* 2020;11(1):1459.
113. Biomarkers and surrogate endpoints: preferred definitions and conceptual framework. *Clin Pharmacol Ther.* 2001;69(3):89-95.
114. Eagle K, Ledermann JA. Tumor markers in ovarian malignancies. *Oncologist.* 1997;2(5):324-9.
115. Vergote I, Banerjee S, Gerdes AM, van Asperen C, Marth C, Vaz F, et al. Current perspectives on recommendations for BRCA genetic testing in ovarian cancer patients. *Eur J Cancer.* 2016;69:127-34.
116. Patch A-M, Christie EL, Etemadmoghadam D, Garsed DW, George J, Fereday S, et al. Whole-genome characterization of chemoresistant ovarian cancer. *Nature.* 2015;521(7553):489-94.
117. Taube JM, Klein A, Brahmer JR, Xu H, Pan X, Kim JH, et al. Association of PD-1, PD-1 ligands, and other features of the tumor immune microenvironment with response to anti-PD-1 therapy. *Clin Cancer Res.* 2014;20(19):5064-74.
118. Ghisoni E, Imbimbo M, Zimmermann S, Valabrega G. Ovarian Cancer Immunotherapy: Turning up the Heat. *Int J Mol Sci.* 2019;20(12).
119. Baci D, Bosi A, Gallazzi M, Rizzi M, Noonan DM, Poggi A, et al. The Ovarian Cancer Tumor Immune Microenvironment (TIME) as Target for Therapy: A Focus on Innate Immunity Cells as Therapeutic Effectors. *Int J Mol Sci.* 2020;21(9).
120. Horowitz M, Esakov E, Rose P, Reizes O. Signaling within the epithelial ovarian cancer tumor microenvironment: the challenge of tumor heterogeneity. *Ann Transl Med.* 2020;8(14):905.
121. Ahmed N, Escalona R, Leung D, Chan E, Kannourakis G, editors. Tumour microenvironment and metabolic plasticity in cancer and cancer stem cells: Perspectives on metabolic and immune regulatory signatures in chemoresistant ovarian cancer stem cells. *Seminars in cancer biology*; 2018: Elsevier.
122. Geistlinger L, Oh S, Ramos M, Schiffer L, LaRue RS, Henzler CM, et al. Multiomic Analysis of Subtype Evolution and Heterogeneity in High-Grade Serous Ovarian Carcinoma. *Cancer Res.* 2020.
123. Varas-Godoy M, Rice G, Illanes SE. The Crosstalk between Ovarian Cancer Stem Cell Niche and the Tumor Microenvironment. *Stem Cells International.* 2017;2017:5263974.

-
124. Jiang Y, Wang C, Zhou S. Targeting tumor microenvironment in ovarian cancer: Premise and promise. *Biochimica et Biophysica Acta (BBA) - Reviews on Cancer*. 2020;1873(2):188361.
 125. Motohara T, Masuda K, Morotti M, Zheng Y, El-Sahhar S, Chong KY, et al. An evolving story of the metastatic voyage of ovarian cancer cells: cellular and molecular orchestration of the adipose-rich metastatic microenvironment. *Oncogene*. 2019;38(16):2885-98.
 126. Yousefi M, Dehghani S, Nosrati R, Ghanei M, Salmaninejad A, Rajaie S, et al. Current insights into the metastasis of epithelial ovarian cancer - hopes and hurdles. *Cellular Oncology*. 2020;43(4):515-38.
 127. Pradeep S, Kim SW, Wu SY, Nishimura M, Chaluvally-Raghavan P, Miyake T, et al. Hematogenous metastasis of ovarian cancer: rethinking mode of spread. *Cancer Cell*. 2014;26(1):77-91.
 128. Ahmed N, Kadife E, Raza A, Short M, Jubinsky PT, Kannourakis G. Ovarian Cancer, Cancer Stem Cells and Current Treatment Strategies: A Potential Role of Magmas in the Current Treatment Methods. *Cells*. 2020;9(3).
 129. Yang Y, Yang Y, Yang J, Zhao X, Wei X. Tumor Microenvironment in Ovarian Cancer: Function and Therapeutic Strategy. *Frontiers in Cell and Developmental Biology*. 2020;8(758).
 130. Gourley C, Miller RE, Hollis RL, Ledermann JA. Role of Poly (ADP-Ribose) Polymerase inhibitors beyond BReast CAncer Gene-mutated ovarian tumours: definition of homologous recombination deficiency? *Curr Opin Oncol*. 2020;32(5):442-50.
 131. Tayama S, Motohara T, Narantuya D, Li C, Fujimoto K, Sakaguchi I, et al. The impact of EpCAM expression on response to chemotherapy and clinical outcomes in patients with epithelial ovarian cancer. *Oncotarget*. 2017;8(27):44312-25.
 132. Ledermann JA, Canevari S, Thigpen T. Targeting the folate receptor: diagnostic and therapeutic approaches to personalize cancer treatments. *Annals of Oncology*. 2015;26(10):2034-43.
 133. Murad JP, Kozłowska AK, Lee HJ, Ramamurthy M, Chang W-C, Yazaki P, et al. Effective Targeting of TAG72+ Peritoneal Ovarian Tumors via Regional Delivery of CAR-Engineered T Cells. *Frontiers in Immunology*. 2018;9(2268).
 134. Hatina J, Boesch M, Sopper S, Kripnerova M, Wolf D, Reimer D, et al. Ovarian Cancer Stem Cell Heterogeneity. *Adv Exp Med Biol*. 2019;1139:201-21.
 135. Lupia M, Cavallaro U. Ovarian cancer stem cells: still an elusive entity? *Molecular Cancer*. 2017;16(1):64.
 136. Behera A, Ashraf R, Srivastava AK, Kumar S. Bioinformatics analysis and verification of molecular targets in ovarian cancer stem-like cells. *Heliyon*. 2020;6(9):e04820.
 137. Muñoz-Galván S, Carnero A. Targeting Cancer Stem Cells to Overcome Therapy Resistance in Ovarian Cancer. *Cells*. 2020;9(6).
 138. F Quail D, J Taylor M, Postovit L-M. Microenvironmental regulation of cancer stem cell phenotypes. *Current stem cell research & therapy*. 2012;7(3):197-216.
 139. Chaffer CL, Weinberg RA. How does multistep tumorigenesis really proceed? *Cancer discovery*. 2015;5(1):22-4.

140. Alvero AB, Chen R, Fu HH, Montagna M, Schwartz PE, Rutherford T, et al. Molecular phenotyping of human ovarian cancer stem cells unravels the mechanisms for repair and chemoresistance. *Cell Cycle*. 2009;8(1):158-66.
141. Liou G-Y. CD133 as a regulator of cancer metastasis through the cancer stem cells. *The International Journal of Biochemistry & Cell Biology*. 2019;106:1-7.
142. Baba T, Convery PA, Matsumura N, Whitaker RS, Kondoh E, Perry T, et al. Epigenetic regulation of CD133 and tumorigenicity of CD133+ ovarian cancer cells. *Oncogene*. 2009;28(2):209-18.
143. Jaggupilli A, Elkord E. Significance of CD44 and CD24 as cancer stem cell markers: an enduring ambiguity. *Clin Dev Immunol*. 2012;2012:708036.
144. Nakamura K, Terai Y, Tanabe A, Ono YJ, Hayashi M, Maeda K, et al. CD24 expression is a marker for predicting clinical outcome and regulates the epithelial-mesenchymal transition in ovarian cancer via both the Akt and ERK pathways. *Oncol Rep*. 2017;37(6):3189-200.
145. Kristiansen G, Denkert C, Schlüns K, Dahl E, Pilarsky C, Hauptmann S. CD24 Is Expressed in Ovarian Cancer and Is a New Independent Prognostic Marker of Patient Survival. *The American Journal of Pathology*. 2002;161(4):1215-21.
146. Luo L, Zeng J, Liang B, Zhao Z, Sun L, Cao D, et al. Ovarian cancer cells with the CD117 phenotype are highly tumorigenic and are related to chemotherapy outcome. *Experimental and Molecular Pathology*. 2011;91(2):596-602.
147. Chau WK, Ip CK, Mak ASC, Lai HC, Wong AST. c-Kit mediates chemoresistance and tumor-initiating capacity of ovarian cancer cells through activation of Wnt/ β -catenin-ATP-binding cassette G2 signaling. *Oncogene*. 2013;32(22):2767-81.
148. Foster BM, Zaidi D, Young TR, Mobley ME, Kerr BA. CD117/c-kit in Cancer Stem Cell-Mediated Progression and Therapeutic Resistance. *Biomedicines*. 2018;6(1).
149. Yang B, Yan X, Liu L, Jiang C, Hou S. Overexpression of the cancer stem cell marker CD117 predicts poor prognosis in epithelial ovarian cancer patients: evidence from meta-analysis. *Onco Targets Ther*. 2017;10:2951-61.
150. Meng E, Mitra A, Tripathi K, Finan MA, Scalici J, McClellan S, et al. ALDH1A1 maintains ovarian cancer stem cell-like properties by altered regulation of cell cycle checkpoint and DNA repair network signaling. *PLoS One*. 2014;9(9):e107142.
151. Januchowski R, Wojtowicz K, Sterzyńska K, Sosińska P, Andrzejewska M, Zawierucha P, et al. Inhibition of ALDH1A1 activity decreases expression of drug transporters and reduces chemotherapy resistance in ovarian cancer cell lines. *The International Journal of Biochemistry & Cell Biology*. 2016;78:248-59.
152. Deng S, Yang X, Lassus H, Liang S, Kaur S, Ye Q, et al. Distinct expression levels and patterns of stem cell marker, aldehyde dehydrogenase isoform 1 (ALDH1), in human epithelial cancers. *PLoS One*. 2010;5(4):e10277.
153. Bandura DR, Baranov VI, Ornatsky OI, Antonov A, Kinach R, Lou X, et al. Mass cytometry: technique for real time single cell multitarget immunoassay based on inductively coupled plasma time-of-flight mass spectrometry. *Anal Chem*. 2009;81(16):6813-22.

-
154. Yan X, Lin Y, Yang D, Shen Y, Yuan M, Zhang Z, et al. A novel anti-CD146 monoclonal antibody, AA98, inhibits angiogenesis and tumor growth. *Blood*. 2003;102(1):184-91.
 155. Carmeliet P, Jain RK. Angiogenesis in cancer and other diseases. *nature*. 2000;407(6801):249-57.
 156. Rask L, Høgdall CK, Kjaer SK, Christensen L, Jensen A, Blaakaer J, et al. Association of CD31 and p53 With Survival of Ovarian Cancer Patients. *Anticancer Res*. 2019;39(2):567-76.
 157. Alvero AB, Fu HH, Holmberg J, Visintin I, Mor L, Marquina CC, et al. Stem-like ovarian cancer cells can serve as tumor vascular progenitors. *Stem Cells*. 2009;27(10):2405-13.
 158. Rubatt JM, Darcy KM, Hutson A, Bean SM, Havrilesky LJ, Grace LA, et al. Independent prognostic relevance of microvessel density in advanced epithelial ovarian cancer and associations between CD31, CD105, p53 status, and angiogenic marker expression: A Gynecologic Oncology Group study. *Gynecologic Oncology*. 2009;112(3):469-74.
 159. Cross MJ, Claesson-Welsh L. FGF and VEGF function in angiogenesis: signalling pathways, biological responses and therapeutic inhibition. *Trends in pharmacological sciences*. 2001;22(4):201-7.
 160. Ahmed Z, Bicknell R. Angiogenic signalling pathways. *Angiogenesis Protocols*: Springer; 2009. p. 3-24.
 161. Sopo M, Anttila M, Hämäläinen K, Kivelä A, Ylä-Herttua S, Kosma V-M, et al. Expression profiles of VEGF-A, VEGF-D and VEGFR1 are higher in distant metastases than in matched primary high grade epithelial ovarian cancer. *BMC cancer*. 2019;19(1):584.
 162. Sallinen H, Heikura T, Koponen J, Kosma V-M, Heinonen S, Ylä-Herttua S, et al. Serum angiopoietin-2 and soluble VEGFR-2 levels predict malignancy of ovarian neoplasm and poor prognosis in epithelial ovarian cancer. *BMC cancer*. 2014;14(1):696.
 163. Lin Z, Liu Y, Sun Y, He X. Expression of Ets-1, Ang-2 and maspin in ovarian cancer and their role in tumor angiogenesis. *Journal of experimental & clinical cancer research*. 2011;30(1):31.
 164. Shen W, Li H, Liu L, Cheng J. Expression levels of PTEN, HIF-1 α , and VEGF as prognostic factors in ovarian cancer. *Eur Rev Med Pharmacol Sci*. 2017;21(11):2596-603.
 165. Cai J, Tang H, Xu L, Wang X, Yang C, Ruan S, et al. Fibroblasts in omentum activated by tumor cells promote ovarian cancer growth, adhesion and invasiveness. *Carcinogenesis*. 2012;33(1):20-9.
 166. Yu Y, Xiao C, Tan L, Wang Q, Li X, Feng Y. Cancer-associated fibroblasts induce epithelial–mesenchymal transition of breast cancer cells through paracrine TGF- β signalling. *British journal of cancer*. 2014;110(3):724-32.
 167. Denton AE, Roberts EW, Fearon DT. Stromal cells in the tumor microenvironment. *Stromal Immunology*: Springer; 2018. p. 99-114.
 168. Sjöberg E, Augsten M, Bergh J, Jirström K, Östman A. Expression of the chemokine CXCL14 in the tumour stroma is an independent marker of survival in breast cancer. *British journal of cancer*. 2016;114(10):1117-24.

169. Yang W, Han W, Ye S, Liu D, Wu J, Liu H, et al. Fibroblast activation protein- α promotes ovarian cancer cell proliferation and invasion via extracellular and intracellular signaling mechanisms. *Experimental and molecular pathology*. 2013;95(1):105-10.
170. Zhao L, Ji G, Le X, Wang C, Xu L, Feng M, et al. Long noncoding RNA LINC00092 acts in cancer-associated fibroblasts to drive glycolysis and progression of ovarian cancer. *Cancer research*. 2017;77(6):1369-82.
171. Mhawech-Fauceglia P, Yan L, Sharifian M, Ren X, Liu S, Kim G, et al. Stromal expression of fibroblast activation protein alpha (FAP) predicts platinum resistance and shorter recurrence in patients with epithelial ovarian cancer. *Cancer Microenvironment*. 2015;8(1):23-31.
172. Givel A-M, Kieffer Y, Scholer-Dahirel A, Sirven P, Cardon M, Pelon F, et al. miR200-regulated CXCL12 β promotes fibroblast heterogeneity and immunosuppression in ovarian cancers. *Nature communications*. 2018;9(1):1-20.
173. Armulik A, Abramsson A, Betsholtz C. Endothelial/pericyte interactions. *Circ Res*. 2005;97(6):512-23.
174. Shepro D, Morel NM. Pericyte physiology. *Faseb j*. 1993;7(11):1031-8.
175. Sinha D, Chong L, George J, Schlüter H, Mönchgesang S, Mills S, et al. Pericytes Promote Malignant Ovarian Cancer Progression in Mice and Predict Poor Prognosis in Serous Ovarian Cancer Patients. *Clin Cancer Res*. 2016;22(7):1813-24.
176. Harper EI, Sheedy EF, Stack MS. With Great Age Comes Great Metastatic Ability: Ovarian Cancer and the Appeal of the Aging Peritoneal Microenvironment. *Cancers (Basel)*. 2018;10(7).
177. Mikula-Pietrasik J, Uruski P, Sosińska P, Maksin K, Piotrowska-Kempisty H, Kucińska M, et al. Senescent peritoneal mesothelium creates a niche for ovarian cancer metastases. *Cell Death Dis*. 2016;7(12):e2565.
178. Mogi K, Yoshihara M, Iyoshi S, Kitami K, Uno K, Tano S, et al. Ovarian Cancer-Associated Mesothelial Cells: Transdifferentiation to Minions of Cancer and Orchestrate Developing Peritoneal Dissemination. *Cancers (Basel)*. 2021;13(6).
179. Rodriguez GM, Galpin KJC, McCloskey CW, Vanderhyden BC. The Tumor Microenvironment of Epithelial Ovarian Cancer and Its Influence on Response to Immunotherapy. *Cancers (Basel)*. 2018;10(8).
180. Ghosn EEB, Cassado AA, Govoni GR, Fukuhara T, Yang Y, Monack DM, et al. Two physically, functionally, and developmentally distinct peritoneal macrophage subsets. *Proceedings of the National Academy of Sciences*. 2010;107(6):2568-73.
181. Sica A, Allavena P, Mantovani A. Cancer related inflammation: the macrophage connection. *Cancer letters*. 2008;267(2):204-15.
182. Grivennikov SI, Greten FR, Karin M. Immunity, inflammation, and cancer. *Cell*. 2010;140(6):883-99.
183. Qian B-Z, Pollard JW. Macrophage diversity enhances tumor progression and metastasis. *Cell*. 2010;141(1):39-51.
184. Sica A. Role of tumour-associated macrophages in cancer-related inflammation. *Exp Oncol*. 2010;32(3):153-8.
185. Gupta V, Yull F, Khabele D. Bipolar tumor-associated macrophages in ovarian cancer as targets for therapy. *Cancers*. 2018;10(10):366.

-
186. Pollard JW. Tumour-educated macrophages promote tumour progression and metastasis. *Nature Reviews Cancer*. 2004;4(1):71-8.
 187. Reinartz S, Schumann T, Finkernagel F, Wortmann A, Jansen JM, Meissner W, et al. Mixed-polarization phenotype of ascites-associated macrophages in human ovarian carcinoma: correlation of CD163 expression, cytokine levels and early relapse. *International journal of cancer*. 2014;134(1):32-42.
 188. Yin M, Li X, Tan S, Zhou HJ, Ji W, Bellone S, et al. Tumor-associated macrophages drive spheroid formation during early transcoelomic metastasis of ovarian cancer. *The Journal of clinical investigation*. 2016;126(11):4157-73.
 189. Li H, Fan X, Houghton J. Tumor microenvironment: the role of the tumor stroma in cancer. *Journal of cellular biochemistry*. 2007;101(4):805-15.
 190. Noy R, Pollard JW. Tumor-associated macrophages: from mechanisms to therapy. *Immunity*. 2014;41(1):49-61.
 191. Galdiero MR, Garlanda C, Jaillon S, Marone G, Mantovani A. Tumor associated macrophages and neutrophils in tumor progression. *Journal of cellular physiology*. 2013;228(7):1404-12.
 192. Mantovani A, Sozzani S, Locati M, Allavena P, Sica A. Macrophage polarization: tumor-associated macrophages as a paradigm for polarized M2 mononuclear phagocytes. *Trends in immunology*. 2002;23(11):549-55.
 193. Coffelt SB, Tal AO, Scholz A, De Palma M, Patel S, Urbich C, et al. Angiopoietin-2 regulates gene expression in TIE2-expressing monocytes and augments their inherent proangiogenic functions. *Cancer research*. 2010;70(13):5270-80.
 194. Ruffell B, Affara NI, Coussens LM. Differential macrophage programming in the tumor microenvironment. *Trends in immunology*. 2012;33(3):119-26.
 195. Finkernagel F, Reinartz S, Lieber S, Adhikary T, Wortmann A, Hoffmann N, et al. The transcriptional signature of human ovarian carcinoma macrophages is associated with extracellular matrix reorganization. *Oncotarget*. 2016;7(46):75339.
 196. Roy A, Li SD. Modifying the tumor microenvironment using nanoparticle therapeutics. *Wiley Interdisciplinary Reviews: Nanomedicine and Nanobiotechnology*. 2016;8(6):891-908.
 197. Fagiani E, Christofori G. Angiopoietins in angiogenesis. *Cancer letters*. 2013;328(1):18-26.
 198. Ngambenjawong C, Gustafson HH, Pun SH. Progress in tumor-associated macrophage (TAM)-targeted therapeutics. *Advanced drug delivery reviews*. 2017;114:206-21.
 199. Ostuni R, Kratochvill F, Murray PJ, Natoli G. Macrophages and cancer: from mechanisms to therapeutic implications. *Trends in immunology*. 2015;36(4):229-39.
 200. Zhang M, He Y, Sun X, Li Q, Wang W, Zhao A, et al. A high M1/M2 ratio of tumor-associated macrophages is associated with extended survival in ovarian cancer patients. *Journal of ovarian research*. 2014;7(1):19.
 201. Cassetta L, Fraggogianni S, Sims AH, Swierczak A, Forrester LM, Zhang H, et al. Human Tumor-Associated Macrophage and Monocyte Transcriptional Landscapes Reveal Cancer-Specific Reprogramming, Biomarkers, and Therapeutic Targets. *Cancer Cell*. 2019;35(4):588-602.e10.
 202. Kim J, Bae J-S. Tumor-associated macrophages and neutrophils in tumor microenvironment. *Mediators of inflammation*. 2016;2016.

203. Yang M, McKay D, Pollard JW, Lewis CE. Diverse functions of macrophages in different tumor microenvironments. *Cancer research*. 2018;78(19):5492-503.
204. Okabe Y, Medzhitov R. Tissue-specific signals control reversible program of localization and functional polarization of macrophages. *Cell*. 2014;157(4):832-44.
205. Stout RD, Jiang C, Matta B, Tietzel I, Watkins SK, Suttles J. Macrophages sequentially change their functional phenotype in response to changes in microenvironmental influences. *The Journal of Immunology*. 2005;175(1):342-9.
206. Lan C, Huang X, Lin S, Huang H, Cai Q, Wan T, et al. Expression of M2-polarized macrophages is associated with poor prognosis for advanced epithelial ovarian cancer. *Technology in cancer research & treatment*. 2013;12(3):259-67.
207. Yuan X, Zhang J, Li D, Mao Y, Mo F, Du W, et al. Prognostic significance of tumor-associated macrophages in ovarian cancer: A meta-analysis. *Gynecologic Oncology*. 2017;147(1):181-7.
208. Fridlender ZG, Sun J, Kim S, Kapoor V, Cheng G, Ling L, et al. Polarization of tumor-associated neutrophil phenotype by TGF-beta: "N1" versus "N2" TAN. *Cancer Cell*. 2009;16(3):183-94.
209. Acuff HB, Carter KJ, Fingleton B, Gorden DL, Matrisian LM. Matrix metalloproteinase-9 from bone marrow-derived cells contributes to survival but not growth of tumor cells in the lung microenvironment. *Cancer Res*. 2006;66(1):259-66.
210. Chen S, Zhang L, Yan G, Cheng S, Fathy AH, Yan N, et al. Neutrophil-to-Lymphocyte Ratio Is a Potential Prognostic Biomarker in Patients with Ovarian Cancer: A Meta-Analysis. *BioMed research international*. 2017;2017:7943467.
211. Sektioglu IM, Carretero R, Bulbuc N, Bald T, Tüting T, Rudensky AY, et al. Basophils Promote Tumor Rejection via Chemotaxis and Infiltration of CD8⁺ T Cells. 2017;77(2):291-302.
212. Varricchi G, Loffredo S, Galdiero MR, Marone G, Cristinziano L, Granata F, et al. Innate effector cells in angiogenesis and lymphangiogenesis. *Current Opinion in Immunology*. 2018;53:152-60.
213. Khan ANH, Emmons TR, Wong JT, Alqassim E, Singel KL, Mark J, et al. Quantification of Early-Stage Myeloid-Derived Suppressor Cells in Cancer Requires Excluding Basophils. 2020;8(6):819-28.
214. Simon SCS, Utikal J, Umansky V. Opposing roles of eosinophils in cancer. *Cancer Immunology, Immunotherapy*. 2019;68(5):823-33.
215. Lotfi R, Lotze MT. Eosinophils induce DC maturation, regulating immunity. 2008;83(3):456-60.
216. Page SM, Gleich GJ, Roebuck KA, Thomas LL. Stimulation of neutrophil interleukin-8 production by eosinophil granule major basic protein. *American journal of respiratory cell and molecular biology*. 1999;21(2):230-7.
217. Labidi-Galy SI, Sisirak V, Meeus P, Gobert M, Treilleux I, Bajard A, et al. Quantitative and functional alterations of plasmacytoid dendritic cells contribute to immune tolerance in ovarian cancer. *Cancer research*. 2011;71(16):5423-34.
218. Vu Manh T-P, Bertho N, Hosmalin A, Schwartz-Cornil I, Dalod M. Investigating evolutionary conservation of dendritic cell subset identity and functions. *Frontiers in immunology*. 2015;6:260.
219. Bol KF, Schreiber G, Gerritsen WR, De Vries IJM, Figdor CG. Dendritic cell-based immunotherapy: state of the art and beyond. *AACR*; 2016.

-
220. Bhatia R, Gautam SK, Cannon A, Thompson C, Hall BR, Aithal A, et al. Cancer-associated mucins: role in immune modulation and metastasis. *Cancer and Metastasis Reviews*. 2019;38(1-2):223-36.
221. DeVito NC, Plebanek M, Thievanthiran B, Hanks BA. Role of tumor-mediated dendritic cell tolerization in immune evasion. *Frontiers in Immunology*. 2019;10:2876.
222. Tang M, Diao J, Cattral MS. Molecular mechanisms involved in dendritic cell dysfunction in cancer. *Cellular and Molecular Life Sciences*. 2017;74(5):761-76.
223. Cubillos-Ruiz JR, Silberman PC, Rutkowski MR, Chopra S, Perales-Puchalt A, Song M, et al. ER stress sensor XBP1 controls anti-tumor immunity by disrupting dendritic cell homeostasis. *Cell*. 2015;161(7):1527-38.
224. Munn DH, Sharma MD, Baban B, Harding HP, Zhang Y, Ron D, et al. GCN2 kinase in T cells mediates proliferative arrest and anergy induction in response to indoleamine 2,3-dioxygenase. *Immunity*. 2005;22(5):633-42.
225. Tanizaki Y, Kobayashi A, Toudjima S, Shiro M, Mizoguchi M, Mabuchi Y, et al. Indoleamine 2,3-dioxygenase promotes peritoneal metastasis of ovarian cancer by inducing an immunosuppressive environment. *Cancer Sci*. 2014;105(8):966-73.
226. Munn DH, Mellor AL. IDO in the Tumor Microenvironment: Inflammation, Counter-Regulation, and Tolerance. *Trends Immunol*. 2016;37(3):193-207.
227. Casey SC, Amedei A, Aquilano K, Azmi AS, Benencia F, Bhakta D, et al. Cancer prevention and therapy through the modulation of the tumor microenvironment. *Semin Cancer Biol*. 2015;35 Suppl(Suppl):S199-s223.
228. MacGregor HL, Sayad A, Elia A, Wang BX, Katz SR, Shaw PA, et al. High expression of B7-H3 on stromal cells defines tumor and stromal compartments in epithelial ovarian cancer and is associated with limited immune activation. *J Immunother Cancer*. 2019;7(1):357.
229. MacGregor HL, Garcia-Batres C, Sayad A, Elia A, Berman HK, Toker A, et al. Tumor cell expression of B7-H4 correlates with higher frequencies of tumor-infiltrating APCs and higher CXCL17 expression in human epithelial ovarian cancer. *Oncoimmunology*. 2019;8(12):e1665460.
230. Scarlett UK, Rutkowski MR, Rauwerdink AM, Fields J, Escovar-Fadul X, Baird J, et al. Ovarian cancer progression is controlled by phenotypic changes in dendritic cells. *J Exp Med*. 2012;209(3):495-506.
231. Atrekhany KN, Drutskaya MS. Myeloid-Derived Suppressor Cells and Proinflammatory Cytokines as Targets for Cancer Therapy. *Biochemistry (Mosc)*. 2016;81(11):1274-83.
232. Gabrilovich DI. Myeloid-Derived Suppressor Cells. *Cancer Immunol Res*. 2017;5(1):3-8.
233. Rodriguez PC, Quiceno DG, Zabaleta J, Ortiz B, Zea AH, Piazuelo MB, et al. Arginase I production in the tumor microenvironment by mature myeloid cells inhibits T-cell receptor expression and antigen-specific T-cell responses. *Cancer Res*. 2004;64(16):5839-49.
234. Srivastava MK, Sinha P, Clements VK, Rodriguez P, Ostrand-Rosenberg S. Myeloid-derived suppressor cells inhibit T-cell activation by depleting cystine and cysteine. *Cancer Res*. 2010;70(1):68-77.

235. Hanson EM, Clements VK, Sinha P, Ilkovitch D, Ostrand-Rosenberg S. Myeloid-derived suppressor cells down-regulate L-selectin expression on CD4+ and CD8+ T cells. *J Immunol.* 2009;183(2):937-44.
236. Sakuishi K, Jayaraman P, Behar SM, Anderson AC, Kuchroo VK. Emerging Tim-3 functions in antimicrobial and tumor immunity. *Trends Immunol.* 2011;32(8):345-9.
237. Gabrilovich DI, Ostrand-Rosenberg S, Bronte V. Coordinated regulation of myeloid cells by tumours. *Nat Rev Immunol.* 2012;12(4):253-68.
238. Ostrand-Rosenberg S, Fenselau C. Myeloid-Derived Suppressor Cells: Immune-Suppressive Cells That Impair Antitumor Immunity and Are Sculpted by Their Environment. *J Immunol.* 2018;200(2):422-31.
239. Bruno A, Mortara L, Baci D, Noonan DM, Albini A. Myeloid Derived Suppressor Cells Interactions With Natural Killer Cells and Pro-angiogenic Activities: Roles in Tumor Progression. *Front Immunol.* 2019;10:771.
240. Balkwill FR, Capasso M, Hagemann T. The tumor microenvironment at a glance. *Journal of Cell Science.* 2012;125(23):5591-6.
241. Ghoneum A, Afify H, Salih Z, Kelly M, Said N. Role of tumor microenvironment in ovarian cancer pathobiology. *Oncotarget.* 2018;9(32):22832-49.
242. Smith-Garvin JE, Koretzky GA, Jordan MS. T cell activation. *Annu Rev Immunol.* 2009;27:591-619.
243. Joyce JA, Pollard JW. Microenvironmental regulation of metastasis. *Nat Rev Cancer.* 2009;9(4):239-52.
244. Zhang N, Bevan MJ. CD8(+) T cells: foot soldiers of the immune system. *Immunity.* 2011;35(2):161-8.
245. Idos GE, Kwok J, Bonthala N, Kysh L, Gruber SB, Qu C. The Prognostic Implications of Tumor Infiltrating Lymphocytes in Colorectal Cancer: A Systematic Review and Meta-Analysis. *Scientific Reports.* 2020;10(1):3360.
246. Galon J, Costes A, Sanchez-Cabo F, Kirilovsky A, Mlecnik B, Lagorce-Pagès C, et al. Type, density, and location of immune cells within human colorectal tumors predict clinical outcome. *Science.* 2006;313(5795):1960-4.
247. Li J, Wang J, Chen R, Bai Y, Lu X. The prognostic value of tumor-infiltrating T lymphocytes in ovarian cancer. *Oncotarget.* 2017;8(9):15621-31.
248. Yang L, Wang S, Zhang Q, Pan Y, Lv Y, Chen X, et al. Clinical significance of the immune microenvironment in ovarian cancer patients. *Mol Omics.* 2018;14(5):341-51.
249. Pinto MP, Balmaceda C, Bravo ML, Kato S, Villarroel A, Owen GI, et al. Patient inflammatory status and CD4+/CD8+ intraepithelial tumor lymphocyte infiltration are predictors of outcomes in high-grade serous ovarian cancer. *Gynecologic Oncology.* 2018;151(1):10-7.
250. Henriksen JR, Donskov F, Waldstrøm M, Jakobsen A, Hjortkjaer M, Petersen CB, et al. Favorable prognostic impact of Natural Killer cells and T cells in high-grade serous ovarian carcinoma. *Acta Oncol.* 2020;59(6):652-9.
251. Goode EL, Block MS, Kalli KR, Vierkant RA, Chen W, Fogarty ZC, et al. Dose-Response Association of CD8+ Tumor-Infiltrating Lymphocytes and Survival Time in High-Grade Serous Ovarian Cancer. *JAMA Oncol.* 2017;3(12):e173290.

-
252. Clarke B, Tinker AV, Lee CH, Subramanian S, van de Rijn M, Turbin D, et al. Intraepithelial T cells and prognosis in ovarian carcinoma: novel associations with stage, tumor type, and BRCA1 loss. *Mod Pathol.* 2009;22(3):393-402.
253. Webb JR, Milne K, Watson P, deLeeuw RJ, Nelson BH. Tumor-Infiltrating Lymphocytes Expressing the Tissue Resident Memory Marker CD103 Are Associated with Increased Survival in High-Grade Serous Ovarian Cancer. *Clinical Cancer Research.* 2014;20(2):434-44.
254. Pardoll DM. The blockade of immune checkpoints in cancer immunotherapy. *Nature Reviews Cancer.* 2012;12(4):252-64.
255. Edwards J, Wilmott JS, Madore J, Gide TN, Quek C, Tasker A, et al. CD103(+) Tumor-Resident CD8(+) T Cells Are Associated with Improved Survival in Immunotherapy-Naïve Melanoma Patients and Expand Significantly During Anti-PD-1 Treatment. *Clin Cancer Res.* 2018;24(13):3036-45.
256. Vignali DA, Collison LW, Workman CJ. How regulatory T cells work. *Nat Rev Immunol.* 2008;8(7):523-32.
257. Facciabene A, Motz GT, Coukos G. T-regulatory cells: key players in tumor immune escape and angiogenesis. *Cancer Res.* 2012;72(9):2162-71.
258. Landskron J, Helland Ø, Torgersen KM, Aandahl EM, Gjertsen BT, Bjørge L, et al. Activated regulatory and memory T-cells accumulate in malignant ascites from ovarian carcinoma patients. *Cancer Immunol Immunother.* 2015;64(3):337-47.
259. Lundgren S, Berntsson J, Nodin B, Micke P, Jirstrom K. Prognostic impact of tumour-associated B cells and plasma cells in epithelial ovarian cancer. *J Ovarian Res.* 2016;9:21.
260. Mauri C, Menon M. Human regulatory B cells in health and disease: therapeutic potential. *J Clin Invest.* 2017;127(3):772-9.
261. Tokunaga R, Naseem M, Lo JH, Battaglin F, Soni S, Puccini A, et al. B cell and B cell-related pathways for novel cancer treatments. *Cancer Treatment Reviews.* 2019;73:10-9.
262. Ljunggren H-G, Malmberg K-J. Prospects for the use of NK cells in immunotherapy of human cancer. *Nature Reviews Immunology.* 2007;7(5):329-39.
263. Nersesian S, Glazebrook H, Toulany J, Grantham SR, Boudreau JE. Naturally Killing the Silent Killer: NK Cell-Based Immunotherapy for Ovarian Cancer. *Front Immunol.* 2019;10:1782.
264. Hoogstad-van Evert JS, Bekkers R, Ottevanger N, Jansen JH, Massuger L, Dolstra H. Harnessing natural killer cells for the treatment of ovarian cancer. *Gynecologic Oncology.* 2020;157(3):810-6.
265. Dong HP, Elstrand MB, Holth A, Silins I, Berner A, Trope CG, et al. NK- and B-Cell Infiltration Correlates With Worse Outcome in Metastatic Ovarian Carcinoma. *American Journal of Clinical Pathology.* 2006;125(3):451-8.
266. Jiménez-Sánchez A, Cybulska P, Mager KL, Koplev S, Cast O, Couturier DL, et al. Unraveling tumor-immune heterogeneity in advanced ovarian cancer uncovers immunogenic effect of chemotherapy. *Nat Genet.* 2020;52(6):582-93.
267. Wu L, Van Kaer L. Natural killer T cells in health and disease. *Frontiers in bioscience (Scholar edition).* 2011;3:236-51.

-
268. Krijgsman D, Hokland M, Kuppen PJK. The Role of Natural Killer T Cells in Cancer—A Phenotypical and Functional Approach. *Frontiers in Immunology*. 2018;9(367).
269. Zhang L, Conejo-Garcia JR, Katsaros D, Gimotty PA, Massobrio M, Regnani G, et al. Intratumoral T cells, recurrence, and survival in epithelial ovarian cancer. *N Engl J Med*. 2003;348(3):203-13.
270. Galon J, Mlecnik B, Bindea G, Angell HK, Berger A, Lagorce C, et al. Towards the introduction of the 'Immunoscore' in the classification of malignant tumours. *J Pathol*. 2014;232(2):199-209.
271. Wei Y, Xiao X, Lao XM, Zheng L, Kuang DM. Immune landscape and therapeutic strategies: new insights into PD-L1 in tumors. *Cell Mol Life Sci*. 2020.
272. Disis ML, Taylor MH, Kelly K, Beck JT, Gordon M, Moore KM, et al. Efficacy and Safety of Avelumab for Patients With Recurrent or Refractory Ovarian Cancer: Phase 1b Results From the JAVELIN Solid Tumor Trial. *JAMA Oncology*. 2019;5(3):393-401.
273. Moore KN, Bookman M, Sehouli J, Miller A, Anderson C, Scambia G, et al. Atezolizumab, Bevacizumab, and Chemotherapy for Newly Diagnosed Stage III or IV Ovarian Cancer: Placebo-Controlled Randomized Phase III Trial (IMagyn050/GOG 3015/ENGOT-OV39). *J Clin Oncol*. 2021;Jco2100306.
274. Vikas P, Borcherding N, Chennamadhavuni A, Garje R. Therapeutic Potential of Combining PARP Inhibitor and Immunotherapy in Solid Tumors. *Front Oncol*. 2020;10:570.
275. Ozbek S, Balasubramanian PG, Chiquet-Ehrismann R, Tucker RP, Adams JC. The evolution of extracellular matrix. *Mol Biol Cell*. 2010;21(24):4300-5.
276. Lu P, Weaver VM, Werb Z. The extracellular matrix: a dynamic niche in cancer progression. *J Cell Biol*. 2012;196(4):395-406.
277. Paszek MJ, Zahir N, Johnson KR, Lakins JN, Rozenberg GI, Gefen A, et al. Tensional homeostasis and the malignant phenotype. *Cancer Cell*. 2005;8(3):241-54.
278. Foster DS, Jones RE, Ransom RC, Longaker MT, Norton JA. The evolving relationship of wound healing and tumor stroma. *JCI Insight*. 2018;3(18).
279. Davidson B, Trope CG, Reich R. The role of the tumor stroma in ovarian cancer. *Front Oncol*. 2014;4:104.
280. Ferrara N. VEGF as a therapeutic target in cancer. *Oncology*. 2005;69 Suppl 3:11-6.
281. Anttila MA, Tammi RH, Tammi MI, Syrjänen KJ, Saarikoski SV, Kosma VM. High levels of stromal hyaluronan predict poor disease outcome in epithelial ovarian cancer. *Cancer Res*. 2000;60(1):150-5.
282. Boyd RS, Balkwill FR. MMP-2 release and activation in ovarian carcinoma: the role of fibroblasts. *Br J Cancer*. 1999;80(3-4):315-21.
283. Freedman RS, Deavers M, Liu J, Wang E. Peritoneal inflammation - A microenvironment for Epithelial Ovarian Cancer (EOC). *J Transl Med*. 2004;2(1):23.
284. Nezhat F, Datta MS, Hanson V, Pejovic T, Nezhat C, Nezhat C. The relationship of endometriosis and ovarian malignancy: a review. *Fertil Steril*. 2008;90(5):1559-70.
285. Jain S, Annett SL, Morgan MP, Robson T. The Cancer Stem Cell Niche in Ovarian Cancer and Its Impact on Immune Surveillance. *Int J Mol Sci*. 2021;22(8).

-
286. Zhang S, Balch C, Chan MW, Lai HC, Matei D, Schilder JM, et al. Identification and characterization of ovarian cancer-initiating cells from primary human tumors. *Cancer Res.* 2008;68(11):4311-20.
287. Auersperg N. The stem-cell profile of ovarian surface epithelium is reproduced in the oviductal fimbriae, with increased stem-cell marker density in distal parts of the fimbriae. *Int J Gynecol Pathol.* 2013;32(5):444-53.
288. Flesken-Nikitin A, Hwang CI, Cheng CY, Michurina TV, Enikolopov G, Nikitin AY. Ovarian surface epithelium at the junction area contains a cancer-prone stem cell niche. *Nature.* 2013;495(7440):241-5.
289. Erickson BK, Conner MG, Landen CN, Jr. The role of the fallopian tube in the origin of ovarian cancer. *Am J Obstet Gynecol.* 2013;209(5):409-14.
290. Paik DY, Janzen DM, Schafenacker AM, Velasco VS, Shung MS, Cheng D, et al. Stem-like epithelial cells are concentrated in the distal end of the fallopian tube: a site for injury and serous cancer initiation. *Stem Cells.* 2012;30(11):2487-97.
291. Abdullah LN, Chow EK-H. Mechanisms of chemoresistance in cancer stem cells. *Clinical and Translational Medicine.* 2013;2(1):e3.
292. Li F, Tiede B, Massagué J, Kang Y. Beyond tumorigenesis: cancer stem cells in metastasis. *Cell Res.* 2007;17(1):3-14.
293. Lawson DA, Bhakta NR, Kessenbrock K, Prummel KD, Yu Y, Takai K, et al. Single-cell analysis reveals a stem-cell program in human metastatic breast cancer cells. *Nature.* 2015;526(7571):131-5.
294. Thibault B, Castells M, Delord JP, Couderc B. Ovarian cancer microenvironment: implications for cancer dissemination and chemoresistance acquisition. *Cancer Metastasis Rev.* 2014;33(1):17-39.
295. Pasquet M, Golzio M, Mery E, Rafii A, Benabbou N, Mirshahi P, et al. Hospicells (ascites-derived stromal cells) promote tumorigenicity and angiogenesis. *Int J Cancer.* 2010;126(9):2090-101.
296. Lane D, Matte I, Laplante C, Garde-Granger P, Carignan A, Bessette P, et al. CCL18 from ascites promotes ovarian cancer cell migration through proline-rich tyrosine kinase 2 signaling. *Mol Cancer.* 2016;15(1):58.
297. Kim S, Kim B, Song YS. Ascites modulates cancer cell behavior, contributing to tumor heterogeneity in ovarian cancer. *Cancer Sci.* 2016;107(9):1173-8.
298. Windmüller C, Zech D, Avril S, Boxberg M, Dawidek T, Schmalfeldt B, et al. CXCR3 mediates ascites-directed tumor cell migration and predicts poor outcome in ovarian cancer patients. *Oncogenesis.* 2017;6(5):e331.
299. Yang S, Wang B, Guan C, Wu B, Cai C, Wang M, et al. Foxp3+IL-17+ T cells promote development of cancer-initiating cells in colorectal cancer. *Journal of Leukocyte Biology.* 2011;89(1):85-91.
300. Seton-Rogers S. Cancer stem cells. VEGF promotes stemness. *Nat Rev Cancer.* 2011;11(12):831.
301. Jang K, Kim M, Gilbert CA, Simpkins F, Ince TA, Slingerland JM. VEGFA activates an epigenetic pathway upregulating ovarian cancer-initiating cells. *EMBO Mol Med.* 2017;9(3):304-18.
302. Kalluri R. The biology and function of fibroblasts in cancer. *Nat Rev Cancer.* 2016;16(9):582-98.

303. Cardenas C, Montagna MK, Pitruzzello M, Lima E, Mor G, Alvero AB. Adipocyte microenvironment promotes Bcl(xl) expression and confers chemoresistance in ovarian cancer cells. *Apoptosis*. 2017;22(4):558-69.
304. Wang D, Xiang T, Zhao Z, Lin K, Yin P, Jiang L, et al. Autocrine interleukin-23 promotes self-renewal of CD133+ ovarian cancer stem-like cells. *Oncotarget*. 2016;7(46):76006-20.
305. Tang S, Xiang T, Huang S, Zhou J, Wang Z, Xie R, et al. Ovarian cancer stem-like cells differentiate into endothelial cells and participate in tumor angiogenesis through autocrine CCL5 signaling. *Cancer Lett*. 2016;376(1):137-47.
306. Drost J, van Jaarsveld RH, Ponsioen B, Zimmerlin C, van Boxtel R, Buijs A, et al. Sequential cancer mutations in cultured human intestinal stem cells. *Nature*. 2015;521(7550):43-7.
307. Li X, Nadauld L, Ootani A, Corney DC, Pai RK, Gevaert O, et al. Oncogenic transformation of diverse gastrointestinal tissues in primary organoid culture. *Nat Med*. 2014;20(7):769-77.
308. Matano M, Date S, Shimokawa M, Takano A, Fujii M, Ohta Y, et al. Modeling colorectal cancer using CRISPR-Cas9-mediated engineering of human intestinal organoids. *Nat Med*. 2015;21(3):256-62.
309. Kretschmar K, Clevers H. Organoids: Modeling Development and the Stem Cell Niche in a Dish. *Dev Cell*. 2016;38(6):590-600.
310. Zong X, Nephew KP. Ovarian Cancer Stem Cells: Role in Metastasis and Opportunity for Therapeutic Targeting. *Cancers (Basel)*. 2019;11(7).
311. Chen EY, Mehra K, Mehrad M, Ning G, Miron A, Mutter GL, et al. Secretory cell outgrowth, PAX2 and serous carcinogenesis in the Fallopian tube. *The Journal of Pathology*. 2010;222(1):110-6.
312. Roh MH, Yassin Y, Miron A, Mehra KK, Mehrad M, Monte NM, et al. High-grade fimbrial-ovarian carcinomas are unified by altered p53, PTEN and PAX2 expression. *Modern Pathology*. 2010;23(10):1316-24.
313. Song H, Kwan SY, Izaguirre DI, Zu Z, Tsang YT, Tung CS, et al. PAX2 Expression in Ovarian Cancer. *Int J Mol Sci*. 2013;14(3):6090-105.
314. Newsted D, Banerjee S, Watt K, Nersesian S, Truesdell P, Blazer LL, et al. Blockade of TGF- β signaling with novel synthetic antibodies limits immune exclusion and improves chemotherapy response in metastatic ovarian cancer models. *OncoImmunology*. 2019;8(2):e1539613.
315. Hudson LG, Zeineldin R, Stack MS. Phenotypic plasticity of neoplastic ovarian epithelium: unique cadherin profiles in tumor progression. *Clinical & Experimental Metastasis*. 2008;25(6):643-55.
316. Ahmed N, Thompson EW, Quinn MA. Epithelial-mesenchymal interconversions in normal ovarian surface epithelium and ovarian carcinomas: An exception to the norm. *Journal of Cellular Physiology*. 2007;213(3):581-8.
317. Ahmed N, Stenvers KL. Getting to know ovarian cancer ascites: opportunities for targeted therapy-based translational research. *Front Oncol*. 2013;3:256.
318. Tan DSP, Agarwal R, Kaye SB. Mechanisms of transcoelomic metastasis in ovarian cancer. *The Lancet Oncology*. 2006;7(11):925-34.
319. Klymenko Y, Kim O, Stack MS. Complex Determinants of Epithelial: Mesenchymal Phenotypic Plasticity in Ovarian Cancer. *Cancers (Basel)*. 2017;9(8).

-
320. Burleson KM, Hansen LK, Skubitz AP. Ovarian carcinoma spheroids disaggregate on type I collagen and invade live human mesothelial cell monolayers. *Clin Exp Metastasis*. 2004;21(8):685-97.
 321. Strobel T, Swanson L, Cannistra SA. In vivo inhibition of CD44 limits intra-abdominal spread of a human ovarian cancer xenograft in nude mice: a novel role for CD44 in the process of peritoneal implantation. *Cancer Res*. 1997;57(7):1228-32.
 322. Lessan K, Aguiar DJ, Oegema T, Siebenson L, Skubitz APN. CD44 and $\alpha 5 \beta 1$ Integrin Mediate Ovarian Carcinoma Cell Adhesion to Peritoneal Mesothelial Cells. *The American Journal of Pathology*. 1999;154(5):1525-37.
 323. Gardner MJ, Catterall JB, Jones LM, Turner GA. Human ovarian tumour cells can bind hyaluronic acid via membrane CD44: a possible step in peritoneal metastasis. *Clin Exp Metastasis*. 1996;14(4):325-34.
 324. Cannistra SA, Kansas GS, Niloff J, DeFranzo B, Kim Y, Ottensmeier C. Binding of ovarian cancer cells to peritoneal mesothelium in vitro is partly mediated by CD44H. *Cancer Res*. 1993;53(16):3830-8.
 325. Chkourko Gusky H, Diedrich J, MacDougald OA, Podgorski I. Omentum and bone marrow: how adipocyte-rich organs create tumour microenvironments conducive for metastatic progression. *Obesity Reviews*. 2016;17(11):1015-29.
 326. Ocaña Oscar H, Córcoles R, Fabra Á, Moreno-Bueno G, Acloque H, Vega S, et al. Metastatic Colonization Requires the Repression of the Epithelial-Mesenchymal Transition Inducer Prrx1. *Cancer Cell*. 2012;22(6):709-24.
 327. Samah R, Yudith Ramos V, Monique B, Jacob M, Michel P, Akira S, et al. TGF β signaling regulates epithelial–mesenchymal plasticity in ovarian cancer ascites-derived spheroids. *Endocrine-Related Cancer*. 2016;23(3):147-59.
 328. Shibue T, Weinberg RA. EMT, CSCs, and drug resistance: the mechanistic link and clinical implications. *Nat Rev Clin Oncol*. 2017;14(10):611-29.
 329. Brabletz T. To differentiate or not--routes towards metastasis. *Nat Rev Cancer*. 2012;12(6):425-36.
 330. Meza-Perez S, Randall TD. Immunological Functions of the Omentum. *Trends Immunol*. 2017;38(7):526-36.
 331. Oosterling SJ, van der Bij GJ, Bögels M, van der Sijp JR, Beelen RH, Meijer S, et al. Insufficient ability of omental milky spots to prevent peritoneal tumor outgrowth supports omentectomy in minimal residual disease. *Cancer Immunol Immunother*. 2006;55(9):1043-51.
 332. Krishnan V, Clark R, Chekmareva M, Johnson A, George S, Shaw P, et al. In Vivo and Ex Vivo Approaches to Study Ovarian Cancer Metastatic Colonization of Milky Spot Structures in Peritoneal Adipose. *J Vis Exp*. 2015(105):e52721.
 333. Gerber SA, Rybalko VY, Bigelow CE, Lugade AA, Foster TH, Frelinger JG, et al. Preferential attachment of peritoneal tumor metastases to omental immune aggregates and possible role of a unique vascular microenvironment in metastatic survival and growth. *Am J Pathol*. 2006;169(5):1739-52.
 334. Clark R, Krishnan V, Schoof M, Rodriguez I, Theriault B, Chekmareva M, et al. Milky spots promote ovarian cancer metastatic colonization of peritoneal adipose in experimental models. *Am J Pathol*. 2013;183(2):576-91.
 335. Liu J, Geng X, Li Y. Milky spots: omental functional units and hotbeds for peritoneal cancer metastasis. *Tumour Biol*. 2016;37(5):5715-26.

-
336. Aras S, Zaidi MR. TAMEless traitors: macrophages in cancer progression and metastasis. *Br J Cancer*. 2017;117(11):1583-91.
337. Pollard JW. Tumour-educated macrophages promote tumour progression and metastasis. *Nat Rev Cancer*. 2004;4(1):71-8.
338. Takaishi K, Komohara Y, Tashiro H, Ohtake H, Nakagawa T, Katabuchi H, et al. Involvement of M2-polarized macrophages in the ascites from advanced epithelial ovarian carcinoma in tumor progression via Stat3 activation. *Cancer Sci*. 2010;101(10):2128-36.
339. Iurlaro R, León-Annicchiarico CL, Muñoz-Pinedo C. Chapter Three - Regulation of Cancer Metabolism by Oncogenes and Tumor Suppressors. In: Galluzzi L, Kroemer G, editors. *Methods in Enzymology*. 542: Academic Press; 2014. p. 59-80.
340. Warburg O, Wind F, Negelein E. THE METABOLISM OF TUMORS IN THE BODY. *J Gen Physiol*. 1927;8(6):519-30.
341. Gouirand V, Guillaumond F, Vasseur S. Influence of the Tumor Microenvironment on Cancer Cells Metabolic Reprogramming. *Frontiers in Oncology*. 2018;8(117).
342. Cortez AJ, Tudrej P, Kujawa KA, Lisowska KM. Advances in ovarian cancer therapy. *Cancer Chemotherapy and Pharmacology*. 2018;81(1):17-38.
343. Hironaka S. Anti-angiogenic therapies for gastric cancer. *Asia-Pacific Journal of Clinical Oncology*. 2019;15(4):208-17.
344. Tanyi JL, Bobisse S, Ophir E, Tuyaerts S, Roberti A, Genolet R, et al. Personalized cancer vaccine effectively mobilizes antitumor T cell immunity in ovarian cancer. *Sci Transl Med*. 2018;10(436).
345. Sanmamed MF, Pastor F, Rodriguez A, Perez-Gracia JL, Rodriguez-Ruiz ME, Jure-Kunkel M, et al. Agonists of Co-stimulation in Cancer Immunotherapy Directed Against CD137, OX40, GITR, CD27, CD28, and ICOS. *Semin Oncol*. 2015;42(4):640-55.
346. Bose C. Immune checkpoint blockers and ovarian cancer. *Indian Journal of Medical and Paediatric Oncology*. 2017;38(2):182-9.
347. Mittica G, Genta S, Aglietta M, Valabrega G. Immune Checkpoint Inhibitors: A New Opportunity in the Treatment of Ovarian Cancer? *Int J Mol Sci*. 2016;17(7).
348. Sheridan C. IDO inhibitors move center stage in immuno-oncology. *Nat Biotechnol*. 2015;33(4):321-2.
349. Chen X, Song E. Turning foes to friends: targeting cancer-associated fibroblasts. *Nature Reviews Drug Discovery*. 2019;18(2):99-115.
350. Barrett R, Puré E. Cancer-associated fibroblasts: key determinants of tumor immunity and immunotherapy. *Current Opinion in Immunology*. 2020;64:80-7.
351. Truffi M, Sorrentino L, Corsi F. Fibroblasts in the Tumor Microenvironment. *Adv Exp Med Biol*. 2020;1234:15-29.
352. Gourley C, Balmaña J, Ledermann JA, Serra V, Dent R, Loibl S, et al. Moving From Poly (ADP-Ribose) Polymerase Inhibition to Targeting DNA Repair and DNA Damage Response in Cancer Therapy. *J Clin Oncol*. 2019;37(25):2257-69.
353. Irish JM, Doxie DB. High-dimensional single-cell cancer biology. *Curr Top Microbiol Immunol*. 2014;377:1-21.
354. Lee JM, Gordon N, Trepel JB, Lee MJ, Yu M, Kohn EC. Development of a multiparameter flow cytometric assay as a potential biomarker for homologous

-
- recombination deficiency in women with high-grade serous ovarian cancer. *J Transl Med.* 2015;13:239.
355. Futamura K, Sekino M, Hata A, Ikebuchi R, Nakanishi Y, Egawa G, et al. Novel full-spectral flow cytometry with multiple spectrally-adjacent fluorescent proteins and fluorochromes and visualization of in vivo cellular movement. *Cytometry A.* 2015;87(9):830-42.
356. Kimball AK, Oko LM, Bullock BL, Nemenoff RA, van Dyk LF, Clambey ET. *A Beginner's Guide to Analyzing and Visualizing Mass Cytometry Data.* 2018;200(1):3-22.
357. Levine JH, Simonds EF, Bendall SC, Davis KL, Amir el AD, Tadmor MD, et al. Data-Driven Phenotypic Dissection of AML Reveals Progenitor-like Cells that Correlate with Prognosis. *Cell.* 2015;162(1):184-97.
358. Qiu P, Simonds EF, Bendall SC, Gibbs KD, Jr., Bruggner RV, Linderman MD, et al. Extracting a cellular hierarchy from high-dimensional cytometry data with SPADE. *Nat Biotechnol.* 2011;29(10):886-91.
359. Van Gassen S, Callebaut B, Van Helden MJ, Lambrecht BN, Demeester P, Dhaene T, et al. FLOW-SOM: Using self-organizing maps for visualization and interpretation of cytometry data. *Cytometry A.* 2015;87(7):636-45.
360. van der Maaten L, Hinton G. Visualizing High-Dimensional Data Using t-SNE.(2008). Reference Source [Google Scholar]. 2008.
361. Pezzotti N, Höllt T, Lelieveldt B, Eisemann E, Vilanova A, editors. Hierarchical stochastic neighbor embedding. *Computer Graphics Forum*; 2016: Wiley Online Library.
362. Becht E, McInnes L, Healy J, Dutertre C-A, Kwok IW, Ng LG, et al. Dimensionality reduction for visualizing single-cell data using UMAP. *Nature biotechnology.* 2019;37(1):38-44.
363. Chevrier S, Levine JH, Zanotelli VRT, Silina K, Schulz D, Bacac M, et al. An immune atlas of clear cell renal cell carcinoma. *Cell.* 2017;169(4):736-49. e18.
364. Wagner J, Rapsomaniki MA, Chevrier S, Anzeneder T, Langwieder C, Dykgers A, et al. A Single-Cell Atlas of the Tumor and Immune Ecosystem of Human Breast Cancer. *Cell.* 2019;177(5):1330-45.e18.
365. Lavin Y, Kobayashi S, Leader A, Amir E-aD, Elefant N, Bigenwald C, et al. Innate immune landscape in early lung adenocarcinoma by paired single-cell analyses. *Cell.* 2017;169(4):750-65. e17.
366. Simoni Y, Becht E, Fehlings M, Loh CY, Koo S-L, Teng KWW, et al. Bystander CD8+ T cells are abundant and phenotypically distinct in human tumour infiltrates. *Nature.* 2018;557(7706):575-9.
367. Goveia J, Rohlenova K, Taverna F, Treps L, Conradi L-C, Pircher A, et al. An integrated gene expression landscape profiling approach to identify lung tumor endothelial cell heterogeneity and angiogenic candidates. *Cancer Cell.* 2020;37(1):21-36. e13.
368. Sankowski R, Böttcher C, Masuda T, Geirsdottir L, Sindram E, Seredenina T, et al. Mapping microglia states in the human brain through the integration of high-dimensional techniques. *Nature neuroscience.* 2019;22(12):2098-110.

-
369. Goswami S, Walle T, Cornish AE, Basu S, Anandhan S, Fernandez I, et al. Immune profiling of human tumors identifies CD73 as a combinatorial target in glioblastoma. *Nature medicine*. 2020;26(1):39-46.
370. Halaby MJ, Hezaveh K, Lamorte S, Kloetgen A, MacLeod BL, Guo M, et al. GCN2 drives macrophage and MDSC function and immunosuppression in the tumor microenvironment. *Science immunology*. 2019;4(42).
371. Helmink BA, Reddy SM, Gao J, Zhang S, Basar R, Thakur R, et al. B cells and tertiary lymphoid structures promote immunotherapy response. *Nature*. 2020;577(7791):549-55.
372. Wei SC, Levine JH, Cogdill AP, Zhao Y, Anang N-AA, Andrews MC, et al. Distinct cellular mechanisms underlie anti-CTLA-4 and anti-PD-1 checkpoint blockade. *Cell*. 2017;170(6):1120-33. e17.
373. Krieg C, Nowicka M, Guglietta S, Schindler S, Hartmann FJ, Weber LM, et al. High-dimensional single-cell analysis predicts response to anti-PD-1 immunotherapy. *Nature medicine*. 2018;24(2):144.
374. Spitzer MH, Carmi Y, Reticker-Flynn NE, Kwek SS, Madhireddy D, Martins MM, et al. Systemic immunity is required for effective cancer immunotherapy. *Cell*. 2017;168(3):487-502. e15.
375. Zhang Q, Lou Y, Yang J, Wang J, Feng J, Zhao Y, et al. Integrated multiomic analysis reveals comprehensive tumour heterogeneity and novel immunophenotypic classification in hepatocellular carcinomas. *Gut*. 2019;68(11).
376. Chew V, Lai L, Pan L, Lim CJ, Li J, Ong R, et al. Delineation of an immunosuppressive gradient in hepatocellular carcinoma using high-dimensional proteomic and transcriptomic analyses. *Proceedings of the National Academy of Sciences*. 2017;114(29):E5900-E9.
377. Baughn LB, Sachs Z, Noble-Orcutt KE, Mitra A, Van Ness BG, Linden MA. Phenotypic and functional characterization of a bortezomib-resistant multiple myeloma cell line by flow and mass cytometry. *Leukemia & lymphoma*. 2017;58(8):1931-40.
378. Hansmann L, Blum L, Ju C-H, Liedtke M, Robinson WH, Davis MM. Mass cytometry analysis shows that a novel memory phenotype B cell is expanded in multiple myeloma. *Cancer immunology research*. 2015;3(6):650-60.
379. Adams III HC, Stevenaert F, Krejcik J, Van der Borght K, Smets T, Bald J, et al. High-parameter mass cytometry evaluation of relapsed/refractory multiple myeloma patients treated with daratumumab demonstrates immune modulation as a novel mechanism of action. *Cytometry Part A*. 2019;95(3):279-89.
380. Marsh-Wakefield F, Kruzins A, McGuire HM, Yang S, Bryant CE, Fazekas De St Groth B, et al. Mass cytometry discovers two discrete subsets of CD39-Treg which discriminate MGUS from Multiple Myeloma. *Frontiers in immunology*. 2019;10:1596.
381. de Vries NL, Van Unen V, Ijsselsteijn ME, Abdelaal T, Van Der Breggen R, Sarasqueta AF, et al. High-dimensional cytometric analysis of colorectal cancer reveals novel mediators of antitumour immunity. *Gut*. 2020;69(4):691-703.
382. Zhang T, Lv J, Tan Z, Wang B, Li Y, Jiang H, et al. Immunocyte profiling using single-cell mass cytometry reveals EpCAM⁺ CD4⁺ T cells abnormal in colon cancer. *Frontiers in immunology*. 2019;10:1571.

-
383. Hartmann FJ, Mrdjen D, McCaffrey E, Glass DR, Greenwald NF, Bharadwaj A, et al. Multiplexed Single-cell Metabolic Profiles Organize the Spectrum of Human Cytotoxic T Cells. *bioRxiv*. 2020.
384. Gonzalez VD, Samusik N, Chen TJ, Savig ES, Aghaeepour N, Quigley DA, et al. Commonly Occurring Cell Subsets in High-Grade Serous Ovarian Tumors Identified by Single-Cell Mass Cytometry. *Cell Rep*. 2018;22(7):1875-88.
385. Toker A, Nguyen LT, Stone SC, Yang C, Katz SR, Shaw PA, et al. Regulatory T cells in ovarian cancer are characterized by a highly activated phenotype distinct from that in melanoma. *Clinical Cancer Research*. 2018:clincanres.0554.2018.
386. Kverneland AH, Pedersen M, Westergaard MCW, Nielsen M, Borch TH, Olsen LR, et al. Adoptive cell therapy in combination with checkpoint inhibitors in ovarian cancer. *Oncotarget*. 2020;11(22).
387. Casado J, Lehtonen O, Rantanen V, Kaipio K, Pasquini L, Häkkinen A, et al. Agile Workflow For Interactive Analysis Of Mass Cytometry Data. *Bioinformatics*. 2020.
388. Bodenmiller B, Zunder ER, Finck R, Chen TJ, Savig ES, Bruggner RV, et al. Multiplexed mass cytometry profiling of cellular states perturbed by small-molecule regulators. *Nature biotechnology*. 2012;30(9):858-67.
389. Kourelis TV, Villasboas JC, Jessen E, Dasari S, Dispenziera A, Jevremovic D, et al. Mass cytometry dissects T cell heterogeneity in the immune tumor microenvironment of common dysproteinemias at diagnosis and after first line therapies. *Blood Cancer Journal*. 2019;9(9):72.
390. Azizi E, Carr AJ, Plitas G, Cornish AE, Konopacki C, Prabhakaran S, et al. Single-Cell Map of Diverse Immune Phenotypes in the Breast Tumor Microenvironment. *Cell*. 2018;174(5):1293-308.e36.
391. Finotello F, Mayer C, Plattner C. Molecular and pharmacological modulators of the tumor immune contexture revealed by deconvolution of RNA-seq data. *Genome Med* 11: 34. 2019.
392. Gerlinger M, Rowan AJ, Horswell S, Larkin J, Endesfelder D, Gronroos E, et al. Intratumor heterogeneity and branched evolution revealed by multiregion sequencing. *N Engl J Med*. 2012;366:883-92.
393. Thorsson V, Gibbs DL, Brown SD, Wolf D, Bortone DS, Yang T-HO, et al. The immune landscape of cancer. *Immunity*. 2018;48(4):812-30. e14.
394. Yeung CLA, Co N-N, Tsuruga T, Yeung T-L, Kwan S-Y, Leung CS, et al. Exosomal transfer of stroma-derived miR21 confers paclitaxel resistance in ovarian cancer cells through targeting APAF1. *Nature communications*. 2016;7(1):1-14.
395. Jiménez-Sánchez A, Cybulska P, Mager KL, Koplev S, Cast O, Couturier D-L, et al. Unraveling tumor-immune heterogeneity in advanced ovarian cancer uncovers immunogenic effect of chemotherapy. *Nature Genetics*. 2020:1-12.
396. Ahmadzadeh M, Pasetto A, Jia L, Deniger DC, Stevanović S, Robbins PF, et al. Tumor-infiltrating human CD4+ regulatory T cells display a distinct TCR repertoire and exhibit tumor and neoantigen reactivity. *Science immunology*. 2019;4(31).
397. Curtis M, Kenny HA, Ashcroft B, Mukherjee A, Johnson A, Zhang Y, et al. Fibroblasts mobilize tumor cell glycogen to promote proliferation and metastasis. *Cell metabolism*. 2019;29(1):141-55. e9.

-
398. Hernandez-Fernaund JR, Ruengeler E, Casazza A, Neilson LJ, Pulleine E, Santi A, et al. Secreted CLIC3 drives cancer progression through its glutathione-dependent oxidoreductase activity. *Nature communications*. 2017;8(1):1-17.
399. Finkernagel F, Reinartz S, Schuldner M, Malz A, Jansen JM, Wagner U, et al. Dual-platform affinity proteomics identifies links between the recurrence of ovarian carcinoma and proteins released into the tumor microenvironment. *Theranostics*. 2019;9(22):6601.
400. Yang SC, Lheureux S, Karakasis K, Burnier JV, Bruce JP, Clouthier DL, et al. Landscape of genomic alterations in high-grade serous ovarian cancer from exceptional long-and short-term survivors. *Genome medicine*. 2018;10(1):81.
401. Pearce OM, Delaine-Smith RM, Maniati E, Nichols S, Wang J, Böhm S, et al. Deconstruction of a metastatic tumor microenvironment reveals a common matrix response in human cancers. *Cancer discovery*. 2018;8(3):304-19.
402. Zhang AW, McPherson A, Milne K, Kroeger DR, Hamilton PT, Miranda A, et al. Interfaces of Malignant and Immunologic Clonal Dynamics in Ovarian Cancer. *Cell*. 2018;173(7):1755-69.e22.
403. Wanderley CW, Colon DF, Luiz JPM, Oliveira FF, Viacava PR, Leite CA, et al. Paclitaxel reduces tumor growth by reprogramming tumor-associated macrophages to an M1 profile in a TLR4-dependent manner. *Cancer research*. 2018;78(20):5891-900.
404. Mak MP, Tong P, Diao L, Cardnell RJ, Gibbons DL, William WN, et al. A patient-derived, pan-cancer EMT signature identifies global molecular alterations and immune target enrichment following epithelial-to-mesenchymal transition. *Clinical Cancer Research*. 2016;22(3):609-20.
405. Buenrostro JD, Giresi PG, Zaba LC, Chang HY, Greenleaf WJ. Transposition of native chromatin for fast and sensitive epigenomic profiling of open chromatin, DNA-binding proteins and nucleosome position. *Nature methods*. 2013;10(12):1213.
406. Frommer M, McDonald LE, Millar DS, Collis CM, Watt F, Grigg GW, et al. A genomic sequencing protocol that yields a positive display of 5-methylcytosine residues in individual DNA strands. *Proceedings of the National Academy of Sciences*. 1992;89(5):1827-31.
407. Schmid M, Durussel T, Laemmli UK. ChIC and ChEC: genomic mapping of chromatin proteins. *Molecular cell*. 2004;16(1):147-57.
408. Dekker J, Rippe K, Dekker M, Kleckner N. Capturing chromosome conformation. *science*. 2002;295(5558):1306-11.
409. Wang Y, Navin NE. Advances and applications of single-cell sequencing technologies. *Molecular cell*. 2015;58(4):598-609.
410. Van Haaften C. 18 - Role of Immunohistochemical Expression of Fas in Ovarian Carcinoma. In: Hayat MA, editor. *Handbook of Immunohistochemistry and in Situ Hybridization of Human Carcinomas*. 4: Academic Press; 2006. p. 457-63.
411. Takai N, Miyakawa I. 22 - Role of Elf-1 in Epithelial Ovarian Carcinoma: Immunohistochemistry. In: Hayat MA, editor. *Handbook of Immunohistochemistry and in Situ Hybridization of Human Carcinomas*. 4: Academic Press; 2006. p. 487-92.
412. Ohishi Y, Kaneki E, Tamiya S, Oda Y, Hirakawa T, Miyamoto S, et al. 7 - Role of Immunohistochemical Expression of Ki-67 in Ovarian Carcinoma. In: Hayat MA,

-
- editor. Handbook of Immunohistochemistry and in Situ Hybridization of Human Carcinomas. 4: Academic Press; 2006. p. 363-70.
413. Nishida N, Yano H, Komai K, Nishida T, Kamura T, Kojiro M. 16 - Role of Immunohistochemical Expression of Vascular Endothelial Growth Factor C and Vascular Endothelial Growth Factor Receptor 2 in Ovarian Cancer. In: Hayat MA, editor. Handbook of Immunohistochemistry and in Situ Hybridization of Human Carcinomas. 4: Academic Press; 2006. p. 441-7.
414. Miyatake T, Shroyer KR. 24 - Immunohistochemical Validation of B7-H4 (DD-O110) as a Biomarker of Ovarian Cancer: Correlation with CA-125. In: Hayat MA, editor. Handbook of Immunohistochemistry and in Situ Hybridization of Human Carcinomas. 4: Academic Press; 2006. p. 499-503.
415. Faleiro-Rodrigues C, Macedo-Pinto I, Pereira D. 12 - Epithelial Ovarian Cancer and the E-Cadherin–Catenin Complex. In: Hayat MA, editor. Handbook of Immunohistochemistry and in Situ Hybridization of Human Carcinomas. 4: Academic Press; 2006. p. 399-403.
416. Aoki Y, Tanaka K. 4 - Role of Immunohistochemical Expression of BRCA1 in Ovarian Carcinoma. In: Hayat MA, editor. Handbook of Immunohistochemistry and in Situ Hybridization of Human Carcinomas. 4: Academic Press; 2006. p. 339-46.
417. Ijsselsteijn ME, Brouwer TP, Abdulrahman Z, Reidy E, Ramalheiro A, Heeren AM, et al. Cancer immunophenotyping by seven-colour multispectral imaging without tyramide signal amplification. *The Journal of Pathology: Clinical Research*. 2019;5(1):3-11.
418. Giesen C, Wang HA, Schapiro D, Zivanovic N, Jacobs A, Hattendorf B, et al. Highly multiplexed imaging of tumor tissues with subcellular resolution by mass cytometry. *Nat Methods*. 2014;11(4):417-22.
419. Angelo M, Bendall SC, Finck R, Hale MB, Hitzman C, Borowsky AD, et al. Multiplexed ion beam imaging of human breast tumors. *Nature medicine*. 2014;20(4):436-42.
420. Chang Q, Ornatsky OI, Siddiqui I, Loboda A, Baranov VI, Hedley DW. Imaging Mass Cytometry. *Cytometry A*. 2017;91(2):160-9.
421. Jackson HW, Fischer JR, Zanotelli VR, Ali HR, Mechera R, Soysal SD, et al. The single-cell pathology landscape of breast cancer. *Nature*. 2020;578(7796):615-20.
422. Schulz D, Zanotelli VRT, Fischer JR, Schapiro D, Engler S, Lun X-K, et al. Simultaneous multiplexed imaging of mRNA and proteins with subcellular resolution in breast cancer tissue samples by mass cytometry. *Cell systems*. 2018;6(1):25-36. e5.
423. Ijsselsteijn ME, van der Breggen R, Farina Sarasqueta A, Koning F, de Miranda NF. A 40-marker panel for high dimensional characterization of cancer immune microenvironments by imaging mass cytometry. *Frontiers in immunology*. 2019;10:2534.
424. Somarakis A, Van Unen V, Koning F, Lelieveldt BP, Höllt T. ImaCytE: Visual Exploration of Cellular Microenvironments for Imaging Mass Cytometry Data. *IEEE Transactions on Visualization and Computer Graphics*. 2019.
425. Schapiro D, Jackson HW, Raghuraman S, Fischer JR, Zanotelli VR, Schulz D, et al. histoCAT: analysis of cell phenotypes and interactions in multiplex image cytometry data. *Nature methods*. 2017;14(9):873.

-
426. Carpenter AE, Jones TR, Lamprecht MR, Clarke C, Kang IH, Friman O, et al. CellProfiler: image analysis software for identifying and quantifying cell phenotypes. *Genome biology*. 2006;7(10):R100.
427. Sommer C, Straehle C, Koethe U, Hamprecht FA, editors. *Ilastik: Interactive learning and segmentation toolkit*. 2011 IEEE international symposium on biomedical imaging: From nano to macro; 2011: IEEE.
428. Zhu Y, Ferri-Borgogno S, Sheng J, Yeung T-L, Burks JK, Cappello P, et al. SIO: A Spatioimageomics Pipeline to Identify Prognostic Biomarkers Associated with the Ovarian Tumor Microenvironment. 2021;13(8):1777.
429. Decalf J, Albert ML, Ziai J. New tools for pathology: a user's review of a highly multiplexed method for in situ analysis of protein and RNA expression in tissue. *The Journal of Pathology*. 2019;247(5):650-61.
430. Momenimovahed Z, Tiznobaik A, Taheri S, Salehiniya H. Ovarian cancer in the world: epidemiology and risk factors. *International journal of women's health*. 2019;11:287-99.
431. Gourley C, Bookman MA. Evolving Concepts in the Management of Newly Diagnosed Epithelial Ovarian Cancer. *J Clin Oncol*. 2019;37(27):2386-97.
432. Labani-Motlagh A, Ashja-Mahdavi M, Loskog A. The Tumor Microenvironment: A Milieu Hindering and Obstructing Antitumor Immune Responses. 2020;11(940).
433. Rundgren IM, Ersvær E, Ahmed AB, Rynningen A, Bruserud Ø. A Pilot Study of Circulating Monocyte Subsets in Patients Treated with Stem Cell Transplantation for High-Risk Hematological Malignancies. 2020;56(1):36.
434. Leelatian N, Doxie DB, Greenplate AR, Mobley BC, Lehman JM, Sinnaeve J, et al. Single Cell Analysis of Human Tissues and Solid Tumors with Mass Cytometry. *Cytometry B Clin Cytom*. 2017.
435. Anandan S, Thomsen LCV, Gullaksen S-E, Abdelaal T, Kleinmanns K, Skavland J, et al. Phenotypic Characterization by Mass Cytometry of the Microenvironment in Ovarian Cancer and Impact of Tumor Dissociation Methods. 2021;13(4):755.
436. Bendall SC, Simonds EF, Qiu P, Amir el AD, Krutzik PO, Finck R, et al. Single-cell mass cytometry of differential immune and drug responses across a human hematopoietic continuum. *Science*. 2011;332(6030):687-96.
437. Polakova I, Pelak O, Thurner D, Pokryvkova B, Tachezy R, Kalina T, et al. Implementation of Mass Cytometry for Immunoprofiling of Patients with Solid Tumors. *J Immunol Res*. 2019;2019:6705949.
438. Brodie TM, Tosevski V, Medova M. OMIP-045: Characterizing human head and neck tumors and cancer cell lines with mass cytometry. *Cytometry A*. 2018;93(4):406-10.
439. Takahashi C, Au-Yeung A, Fuh F, Ramirez-Montagut T, Bolen C, Mathews W, et al. Mass cytometry panel optimization through the designed distribution of signal interference. *Cytometry Part A : the journal of the International Society for Analytical Cytology*. 2016;91.
440. Liu X, Song W, Wong BY, Zhang T, Yu S, Lin GN, et al. A comparison framework and guideline of clustering methods for mass cytometry data. *Genome Biology*. 2019;20(1):297.





-
441. Samusik N, Good Z, Spitzer MH, Davis KL, Nolan GP. Automated mapping of phenotype space with single-cell data. *Nat Methods*. 2016;13(6):493-6.
 442. Amir E-aD, Lee B, Badoual P, Gordon M, Guo XV, Merad M, et al. Development of a Comprehensive Antibody Staining Database Using a Standardized Analytics Pipeline. 2019;10(1315).
 443. Robinson MD, McCarthy DJ, Smyth GK. edgeR: a Bioconductor package for differential expression analysis of digital gene expression data. *Bioinformatics*. 2010;26(1):139-40.
 444. Finak G, Langweiler M, Jaimes M, Malek M, Taghiyar J, Korin Y, et al. Standardizing Flow Cytometry Immunophenotyping Analysis from the Human ImmunoPhenotyping Consortium. *Sci Rep*. 2016;6:20686.
 445. Lun ATL, Richard AC, Marioni JC. Testing for differential abundance in mass cytometry data. *Nat Methods*. 2017;14(7):707-9.
 446. Maecker HT, McCoy JP, Nussenblatt R. Standardizing immunophenotyping for the Human Immunology Project. *Nat Rev Immunol*. 2012;12(3):191-200.
 447. McCarthy DJ, Chen Y, Smyth GK. Differential expression analysis of multifactor RNA-Seq experiments with respect to biological variation. *Nucleic acids research*. 2012;40(10):4288-97.
 448. Darvin P, Toor SM, Sasidharan Nair V, Elkord E. Immune checkpoint inhibitors: recent progress and potential biomarkers. *Experimental & Molecular Medicine*. 2018;50(12):1-11.
 449. Moore KN, Pignata S. Trials in progress: IMagyn050/GOG 3015/ENGOT-OV39. A Phase III, multicenter, randomized study of atezolizumab versus placebo administered in combination with paclitaxel, carboplatin, and bevacizumab to patients with newly-diagnosed stage III or stage IV ovarian, fallopian tube, or primary peritoneal cancer. *Int J Gynecol Cancer*. 2019.
 450. Deshpande M, Romanski PA, Rosenwaks Z, Gerhardt J. Gynecological Cancers Caused by Deficient Mismatch Repair and Microsatellite Instability. 2020;12(11):3319.
 451. Zhang T, Warden AR, Li Y, Ding X. Progress and applications of mass cytometry in sketching immune landscapes. 2020;10(6):e206.
 452. Hartmann FJ, Babbord J, Gherardini PF, Amir ED, Jones K, Sahaf B, et al. Comprehensive Immune Monitoring of Clinical Trials to Advance Human Immunotherapy. *Cell Rep*. 2019;28(3):819-31.e4.
 453. Olsen LR, Leipold MD, Pedersen CB, Maecker HT. The anatomy of single cell mass cytometry data. 2019;95(2):156-72.
 454. Bobisse S, Genolet R, Roberti A, Tanyi JL, Racle J, Stevenson BJ, et al. Sensitive and frequent identification of high avidity neo-epitope specific CD8⁺T cells in immunotherapy-naïve ovarian cancer. *Nature Communications*. 2018;9(1):1092.
 455. Hornburg M, Desbois M, Lu S, Guan Y, Lo AA, Kaufman S, et al. Single-cell dissection of cellular components and interactions shaping the tumor immune phenotypes in ovarian cancer. *Cancer Cell*. 2021.
 456. Tricot S, Meyrand M, Sammicheli C, Elhmouzi-Younes J, Corneau A, Bertholet S, et al. Evaluating the efficiency of isotope transmission for improved panel design and a comparison of the detection sensitivities of mass cytometer instruments. 2015;87(4):357-68.

-
457. Takahashi C, Au-Yeung A, Fuh F, Ramirez-Montagut T, Bolen C, Mathews W, et al. Mass cytometry panel optimization through the designed distribution of signal interference. 2017;91(1):39-47.
458. Gonder S, Fernandez Botana I, Wierz M, Pagano G, Gargiulo E, Cosma A, et al. Method for the Analysis of the Tumor Microenvironment by Mass Cytometry: Application to Chronic Lymphocytic Leukemia. 2020;11(2730).
459. Han G, Spitzer MH, Bendall SC, Fantl WJ, Nolan GP. Metal-isotope-tagged monoclonal antibodies for high-dimensional mass cytometry. *Nature Protocols*. 2018;13(10):2121-48.
460. Sakkestad ST, Skavland J, Hanevik K. Whole blood preservation methods alter chemokine receptor detection in mass cytometry experiments. *Journal of Immunological Methods*. 2020;476:112673.
461. Spitzer Matthew H, Nolan Garry P. Mass Cytometry: Single Cells, Many Features. *Cell*. 2016;165(4):780-91.
462. Konstantinopoulos PA, Cannistra SA. Immune Checkpoint Inhibitors in Ovarian Cancer: Can We Bridge the Gap Between IMagynation and Reality? ;0(0):JCO.21.00571.
463. Bashashati A, Ha G, Tone A, Ding J, Prentice LM, Roth A, et al. Distinct evolutionary trajectories of primary high-grade serous ovarian cancers revealed through spatial mutational profiling. *J Pathol*. 2013;231(1):21-34.
464. McGranahan N, Swanton C. Clonal Heterogeneity and Tumor Evolution: Past, Present, and the Future. *Cell*. 2017;168(4):613-28.
465. Drakes ML, Stiff PJ. Regulation of Ovarian Cancer Prognosis by Immune Cells in the Tumor Microenvironment. *Cancers (Basel)*. 2018;10(9).
466. Schauer IG, Sood AK, Mok S, Liu J. Cancer-Associated Fibroblasts and Their Putative Role in Potentiating the Initiation and Development of Epithelial Ovarian Cancer. *Neoplasia*. 2011;13(5):393-405.
467. Sahai E, Astsaturov I, Cukierman E, DeNardo DG, Egeblad M, Evans RM, et al. A framework for advancing our understanding of cancer-associated fibroblasts. *Nature Reviews Cancer*. 2020;20(3):174-86.
468. Hegde PS, Karanikas V, Evers SJCCR. The where, the when, and the how of immune monitoring for cancer immunotherapies in the era of checkpoint inhibition. 2016;22(8):1865-74.
469. Drakes ML, Czerlanis CM, Stiff PJ. Immune Checkpoint Blockade in Gynecologic Cancers: State of Affairs. 2020;12(11):3301.
470. Hegde PS, Chen DSJI. Top 10 challenges in cancer immunotherapy. 2020;52(1):17-35.
471. Zielinski JM, Luke JJ, Guglietta S, Krieg C. High Throughput Multi-Omics Approaches for Clinical Trial Evaluation and Drug Discovery. *Front Immunol*. 2021;12:590742.
472. Kay AW, Strauss-Albee DM, Blish CA. Application of Mass Cytometry (CyTOF) for Functional and Phenotypic Analysis of Natural Killer Cells. *Methods in molecular biology (Clifton, NJ)*. 2016;1441:13-26.

I

Article

Phenotypic Characterization by Mass Cytometry of the Microenvironment in Ovarian Cancer and Impact of Tumor Dissociation Methods

Shamundeewari Anandan^{1,2,†}, Liv Cecilie V. Thomsen^{1,2,†}, Stein-Erik Gullaksen¹ , Tamim Abdelaal³, Katrin Kleinmanns¹ , Jørn Skavland¹, Geir Bredholt¹, Bjørn Tore Gjertsen^{1,4} , Emmet McCormack^{1,5} and Line Bjørge^{1,2,*} 

- ¹ Centre for Cancer Biomarkers, Department of Clinical Science, University of Bergen, 5021 Bergen, Norway; Shamundeewari.Anandan@uib.no (S.A.); liv.vestheim@uib.no (L.C.V.T.); stein.gullaksen@uib.no (S.-E.G.); katrin.kleinmanns@uib.no (K.K.); Jørn.Skavland@uib.no (J.S.); Geir.Bredholt@uib.no (G.B.); bjorn.gjertsen@uib.no (B.T.G.); Emmet.Mc.Cormack@uib.no (E.M.)
- ² Department of Obstetrics and Gynecology, Haukeland University Hospital, 5021 Bergen, Norway
- ³ Delft Bioinformatics Lab, Delft University of Technology, 2600 AA Delft, The Netherlands; T.R.M.Abdelaal-1@tudelft.nl
- ⁴ Department of Internal Medicine, Hematology Section, Haukeland University Hospital, 5021 Bergen, Norway
- ⁵ Centre for Pharmacy, Department of Clinical Science, The University of Bergen, Jonas Lies vei 65, 5021 Bergen, Norway
- * Correspondence: Line.Bjorge@uib.no
- † These authors contributed equally to this work.



Citation: Anandan, S.; Thomsen, L.C.V.; Gullaksen, S.-E.; Abdelaal, T.; Kleinmanns, K.; Skavland, J.; Bredholt, G.; Gjertsen, B.T.; McCormack, E.; Bjørge, L. Phenotypic Characterization by Mass Cytometry of the Microenvironment in Ovarian Cancer and Impact of Tumor Dissociation Methods. *Cancers* **2021**, *13*, 755. <https://doi.org/10.3390/cancers13040755>

Academic Editor:

Ronald Buckanovich

Received: 4 January 2021

Accepted: 9 February 2021

Published: 11 February 2021

Publisher's Note: MDPI stays neutral with regard to jurisdictional claims in published maps and institutional affiliations.



Copyright: © 2021 by the authors. Licensee MDPI, Basel, Switzerland. This article is an open access article distributed under the terms and conditions of the Creative Commons Attribution (CC BY) license (<https://creativecommons.org/licenses/by/4.0/>).

Simple Summary: High-grade serous ovarian cancer (HGSOC) is the deadliest gynecological malignancy. Despite increasing research on HGSOC, biomarkers for individualized selection of therapy are scarce. In this study, we develop a multiparametric mass cytometry antibody panel to identify differences in the cellular composition of the microenvironment of tumor tissues dissociated to single-cell suspensions. We also investigate how dissociation methods impact results. Application of our antibody panel to HGSOC tissues showed its ability to identify established main cell subsets and subpopulations of these cells. Comparisons between dissociation methods revealed differences in cell fractions for one immune, two stromal, and three tumor cell subpopulations, while functional marker expression was not affected by the dissociation method. The interpatient disparities identified in the tumor microenvironment were more significant than those identified between differently dissociated tissues from one patient, indicating that the panel facilitates the mapping of individual tumor microenvironments in HGSOC patients.

Abstract: Improved molecular dissection of the tumor microenvironment (TME) holds promise for treating high-grade serous ovarian cancer (HGSOC), a gynecological malignancy with high mortality. Reliable disease-related biomarkers are scarce, but single-cell mapping of the TME could identify patient-specific prognostic differences. To avoid technical variation effects, however, tissue dissociation effects on single cells must be considered. We present a novel Cytometry by Time-of-Flight antibody panel for single-cell suspensions to identify individual TME profiles of HGSOC patients and evaluate the effects of dissociation methods on results. The panel was developed utilizing cell lines, healthy donor blood, and stem cells and was applied to HGSOC tissues dissociated by six methods. Data were analyzed using Cytobank and X-shift and illustrated by t-distributed stochastic neighbor embedding plots, heatmaps, and stacked bar and error plots. The panel distinguishes the main cellular subsets and subpopulations, enabling characterization of individual TME profiles. The dissociation method affected some immune ($n = 1$), stromal ($n = 2$), and tumor ($n = 3$) subsets, while functional marker expressions remained comparable. In conclusion, the panel can identify subsets of the HGSOC TME and can be used for in-depth profiling. This panel represents a promising profiling tool for HGSOC when tissue handling is considered.

Keywords: high-grade serous ovarian cancer (HGSOC); single-cell mass cytometry; Cytometry by Time-of-Flight (CyTOF); tumor microenvironment (TME); cell expression profile; tumor dissociation; characterization

1. Introduction

The five-year survival rate is low for high-grade serous ovarian cancer (HGSOC), the most common epithelial ovarian cancer subtype, and long-term survival rates have improved only modestly over the last three decades despite increasingly aggressive surgical and chemotherapeutic approaches [1].

Like other malignant tumors, HGSOC consists not only of aggregates of heterogeneous populations of cancer cells but also of a variety of stromal and infiltrating immune cells, extracellular matrix proteins, and secreted molecules, collectively known as the tumor microenvironment (TME) [2,3]. This complex and dynamic interactive entity contributes to tumor growth through a reciprocal interplay between cancer and host cells [2,4].

The characterization of the composition, organization, and functionality of the HGSOC TME using sensitive tools [5] is fundamental for developing new management strategies and improving survival rates [6]. Traditionally, immunohistochemistry analysis and large-scale high-throughput omics technologies have been used for HGSOC TME characterization on the single-cell level [7–11]. Some components of the TME have been described using various methods, such as gene expression analyses of mRNA and microRNA, genetic mapping of promoter methylation and DNA copy numbers, and immune cell-focused analysis of the T cell receptor. However, a global depiction of the constituent cells of the TME is still required [6–10]. Single-cell Cytometry by Time-of-Flight (CyTOF), a relatively new method for single-cell profiling, utilizes stable isotopes combined with monoclonal antibodies as reporters. The method enables detailed phenotypic characterization and simultaneous detection of over 40 parameters per cell at a single-cell level [12]. However, few studies using this method of single-cell phenotyping of HGSOC tissues have been published. Those that are available describe novel cellular phenotypes associated with a specific immunological TME [13–17]. Gonzalez et al. applied a CyTOF panel of 41 antibody markers to dissociated tumors. Four of the markers were used to identify viable tumor cells and exclude stromal, immune, and blood vessel cells, and the remaining markers were used to interrogate HGSOC tumor cell biology [13]. Toker et al. and Kverneland et al. applied the CyTOF method to dissociated HGSOC tissues, focusing exclusively on the different T cell subsets of the ovarian cancer TME [14,15], while Casado et al. applied a new analysis tool combined with a HGSOC mass cytometry panel, which enabled them to identify different subsets of cells, mainly tumor and immune cells, in dissociated tissues [16]. Currently, except for Casado et al.'s study, the published research has been largely restricted to comparisons within tumor or immune cell subsets, while a more global characterization of all major cell subsets of the TME is lacking.

Due to the underlying complexity of data generated through CyTOF analyses, adequate attention to sample preparation is crucial to avoid introducing technically induced variation that may obscure biological insights. A common goal when preparing single-cell suspensions from solid tumors is to preserve cell viability and cellular diversity [18]. However, the extent to which the expression of certain markers is disrupted by the process of common tissue dissociation methods is incompletely understood. To interpret in-depth single-cell phenotyping results, it is important to establish a comprehensive understanding of the effects of sample conditioning. This information should also be included in the standard protocols for tissue dissociation to avoid unacknowledged methodological bias introduced by the sample treatment. Systematic comparisons of the cellular effects of tissue preparation techniques have previously been carried out in CyTOF analyses of gliomas, melanomas, small cell lung cancer, and tonsil tissues but not in HGSOC [18,19].

In this study, we present a novel TME-based 35-marker CyTOF panel to identify patient-specific tumor phenotypes. The CyTOF panel is optimized for single-cell suspensions of HGSOC tissues and delineates the main cell subsets of the TME: tumor cells, the immune cell subset, and the stromal niche. By applying the CyTOF panel to patient material, we evaluated the effects of six different tissue dissociation methods on cellular expression and demonstrated the impact of different techniques on antigen expression profiles. This is an important consideration when single-cell tumor suspensions are used to examine the HGSOC TME. However, we demonstrate how interpatient differences in the TME can be identified independent of the dissociation technique applied to the tissues. As the panel can be used to identify the main populations of immune, stromal, and tumor cells in the TME, as well as potential new cellular subsets within specific populations, its application, and the combination of the results with clinical data could provide insights into how differences in the TME composition impact clinical outcomes.

2. Results

2.1. Development of a Novel HGSOC TME-Based CyTOF Panel

The development of the CyTOF panel was the foundation for all further analyses. Based on a literature review, we designed a panel to define the major immune, stromal, and tumor subsets of the HGSOC TME [20,21] (Table S1). The panel was developed according to an optimization process, whereby all antibodies were titrated on a mixture of cells to include positive and negative marker controls (Figure 1, Table S1). A backbone panel containing immune markers ($n = 15$) identified either on the cell surface or intracellularly was titrated on unstimulated healthy peripheral blood mononuclear cells (PBMCs). Then, healthy PBMCs, both unstimulated and stimulated by the cytokine-producing agents phorbol 12-myristate 13-acetate (PMA), ionomycin, phytohemagglutinin (PHA), and interleukin 2 (IL-2), were used to determine optimized titer values of the cell surface antibodies that identify immune checkpoints ($n = 6$). The tumor ($n = 11$) and stromal ($n = 4$) markers were titrated on a mixture of two HGSOC cell lines, two dissociated primary tumor tissues, CD34+ cells, and unstimulated and stimulated healthy PBMCs (Figure 1, Table S1 and Figures S2–S6).

As a final step, all markers in the panel were titrated on a mix of four primary patient samples, as well as on two HGSOC cell lines, one CD34+ cell line, and PBMCs (Figure 1, Table S1, Supplementary Material 4). After initial gating steps, including Gaussian gating [22], the X-shift algorithm [23] was applied to the debarcoded CyTOF files. The cellular expression patterns of the panel markers were identified in the positive and not in the negative controls, which confirmed the specificity of marker expression. When the antibody panel was applied to dissociated primary tumor tissues, the resulting data confirmed that the panel could identify tumor cells and common infiltrating immune cells, such as T cells, B cells, resident tissue macrophages/monocytes, and natural killer cells. Cells belonging to the tumor stroma, including pericytes, endothelial cells, and fibroblasts, could also be distinguished successfully, and the data analyses could identify markers expressed either on cell subsets (such as stem cells) or activated cells or antibodies that are classified as immune checkpoint markers.

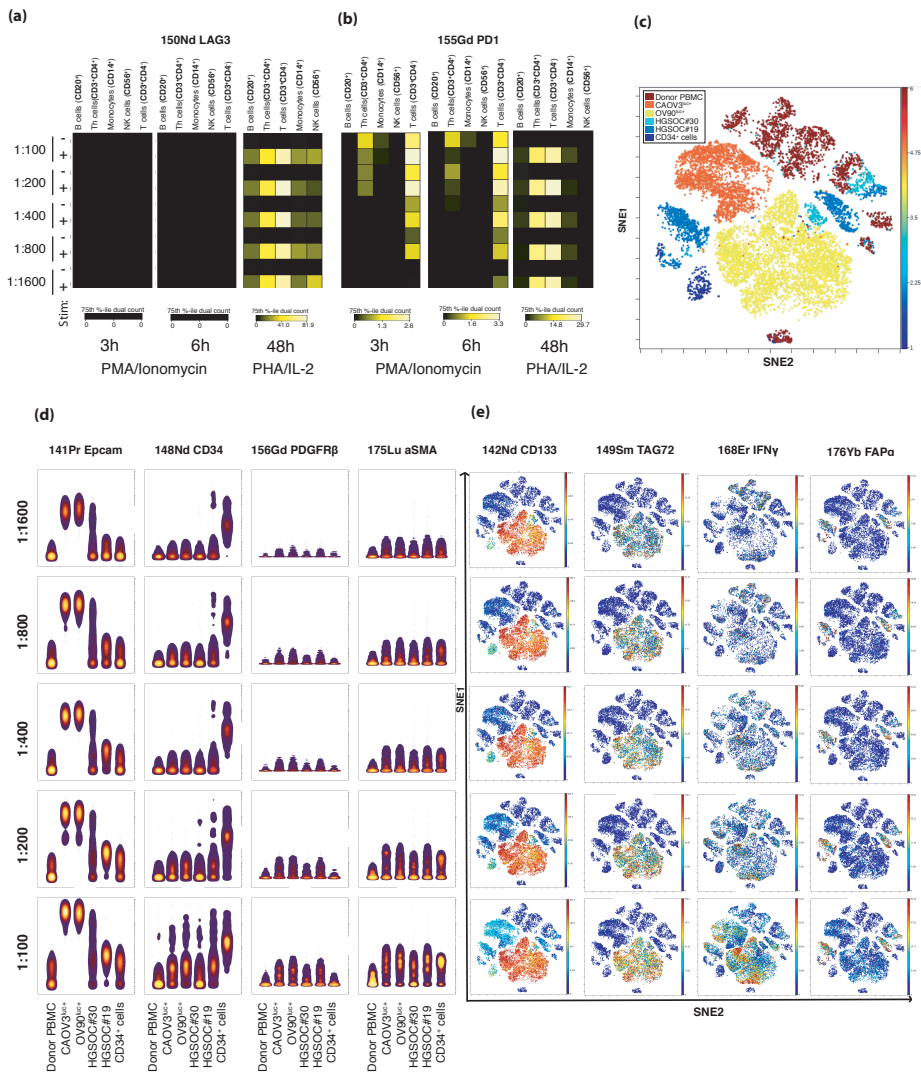


Figure 1. Titration of the panel antibodies using Cytobank software. **(a,b)** Immune checkpoint antibodies were titrated on both peripheral blood mononuclear cells (PBMCs) stimulated by phorbol 12-myristate 13-acetate (PMA) (25 ng/mL) + ionomycin (1 μ g/mL) and PBMCs stimulated by phytohemagglutinin (PHA) (2.5 μ g/mL) + interleukin 2 (IL-2). Heatmaps show that LAG-3 **(a)** was only expressed after stimulation by PHA/IL-2 and that PD-1 expression **(b)** differed with the dilution in the cells stimulated by PMA/ionomycin, while expression was consistent across all dilutions tested on PHA/IL-2-stimulated cells. **(c)** A viSNE plot was generated after pooling all samples from the stromal marker and tumor cell marker titration experiments, and the different samples were color coded. The results demonstrate a distinct separation of ovarian cancer cell lines (Caov-3 and OV-90) from the other samples, while the two dissociated tumor samples (HGSOC#19 and HGSOC#30) and the stem cells (CD34⁺ cells) show overlapping phenotypes, as well as some cellular similarity with the healthy donor sample (donor PBMCs). **(d)** Illustration of the gating strategy of the concatenated .fcs files to visualize immune staining. Plots display the sample-wise staining pattern in six samples (in the columns) of four selected markers, two tumor (EpcAM and CD34) and two stromal (PDGFR β and α SMA) antibodies (horizontally) in a dilution series from 1:100 to 1:1600 (vertically). **(e)** The viSNE plot in **(c)** color coded according to the specific antibody expression of four antibodies (horizontally) in the combined samples according to titration levels (vertically), from the most diluted on the top to the least diluted on the bottom.

2.2. In-Depth Tissue and Cell Phenotyping of the Major TME Cell Populations

An analysis of the data from three patient samples dissociated by six different methods resulted in the identification of 28 populations for further analysis. When all data were combined, common infiltrating immune cell subsets were distinguishable, including three T cell subsets (CD3+ cells), antigen-presenting cells (HLA-DR+ cells), macrophages/monocytes (CD14+ cells), and granulocytes (CD11b+ cells) (Figure 2). Among the tumor cell clusters identified, two separately clustered categories of cells were observed: tumor cells expressing EpCAM, FOLR1, or both, with high expression of CD47 and those without high expression of CD47 (total clusters $n = 10$). The most abundant stromal populations of the three tumors included in the experiment were endothelial cells (PDGFR β +), fibroblasts (CD56+ cells), and cancer-associated fibroblasts expressing α SMA and FAP α (Figure 2). A separate hierarchical cluster of immature or stem-like cell populations ($n = 4$) was identified, which expressed CD133, CD34, or both, as well as CD24, a marker found on both immature leukocytes and ovarian cancer cells [24,25].

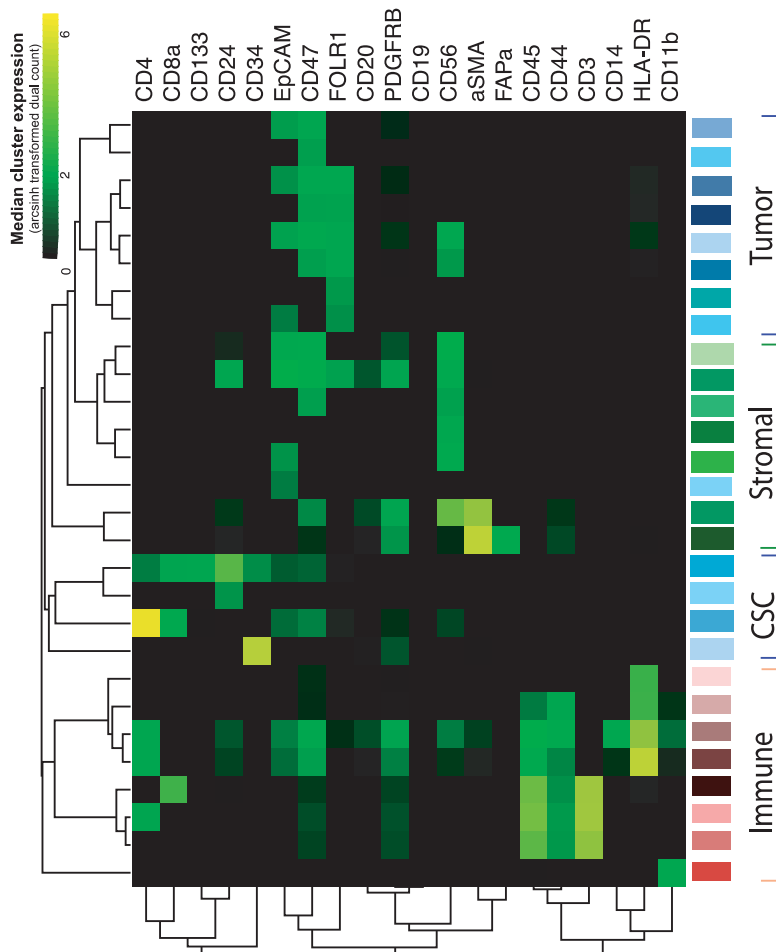


Figure 2. Heatmap showing the hierarchical clustering of data based on the identification of the main cellular subsets (tumor cells, stromal cells, immature or stem cells [CSC], and immune cells; y-axis) by the cellular expression of antibodies (x-axis). Data were generated from all dissociated samples from three patients and illustrate the 28 most common cell populations detected in the combined data set.

Among the stem-like populations, one seems to be previously undetected in ovarian tumors (the uppermost CSC cluster in Figure 2), where the cells express the stem cell markers CD133, CD34, CD47 and the lymphocyte markers CD4 and CD8 but not CD3, in addition to the tumor markers CD24 and EpCAM.

2.3. Phenotypic Differences between the Patient Samples

Data from the tumor tissues of three patients, with each tumor dissociated by six separate methods, were combined, and the proportions of the main cell subsets were compared. This showed that the cellular composition varied greatly across tumor tissues (Figure 3). While patient 1’s tumor showed the presence of several CD45+ cell subsets regardless of the dissociation method, the tumors of patients 2 and 3 only showed cell expression of CD14+ leukocytes and HLA-DR positive cells, respectively. For the stromal cell subsets, all dissociated tissues from patient 1 showed expression of αSMA, while this marker was only found in tissues from patient 2 that were dissociated by the Miltenyi cocktail (for either 1 h or 2 h.) and was not found in any of the tissue samples from patient 3. Regarding the tumor cells, all dissociated tumors from all three patients contained cells expressing EpCAM and CD47, with and without positive CD56 expression. However, the EpCAM+ CD47+ CD56+ cell subset showed a method-independent higher number of these cells (event count) in the tumor of patient 2. The cells with FOLR1 expression were mainly found in the tumor tissues from patient 3, but the mechanically dissociated tissue of patient 1 also contained this cell subset. Regarding the fibroblast subsets defined as CD56+, those coexpressing CD47 were predominantly found in tumor samples from patients 2 and 3, while the cell subset defined singly by CD56 expression was mainly found in the mechanically dissociated tissues from all three patients.

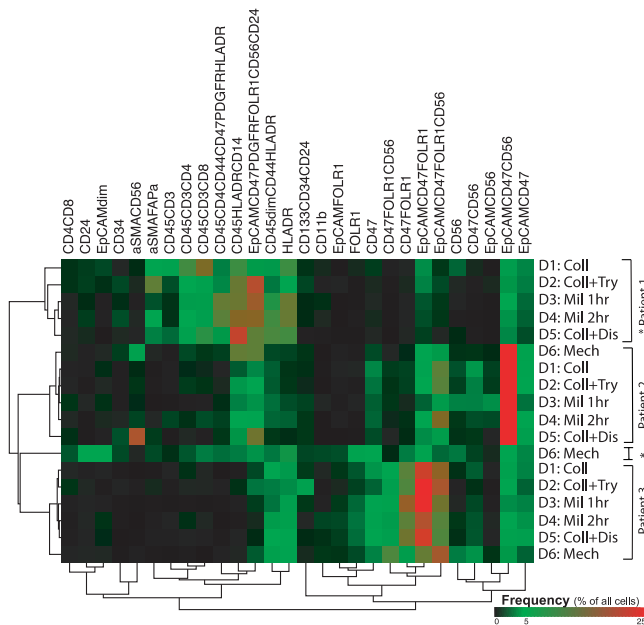


Figure 3. Hierarchically clustered heatmap showing variation in antibody expression (columns) in ovarian tissues from three patients using six different tissue dissociation methods (rows): collagenase, collagenase, and trypsin, Miltenyi enzyme mixture for 1 h, Miltenyi enzyme mixture for 2 h, collagenase and dispase, and mechanical dissociation. When the samples were clustered hierarchically according to antibody expression, the mechanically dissociated (D6) Patient 1 tumor, marked *, did separate from the rest of the samples and clustered between the samples from Patient 2 and Patient 3. The other samples cluster according to patient rather than according to dissociation method applied to the tissue.

2.4. Dissociation Method-Related Differences

In a hierarchical clustering of all samples, marker expression differed somewhat between disparately treated tissues from the same patient, in accordance with the results demonstrated in Figure 3. However, all but one mechanically dissociated sample (from patient 1) clustered according to the patient from whom the sample originated rather than according to the dissociating enzyme mixture used on the sample.

When the three main cellular subsets—the immune, stromal, and tumor cells—were examined separately in the combined patient pool, a dissociation method effect was reflected in the resulting proportions of specific cell clusters that contributed to one main subset, as illustrated by the stacked heatmaps in Figure 4b,d,f. Mechanically dissociated tissues and single cells resulting from enzymatic dissociation by collagenase alone demonstrated lower fractions of immune cluster 7 and stromal cluster 5 compared to cell suspensions generated by the Miltenyi enzymatic cocktail (Figure 4c,e). For the stromal cluster 6 the opposite effect was seen as the percentage of cells in this cluster was higher when tissues were treated enzymatically by collagenase than by the Miltenyi cocktail for 2 h. Cells dissociated using the mechanical dissociation method differed from those dissociated by most enzymatic methods in terms of the expression of tumor cell clusters 2 and 4, while the expression of tumor cell cluster 5 differed significantly between tissues treated enzymatically by collagenase alone and those treated by the Miltenyi cocktail for two hours (Figure 4g). An overview over the markers defining the cell clusters which were affected discordantly by different dissociation methods (Figure 4c,e,g) can be found in Table S2.

An investigation of functional markers in each of the 28 identified main cell clusters according to dissociation method showed no significant differences in the median marker expression despite a trend toward lower expression in the mechanically dissociated tissues compared to samples dissociated by other methods (Figure S6). The functional markers demonstrated expression in cellular subsets similar to that commonly reported in the literature; T cells and some tumor clusters expressed markers for immune checkpoints, while tumor-associated fibroblasts (CD47+ CD56+ cells) and some tumor cell subsets (CD47+ FOLR1+ cells) did not demonstrate any increased expression of functional markers. Further analysis indicated mutually exclusive PD-1 expression on CD4-positive T cells and PD-L1 expression on the population of CD14+ monocytes/macrophages.

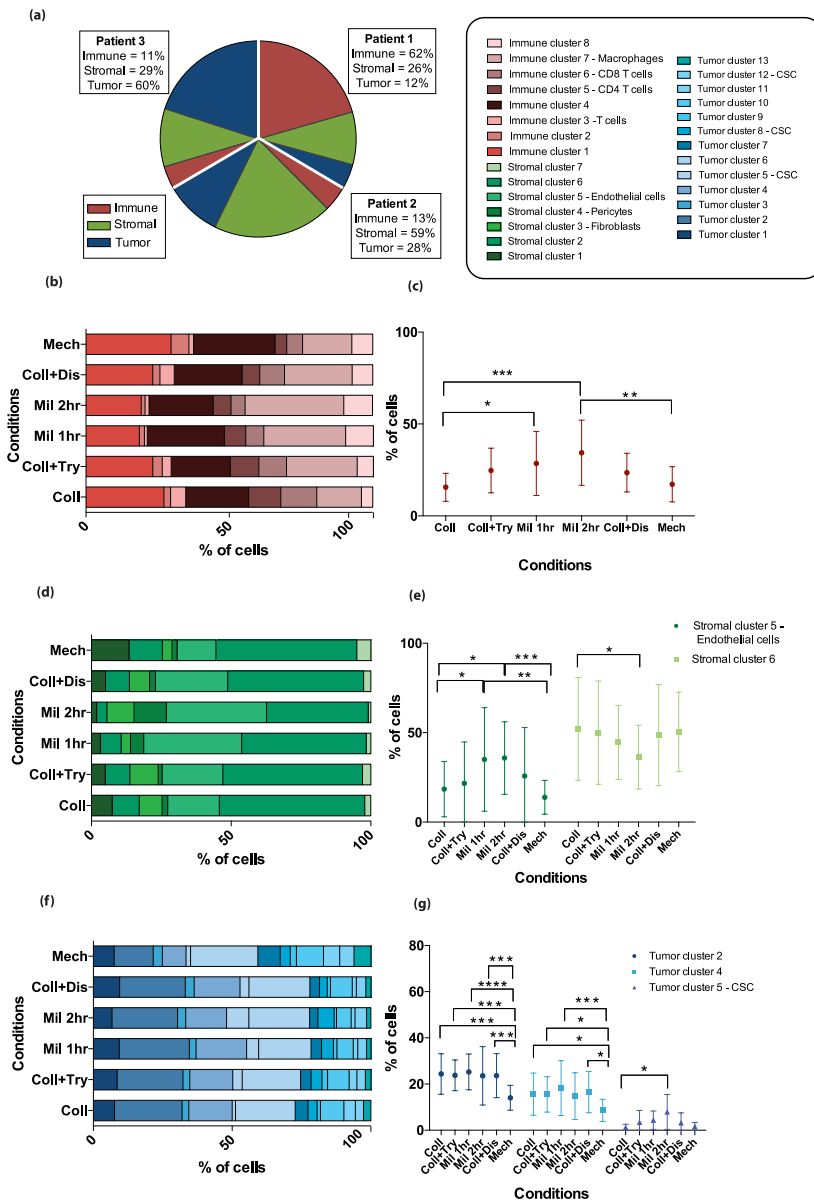


Figure 4. Differences in specific cell cluster proportions of the total cell population by dissociation method. **(a)** The pie chart displays the proportions of the three different metaclusters—immune cells in red, stromal cells in green, and tumor cells in blue—in three patients, out of a total of 300%. The graph is based on the pooled results from the six dissociation methods. The patient-specific fractions of each metacluster are shown in the text boxes. **(b,d,f)** Stacked bar plots illustrate how the identified clusters (color coded according to legend in **(a)**) within the metaclusters are proportioned in the combined patient samples according to the dissociation method applied for **(b)** immune cells, **(d)** stromal cells, and **(f)** tumor cells. **(c,e,g)** Error plots displaying the mean percentage of cells in the combined data from three patient samples with standard deviations. The specific clusters included in the figure are those where significant differences between dissociation methods were found by a two-way ANOVA analysis with Tukey’s multiple comparisons test. * *p*-value less than or equal to 0.05. ** *p*-value less than or equal to 0.01. *** *p*-value less than or equal to 0.001. **** *p*-value less than or equal to 0.0001.

3. Discussion

In solid cancers, the TME can promote immunosuppressive mechanisms, tumor vascularization, growth, and metastasis [26–28]. The challenging heterogeneity and dynamic nature of solid tumors, as well as the inherent chemo-resistance present in many tumors, appear to be influenced considerably by the cellular composition of, and interactions within the TME [26–28]. Consequently, a significant number of studies have been conducted to identify predictive or prognostic markers in the TME of HGSOE using molecular methods [2,9,29–33]. Published research on the TME often focuses on one main cellular subset, usually tumor cells or immune cells [4,7,13–16]. However, the impacts of cancer stromal cells on clinical outcomes are also increasingly being investigated [2,34–36]. A more comprehensive mapping of the tissue composition of the TME could help reveal the phenotypic diversity of tumors [7]. The development of a mass cytometry panel involves a step-by-step optimization process [37,38]. In the recent past, several mass cytometry panels have been developed to investigate a range of dissociated cancers [19,37,39–41], but only a few of these publications have focused on the panel development process [19,37,42]. As all molecular or analytical techniques entail inherent biases, an awareness of how the techniques contribute to skewing results can prevent undetected weaknesses, facilitate more precise comparisons, and improve the reproducibility of experiments. Here, we describe the development of a CyTOF panel to identify the tumor, stromal, and immune cell subsets found in HGSOE tissues, as well as potential novel cell subgroups. We also examine how different commonly used methods for dissociating tumors into single cells in suspension can impact the results of CyTOF analyses.

Dissociated tissues can be examined by multiparameter flow cytometry with a relatively high cell throughput, but the overlapping emission spectra of the fluorescent dyes restrict the possibility for simultaneous examination of over 20 antibodies, although new methods are being developed to circumvent this restriction [43,44]. Histopathologic examination with immunohistochemistry analyses is another commonly applied method used both clinically and in research to identify the cellular composition of tumors and phenotype the cancer based on both morphology and antibody expression. While this method provides spatial information that will be lost in analyses of disseminated tissues, an advantage of the CyTOF method over both immunohistochemistry and flow cytometry is that the cellular expression of over 30 antibodies can be examined simultaneously [45].

Only a few studies using the suspension CyTOF technique on tumor tissues have been published. In our study, the fcs. file debarcoding process posed a major challenge, as the data in the generated files represented a mix of cells with vastly varying cell sizes and iridium content, which is not the case with data generated from experiments focusing on PBMCs. Gonzalez et al. addressed this issue by writing a debarcoding algorithm to apply to CyTOF data from HGSOE tumors [13]. For the current study, we manually debarcoded each of the files separately to achieve a balance between including as many live cells as possible from each sample and excluding debris. This process was performed using the debarcoding tool in the Fluidigm software and adapting both the barcode separation and Mahalanobis distance according to the barcode pattern seen in the files.

Gonzalez et al. developed a panel of 41 antibodies to interrogate the HGSOE tumor compartment [13], while Toker et al. used a panel focusing on the infiltrating T cell populations of the TME [14]. Each study interrogated specific compartments of the TME in detail. By contrast, our panel provides a broader overview of the main populations of the HGSOE TME. Like the other researchers, we were able to identify potential new cellular subsets within the specific populations when the panel was used on HGSOE tissues. Gonzalez et al. identified how tumor resistance to the chemotherapy drug carboplatin differed in two novel vimentin-positive subpopulations according to the expression of cMyc and human epididymis secretory protein 4 (HE4) [13]. Similarly, Casado et al. show how specific, previously undescribed, tumor subsets seem to be associated with the disease state. These subsets include cells with high expression of MUC1 and CD147, minimal Ki67 enrichment, and low ERK1-2 signaling, which were found to be present in greater

numbers in recurrent tumors than in samples from a primary treatment setting [16]. In the present study, a previously undescribed stem-like cell subset is detected, expressing the following markers: CD24, EpCAM, CD133, CD34, CD47, CD4, and CD8. As the study cohort consists of only three patients, further validation of the finding in a larger patient material is warranted. Furthermore, an exploration of how presence or distribution of this cell subset associates with specific phenotypic outcomes, such as tumor resection rates or progression-free intervals could add translationally applicable information.

Application of our panel enables the TME profiles of the individual patient to be distinguished, and it is hoped that further use of the method on different patient cohorts could contribute to identifying how differences in TME composition impact clinical outcomes. The results of this study illustrate a sufficient depth of phenotyping when the developed CyTOF panel is applied to patient samples. For a more in-depth characterization of particular cell populations, possible solutions [13,14] include using dedicated panels with a focus on specific cell subsets, increasing the sample sizes or combining different panels using panel merging algorithms [6]. Combining the results from tumor analyses with clinical data from prospectively collected biobanks and implementing the method in clinical trials could increase its clinical translatability.

Our panel was optimized for single-cell suspensions obtained from primary tumor samples, and the six dissociation methods were selected to cover the spectrum of regular dissociation protocols applied to ovarian tumors [13,46]. In our study, we found that the method of tissue dissociation affected the marker expression of a few subgroups within the three major cell subsets. Similar effects on immune cells have been identified by Poláková et al. [19], who compared dissociation of tonsillar carcinoma tissues by two collagenases combined with Dnase 1. They found that the dissociation method significantly affected the expression of major lymphocyte markers [19]. Leelatian et al. examined the cellular effects of tumor dissociation methods on tissues from gliomas, tonsils, and melanomas and found that disaggregation conditions affected the various cell populations differently [18]. The observations from these studies and our own indicate that the lack of reproducibility of results from tissue-focused CyTOF studies may be partly due to the application of different tissue dissociation methods. Furthermore, our findings demonstrate the need for careful selection of dissociation method to suit the study hypothesis when planning experiments, as some markers of interest might be dimly or not expressed if particular dissociations are used, which may lead to a failure to detect important cell subsets. In particular, the cell subset-related results from studies applying mechanical dissociation of tissues needs to be interpreted with caution.

There are several limitations to this study, including a lack of validation of the findings by other methods. By adding more antibody-positive controls to the experiments, particularly for the stromal markers, and allocating part of the tumor sample for immunohistochemistry examination of the fresh frozen tissue it would be feasible to validate the presence of the cell subsets identified in the dissociated tumor samples. The sample size is small, which might cause dissociation method-related differences to go undetected. Still, with these three samples it was possible to detect changes in antigen expression in different cellular subsets that are important to recognize when future studies applying dissociated HGSOC tissues are planned.

In our experiment, we examined three patient samples dissociated by six different methods to ensure that we would be able to detect the different main cell subsets and investigate the potential impacts of the dissociation methods. The results of this study demonstrate greater interpatient differences than intrapatient differences and confirm the acknowledged tumor heterogeneity, as each patient sample displayed a unique combination of tumor, immune, and stromal cells, regardless of the method used for tumor dissociation. Several authors have illustrated the challenges of developing reliable diagnostic and therapy-related methods that can be applied to heterogeneous cancer tissues [13,47–49]. The polyclonality and heterogeneity of HGSOC tumors, which has been established through single-cell experiments [13,47–49], indicate a need for better profiling tools. Application

of CyTOF in studies of HGSOc to detect cellular patterns rather than single biomarkers, potentially in combination with genetic biomarkers and preclinical modeling systems may provide breakthroughs. The CyTOF methodology has been extended during the last years, with the introduction of a method that combines CyTOF with imaging to examine single cells in tissue sections [50]. Thus, the adaptation of CyTOF panels for examination of solid tissues by this combined method is ongoing. It is our hope that as an increasing number of studies using imaging mass cytometry are published, concerns regarding the effects of the tumor dissociation methods on data generation will be eliminated. Studies on the cellular components of tumors and their impact on clinical outcomes often cannot be reproduced and differences in methodology, and such tumor dissociation methods could be a factor contributing to discrepancies in results. Hopefully, in future studies the variability in antibody expression induced by the dissociation method will be considered during the planning phase of new experiments.

4. Materials and Methods

4.1. Samples

4.1.1. Patient Sample Collection

We used samples from four patients with primary advanced HGSOc (Stages IIc–IIIC) admitted to the Department of Obstetrics and Gynecology, Haukeland University Hospital (HUS), Bergen, Norway. All samples were included in the Bergen Gynecologic Cancer Biobank (GYNCAN). The tumor samples resected during primary debulking procedures were obtained from the primary ovarian tumors and placed directly in Dulbecco's Modified Eagle's Medium (DMEM) and transferred to the laboratory for immediate processing. However, our experiments on dissociation method effects required sufficient tissue for the application of six separate dissociation methods, which we could only obtain from three of the four patients. Clinical and histopathological data on these three patients can be found in the Table S3. Informed consent was obtained from the women before collection of the tumor samples was initiated.

4.1.2. Ovarian Cancer Cell Lines

The human ovarian serous adenocarcinoma cell lines OV-90 (American Type Culture Collection [ATCC][®]CRL-11732[™]) and Caov-3 (ATCC[®]HTB-75[™]) were obtained from ATCC, VA. The OV-90 cells were cultivated in RPMI 1640 medium, and the Caov-3 cells were cultivated in DMEM medium. Both media were supplemented with 10% heat-inactivated fetal calf serum (FCS), 2 mM L-glutamine, and penicillin 100 IU/mL (all from Gibco, Thermo Fisher Scientific, Waltham, MA, USA). Cells were grown in 75 cm² cell culture flasks (Costar, MA, USA) at 37 °C in a humidified atmosphere with 5% CO₂ and subcultured twice a week. Single-cell suspensions were obtained by washing the cells twice with phosphate buffered saline (PBS) (1:10 dilution of 10× stock PBS; Dulbecco's tablets, Oxoid Limited, Thermo Fisher Scientific, Waltham, MA, USA) before incubation with trypsin (Gibco, Thermo Fisher Scientific). As a final step, cells were washed one last time, freezing media (90% FCS and 10% dimethyl sulfoxide (DMSO) (Sigma Aldrich, St. Louis, MO, USA)) was added, and the cells were cryopreserved.

4.1.3. Stem Cells

The CD34+ stem cells had been collected as part of the Research Biobank for Blood Diseases (REC ID 2015/1759), HUS, Bergen, Norway, by a standardized process described elsewhere [51].

4.1.4. Healthy Donor Peripheral Blood Mononuclear Cells (PBMCs)

Peripheral blood from healthy donors was collected at the Blood bank, Department of Immunology and Transfusion Medicine, HUS, Bergen, Norway. The sampling was approved by the REC (REC ID 2012/2247). The PBMCs were isolated by density gradient centrifugation with Lymphoprep (Axis-Shield, Oslo, Norway), cryopreserved in 90% FCS

and 10% DMSO and frozen in a Mr. Frosty container (Thermo Fisher Scientific) at -80°C for 24 h before being stored at -150°C .

4.2. Stimulation of PBMCs

To enable identification of the optimal dilution of antibody markers for use in further experiments, including markers expressed in activated cells only, all markers for immune cells and immune checkpoints were titrated concomitantly on unstimulated and stimulated PBMCs. Prior to stimulation, a batch of cryopreserved PBMCs were thawed, slow diluted (1:12) in RPMI 1640 medium at room temperature, and pelleted at 300 g for 5 min. The cells (3×10^6 cells/mL) were then resuspended in complete RPMI 1640 medium and incubated for an hour at 37°C in a humidified atmosphere with 5% CO_2 , prior to stimulation with either phorbol 12-myristate 13-acetate (PMA) (25 ng/mL) and ionomycin (1 $\mu\text{g}/\text{mL}$) for 3 or 6 h, or 2.5 $\mu\text{g}/\text{mL}$ phytohemagglutinin (PHA, Sigma Aldrich) and 100 IU/mL Human Interleukin-2 (IL-2) Recombinant Protein (Gibco, Thermo Fischer Scientific) for 48 h under the same incubation conditions. After stimulation, the cells were fixed using Stable-Lyse and Stable-Store (Smart Tube Inc., San Carlos, CA, USA) as per the manufacturer's protocol (Protocol number: SLSSP1TF-150203).

4.3. Tumor Dissociation Methods

Each tumor piece was divided into cubes (1 mm^3) using a sterile scalpel, and the cubes were randomly assigned to dissociation methods. Tissue pieces were washed with either Hanks' Balanced Salt Solution (Thermo Fischer Scientific) or PBS and transferred to 50 mL Falcon tubes filled with the respective pre-warmed (37°C) enzyme mixtures. Each patient tumor sample was treated by six different dissociation methods (Table 1): five enzymatic and one mechanical (Mech). The enzymatic methods were collagenase II + calcium chloride (CaCl_2) (Coll), collagenase + CaCl_2 + TrypLE (Coll+Try), Miltenyi for one hour (Mil 1 h), Miltenyi for two hours (Mil 2 h), and collagenase + CaCl_2 + dispase (Coll+Dis). The enzymatic dissociations were performed (1) by collagenase type II (1 mg/mL, Gibco, Thermofischer) in combination with CaCl_2 (3 mM, Sigma Aldrich) for either two hours without (Coll), or with (Coll+Try) TrypLE Express Enzyme (1 \times) added afterwards for 5–10 min with no phenol red (Thermo Fisher Scientific); (2) by collagenase for 1 h with dispase (50 U/mL, Thermo Fisher Scientific) (Coll+Dis); or (3) by application of the Tumor Dissociation Kit from Miltenyi Biotec (as per manufacturer's recommendations) for either 1 h (Mil 1 h) or 2 h (Mil 2 h).

Table 1. The six tumor dissociation methods evaluated using the CyTOF panel.

Dissociations/ Conditions	Primary Enzyme	Duration	Additional Enzyme	Duration
1. Coll	Collagenase II + CaCl_2	2 h		
2. Coll+Try	Collagenase II + CaCl_2	2 h	TrypLE	5 min
3. Mil 1 h	Miltenyi	1 h		
4. Mil 2 h	Miltenyi	2 h		
5. Coll+Dis	Collagenase II + CaCl_2	1 h	Dispase	30 min
6. Mech	Mechanical. – No enzyme added.	-	-	-

The tissue samples in the different enzyme mixtures were transferred to a 37 °C incubator with 5% CO₂ with continuous shaking at 250 rpm for the respective durations required for each dissociation method. Conventional mechanical dissociation (Mech, Table 1) entailed fine mincing of the tissue with sterile glass slides. After tissue dissociation, all cells, regardless of the dissociation method used, were strained through a 40 µm cell strainer, checked for cell viability with trypan blue staining, centrifuged (300 g, 5 min, room temperature), and cryopreserved in freezing media (90% FBS [Gibco] with 10% DMSO [Sigma Aldrich]) in a Mr. Frosty container at −80 °C for 24 h before being stored at −150 °C. The viability of cells in the dissociated tissues varied between patient samples and dissociation methods, with the lowest fractions of viable cells after mechanical dissociation (Table S4).

4.4. The CyTOF Panel

A 35-marker panel was developed with a focus on three components of the HGSOc tumor microenvironment: tumor cells, immune cells, and stromal cells (Figure S1, Supplementary Material 1, Table S1). The markers included in the panel were selected after a review of the literature. The associated metal conjugates were chosen based on information found in the web-based application Maxpar Panel Designer (Fluidigm, Markham, ON, Canada). Pre-conjugated antibodies ($n = 24$) were purchased from Fluidigm. For antibodies in the panel that were unavailable in the pre-conjugated form, in-house conjugation of carrier-free antibodies ($n = 11$) to metal-chelated polymers (Maxpar X8 Antibody Labeling Kits, Fluidigm) was performed according to the manufacturer's protocol (PRD002 Version 11). The in-house-conjugated metal-labeled antibodies (Table S1, Supplementary Material 2) were diluted to 0.5 mg/mL in antibody stabilization solution (CANDOR Bioscience GmbH, Wangen, Germany) and stored at 4 °C.

4.5. Antibody Titration

All markers were initially validated and titrated on the ovarian cell lines OV-90 and Caov-3 and on the CD34+ cells and unstimulated and stimulated PBMCs (Figure S2, Figure S3, Supplementary Material 3). Then, the selected dilution of each marker in the panel was validated on cell suspensions from four human tumor samples (Figure S4, Supplementary Material 4). The provider, clone, and metal tag of each antibody and the controls used for titrations are listed in the (Supporting Information Table S1). Next, the selected dilutions of antibodies were further titrated on two primary tumor tissues dissociated by collagenase [D1] and Miltenyi 1 h [D3], respectively, as well as on the biobanked stem-cell-derived CD34+ cells and unstimulated and stimulated PBMCs. As a final step, all markers in the panel were titrated on primary patient samples ($n = 4$), each dissociated by one of the five methods: Coll [D1], Coll+Try [D2], Mil 1hr [D3], Coll+Dis [D5], or Mech [D6].

To investigate the effects of the dissociation methods, 18 barcoded samples (three patients with six dissociated samples per patient) and two barcoded controls (OV-90 cells and unstimulated PBMCs) were resuspended in cell staining buffer (CSB), pooled, pelleted, and washed twice with CSB at 800 g for 4 min at 4 °C.

4.6. Sample Preparation for Mass Cytometry Analysis

All analyzed samples were treated in the following way: Cryopreserved samples from the single-cell suspensions from the different dissociations and the control cells (OV-90, Caov-3, and from unstimulated and stimulated PBMCs) were rapidly thawed in a water bath, diluted (1:10) in their respective culture media, and centrifuged at 300 g for 5 min at room temperature. To assess cell viability, 5 µM of Cell-ID™ Cisplatin (Fluidigm) was added to each sample for 60 s, before the effect of the cisplatin was quenched by Maxpar CSB (Fluidigm) and the cells were fixed according to the Stable-Lyse and Stable-Store protocol (No: SLSSP1TF-150203). The samples were counted and 1–3 × 10⁶ cells from each sample were barcoded using the 20-plex metal barcoding kit (Fluidigm) as per the

Fluidigm user guide (version PN PRD023 B1). All the following steps were conducted at room temperature. For extracellular staining, samples were incubated with FcR blocking reagent (Miltenyi Biotec) at 1:10 dilution for 20 min, followed by antibody staining with 50 μ L of a mixture containing CSB and 33 antibodies per 50 μ L of cell sample (1:1 ratio) for 20 min. Cells were then washed twice at 800 g with CSB before 1 mL of methanol was added to each sample. The samples were incubated for 15 min, after which cells were washed twice with CSB and the pellets resuspended with CSB to a total of 50 μ L. Then, 50 μ L of the intracellular antibody cocktail containing antibodies against FoxP3 and interferon gamma was added to each sample to a ratio of 1:1, and the samples were incubated for 30 min. Cells were then washed twice at 500 g with CSB prior to resuspension for 1 h in 1 mL (125 nM/mL) of Cell-ID Intercalator-Ir (Fluidigm). After washing (800 g , 4 min) once with CSB and once with PBS, samples were diluted to 1×10^6 cells/mL in Maxpar Cell Acquisition Solution containing 10% of EQ™ Four Element Calibration Beads (all reagents from Fluidigm) and run sequentially on a Helios mass cytometer (Fluidigm) through a wide bore injector system (Fluidigm).

4.7. Data Analysis

The .fcs files resulting from the mass cytometry experiments were normalized using internal bead standards, and the normalization algorithm in the CyTOF software v.6.7 (Fluidigm) was conducted before further analysis.

4.7.1. Initial Gating and Debarcoding

Using analysis tools from the Cytobank platform (v7.2.0 and v7.3.0, Beckman Coulter, Inc., Indianapolis, IN, USA), initial gating of live singlets was performed using manual gating according to the four Gaussian parameters: center, width, offset, and residual [22]. Files were debarcoded with a 20-plex-debarcoding key (Fluidigm) using the Premessa debarcoder GUI package (<https://github.com/ParkerICI/premessa>, accessed on 4 December 2018) in R (version R 3.4.1 GUI 1.70 El Capitan build (7375)).

4.7.2. Visualization Methods

T-Distributed Stochastic Neighbor Embedding (tSNE) is a nonlinear dimensionality reduction algorithm that reduces high-dimensional data down to two dimensions for easy visualization and rapid exploratory data analysis of any data type [13,52]. To visualize the expression pattern of the panel markers in two dimensions, tSNE maps were plotted in Cytobank (Figure 1b,d). The main cell populations were defined by manual gating according to marker expression and overlaid on the corresponding tSNE plot (Figure 1b).

To further compare the effects of the six dissociation methods on the individual panel markers (and interpatient differences in the individual markers), live singlet cells were gated out according to the Gaussian parameters after CATALYST debarcoding of .fcs files. All live single cells from all files generated from the dissociated patient samples ($n = 18$) were then grouped separately according to the dissociation method and patient tissue used, and histograms displaying $\times/5$ arcsin-transformed median expression of marker distributions were plotted in MATLAB v.R2019a (The MathWorks Inc., Natick, MA, USA) (Figure S5).

4.7.3. Clustering

Debarcoded files containing the live single cells were concatenated for the purpose of unsupervised clustering according to cellular phenotypical resemblances by a density-based clustering method called X-shift (VorteX, Java version 1.0) [23]. X-shift finds the local density maxima of each data point (cell event), which becomes the cell cluster centroid in a nearest neighbor graph, using the weighted K-nearest-neighbor density estimation in a multidimensional marker space. The K value was automatically selected as 28 from the elbow point in a number of cell clusters versus K plot, with the software merging clusters by a Mahalanobis distance of less than 2.0.

4.7.4. Bar Plots and Pie Charts

To visualize the differences in the percentage of the cell clusters between the tumor dissociation conditions for the different patients, Prism (6.0c version; GraphPad) was used to plot stacked bar plots in an XY table format using the clustering data obtained from X-shift (Figure 4). Prism software was also used to generate pie charts and compare cell subset fractions according to dissociation method (Figure 4).

4.7.5. Heatmaps and Cox Proportional-Hazards Models

Heatmaps were generated in X-shift to efficiently visualize patterns and relationships in the high-dimensional mass cytometry data from the differently dissociated tumors. Using proportional numbers of live single cells from all the quality-controlled files, X-shift identified 91 cellular subsets. To enable identification of dissociation method effects on the main cellular subsets and their marker expression, all clusters constituting an average of <0.5% of the total cell numbers of each sample were excluded from further analyses. Based on the resulting 34 clusters, a hierarchically clustered heatmap was generated, and the cellular subsets that deviated only according to HLA-DR expression ($n = 6$ pairs) were manually merged. This resulted in 28 clusters on which the analyses were performed.

Arcsin-transformed dual counts of the median expression of functional markers in the panel were investigated using Cox proportional-hazards models for the cellular populations according to dissociation method (Figure S6).

5. Conclusions

The TME must be better understood if survival rates are to be improved for HGSOc. New tools for phenotypic characterization are necessary, especially when information on all the different components of the TME is needed at a single-cell resolution. This study describes how a 35-marker CyTOF panel for single-cell suspensions of HGSOc tissues can be used to define the three main parts of the TME. The study also provides an overview of the effects of dissociation methods on the cell subsets. The results show that the panel will be useful for investigating HGSOc tumors. Further, this study demonstrates how the reproducibility of study outcomes can improve if researchers take appropriate measures when generating single-cell suspensions. A combinatorial analysis method, such as that presented here, could replace single phenotype biomarker approaches and make it possible to identify treatment options in a more refined and personalized way.

Supplementary Materials: The following are available online at <https://www.mdpi.com/2072-6694/13/4/755/s1>, Figure S1: Overview of ovarian mass cytometry panel development, Figure S2: Antibody staining on unstimulated and PHA-stimulated PBMCs, Figure S3: Stromal and tumor panels were titrated on ovarian cancer cell lines and a mixture of the patient samples, Figure S4: Panel validation on pooled patient data, Figure S5: Histograms illustrating antibody expression according to three separate patient samples, Figure S6: Cox proportional-hazard models of median expression of the functional markers. Table S1: Overview of antibodies and metal conjugates (Tags) included in the HGSOc TME-based mass cytometry by time-of-flight (CyTOF) panel, the positive and negative controls used for each antibody, and the final antibody dilutions that should be applied to tissues, Table S2: Antibody-expression of the cell clusters significantly affected by the different dissociation methods, Table S3: Overview of the patient cohort ($n = 3$), Table S4: Viability of the cells in the dissociated tissues. For each patient sample and the six dissociation methods the percentage of dead cells in the sample is listed. The viability was measured directly after dissociation of the tumor before freezing.

Author Contributions: Conceptualization, S.A., L.C.V.T., E.M. and L.B.; Formal analysis, S.A., L.C.V.T., S.-E.G., T.A., K.K., J.S. and G.B.; Funding acquisition, E.M. and L.B.; Investigation, S.A., L.C.V.T., S.-E.G., T.A., K.K., J.S. and G.B.; Methodology, S.A., L.C.V.T., S.-E.G., G.B. and L.B.; Supervision, B.T.G., E.M. and L.B.; Visualization, S.A., S.-E.G. and T.A.; Writing—original draft, S.A., L.C.V.T. and L.B.; Writing—review and editing, S.A., L.C.V.T., S.-E.G., T.A., K.K., J.S., G.B., B.T.G., E.M. and L.B. All authors have read and agreed to the published version of the manuscript.

Funding: This research was funded by Helse Vest RHF and Helse Bergen HF (project numbers 911809, 911852, 912171, 240222, HV1269), the Norwegian Cancer Society (182735, 100933), and the Research Council of Norway through its Centers of Excellence funding scheme (project number 223250, 262652). The authors Anandan and Kleinmanns are part of the project Image-Guided Surgery and Personalised Postoperative Immunotherapy to Improving Cancer Outcome (ISPIC), which is funded through the H2020 program MSCA-ITN under grant agreement number 675743.

Institutional Review Board Statement: All investigations were carried out according to the 2013 revision of the Declaration of Helsinki. The regional ethics committee approved the biobanking of tumor tissues from women with gynecological cancers (the Norwegian Regional Committees for Medical and Health Research Ethics West [REC West] ID 2014/1907) and the present study (REC West ID 2017/623).

Informed Consent Statement: Informed consent was obtained from all subjects involved in the study.

Data Availability Statement: The data presented in this study are available on request from the corresponding author. The data are not publicly available due to ethical restrictions.

Acknowledgments: The mass cytometry was performed at the Flow Cytometry Core Facility, Department of Clinical Science, University of Bergen. The Helios Mass Cytometer was funded by Bergen Research Foundation. The figures were designed with Adobe Illustrator (Adobe Inc. (2020)), retrieved from <https://adobe.com/products/illustrator>, and the graphical abstract was created with BioRender (BioRender.com).

Conflicts of Interest: Thomsen reports personal fees from Bayer and AstraZeneca, and Thomsen and Bjørge report financial support from AstraZeneca for a researcher-initiated trial. The other authors declare no conflict of interest.

References

1. Miller, K.D.; Siegel, R.L.; Lin, C.C.; Mariotto, A.B.; Kramer, J.L.; Rowland, J.H.; Stein, K.D.; Alteri, R.; Jemal, A. Cancer treatment and survivorship statistics, 2016. *CA Cancer J. Clin.* **2016**, *66*, 271–289. [[CrossRef](#)]
2. Nwani, N.G.; Sima, L.E.; Nieves-Neira, W.; Matei, D. Targeting the Microenvironment in High Grade Serous Ovarian Cancer. *Cancers (Basel)* **2018**, *10*, 266. [[CrossRef](#)]
3. Freedman, R.S.; Deavers, M.; Liu, J.; Wang, E. Peritoneal inflammation—A microenvironment for Epithelial Ovarian Cancer (EOC). *J. Transl. Med.* **2004**, *2*, 23. [[CrossRef](#)]
4. Zhang, L.; Conejo-Garcia, J.R.; Katsaros, D.; Gimotty, P.A.; Massobrio, M.; Regnani, G.; Makrigiannakis, A.; Gray, H.; Schlienger, K.; Liebman, M.N.; et al. Intratumoral T cells, recurrence, and survival in epithelial ovarian cancer. *N. Engl. J. Med.* **2003**, *348*, 203–213. [[CrossRef](#)]
5. Petitprez, F.; Sun, C.M.; Lacroix, L.; Sautès-Fridman, C.; de Reyniès, A.; Fridman, W.H. Quantitative Analyses of the Tumor Microenvironment Composition and Orientation in the Era of Precision Medicine. *Front. Engl.* **2018**, *8*, 390. [[CrossRef](#)]
6. Abdelaal, T.; Hollt, T.; van Unen, V.; Lelieveldt, B.P.F.; Koning, F.; Reinders, M.J.T.; Mahfouz, A. CyTOFmerge: Integrating mass cytometry data across multiple panels. *Bioinformatics* **2019**. [[CrossRef](#)]
7. Drakes, M.L.; Stiff, P.J. Regulation of Ovarian Cancer Prognosis by Immune Cells in the Tumor Microenvironment. *Cancers (Basel)* **2018**, *10*, 302. [[CrossRef](#)]
8. Jiménez-Sánchez, A.; Memon, D.; Pourpe, S.; Veeraghavan, H.; Li, Y.; Vargas, H.A.; Gill, M.B.; Park, K.J.; Zivanovic, O.; Konner, J.; et al. Heterogeneous Tumor-Immune Microenvironments among Differentially Growing Metastases in an Ovarian Cancer Patient. *Cell* **2017**, *170*, 927–938.e920. [[CrossRef](#)] [[PubMed](#)]
9. Kreuzinger, C.; Geroldinger, A.; Smeets, D.; Braicu, E.I.; Sehouli, J.; Koller, J.; Wolf, A.; Darb-Esfahani, S.; Joehrens, K.; Vergote, I.; et al. A Complex Network of Tumor Microenvironment in Human High-Grade Serous Ovarian Cancer. *Clin. Cancer Res.* **2017**, *23*, 7621–7632. [[CrossRef](#)] [[PubMed](#)]
10. Zhang, A.W.; McPherson, A.; Milne, K.; Kroeger, D.R.; Hamilton, P.T.; Miranda, A.; Funnell, T.; Little, N.; de Souza, C.P.E.; Laan, S.; et al. Interfaces of Malignant and Immunologic Clonal Dynamics in Ovarian Cancer. *Cell* **2018**, *173*, 1755–1769.e1722. [[CrossRef](#)] [[PubMed](#)]
11. Corvigno, S.; Wisman, G.B.; Mezheyski, A.; van der Zee, A.G.; Nijman, H.W.; Avall-Lundqvist, E.; Ostman, A.; Dahlstrand, H. Markers of fibroblast-rich tumor stroma and perivascular cells in serous ovarian cancer: Inter- and intra-patient heterogeneity and impact on survival. *Oncotarget* **2016**, *7*, 18573–18584. [[CrossRef](#)] [[PubMed](#)]
12. Bandura, D.R.; Baranov, V.I.; Ornatsky, O.I.; Antonov, A.; Kinach, R.; Lou, X.; Pavlov, S.; Vorobiev, S.; Dick, J.E.; Tanner, S.D. Mass cytometry: Technique for real time single cell multitarget immunoassay based on inductively coupled plasma time-of-flight mass spectrometry. *Anal. Chem.* **2009**, *81*, 6813–6822. [[CrossRef](#)] [[PubMed](#)]

13. Gonzalez, V.D.; Samusik, N.; Chen, T.J.; Savig, E.S.; Aghaeepour, N.; Quigley, D.A.; Huang, Y.W.; Giangarra, V.; Borowsky, A.D.; Hubbard, N.E.; et al. Commonly Occurring Cell Subsets in High-Grade Serous Ovarian Tumors Identified by Single-Cell Mass Cytometry. *Cell Rep.* **2018**, *22*, 1875–1888. [[CrossRef](#)]
14. Toker, A.; Nguyen, L.T.; Stone, S.C.; Yang, C.; Katz, S.R.; Shaw, P.A.; Clarke, B.A.; Ghazarian, D.A.; Al Habeeb, A.S.; Easson, A.M.; et al. Regulatory T cells in ovarian cancer are characterized by a highly activated phenotype distinct from that in melanoma. *Clin. Cancer Res.* **2018**. [[CrossRef](#)] [[PubMed](#)]
15. Kverneland, A.H.; Pedersen, M.; Westergaard, M.C.W.; Nielsen, M.; Borch, T.H.; Olsen, L.R.; Aasbjerg, G.; Santegoets, S.J.; Burg, S.H.v.d.; Milne, K.; et al. Adoptive cell therapy in combination with checkpoint inhibitors in ovarian cancer. *Oncotarget* **2020**, *11*, 2092. [[CrossRef](#)] [[PubMed](#)]
16. Casado, J.; Lehtonen, O.; Rantanen, V.; Kaipio, K.; Pasquini, L.; Häkkinen, A.; Petrucci, E.; Hynninen, J.; Hietanen, S.; Carpén, O.; et al. Agile Workflow For Interactive Analysis Of Mass Cytometry Data. *Bioinformatics* **2020**. [[CrossRef](#)]
17. Comsa, E.; Nguyen, K.A.; Loghin, F.; Boumendjel, A.; Peuchmaur, M.; Andrieu, T.; Falson, P. Ovarian cancer cells cisplatin sensitization agents selected by mass cytometry target ABCC2 inhibition. *Future Med. Chem.* **2018**, *10*, 1349–1360. [[CrossRef](#)]
18. Leelatian, N.; Doxie, D.B.; Greenplate, A.R.; Mobley, B.C.; Lehman, J.M.; Sinnaeve, J.; Kauffman, R.M.; Werkhaven, J.A.; Mistry, A.M.; Weaver, K.D.; et al. Single Cell Analysis of Human Tissues and Solid Tumors with Mass Cytometry. *Cytom. B Clin. Cytom.* **2017**. [[CrossRef](#)]
19. Polakova, I.; Pelak, O.; Thurner, D.; Pokryvkova, B.; Tachezy, R.; Kalina, T.; Smahel, M. Implementation of Mass Cytometry for Immunoprofiling of Patients with Solid Tumors. *J. Immunol. Res.* **2019**, *2019*, 6705949. [[CrossRef](#)] [[PubMed](#)]
20. Luo, Z.; Wang, Q.; Lau, W.B.; Lau, B.; Xu, L.; Zhao, L.; Yang, H.; Feng, M.; Xuan, Y.; Yang, Y.; et al. Tumor microenvironment: The culprit for ovarian cancer metastasis? *Cancer Lett.* **2016**, *377*, 174–182. [[CrossRef](#)] [[PubMed](#)]
21. Ghoneum, A.; Afify, H.; Salih, Z.; Kelly, M.; Said, N. Role of tumor microenvironment in ovarian cancer pathobiology. *Oncotarget* **2018**, *9*, 22832–22849. [[CrossRef](#)] [[PubMed](#)]
22. Bagwell, C.B.; Inokuma, M.; Hunsberger, B.; Herbert, D.; Bray, C.; Hill, B.; Stelzer, G.; Li, S.; Kollipara, A.; Ornatsky, O.; et al. Automated Data Cleanup for Mass Cytometry. *Cytom. Part A* **2020**, *97*, 184–198. [[CrossRef](#)] [[PubMed](#)]
23. Samusik, N.; Good, Z.; Spitzer, M.H.; Davis, K.L.; Nolan, G.P. Automated mapping of phenotype space with single-cell data. *Nat. Methods* **2016**, *13*, 493–496. [[CrossRef](#)] [[PubMed](#)]
24. Tan, Y.; Zhao, M.; Xiang, B.; Chang, C.; Lu, Q. CD24: From a Hematopoietic Differentiation Antigen to a Genetic Risk Factor for Multiple Autoimmune Diseases. *Clin. Rev. Allergy Immunol.* **2016**, *50*, 70–83. [[CrossRef](#)]
25. Liu, Y.; Zheng, P. CD24: A genetic checkpoint in T cell homeostasis and autoimmune diseases. *Trends Immunol.* **2007**, *28*, 315–320. [[CrossRef](#)]
26. Hanahan, D.; Weinberg, R.A. Hallmarks of cancer: The next generation. *Cell* **2011**, *144*, 646–674. [[CrossRef](#)]
27. Fane, M.; Weeraratna, A.T. How the ageing microenvironment influences tumour progression. *Nat. Rev. Cancer* **2020**, *20*, 89–106. [[CrossRef](#)]
28. Jin, M.-Z.; Jin, W.-L. The updated landscape of tumor microenvironment and drug repurposing. *Signal Transduct. Target. Ther.* **2020**, *5*, 1–16. [[CrossRef](#)]
29. Heindl, A.; Lan, C.; Rodrigues, D.N.; Koelble, K.; Yuan, Y. Similarity and diversity of the tumor microenvironment in multiple metastases: Critical implications for overall and progression-free survival of high-grade serous ovarian cancer. *Oncotarget* **2016**, *7*, 71123–71135. [[CrossRef](#)]
30. Ciucci, A.; Zannoni, G.F.; Buttarelli, M.; Martinelli, E.; Mascilini, F.; Petrillo, M.; Ferrandina, G.; Scambia, G.; Gallo, D. Ovarian low and high grade serous carcinomas: Hidden divergent features in the tumor microenvironment. *Oncotarget* **2016**, *7*, 68033–68043. [[CrossRef](#)]
31. Koti, M.; Siu, A.; Clément, I.; Bidarimath, M.; Turashvili, G.; Edwards, A.; Rahimi, K.; Mes-Masson, A.M.; Squire, J.A. A distinct pre-existing inflammatory tumour microenvironment is associated with chemotherapy resistance in high-grade serous epithelial ovarian cancer. *Br. J. Cancer* **2015**, *112*, 1215–1222. [[CrossRef](#)] [[PubMed](#)]
32. Verardo, R.; Piazza, S.; Klaric, E.; Ciani, Y.; Bussadori, G.; Marzinotto, S.; Mariuzzi, L.; Cesselli, D.; Beltrami, A.P.; Mano, M.; et al. Specific mesothelial signature marks the heterogeneity of mesenchymal stem cells from high-grade serous ovarian cancer. *Stem Cells* **2014**, *32*, 2998–3011. [[CrossRef](#)]
33. Leinster, D.A.; Kulbe, H.; Everitt, G.; Thompson, R.; Perretti, M.; Gavins, F.N.; Cooper, D.; Gould, D.; Ennis, D.P.; Lockley, M.; et al. The peritoneal tumour microenvironment of high-grade serous ovarian cancer. *J. Pathol.* **2012**, *227*, 136–145. [[CrossRef](#)]
34. Garin-Chesa, P.; Old, L.J.; Rettig, W.J. Cell surface glycoprotein of reactive stromal fibroblasts as a potential antibody target in human epithelial cancers. *Proc. Natl. Acad. Sci. USA* **1990**, *87*, 7235–7239. [[CrossRef](#)]
35. Yang, W.; Han, W.; Ye, S.; Liu, D.; Wu, J.; Liu, H.; Li, C.; Chen, H.J.E. Fibroblast activation protein- α promotes ovarian cancer cell proliferation and invasion via extracellular and intracellular signaling mechanisms. *Exp. Mol. Pathol.* **2013**, *95*, 105–110. [[CrossRef](#)] [[PubMed](#)]
36. Mhawech-Fauceglia, P.; Yan, L.; Sharifian, M.; Ren, X.; Liu, S.; Kim, G.; Gayther, S.A.; Pejovic, T.; Lawrenson, K.J.C.M. Stromal expression of fibroblast activation protein alpha (FAP) predicts platinum resistance and shorter recurrence in patients with epithelial ovarian cancer. *Cancer Microenviron.* **2015**, *8*, 23–31. [[CrossRef](#)] [[PubMed](#)]
37. Brodie, T.M.; Tosevski, V.; Medova, M. OMIP-045: Characterizing human head and neck tumors and cancer cell lines with mass cytometry. *Cytom. A* **2018**, *93*, 406–410. [[CrossRef](#)] [[PubMed](#)]

38. Gadalla, R.; Noamani, B.; MacLeod, B.L.; Dickson, R.J.; Guo, M.; Xu, W.; Lukhele, S.; Elsaesser, H.J.; Razak, A.R.A.; Hirano, N.; et al. Validation of CyTOF Against Flow Cytometry for Immunological Studies and Monitoring of Human Cancer Clinical Trials. *Front. Oncol.* **2019**, *9*, 415. [[CrossRef](#)] [[PubMed](#)]
39. Wei, S.C.; Levine, J.H.; Cogdill, A.P.; Zhao, Y.; Anang, N.-A.A.S.; Andrews, M.C.; Sharma, P.; Wang, J.; Wargo, J.A.; Pe'er, D.; et al. Distinct Cellular Mechanisms Underlie Anti-CTLA-4 and Anti-PD-1 Checkpoint Blockade. *Cell* **2017**, *170*, 1120–1133. [e1117](#). [[CrossRef](#)]
40. Datar, I.; Sanmamed, M.F.; Wang, J.; Henick, B.S.; Choi, J.; Badri, T.; Dong, W.; Mani, N.; Toki, M.; Mejías, L.D.; et al. Expression Analysis and Significance of PD-1, LAG-3, and TIM-3 in Human Non-Small Cell Lung Cancer Using Spatially Resolved and Multiparametric Single-Cell Analysis. *J. Clin. Cancer Res.* **2019**, *25*, 4663–4673. [[CrossRef](#)]
41. Mistry, A.M.; Greenplate, A.R.; Ihrie, R.A.; Irish, J.M. Beyond the message: Advantages of snapshot proteomics with single-cell mass cytometry in solid tumors. *FEBS J.* **2019**, *286*, 1523–1539. [[CrossRef](#)] [[PubMed](#)]
42. Takahashi, C.; Au-Yeung, A.; Fuh, F.; Ramirez-Montagut, T.; Bolen, C.; Mathews, W.; O’Gorman, E.W. Mass cytometry panel optimization through the designed distribution of signal interference. *Cytom. Part A J. Int. Soc. Anal. Cytol.* **2016**, *91*. [[CrossRef](#)] [[PubMed](#)]
43. McKinnon, K.M. Flow Cytometry: An Overview. *Curr. Protoc. Immunol.* **2018**, *120*, 5.1.1–5.1.11. [[CrossRef](#)] [[PubMed](#)]
44. Dunbar, S.A. Applications of Luminex xMAP technology for rapid, high-throughput multiplexed nucleic acid detection. *Clin. Chim. Acta* **2006**, *363*, 71–82. [[CrossRef](#)] [[PubMed](#)]
45. Spitzer, M.H.; Nolan, G.P. Mass Cytometry: Single Cells, Many Features. *Cell* **2016**, *165*, 780–791. [[CrossRef](#)]
46. Pribyl, L.J.; Coughlin, K.A.; Sueblinvong, T.; Shields, K.; Iizuka, Y.; Downs, L.S.; Ghebre, R.G.; Bazzaro, M. Method for obtaining primary ovarian cancer cells from solid specimens. *J. Vis. Exp.* **2014**. [[CrossRef](#)]
47. Lohr, J.G.; Stojanov, P.; Carter, S.L.; Cruz-Gordillo, P.; Lawrence, M.S.; Auclair, D.; Sougnez, C.; Knoechel, B.; Gould, J.; Saksena, G.; et al. Widespread genetic heterogeneity in multiple myeloma: Implications for targeted therapy. *Cancer Cell* **2014**, *25*, 91–101. [[CrossRef](#)]
48. Winterhoff, B.J.; Maile, M.; Mitra, A.K.; Sebe, A.; Bazzaro, M.; Geller, M.A.; Abraham, J.E.; Klein, M.; Hellweg, R.; Mullany, S.A.; et al. Single cell sequencing reveals heterogeneity within ovarian cancer epithelium and cancer associated stromal cells. *Gynecol. Oncol.* **2017**, *144*, 598–606. [[CrossRef](#)]
49. Geistlinger, L.; Oh, S.; Ramos, M.; Schiffer, L.; LaRue, R.S.; Henzler, C.M.; Munro, S.A.; Daughters, C.; Nelson, A.C.; Winterhoff, B.J.; et al. Multiomic Analysis of Subtype Evolution and Heterogeneity in High-Grade Serous Ovarian Carcinoma. *Cancer Res.* **2020**. [[CrossRef](#)]
50. Giesen, C.; Wang, H.A.; Schapiro, D.; Zivanovic, N.; Jacobs, A.; Hattendorf, B.; Schuffler, P.J.; Grolimund, D.; Buhmann, J.M.; Brandt, S.; et al. Highly multiplexed imaging of tumor tissues with subcellular resolution by mass cytometry. *Nat. Methods* **2014**, *11*, 417–422. [[CrossRef](#)] [[PubMed](#)]
51. Rundgren, I.M.; Ersvær, E.; Ahmed, A.B.; Rynningen, A.; Bruslerud, Ø. A Pilot Study of Circulating Monocyte Subsets in Patients Treated with Stem Cell Transplantation for High-Risk Hematological Malignancies. *Medicina* **2020**, *56*, 36. [[CrossRef](#)] [[PubMed](#)]
52. Amir, E.A.D.; Davis, K.L.; Tadmor, M.D.; Simonds, E.F.; Levine, J.H.; Bendall, S.C.; Shenfeld, D.K.; Krishnaswamy, S.; Nolan, G.P.; Pe’er, D. viSNE enables visualization of high dimensional single-cell data and reveals phenotypic heterogeneity of leukemia. *Nat. Biotechnol.* **2013**, *31*, 545–552. [[CrossRef](#)] [[PubMed](#)]

Phenotypic Characterization by Mass Cytometry of the Microenvironment in Ovarian Cancer and Impact of Tumor Dissociation Methods

Shamundeewari Anandan, Liv Cecilie V. Thomsen, Stein-Erik Gullaksen, Tamim Abdelaal, Katrin Kleinmanns, Jørn Skavland, Geir Bredholt, Bjørn Tore Gjertsen, Emmet McCormack and Line Bjørge

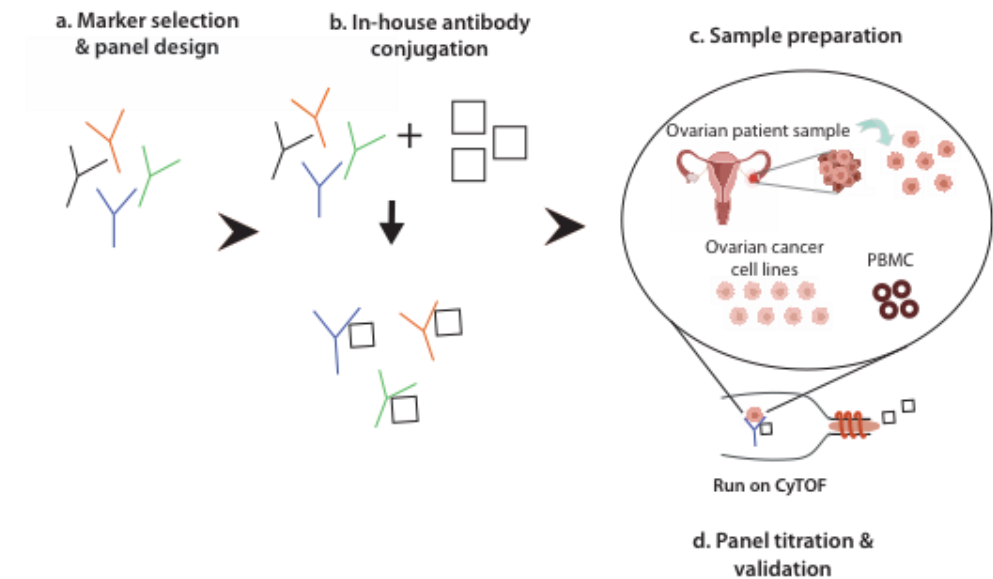


Figure S1. Overview of ovarian mass cytometry panel development.

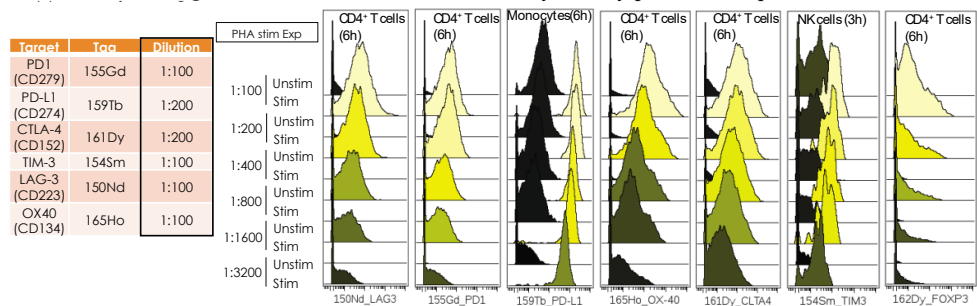


Figure S2. Antibody staining on unstimulated and PHA-stimulated PBMCs. On the left are the markers defined as immune checkpoints in this experiment, the associated metal tags, and the final dilutions selected for further experiments. On the right are the overlaid histograms for each marker in the relevant cell subsets (horizontally) according to dilution (vertically) from the lowest uppermost in the figure to

the highest lowermost, alternating between expression demonstrated in unstimulated (Unstim) PBMCs and stimulated (Stim) PBMCs.

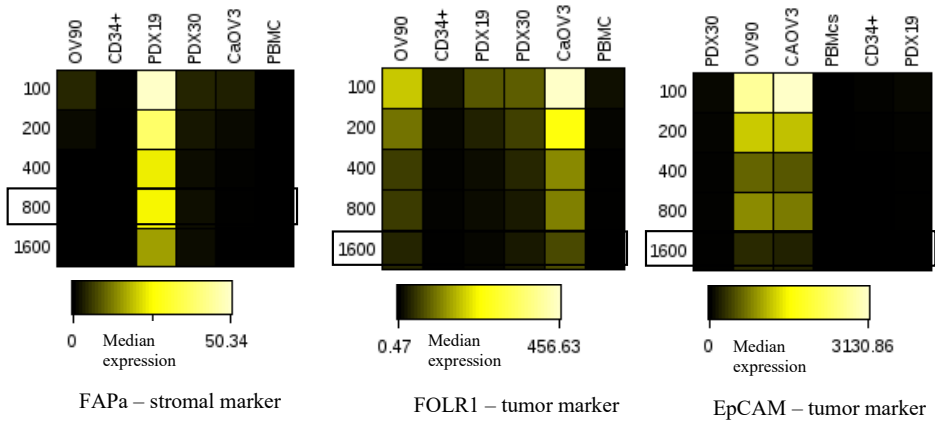


Figure S3. Stromal and tumor panels were titrated on ovarian cancer cell lines and a mixture of the patient samples. Since the stromal marker fibroblast activation protein alpha (FAP α ; left) demonstrated good signals at all dilutions in the patient sample, a lower dilution of 1:800 was selected for this marker. The tumor markers folate receptor (FOLR1; center) and epithelial cell adhesion molecule (EpCAM; right) showed decreasing marker expression with higher dilutions. Still, as the antibodies were expressed at the high dilution (1:1600), this was selected for these markers.

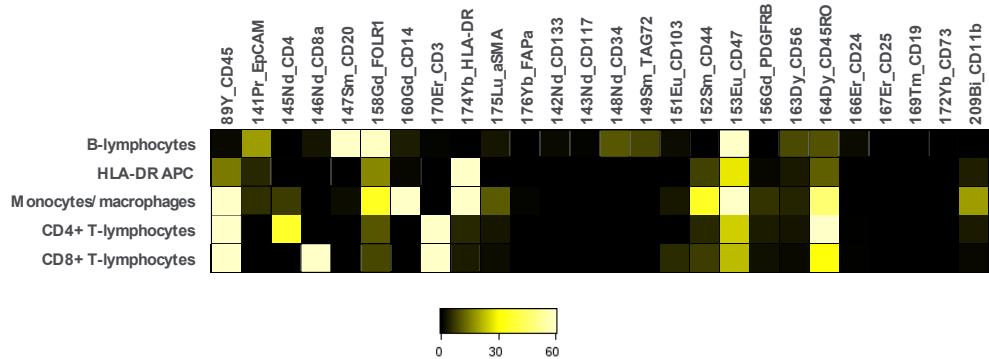


Figure S4. Panel validation on pooled patient data. The antibody panel was applied to a pool of dissociated patient tumors ($n = 4$, each dissociated by a different method) with the antibodies diluted according to the results from the previous titration steps. The generated CyTOF data were analyzed in Cytobank, and a heatmap was generated. The main cell subsets (vertically) were defined according to cellular antibody expression (horizontally). The major immune phenotypes (CD45+ cells) were identified, including CD8+cytotoxic T cells, CD4+ T helper cells, CD20+ B cells, and HLA DR+ antigen-presenting cells. Stromal and tumor cells were also identified.

Figure S5. Histograms illustrating antibody expression according to three separate patient samples. Marker distribution per patient is displayed for all conditions. Probability density function of each marker show distribution differences across patients for all conditions. The x-axis represents marker expression values arcsin-transformed using a cofactor of 5. The marker expression range is limited to between 0.1 and 6 (ignoring the zero peak for visualization purposes). The y-axis represents the probability density, which is the occurrence frequency for different marker expression values. (This is enclosed as a separate file due to size.)

Figure S6. Cox proportional-hazard models of median expression of the functional markers. (This is enclosed as a separate file due to size.)

Table S1: Overview of antibodies and metal conjugates (Tags) included in the HGSOc TME-based mass cytometry by time-of-flight (CyTOF) panel, the positive and negative controls used for each antibody, and the final antibody dilutions that should be applied to tissues

Markers	Clone	Tag	Positive control	Negative control	Dilution
CD8a	RPAT8	146Nd	PBMC	OV90 <i>luc</i> ⁺ and CAOv3 <i>luc</i> ⁺	1:400
CD4	RPAT4	145Nd	PBMC	OV90 <i>luc</i> ⁺ and CAOv3 <i>luc</i> ⁺	1:100
CD3	UCHT1	170Er	PBMC	OV90 <i>luc</i> ⁺ and CAOv3 <i>luc</i> ⁺	1:6400
CD45RO	UCHL1	164Dy	PBMC	OV90 <i>luc</i> ⁺ and CAOv3 <i>luc</i> ⁺	1:200
HLA-DR	L243	174Yb	PBMC	OV90 <i>luc</i> ⁺ and CAOv3 <i>luc</i> ⁺	1:6400
CD20	2H7	147Sm	PBMC	OV90 <i>luc</i> ⁺ and CAOv3 <i>luc</i> ⁺	1:50
CD25	2A3	167Er	PBMC	OV90 <i>luc</i> ⁺ and CAOv3 <i>luc</i> ⁺	1:50
CD56	NCAM16.2	163Dy	PBMC	OV90 <i>luc</i> ⁺ and CAOv3 <i>luc</i> ⁺	1:12800
CD19	HIB19	169Tm	PBMC	OV90 <i>luc</i> ⁺ and CAOv3 <i>luc</i> ⁺	1:200
CD14	M5E2	160Gd	PBMC	OV90 <i>luc</i> ⁺ and CAOv3 <i>luc</i> ⁺	1:200
CD11b	ICRF44	209Bi	PBMC	OV90 <i>luc</i> ⁺ and CAOv3 <i>luc</i> ⁺	1:400
CD45	HI30	89Y	PBMC	OV90 <i>luc</i> ⁺ and CAOv3 <i>luc</i> ⁺	1:1600
CD103	BER-ACT8	151Eu	PBMC	OV90 <i>luc</i> ⁺ and CAOv3 <i>luc</i> ⁺	1:200
CD47*	CC2C6	153Eu	PBMC	OV90 <i>luc</i> ⁺ and CAOv3 <i>luc</i> ⁺	1:12800
PD1/CD279	EH12. 2H7	155Gd	Stimulated PBMC	PBMC	1:100
PD-L1/CD274	29E.2A3	159Tb	Stimulated PBMC	PBMC	1:200
CTLA-4/CD152	14D3	161Dy	Stimulated PBMC	PBMC	1:200

TIM-3	F38-2E2	154Sm	Stimulated PBMC	PBMC	1:50
LAG-3/CD223	11C3C65	150Nd	Stimulated PBMC	PBMC	1:50
OX40/CD134*	Ber-ACT35 (ACT35)	165Ho	Stimulated PBMC	PBMC	1:100
Foxp3	259D/C7	162Dy	Stimulated PBMC	PBMC	1:800
IFN γ	B27	168Er	OV90 <i>luc</i> ⁺ and CAOV3 <i>luc</i> ⁺	PBMC	1:50
CD34	581	148Nd	OV90 <i>luc</i> ⁺ and CAOV3 <i>luc</i> ⁺	PBMC	1:3200
CD73*	AD2	172Yb	OV90 <i>luc</i> ⁺ and CAOV3 <i>luc</i> ⁺	PBMC	1:1600
CD24	ML5	166Er	OV90 <i>luc</i> ⁺ and CAOV3 <i>luc</i> ⁺	PBMC	1:200
CD44*	BJ18	152Sm	OV90 <i>luc</i> ⁺ and CAOV3 <i>luc</i> ⁺	PBMC	1:400
CD133*	5-E3 (5E3)	142Nd	OV90 <i>luc</i> ⁺ and CAOV3 <i>luc</i> ⁺	PBMC	1:200
CD117	104D2	143Nd	OV90 <i>luc</i> ⁺ and CAOV3 <i>luc</i> ⁺	PBMC	1:50
EpCAM/CD326	9C4	141Pr	OV90 <i>luc</i> ⁺ and CAOV3 <i>luc</i> ⁺	PBMC	1:6400
TAG72*	0.N.561	149Sm	OV90 <i>luc</i> ⁺ and CAOV3 <i>luc</i> ⁺	PBMC	1:50
FOLR1*	548908	158Gd	OV90 <i>luc</i> ⁺ and CAOV3 <i>luc</i> ⁺	PBMC	1:6400
PDGFRB/CD140b	18A2	156Gd	OV90 <i>luc</i> ⁺ and CAOV3 <i>luc</i> ⁺	PBMC	1:50
FAPalpha*	F11-24	176Yb	OV90 <i>luc</i> ⁺ and CAOV3 <i>luc</i> ⁺	PBMC	1:800
aSMA*	1A4	175Lu	OV90 <i>luc</i> ⁺ and CAOV3 <i>luc</i> ⁺	PBMC	1:6400
AXL*	MM0098- 2N33	171Yb	OV90 <i>luc</i> ⁺ and CAOV3 <i>luc</i> ⁺	PBMC	1:200

*In-house conjugated antibodies

Table S2 Antibody-expression of the cell clusters significantly affected by the different dissociation methods

Cluster name	Antigen expression
Immune cluster 7	CD45+HLA-DR+CD14+
Stromal cluster 5	EpCAM+CD47+PDGFR+FOLR1+CD56+CD24+
Stromal cluster 6	EpCAM+CD47+CD56+

Tumor cluster 2	EpCAM+CD47+FOLR1+
Tumor cluster 4	EpCAM+CD47+
Tumor cluster 5 - Cancer stem cells	CD34+

Table S3 Overview of the patient cohort ($n = 3$).

Patient	Age	Stage	Morphology	Chemonaïve	Progression-free survival (days)	Status
1	71	IIIc	High-grade serous ovarian adenocarcinoma	No	1516	Alive without disease
2	61	IIc	High-grade serous ovarian adenocarcinoma	Yes	449	Alive with disease
3	69	IIIc	High-grade serous ovarian adenocarcinoma	Yes	549	Alive without disease

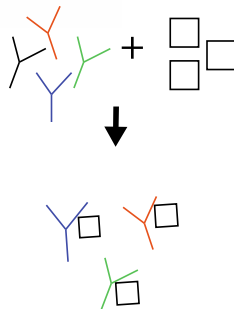
Table S4. Viability of the cells in the dissociated tissues. For each patient sample and the six dissociation methods the percentage of dead cells in the sample is listed. The viability was measured directly after dissociation of the tumor before freezing.

Patient	Collagenase	Collagenase + trypsin	Miltenyi 1 hr	Miltenyi 2 hrs	Dispase	Mechanical
1	5.6	6.56	5.1	5.9	4.5	11.9
2	15	14	19	16	14	30
3	3.99	8.1	9.65	24.8	8.56	35.7

Supplementary Material 1. Marker selection and panel design

A 35-antibody HGSOc panel focusing on cellular components of the tumor microenvironment was developed using markers selected on the basis of a literature review and designed with the panel designer (Fluidigm, CA). The panel comprised three major categories: tumor, stromal, and immune markers. These included 33 surface antibodies and two intercellular antibodies. The 33 selected surface markers included general immune lineage markers ($n = 15$), ovarian stromal, tumor, and stem cell markers ($n = 12$), and immune checkpoint antibodies ($n = 6$). Pre-conjugated antibodies ($n = 24$) were purchased from Fluidigm (Supplementary Table 1).

Supplementary Material 2. In-house antibody conjugation to rare metals

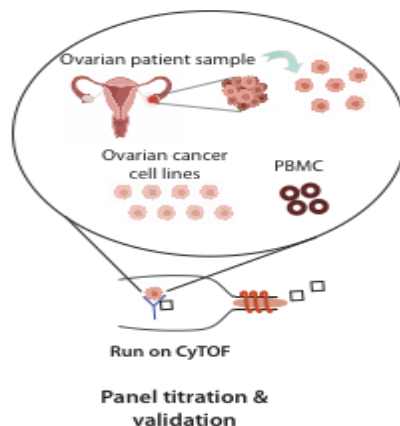


Apart from the 24 pre-conjugated antibodies purchased, a total of 11 antibodies were successfully conjugated in house. In-house conjugation of carrier-free antibodies ($n = 11$) to metal-chelated polymers (MaxPAR antibody conjugation kit, Fluidigm) was performed according to the manufacturer's protocol (PRD002 Version 11). The in-house conjugated metal-labeled antibodies were diluted to 0.5mg/mL in antibody stabilization solution (CANDOR Biosciences, Wangen im Allgäu, Germany) and stored at 4°C until required.

Supplementary Material 3. *Ex vivo* stimulation of peripheral blood mononuclear cells

Immune checkpoint antibodies were titrated on stimulated peripheral blood mononuclear cells (PBMCs). Prior to stimulation, a batch of cryopreserved PBMCs (collected from healthy donors, as mentioned above) were thawed, slow diluted (1:12) in RPMI 1640 media at room temperature, and pelleted at 300 g for 5 minutes. The cells (3×10^6 cells/mL) were then resuspended in complete RPMI 1640 medium supplemented with 10% FCS, 2 mM L-glutamine, penicillin 100 IU/mL, and 100U/mL Interleukin-2 (IL-2) (Gibco, Thermo Fischer Scientific) and incubated for an hour at 37 °C in a humidified atmosphere with 5% CO₂, prior to stimulation with 2.5 µg/mL phytohemagglutinin (PHA, Sigma Aldrich) for 48 hours under the same incubation conditions. After stimulation, the cells were fixed using Stable-Lyse and Stable-Store (Smart Tube Inc., CA) as per the manufacturer's protocol (Protocol number: SLSSP1TF-150203). Healthy non-stimulated PBMCs used for titrations were fixed following the same protocol.

Supplementary Material 4. Panel titration and validation



The 35-antibody panel was split into smaller titration panels (immune, stromal/tumor). Two main criteria were included in the design of these titration panels, namely, antibodies with the same metal tags were excluded, and the corresponding M±1 and +16 channels were left open and empty to avoid spillovers and oxide interference.

Initially, a backbone panel with common immune lineage markers was designed, and the rest of the panel was built on this. Immune antibodies were titrated on unstimulated PBMCs and PBMCs stimulated by either phorbol 12-myristate 13-acetate (PMA) (25 ng/mL) and ionomycin (1ug/mL) for 3 or 6 hours or 2.5 µg/mL phytohemagglutinin (PHA) and 100 IU/ml Human Interleukin-2 (IL-2) Recombinant Protein. The immune checkpoint antibodies were titrated successfully when applied to unstimulated and stimulated PBMCs (Figure S2).

Supplementary Material 5. Expression of functional markers

The median expression of each of the functional markers included in the panel was evaluated using Cox proportional-hazard models to investigate whether expression levels within the cell populations differed significantly when the six different dissociation methods were applied to the same tissues (Supplementary Figure S6).

Figure S3.1: Histogram - aSMA

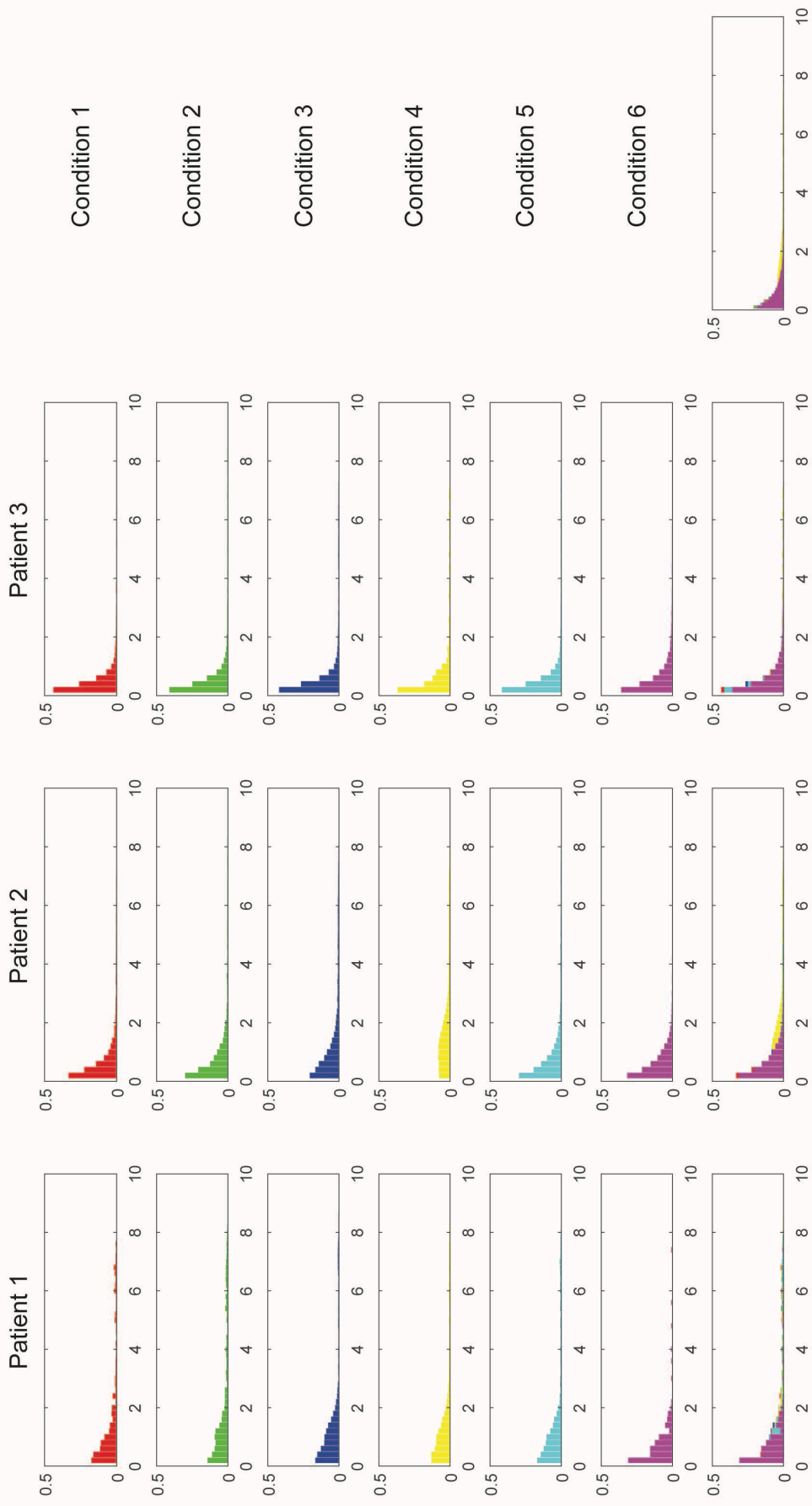


Figure S3.2: Histogram - Ax1

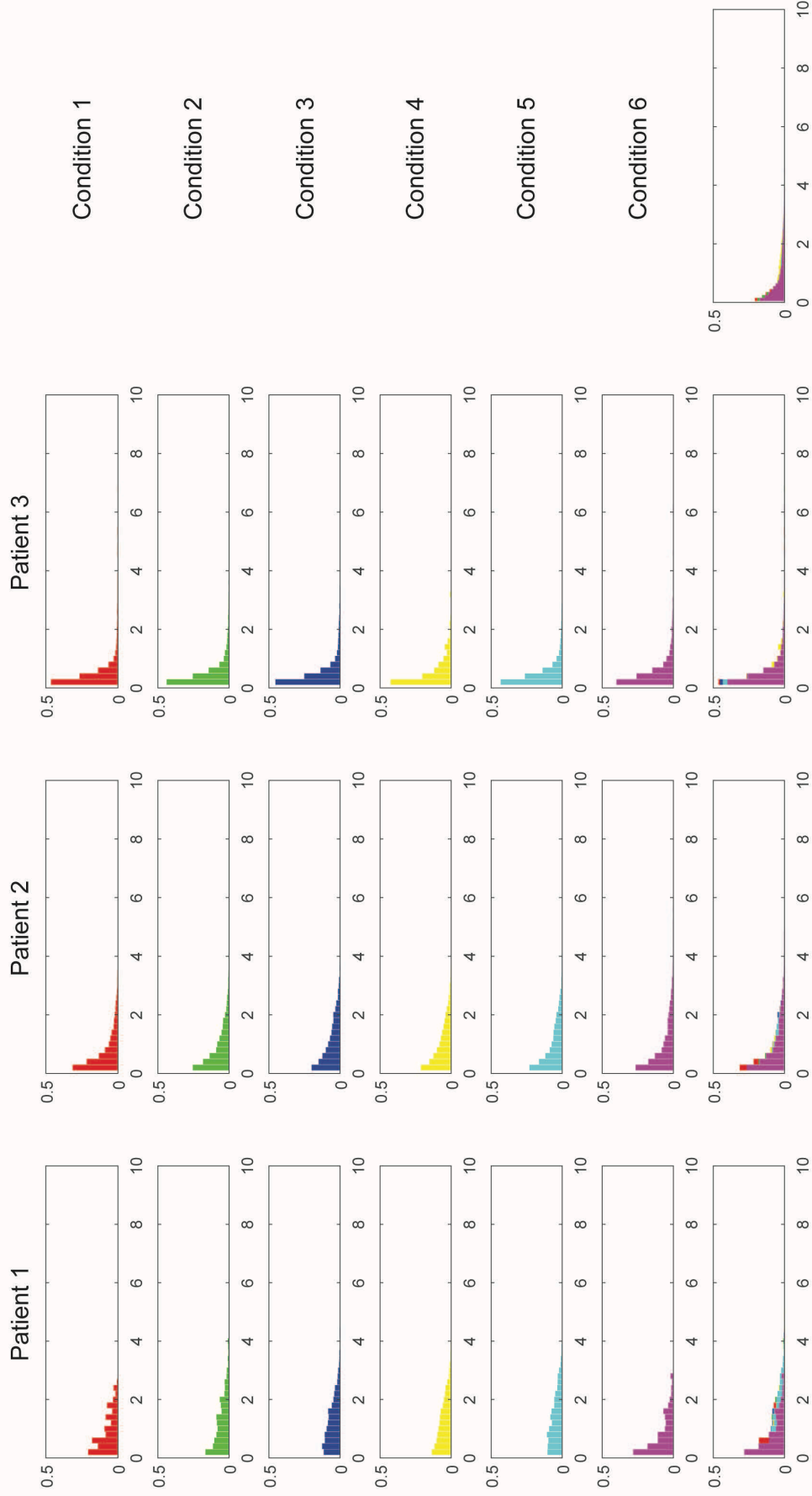


Figure S3.3: Histogram - CD3

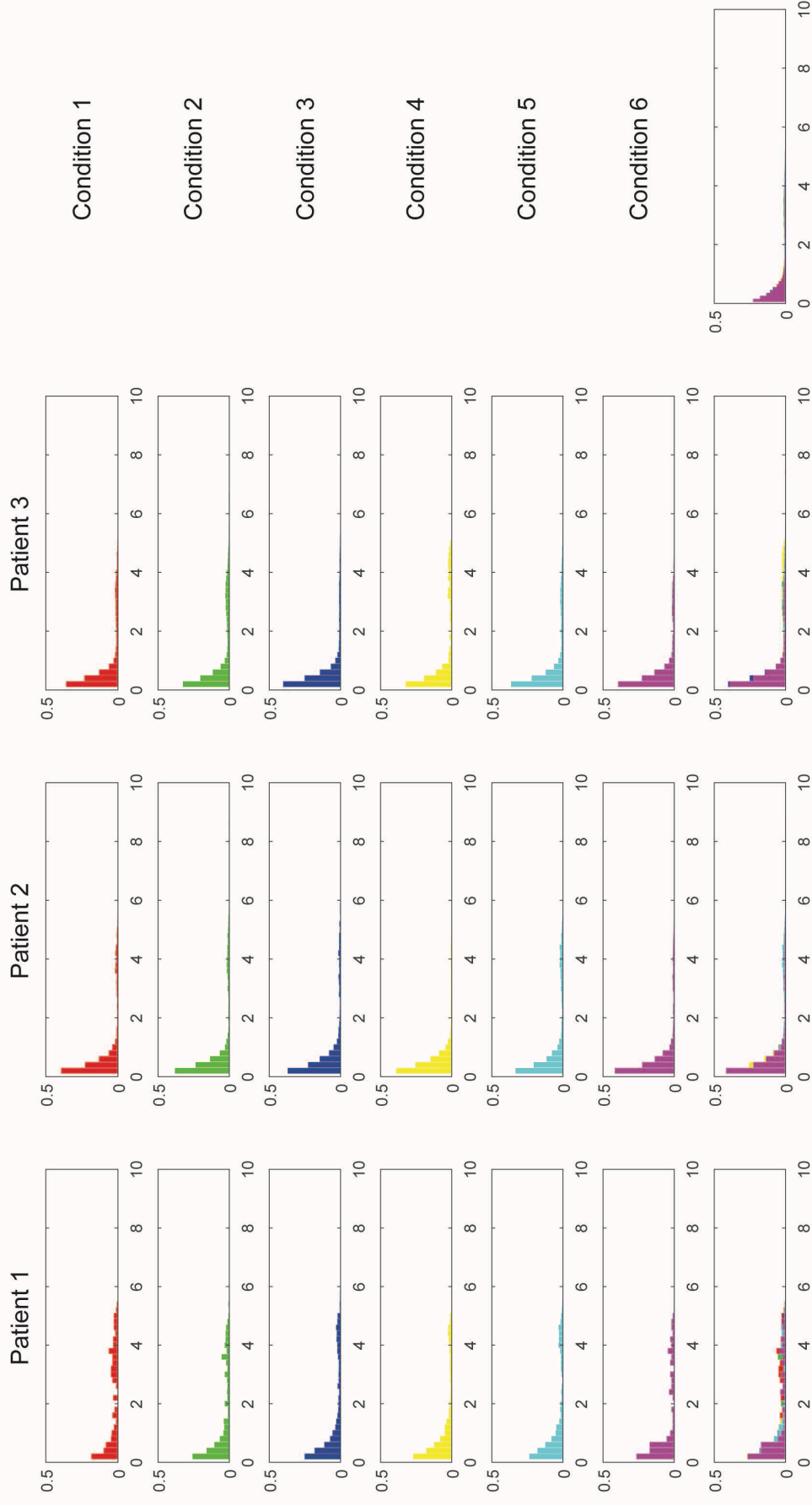


Figure S3.4: Histogram - CD4

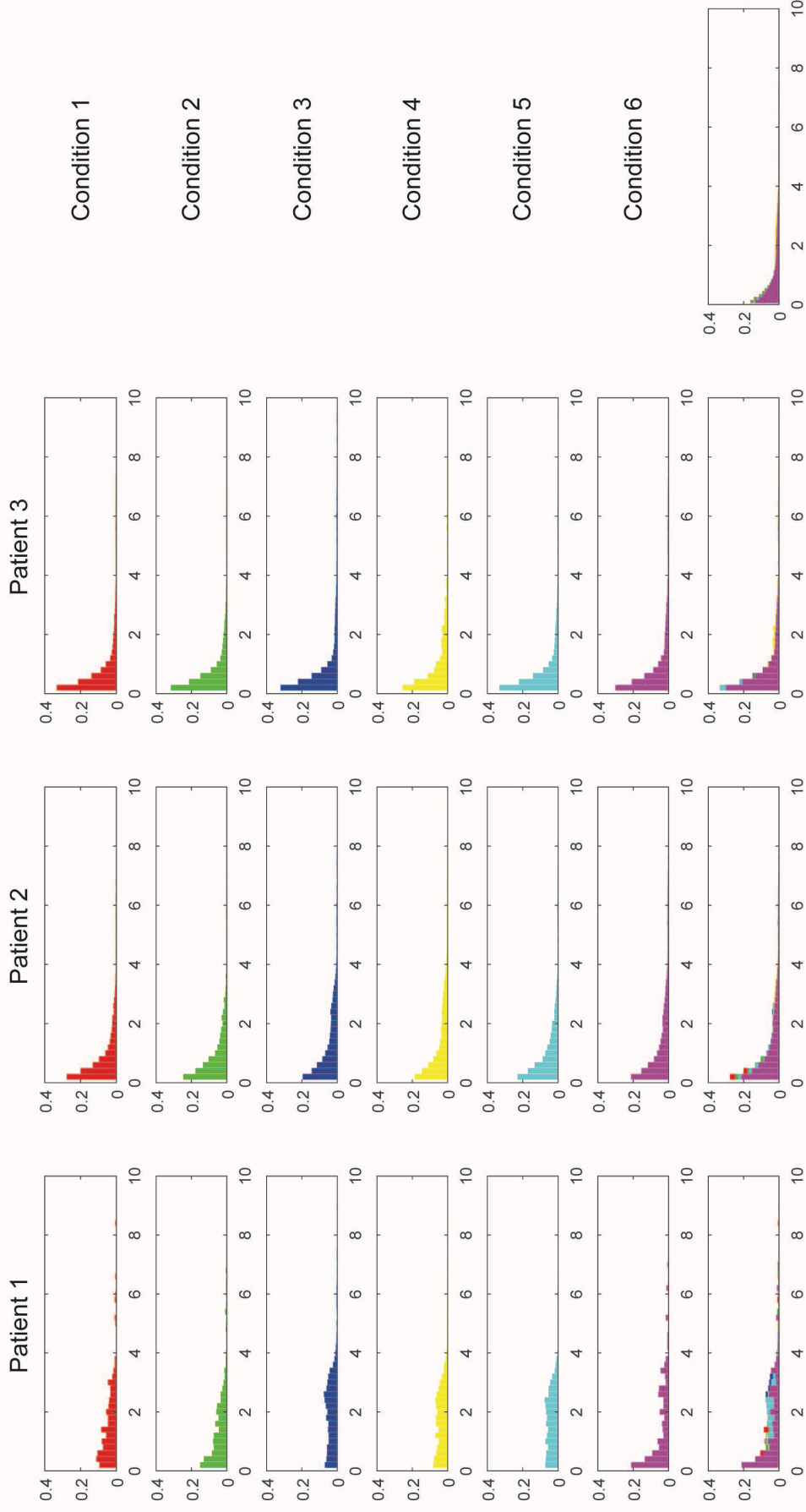


Figure S3.5: Histogram - CD8a

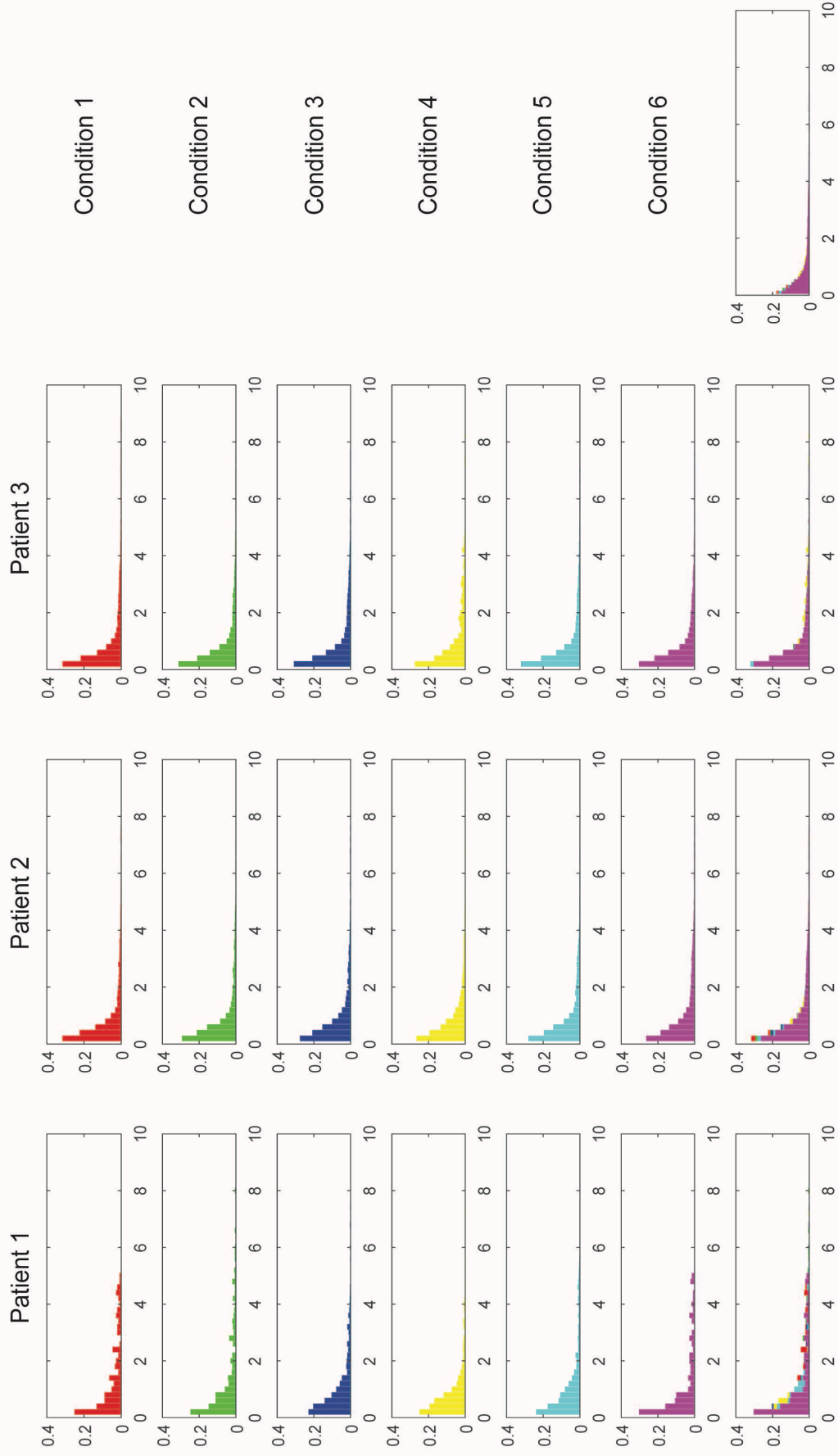


Figure S3.6: Histogram - CD11b

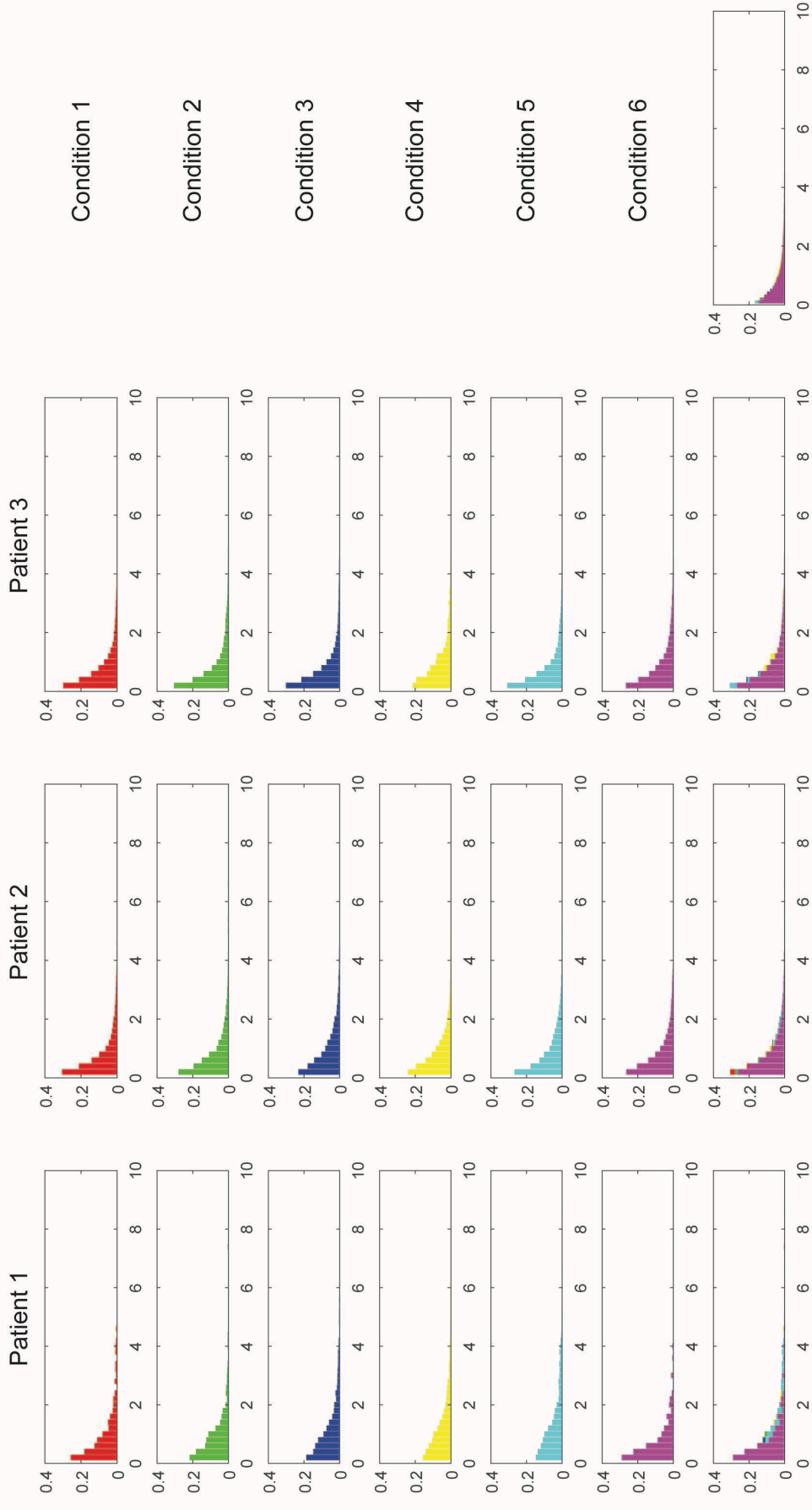


Figure S3.7: Histogram - CD14

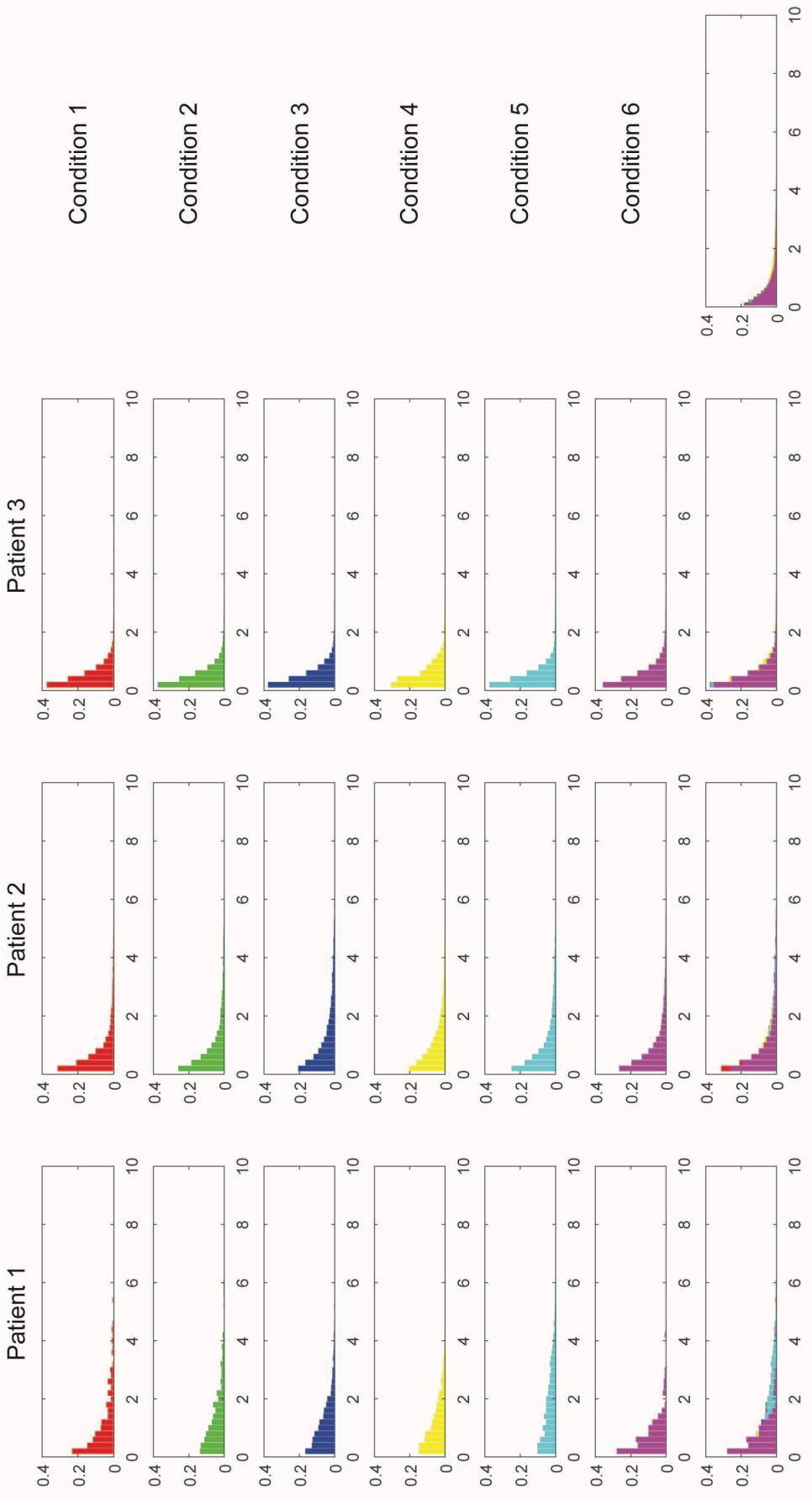


Figure S3.8: Histogram - CD19

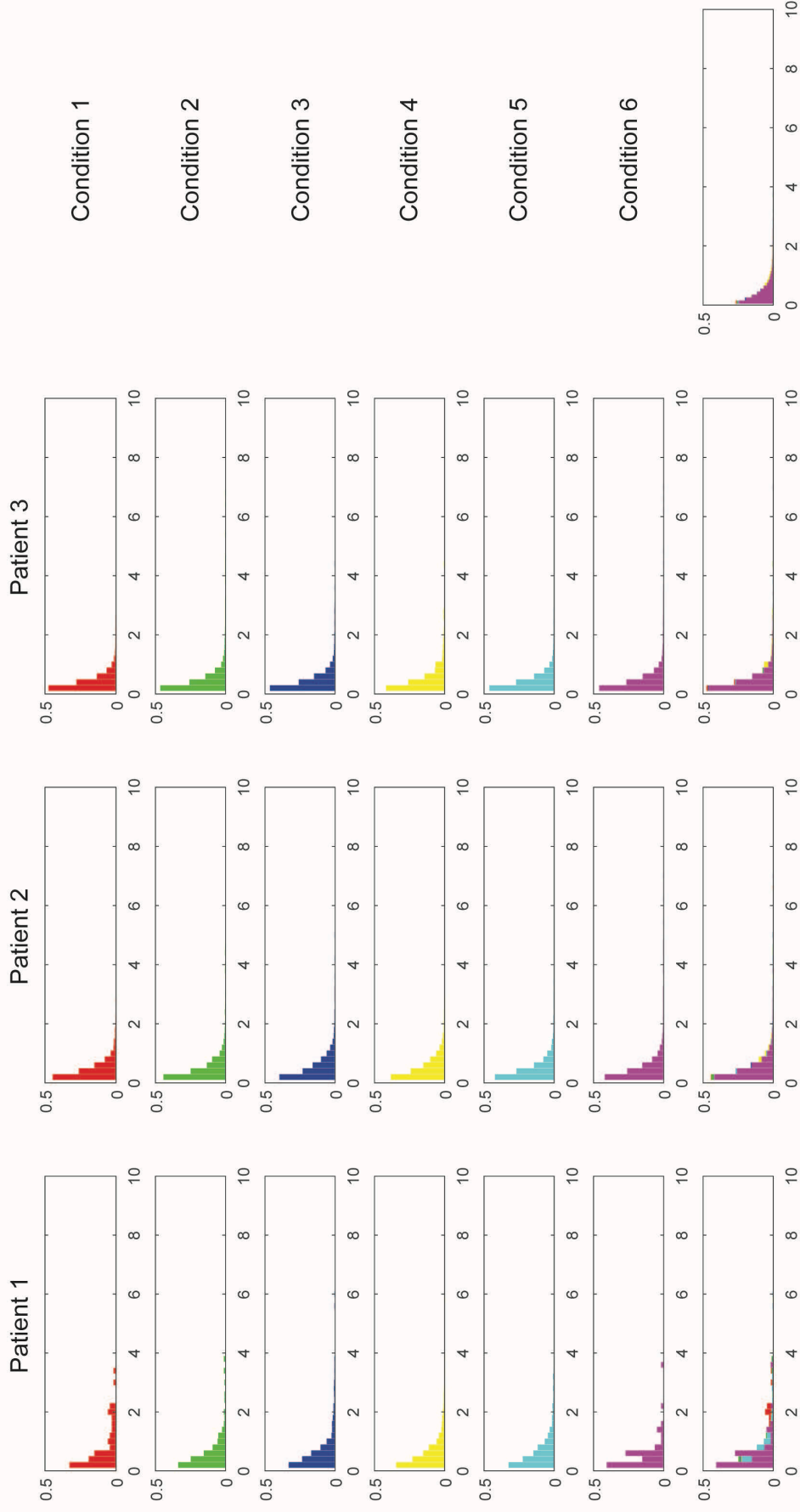


Figure S3.9: Histogram - CD20

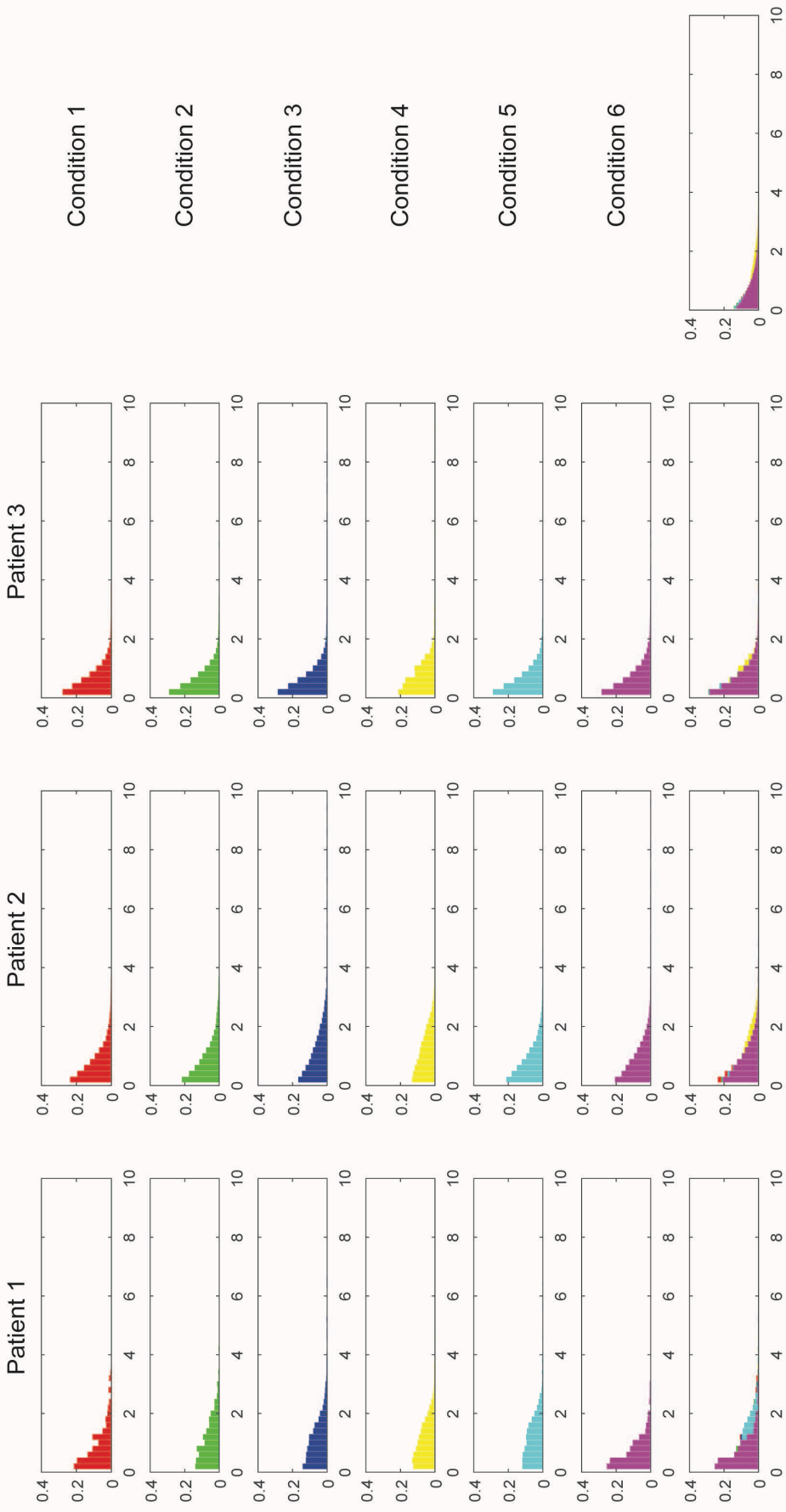


Figure S3.10: Histogram - CD24

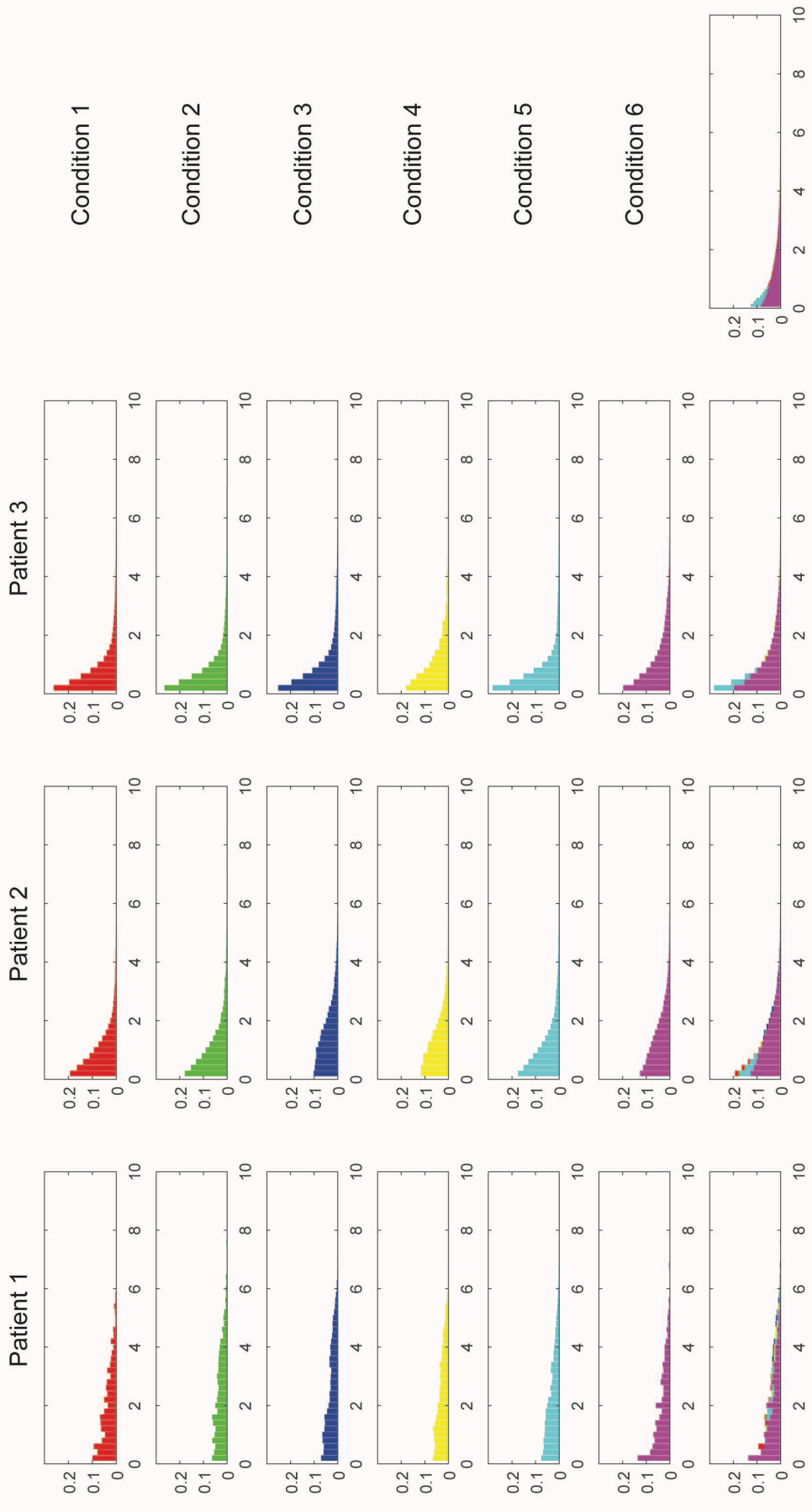


Figure S3.11: Histogram - CD25

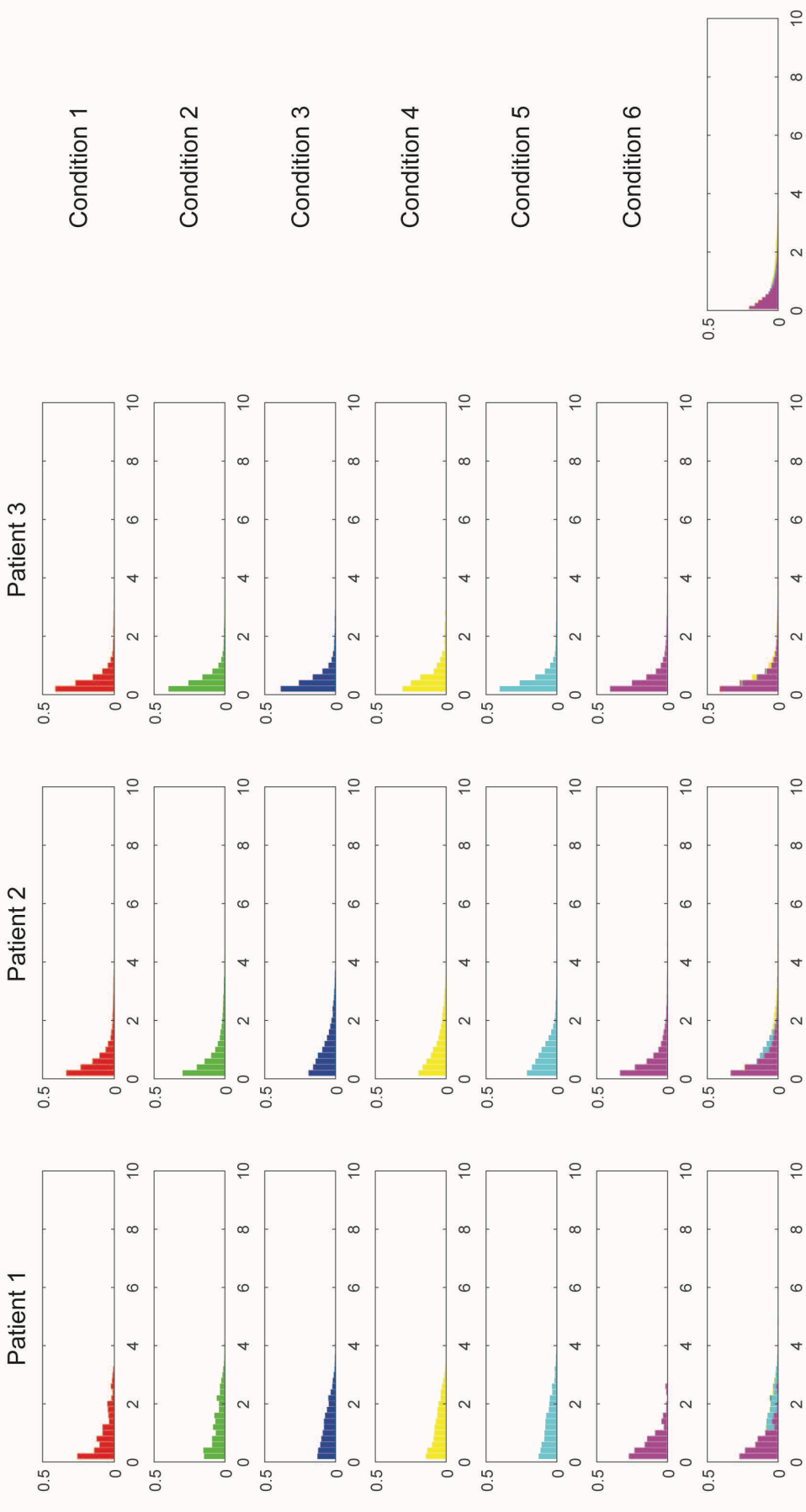


Figure S3.12: Histogram - CD34

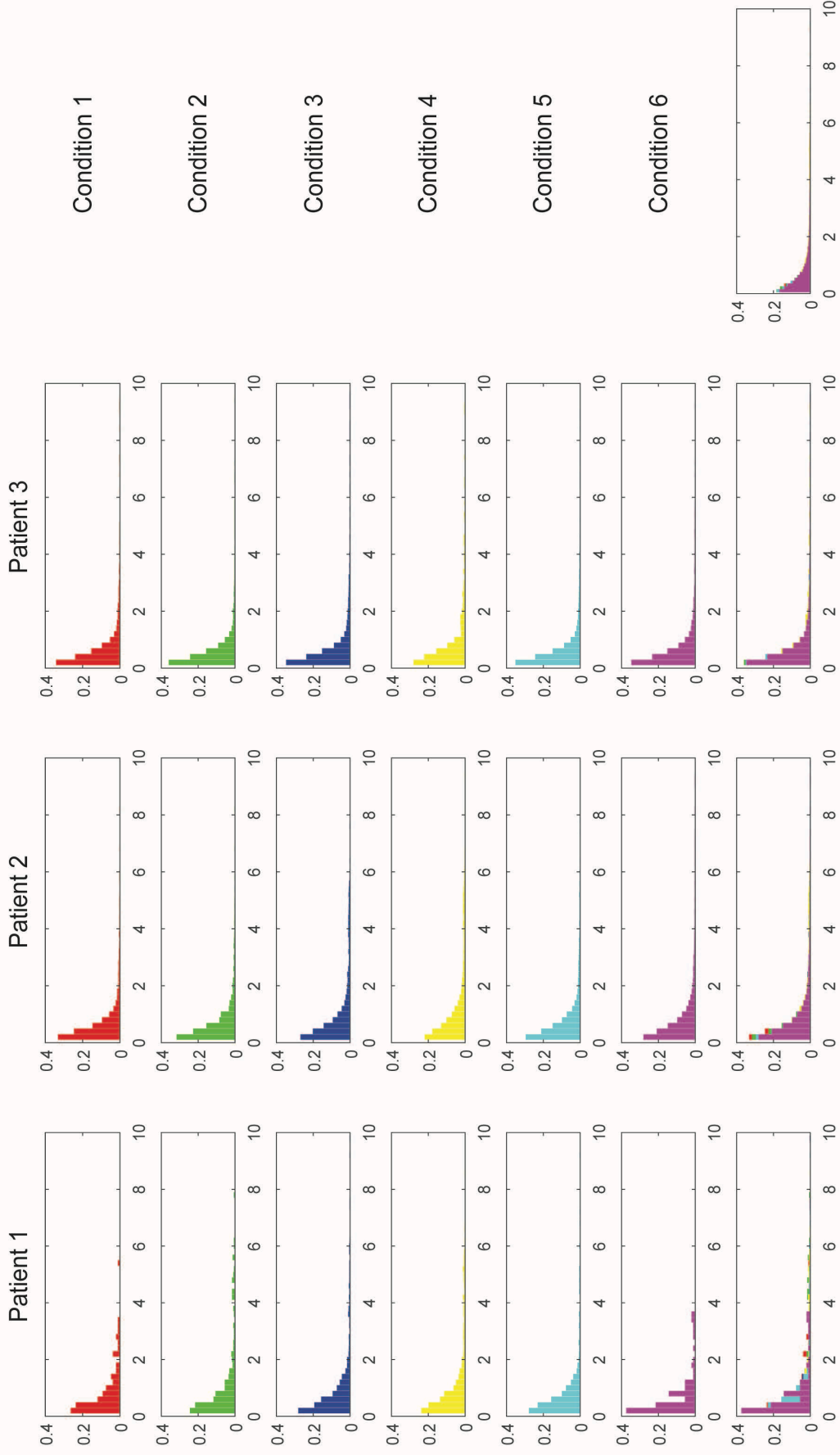


Figure S3.13: Histogram - CD44

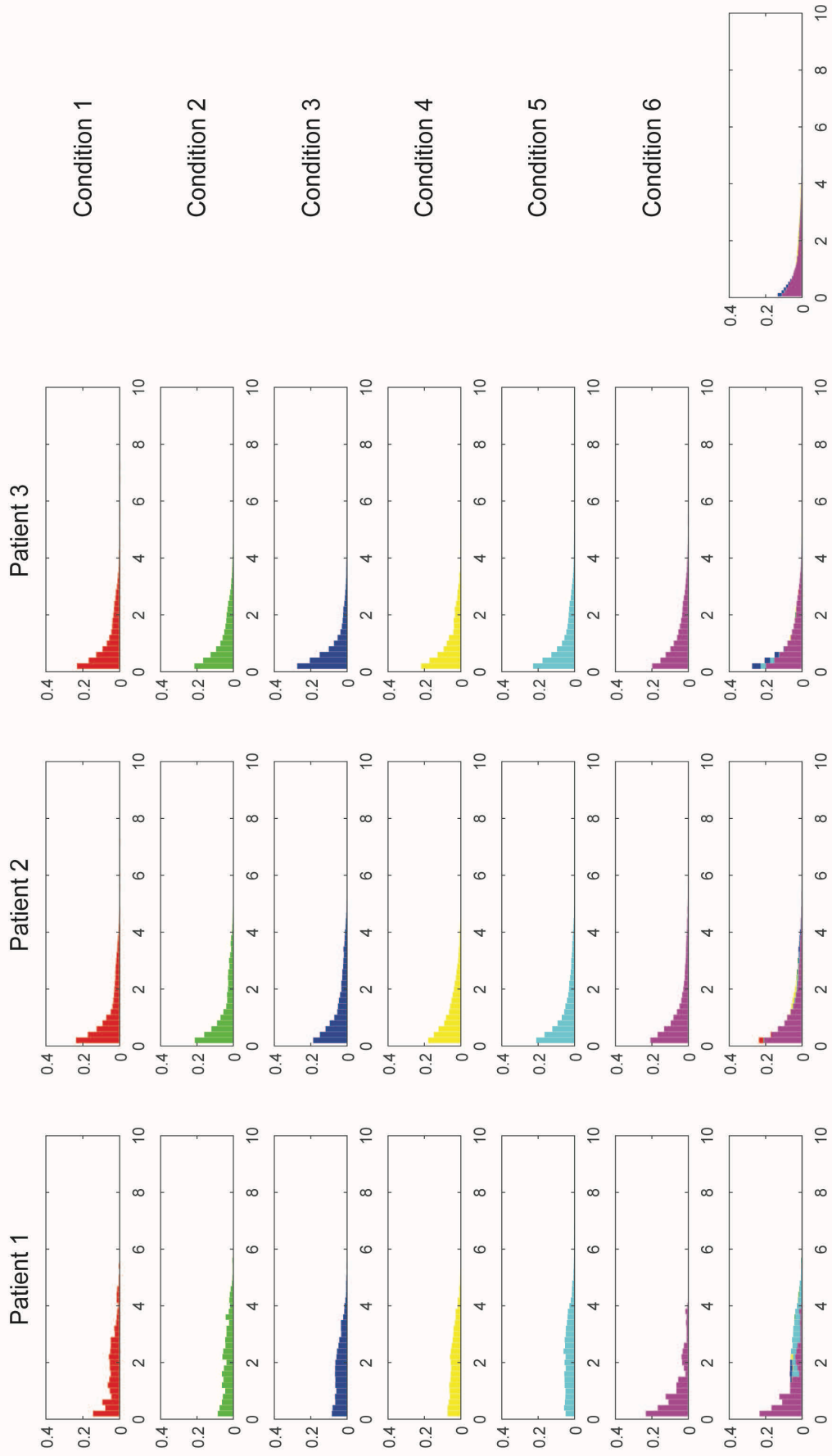


Figure S3.14: Histogram - CD45

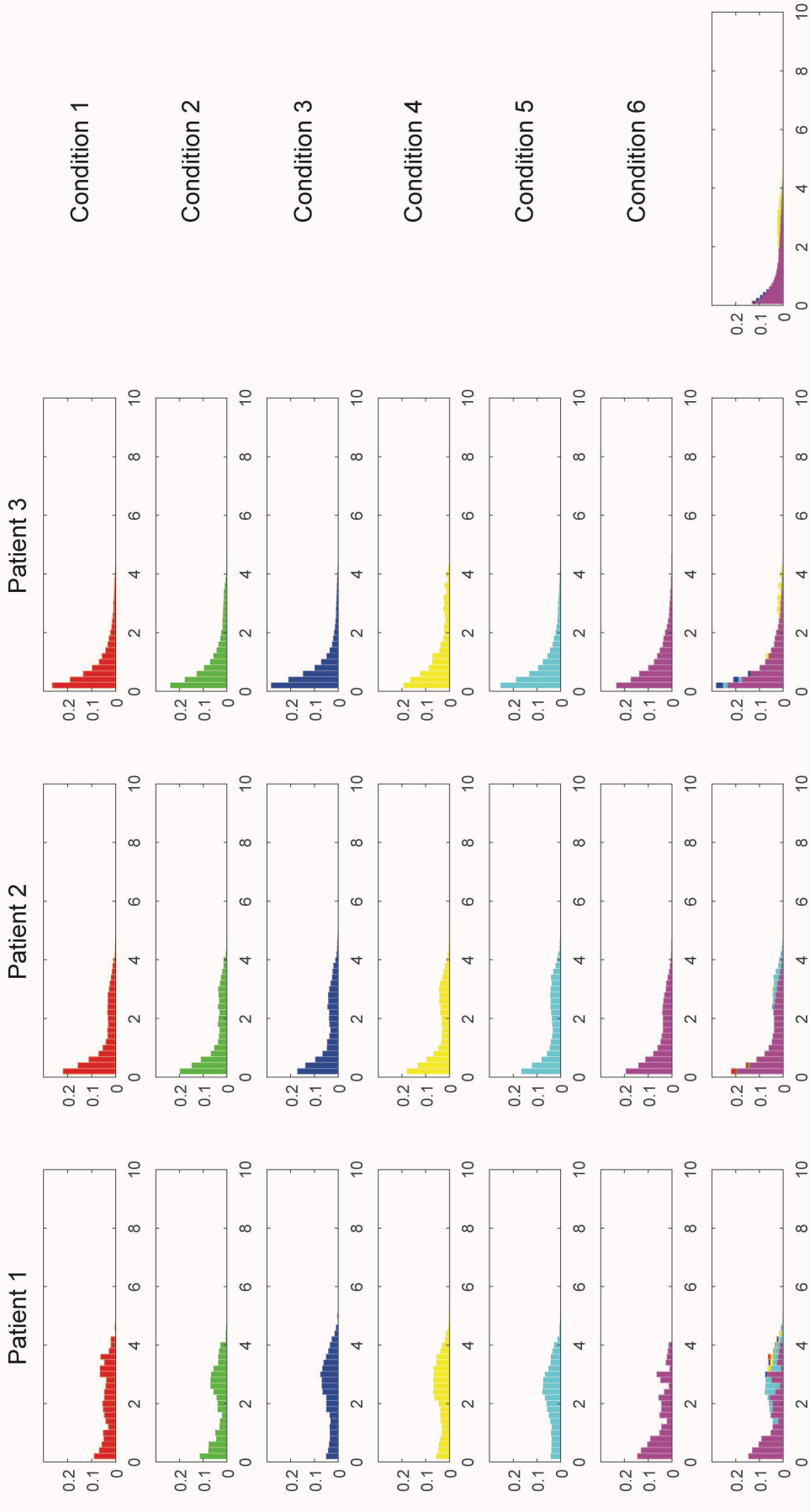


Figure S3.15: Histogram - CD45RO

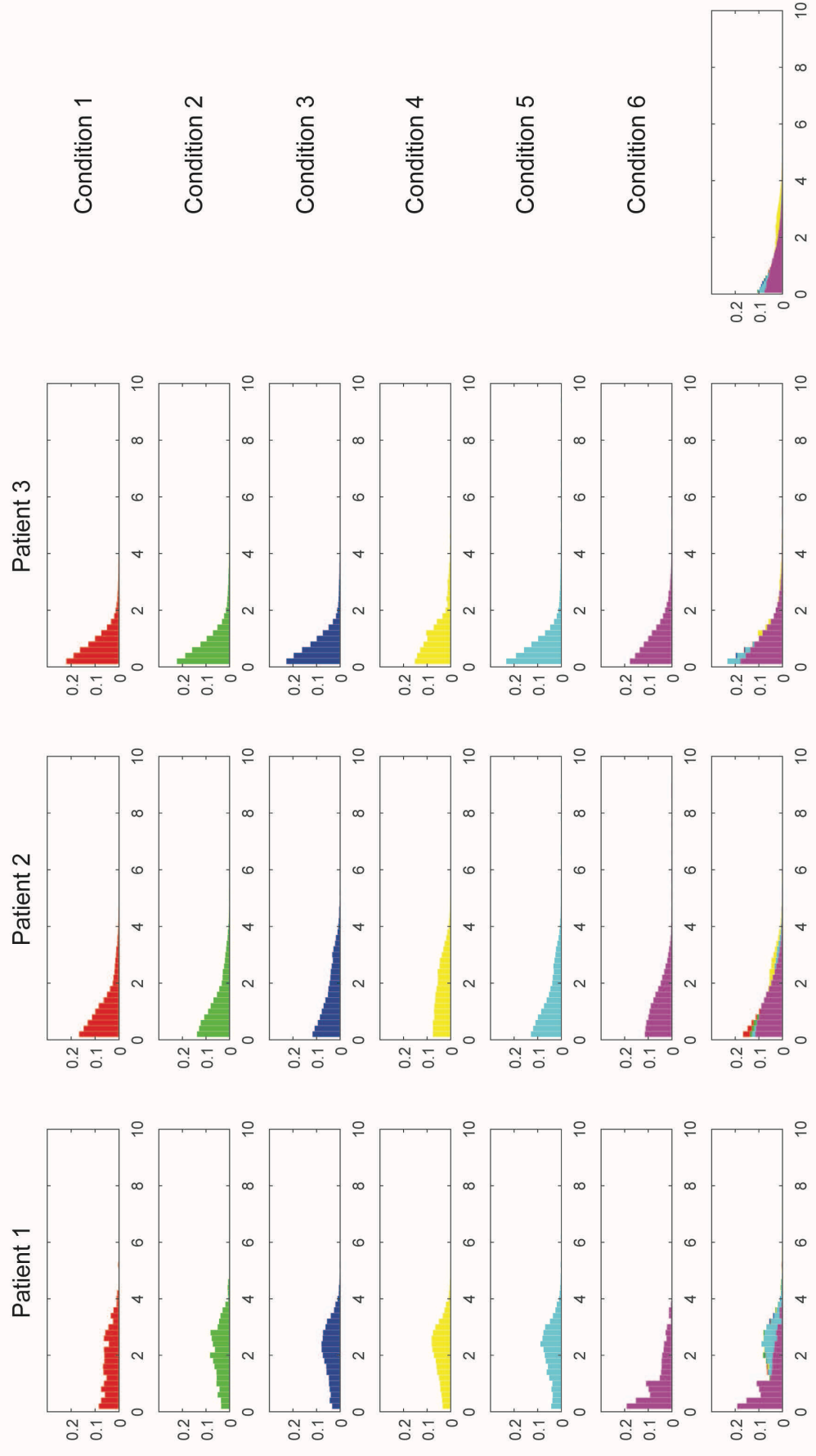


Figure S3.16: Histogram - CD47

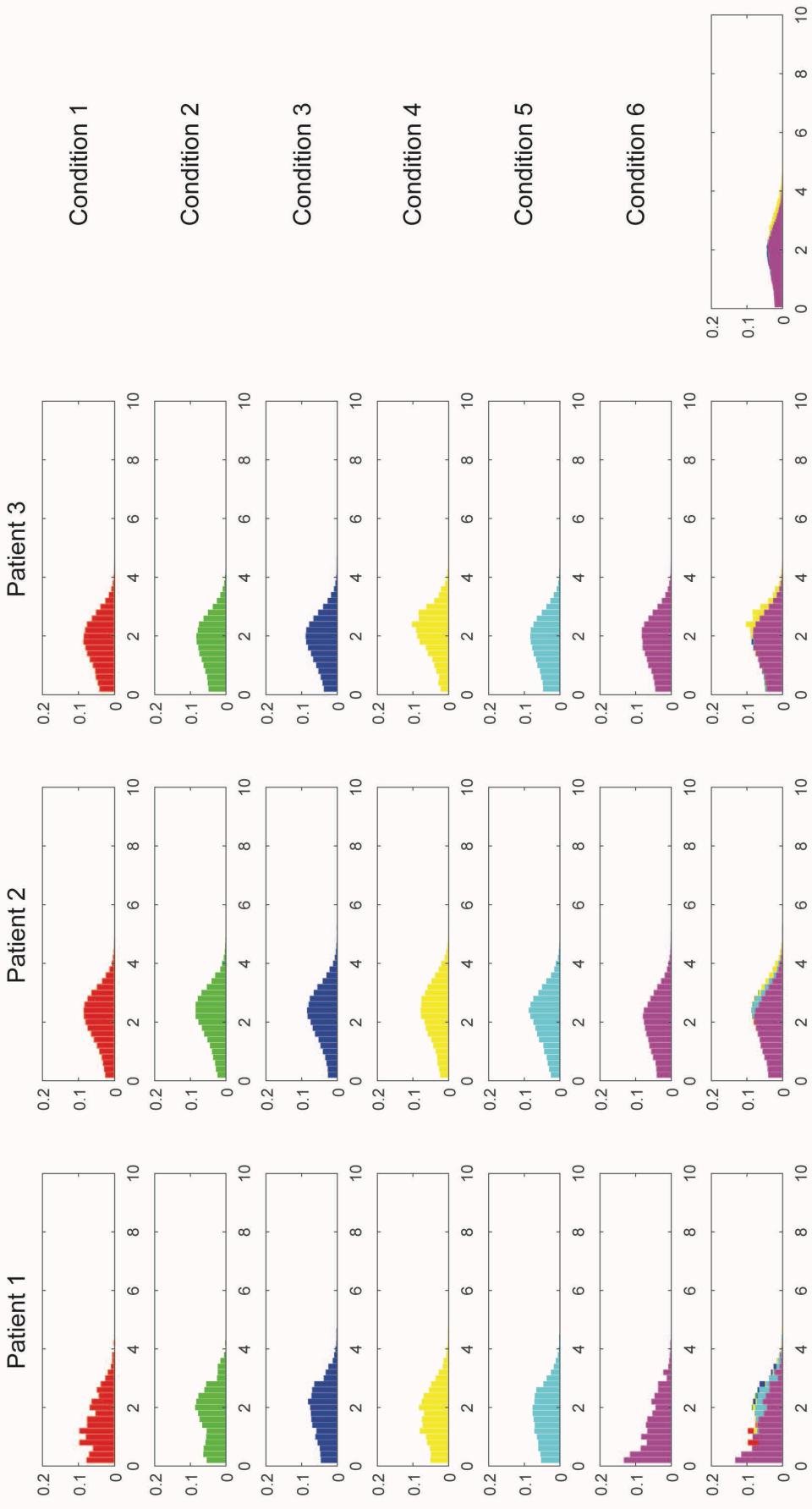


Figure S3.17: Histogram - CD56

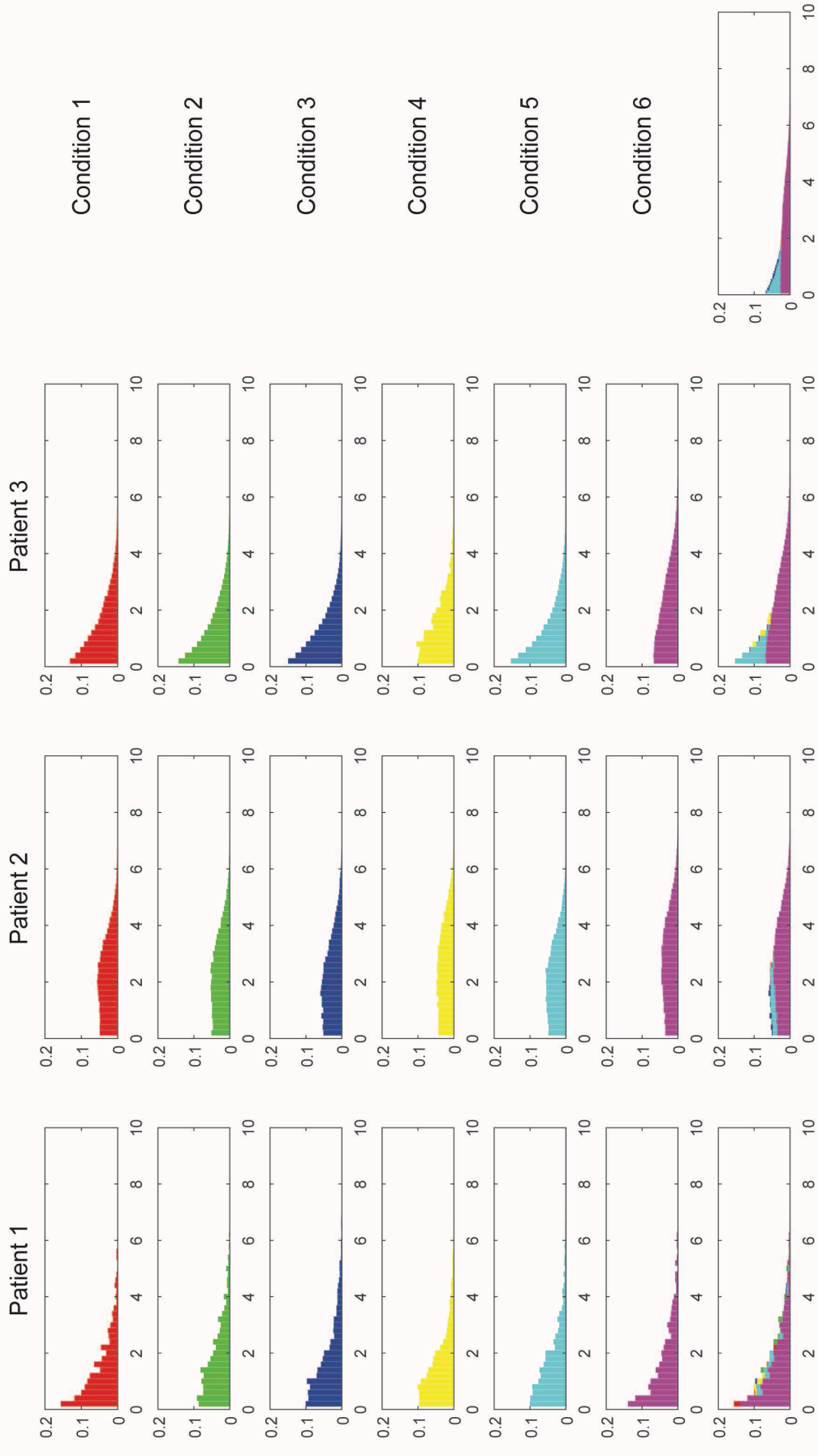


Figure S3.18: Histogram - CD73

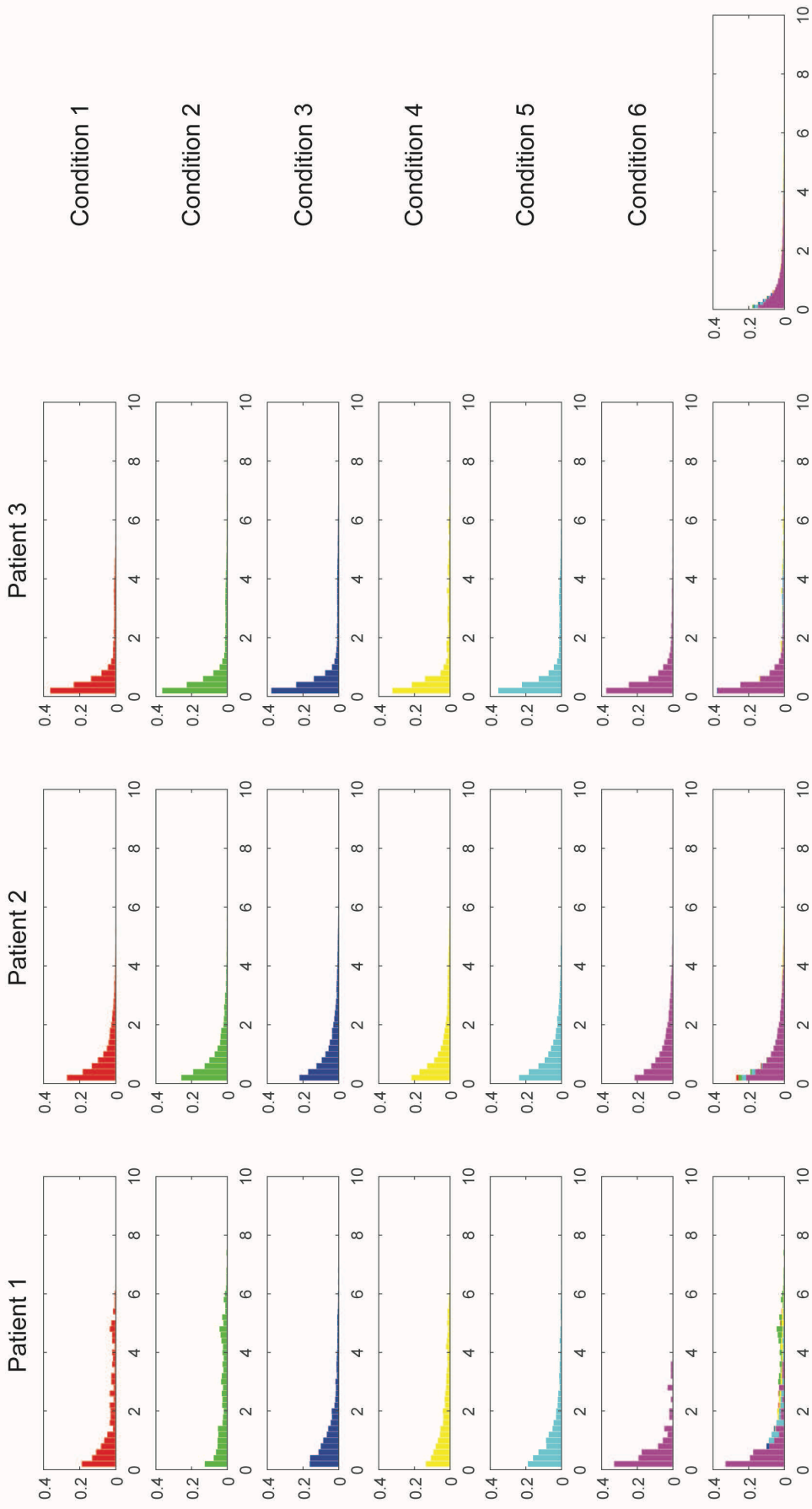


Figure S3.19: Histogram - CD103

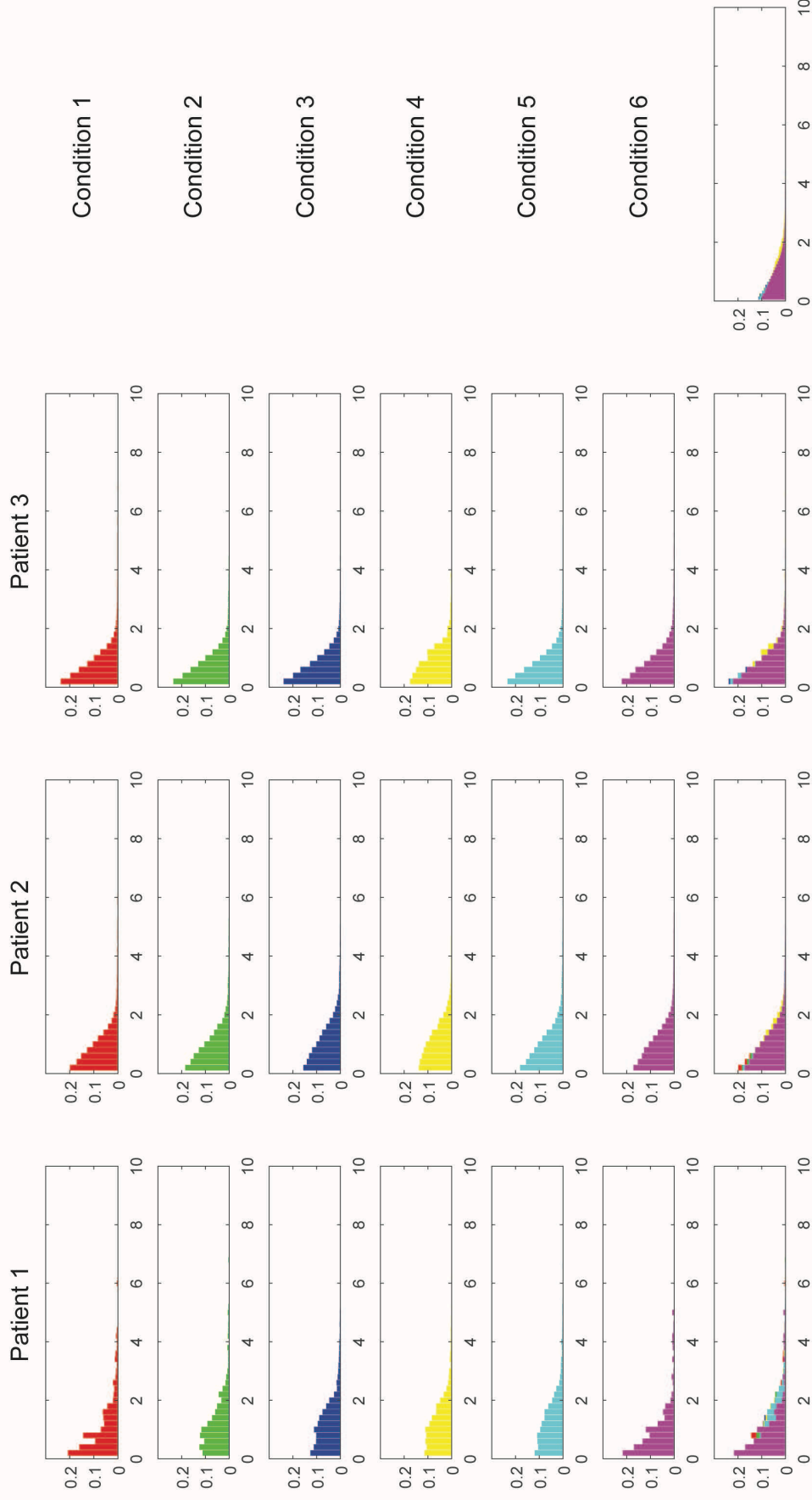


Figure S3.20: Histogram - CD117

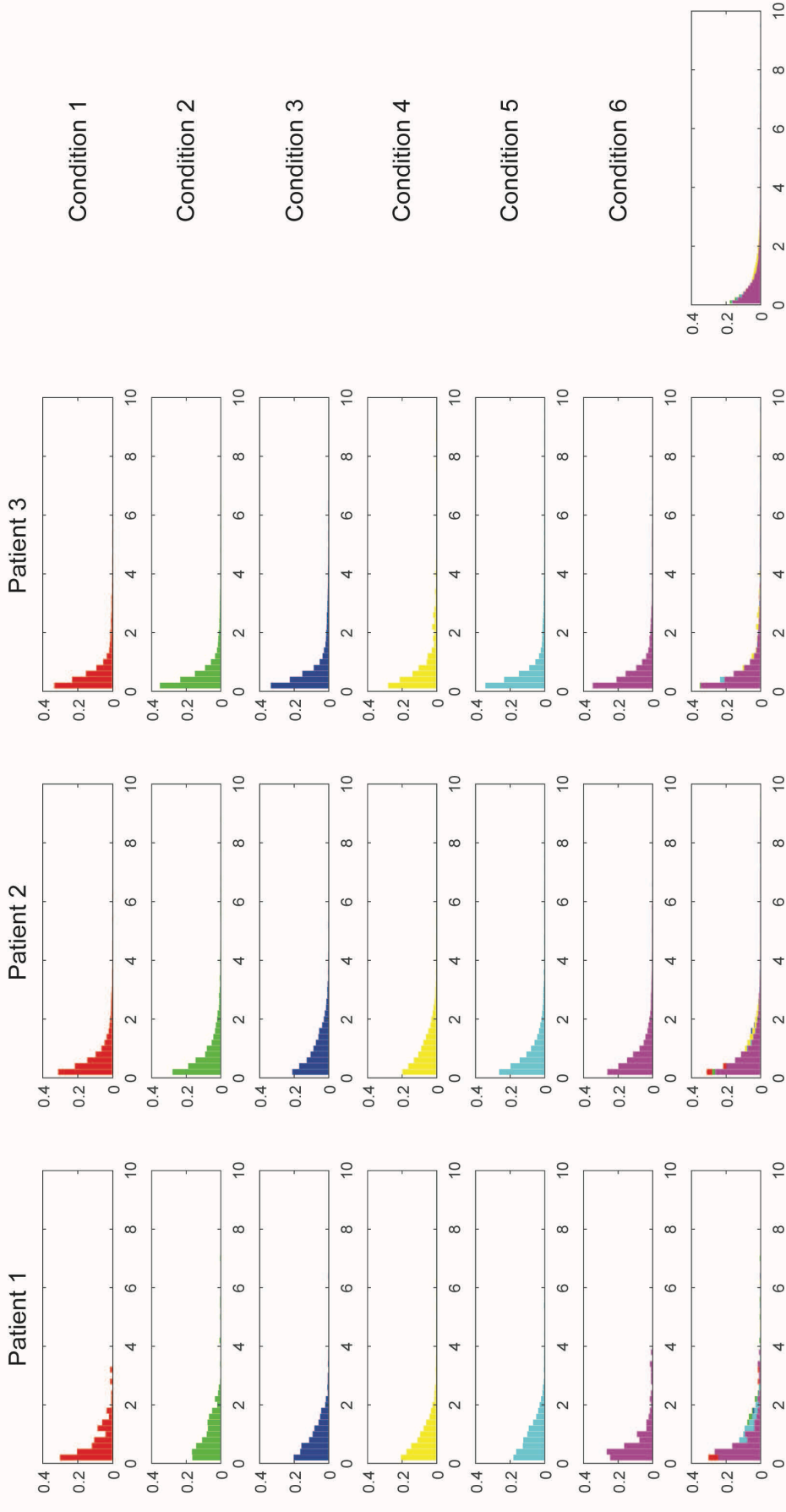


Figure S3.21: Histogram - CD133

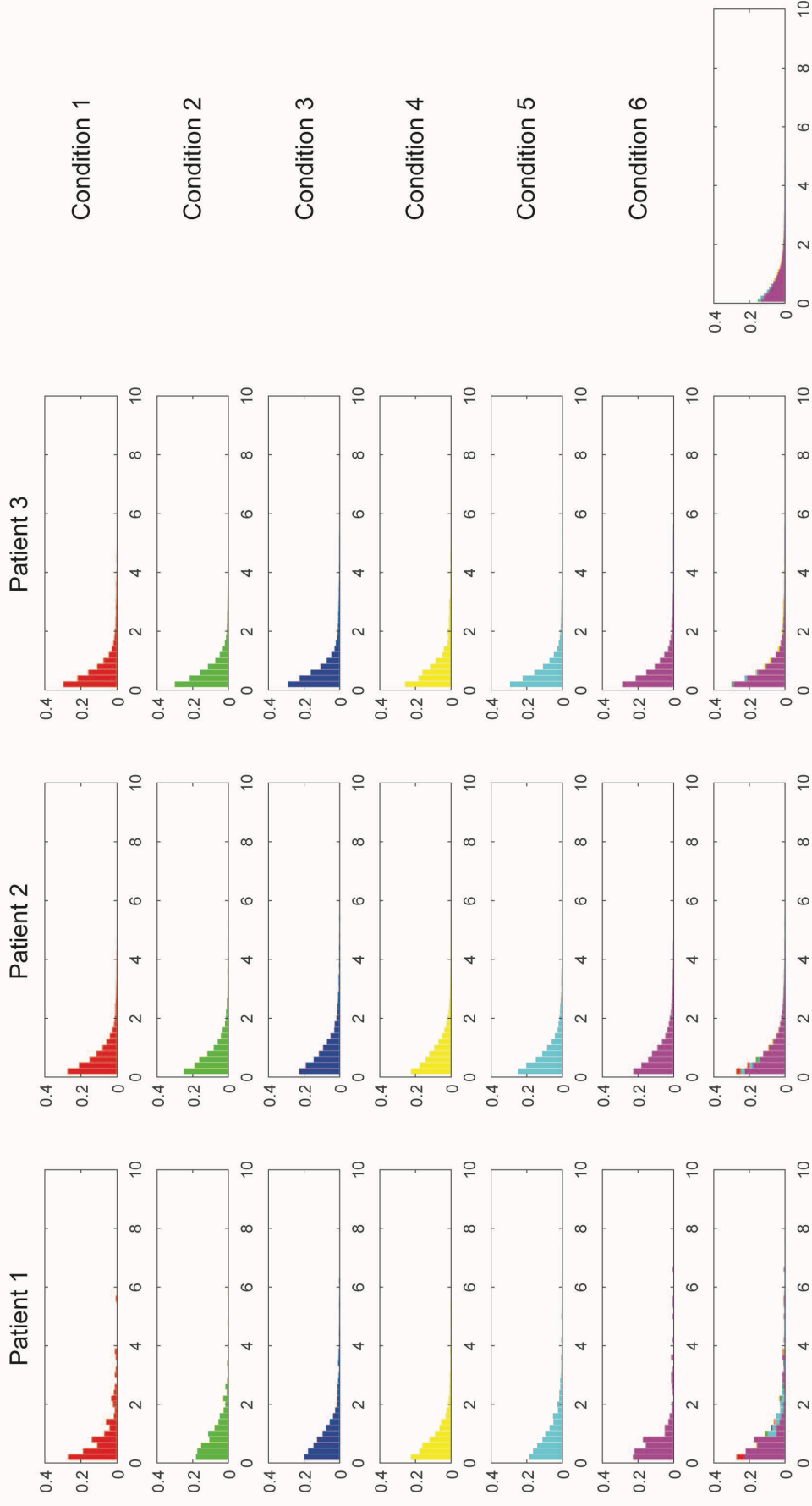


Figure S3.22: Histogram - CTLA4

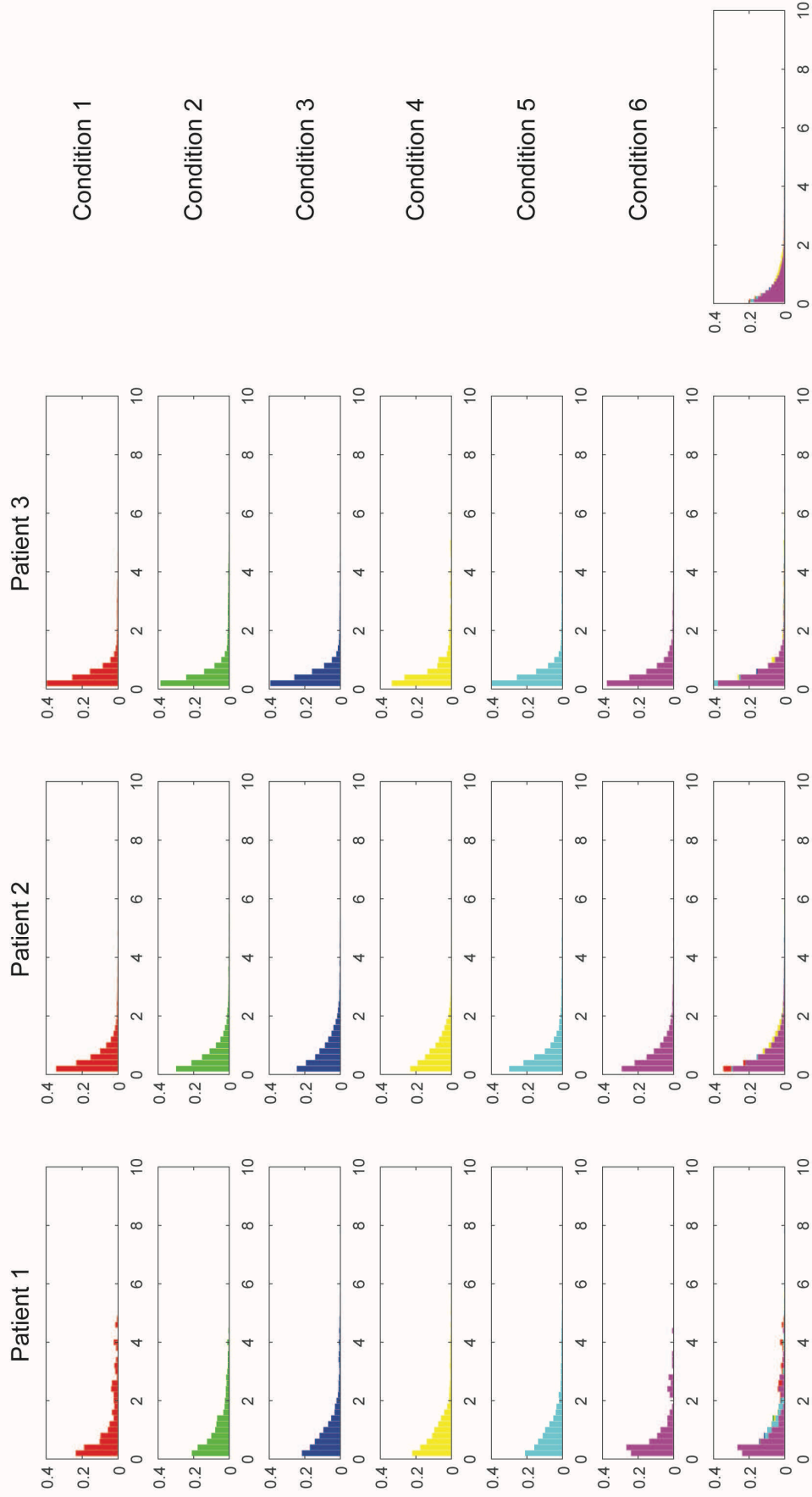


Figure S3.23: Histogram - EpCAM

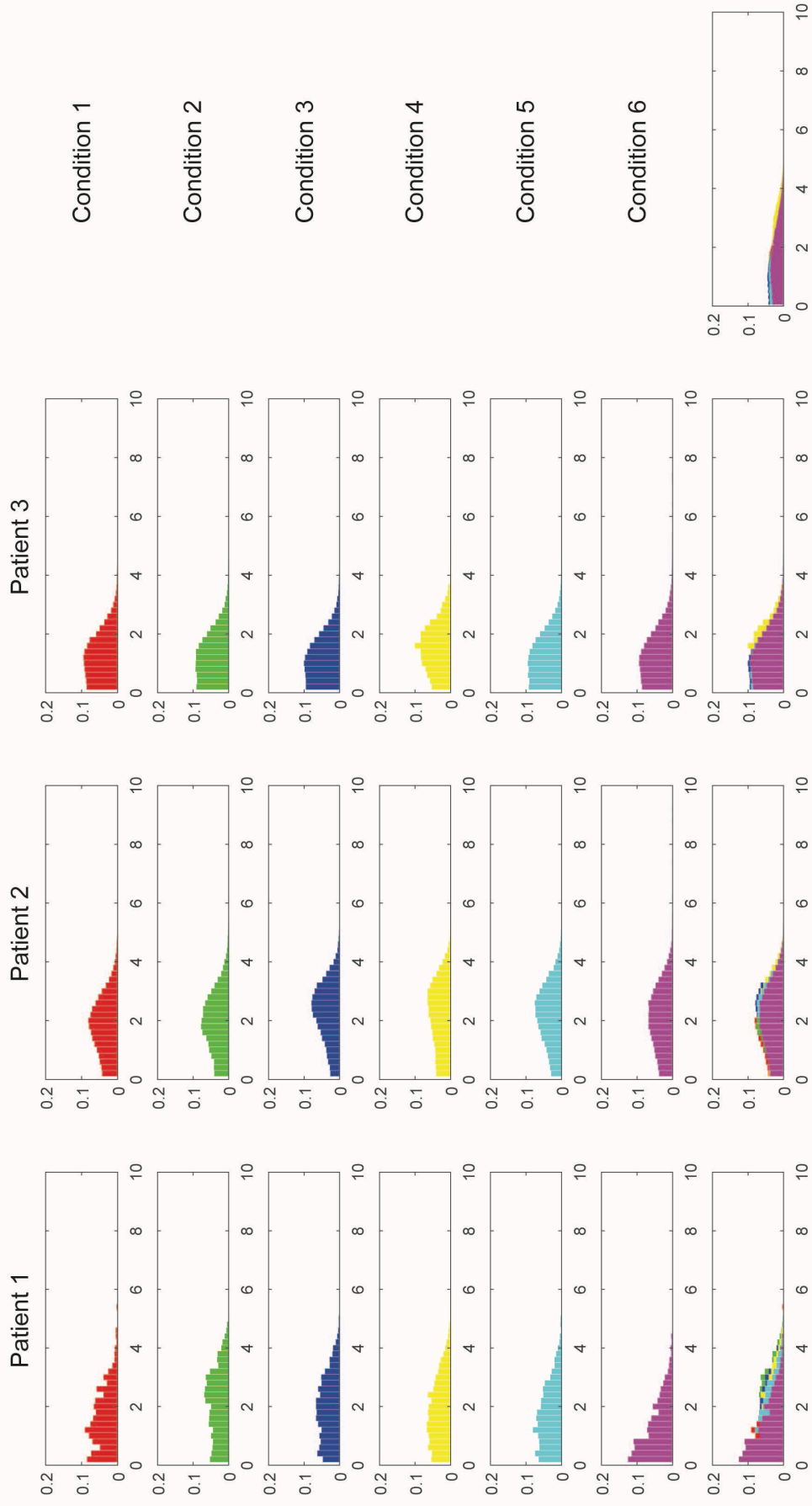


Figure S3.24: Histogram - FAPa

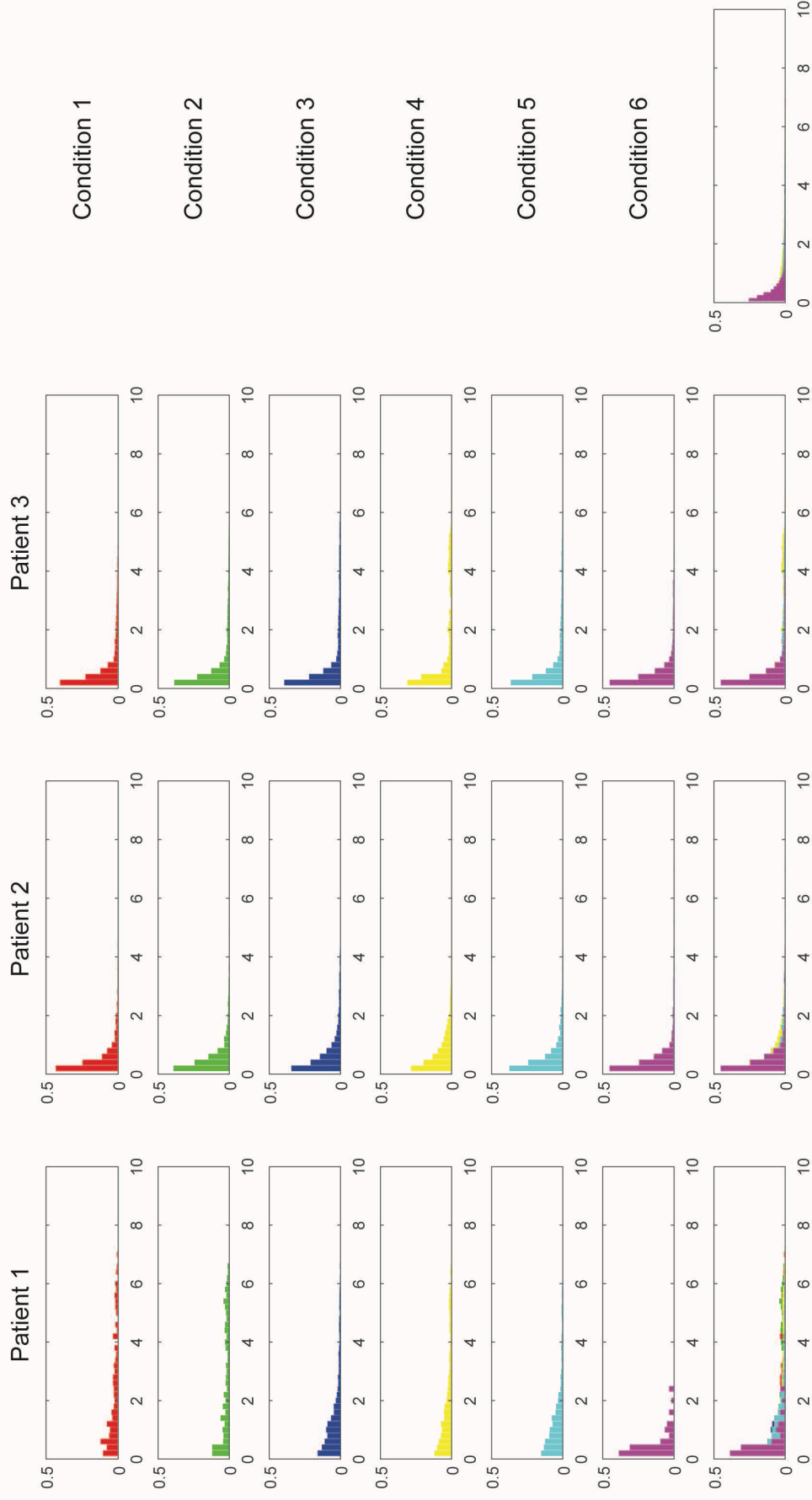


Figure S3.25: Histogram - FOLR1

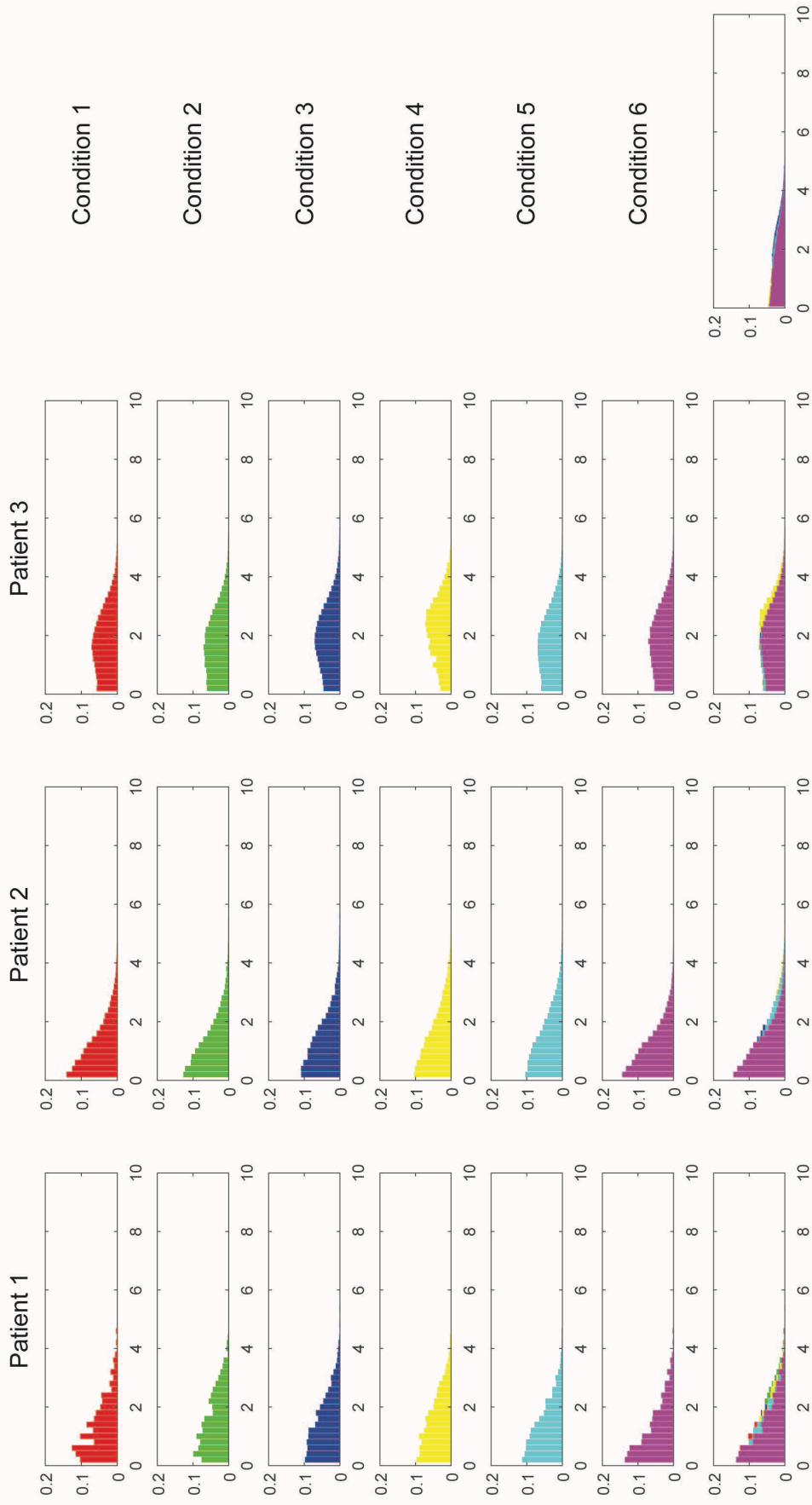


Figure S3.26: Histogram - Foxp3

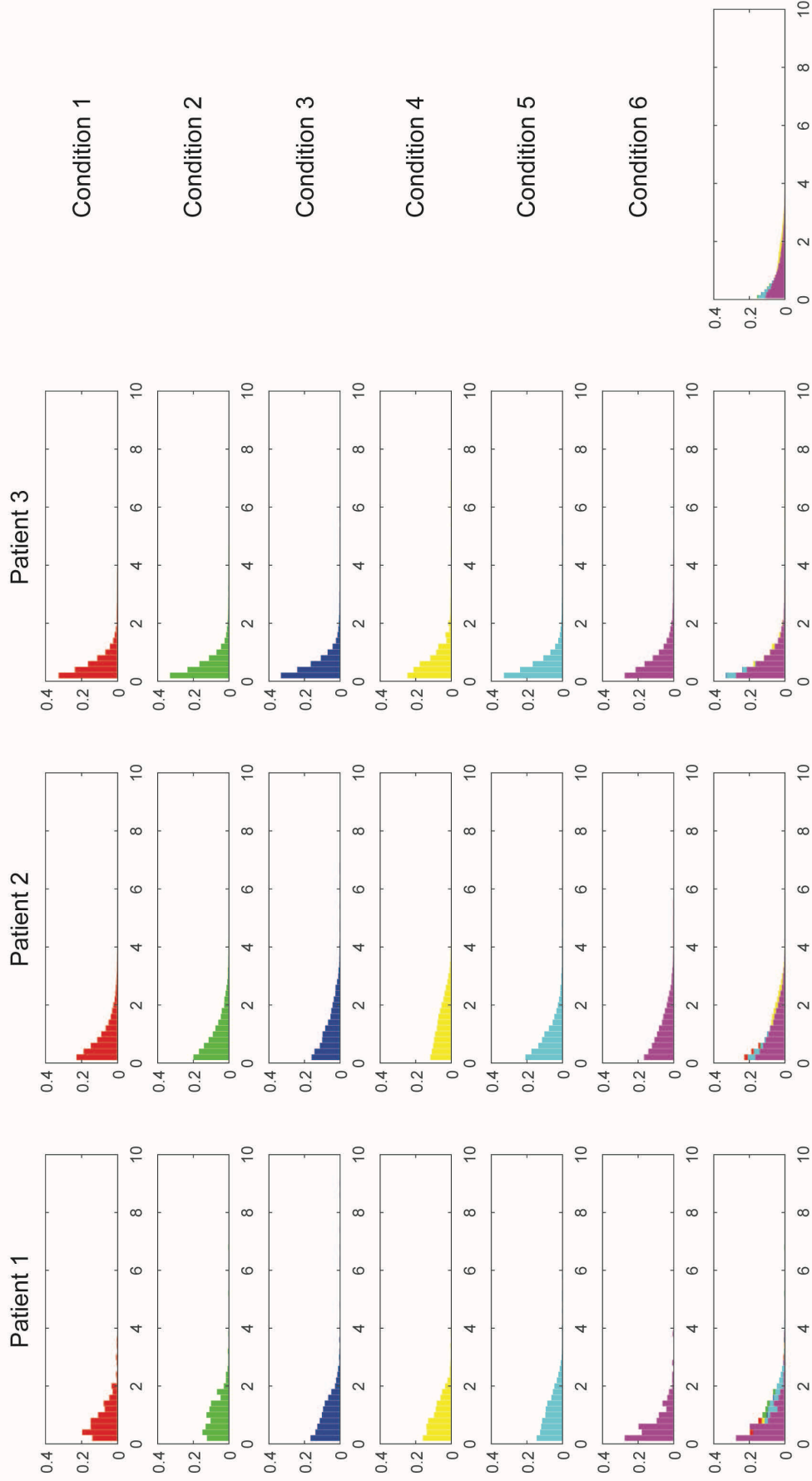


Figure S3.27: Histogram - HLA-DR

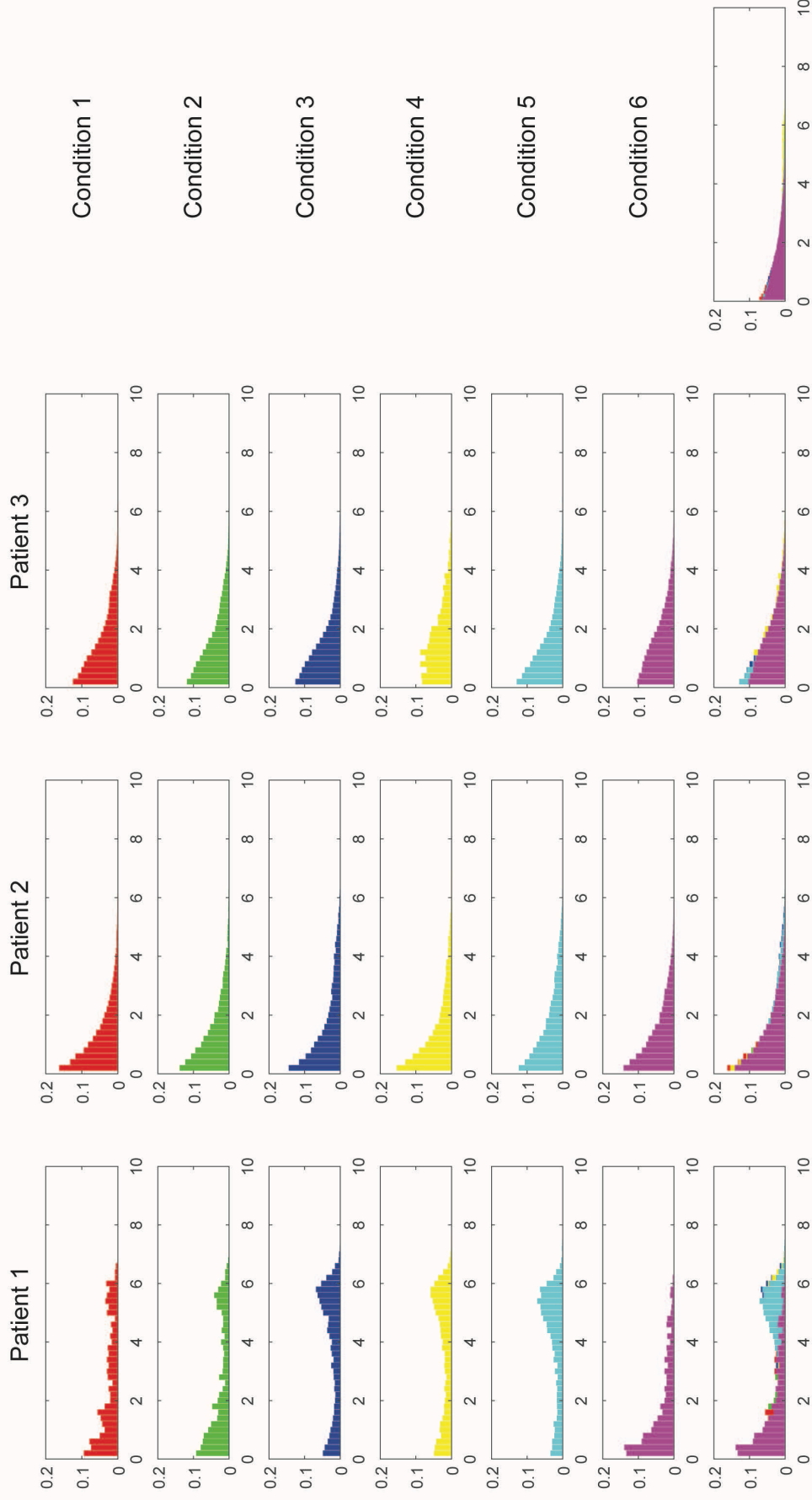


Figure S3.28: Histogram - IFNg

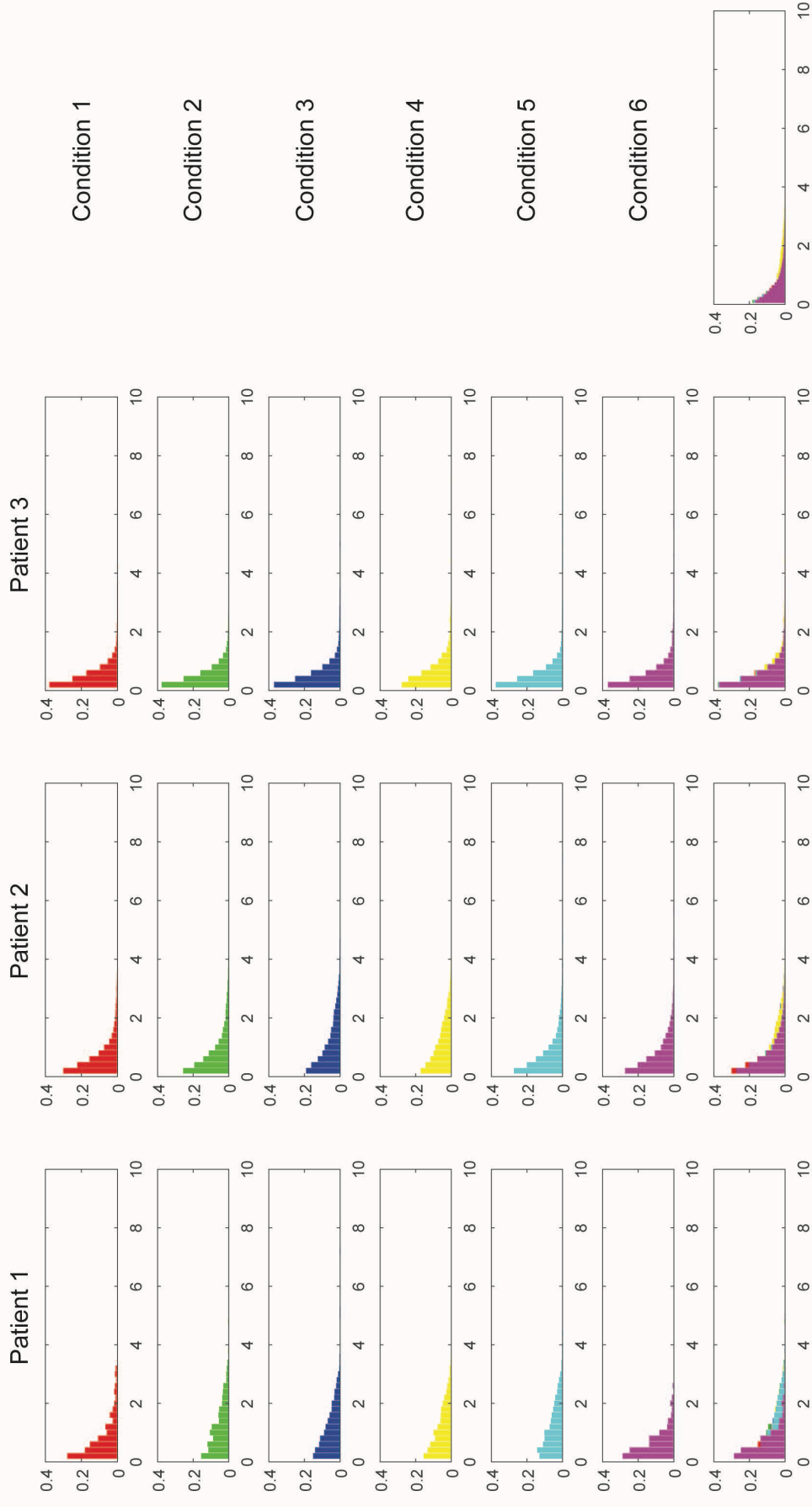


Figure S3.29: Histogram - Lag3

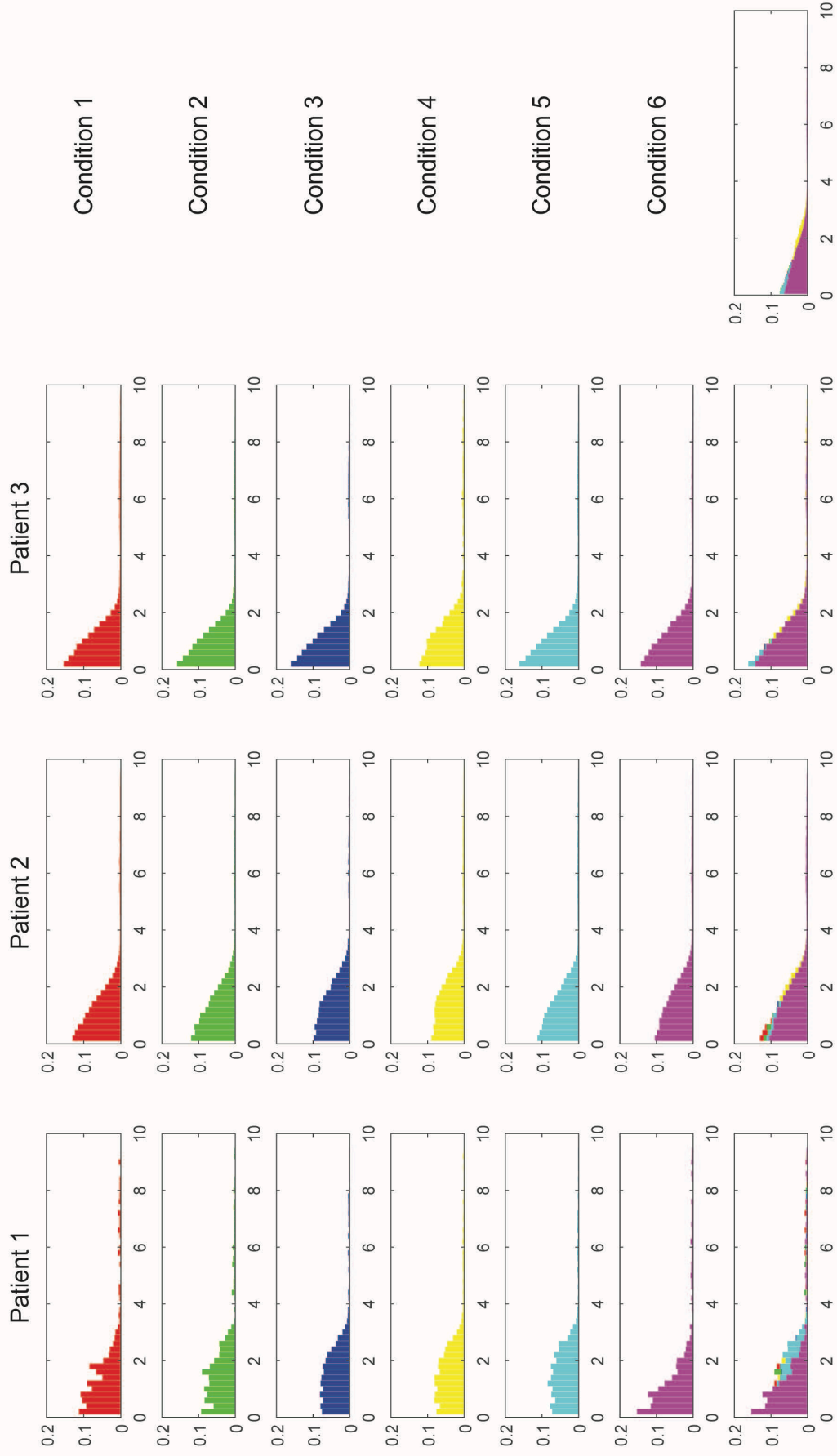


Figure S3.31: Histogram - PD1

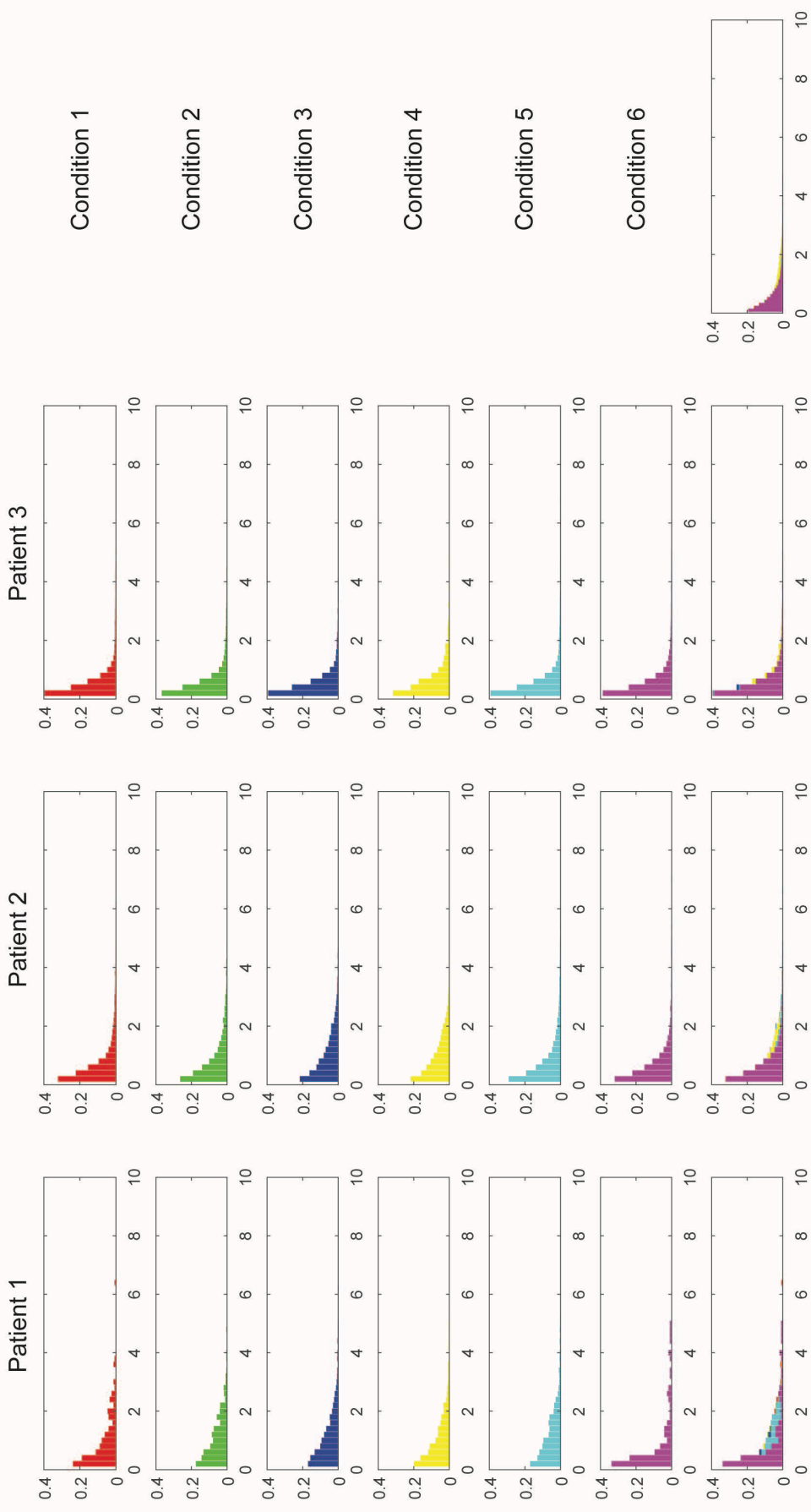


Figure S3.32: Histogram - PDGFRb

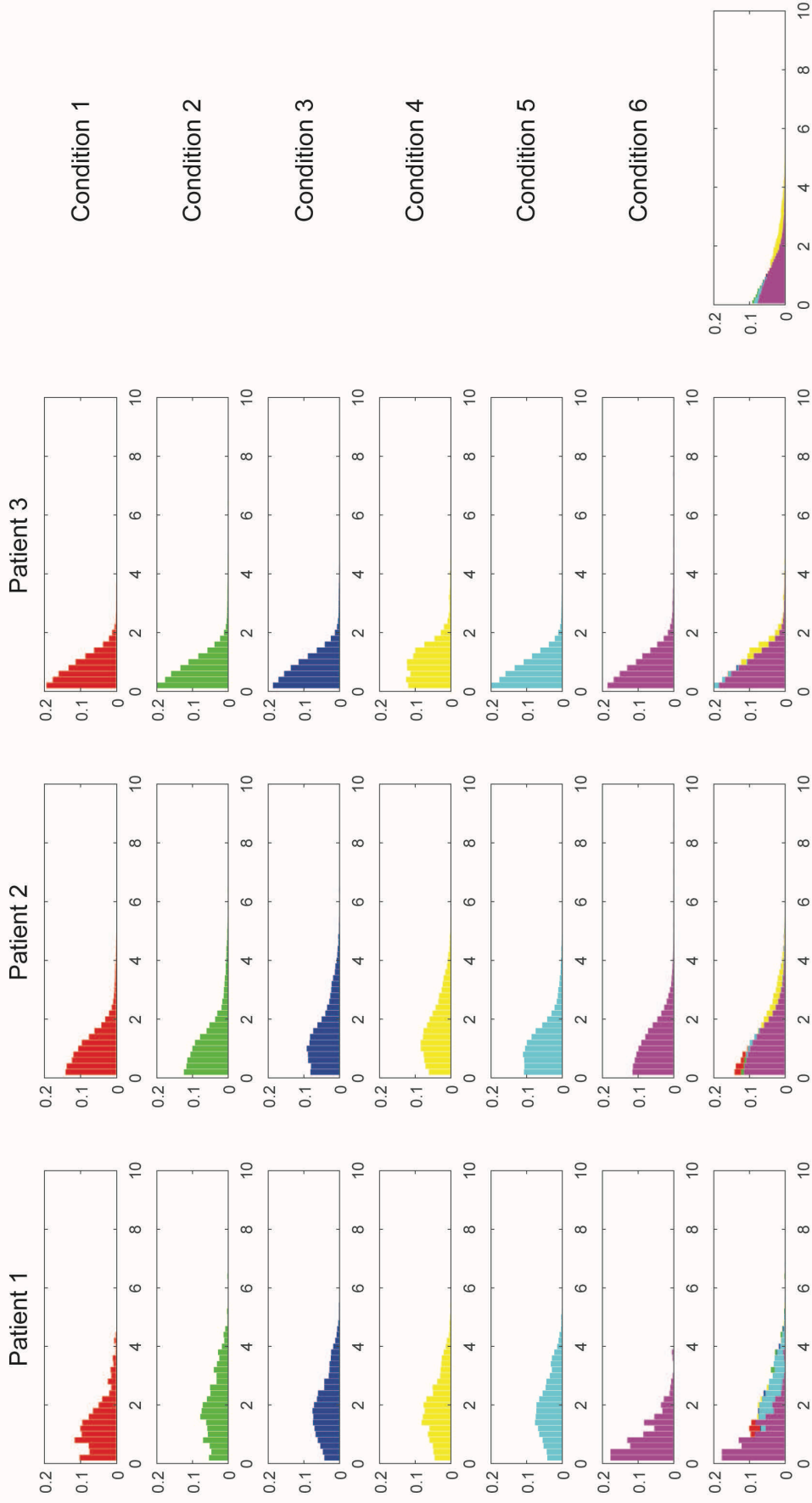


Figure S3.33: Histogram - PDL1

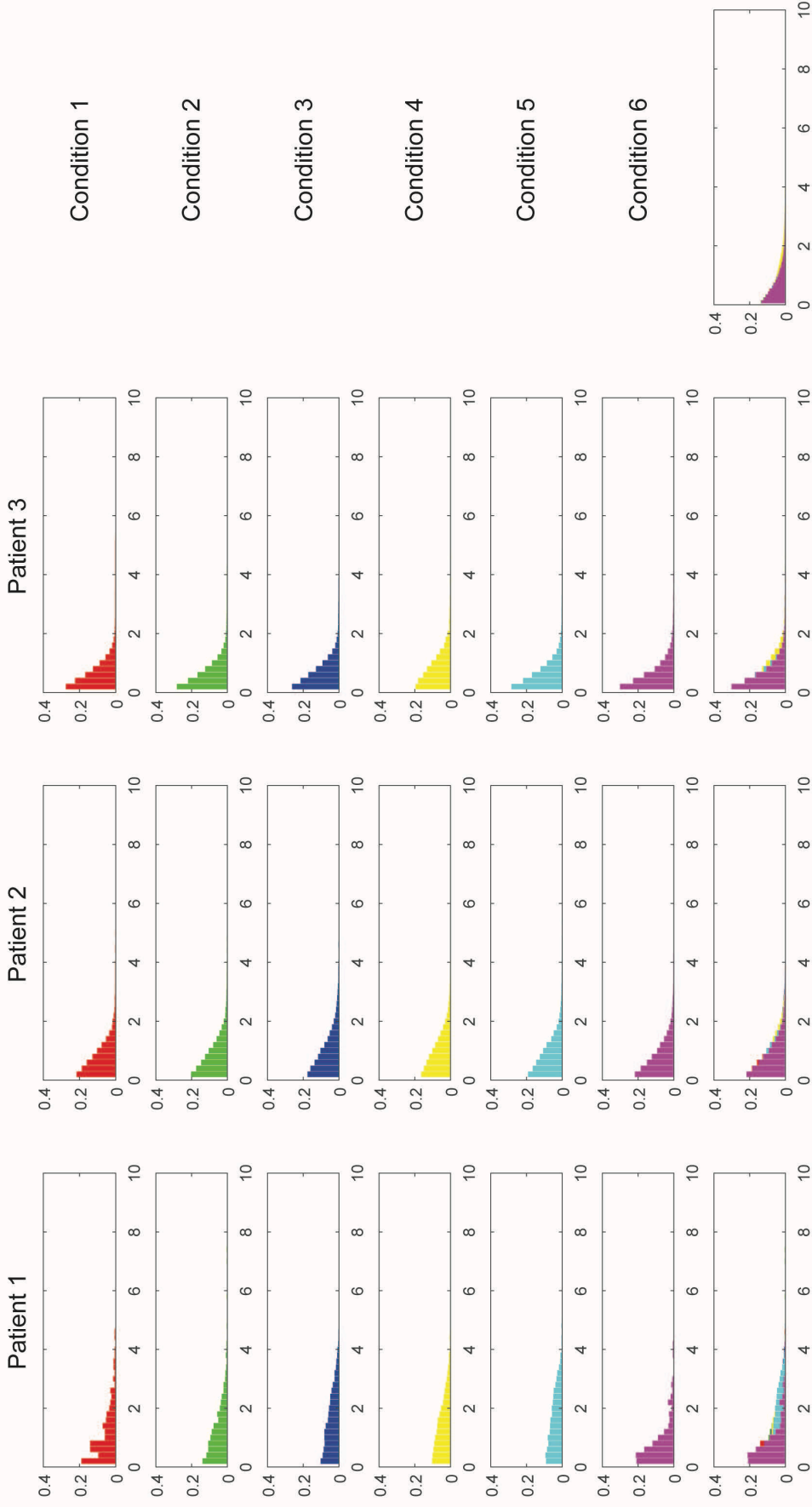


Figure S3.34: Histogram - TAG72

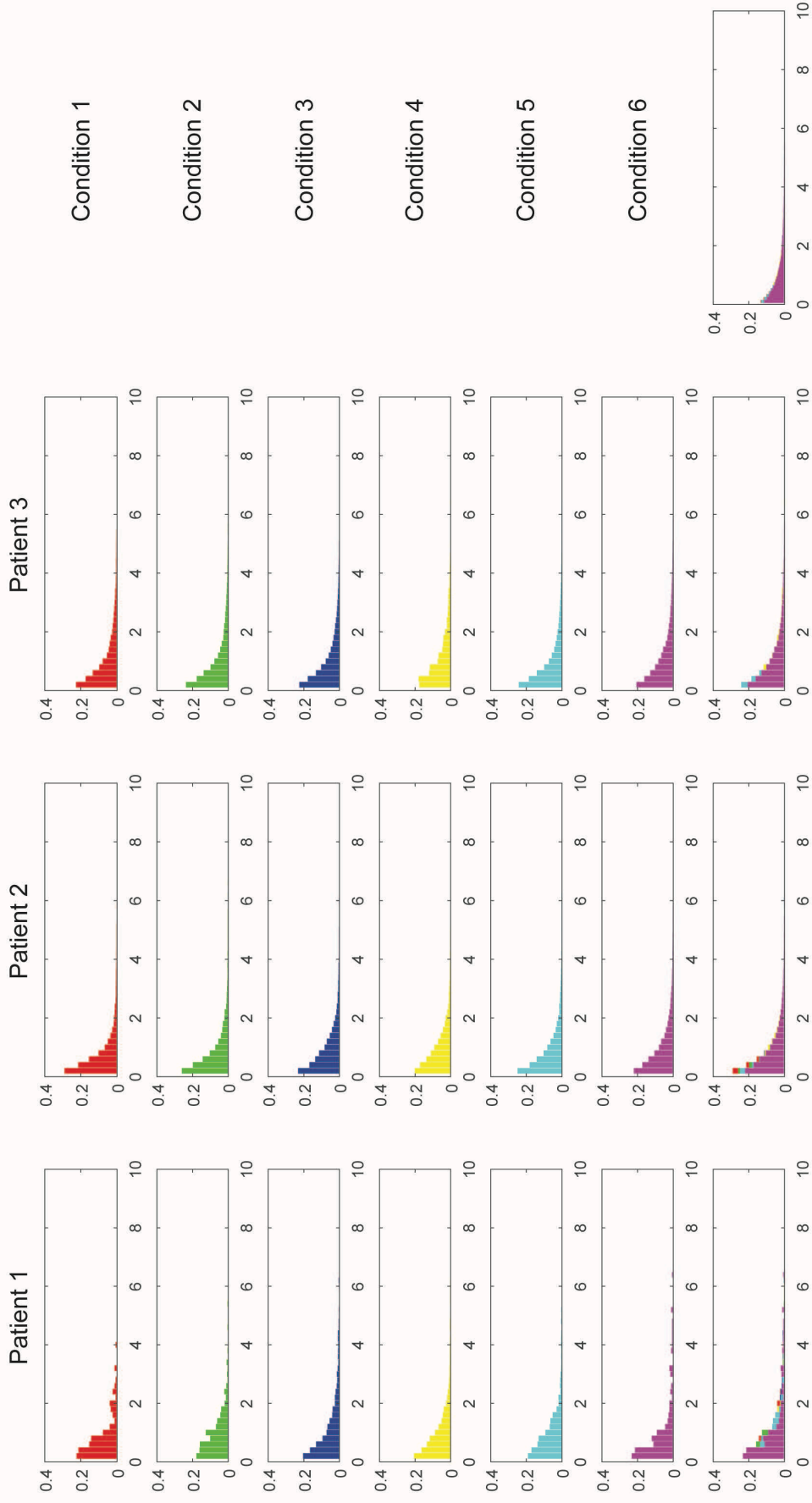
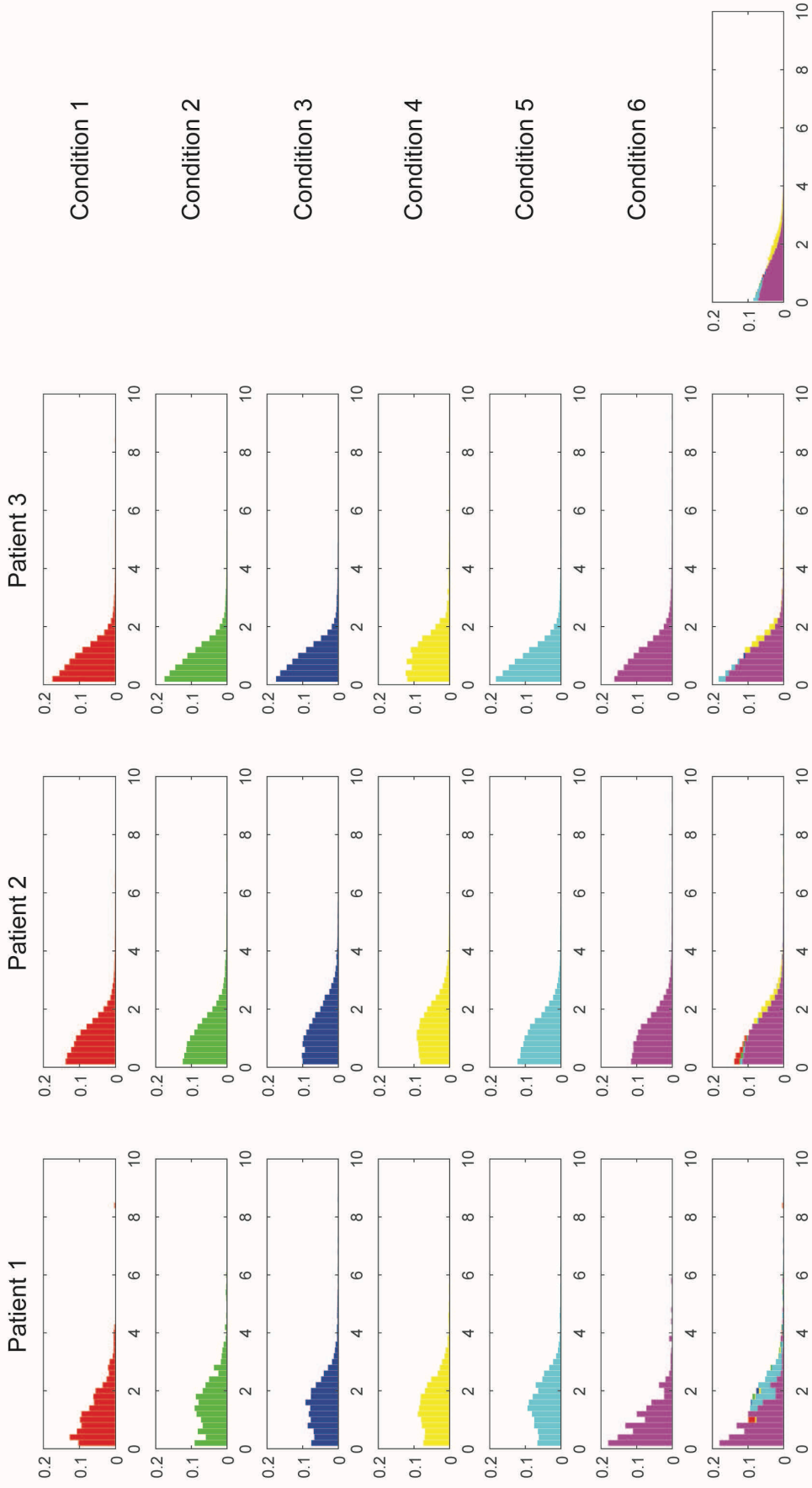
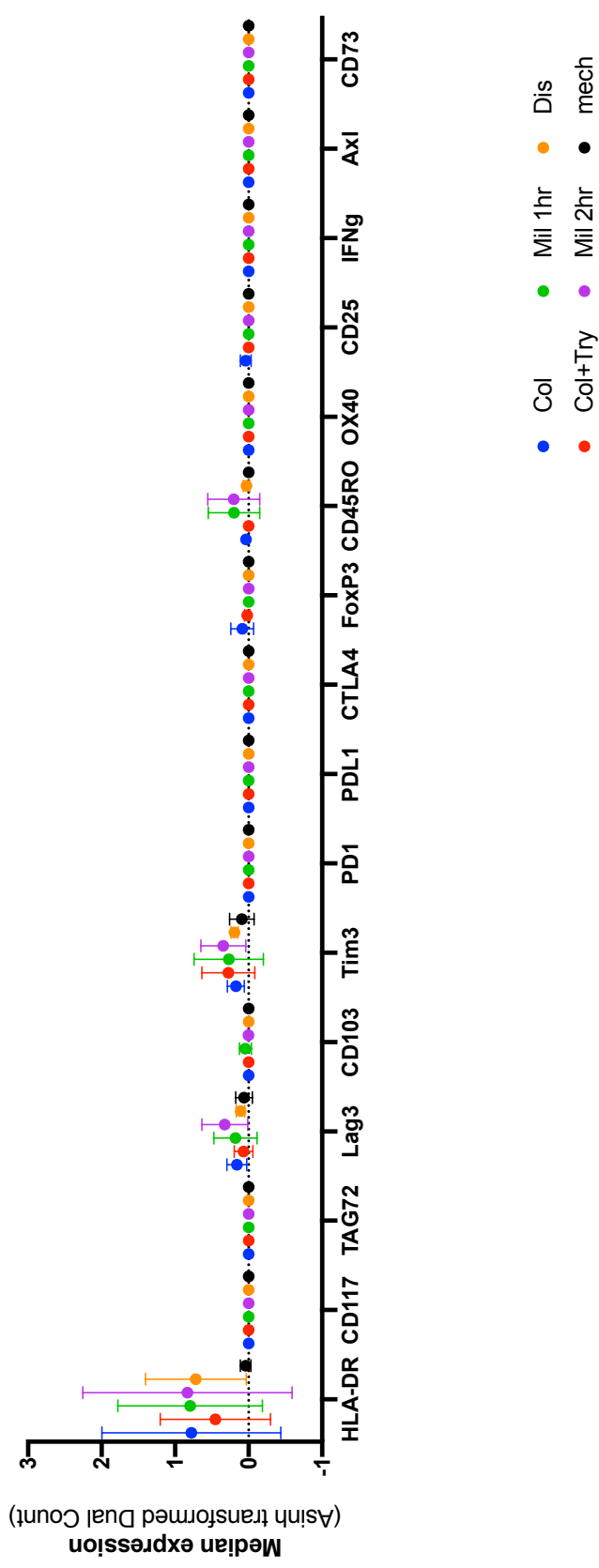


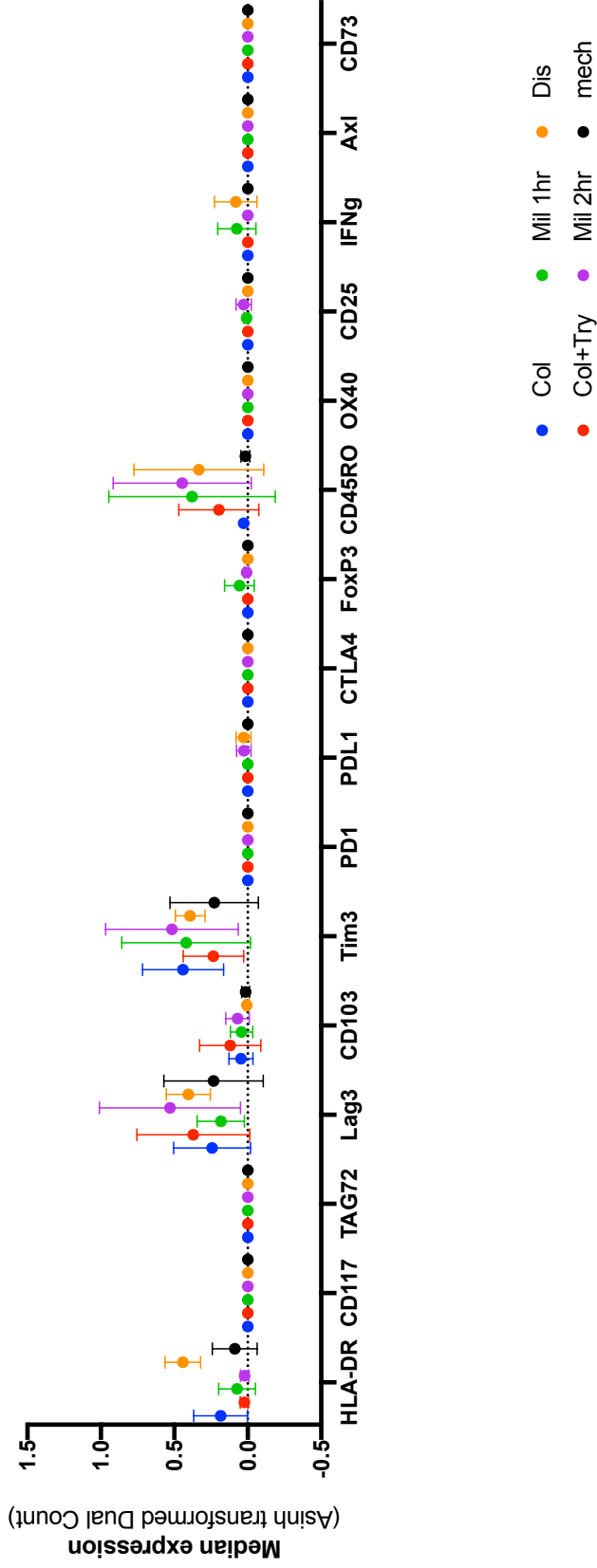
Figure S3.35: Histogram - Tim3



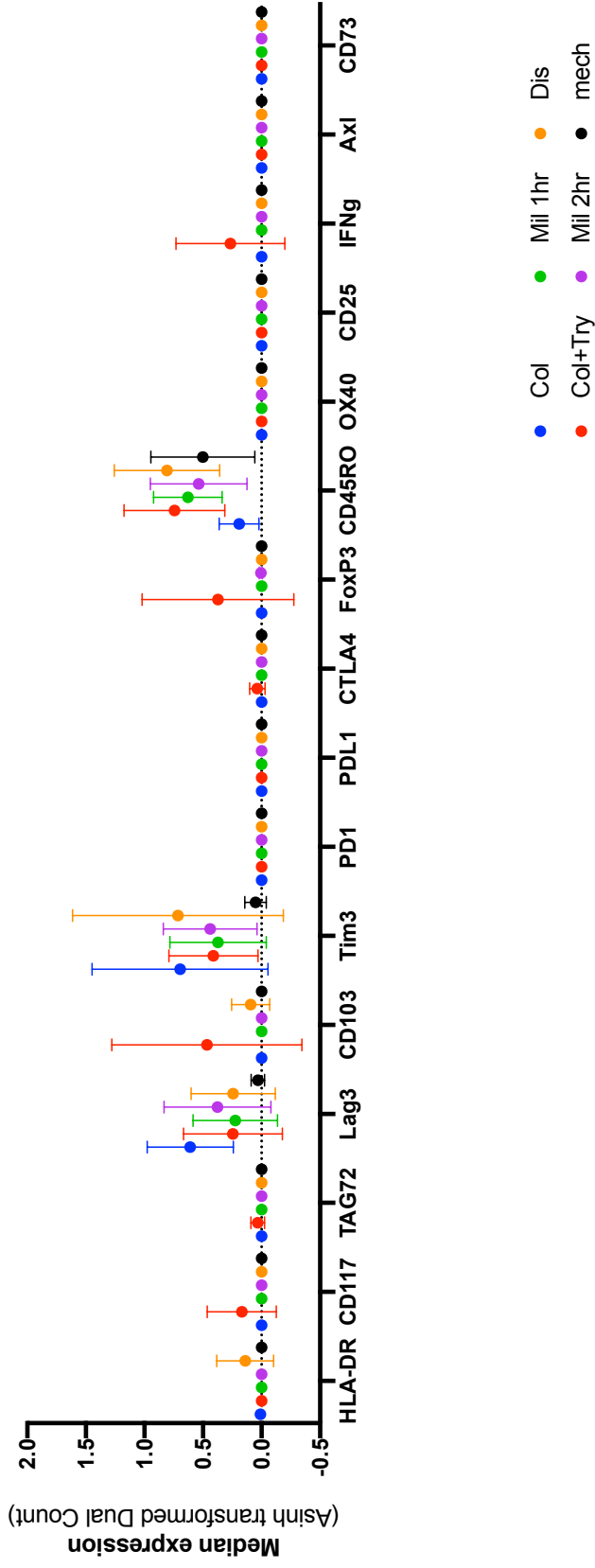
CD47FOLR1 phenotype (Mean with SD, n=3)



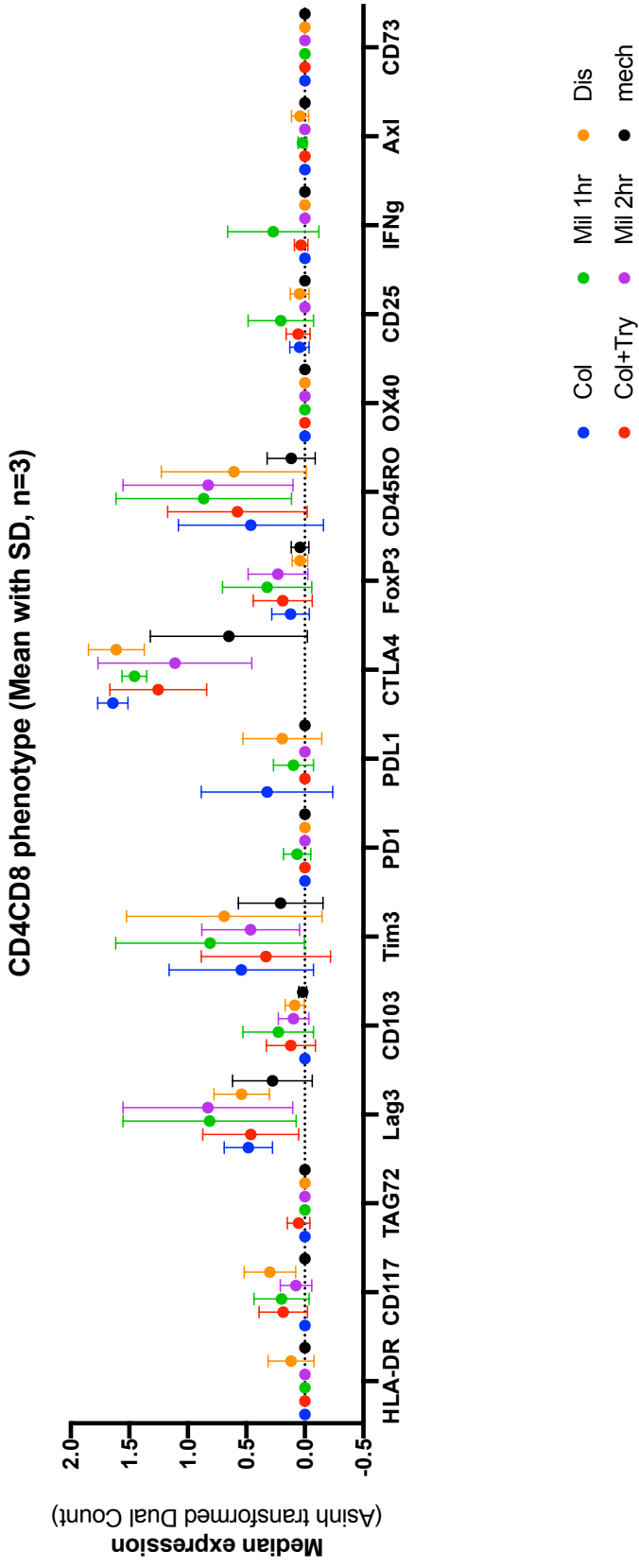
EpCAMCD47FOLR1 phenotype (Mean with SD, n=3)



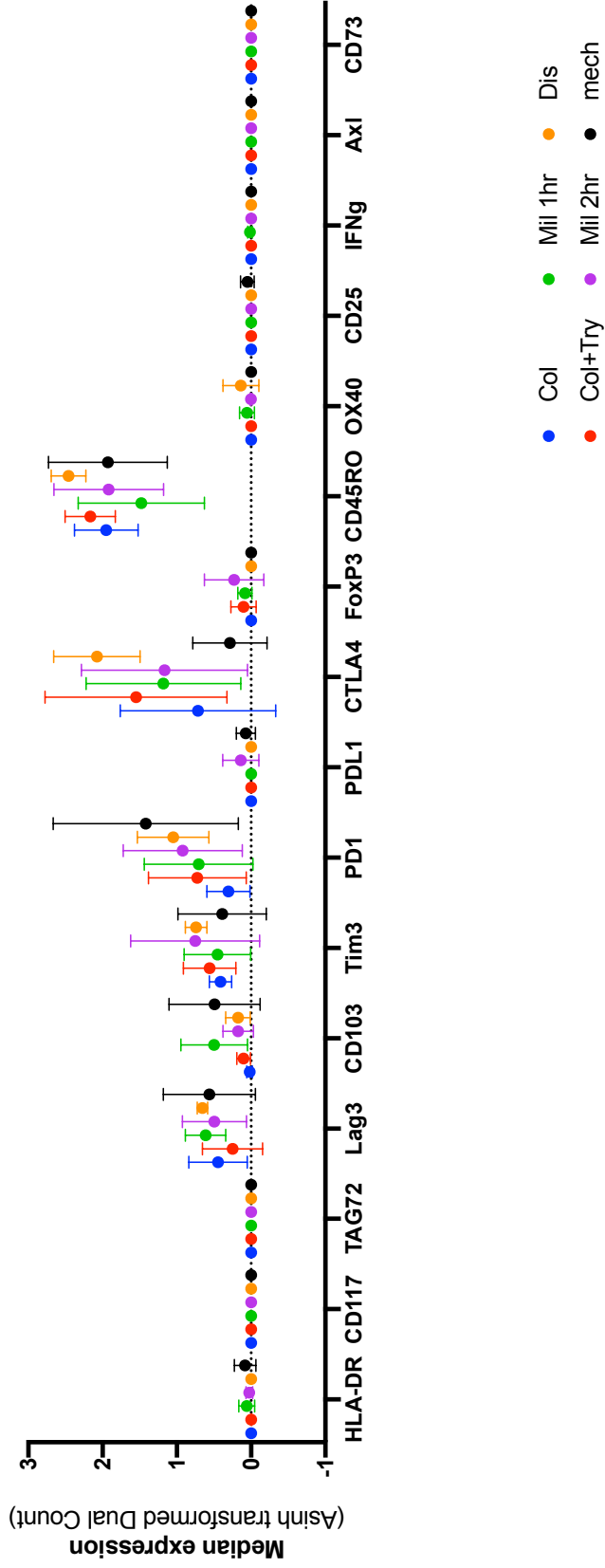
CD11b phenotype (Mean with SD, n=3)



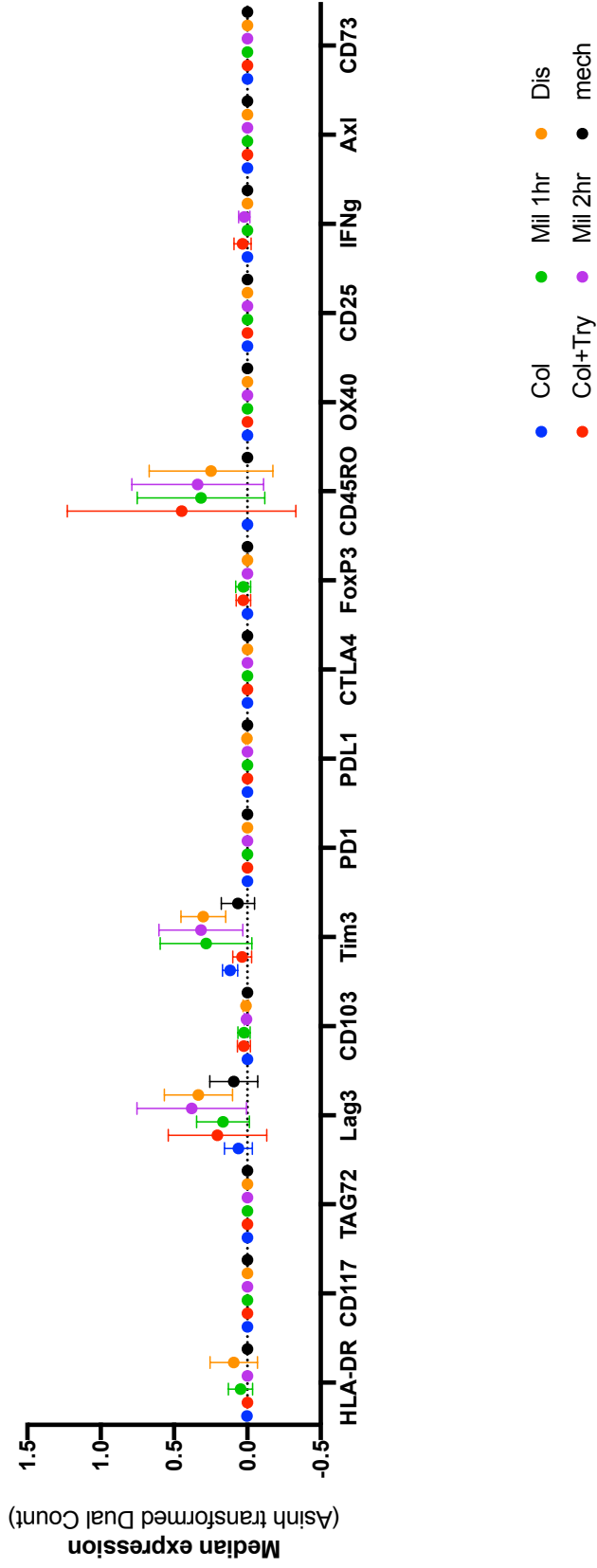
CD3 negative!



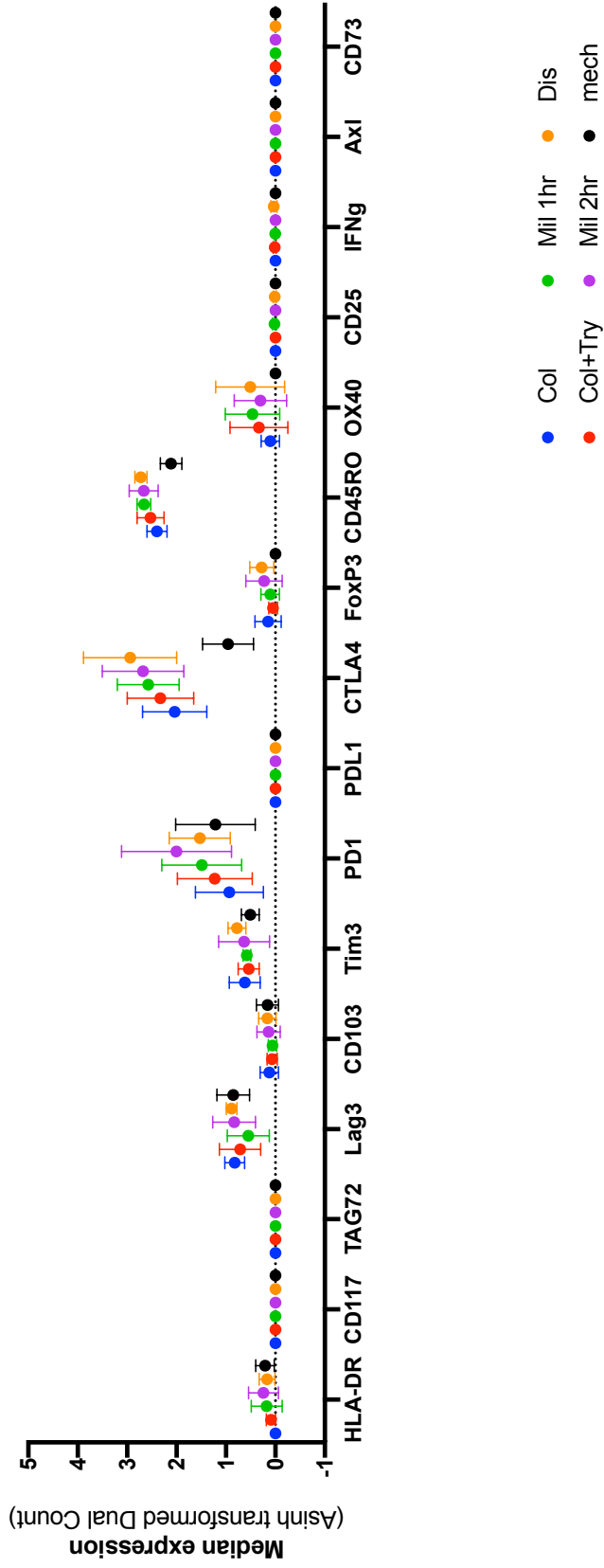
CD45CD3 phenotype (Mean with SD, n=3)



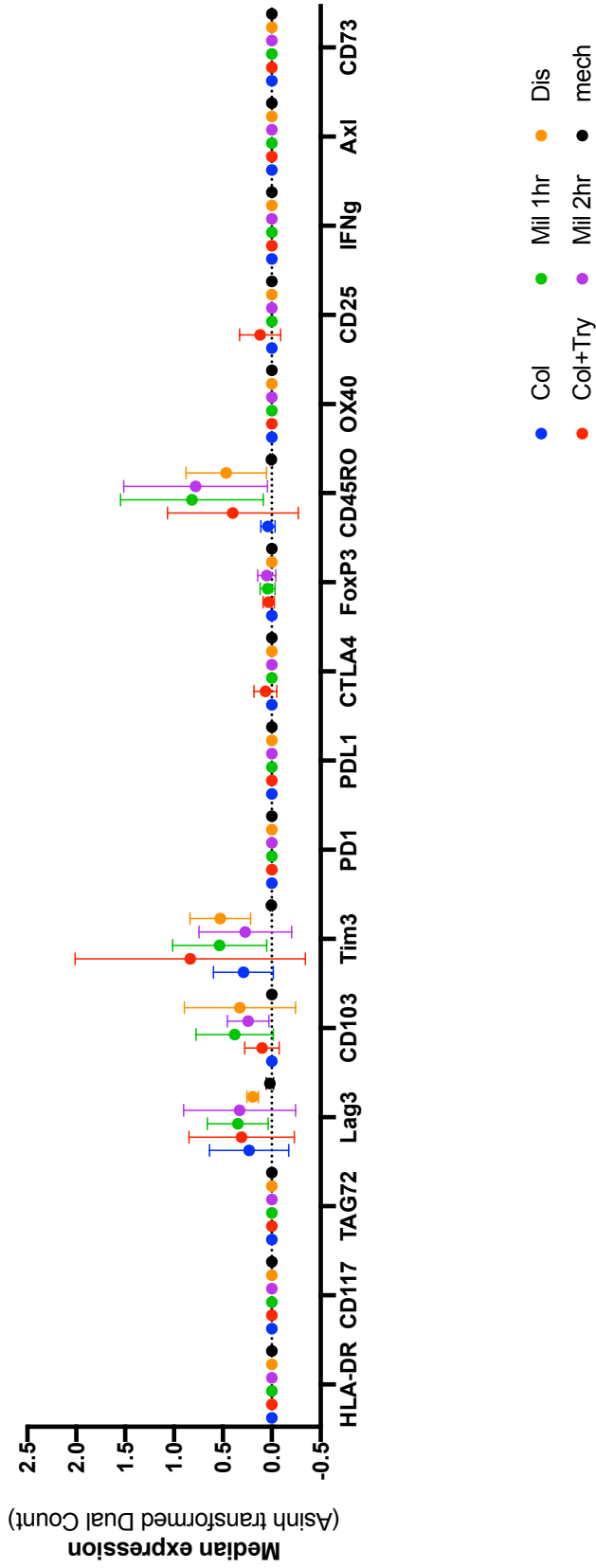
EpCAMCD47 phenotype (Mean with SD, n=3)



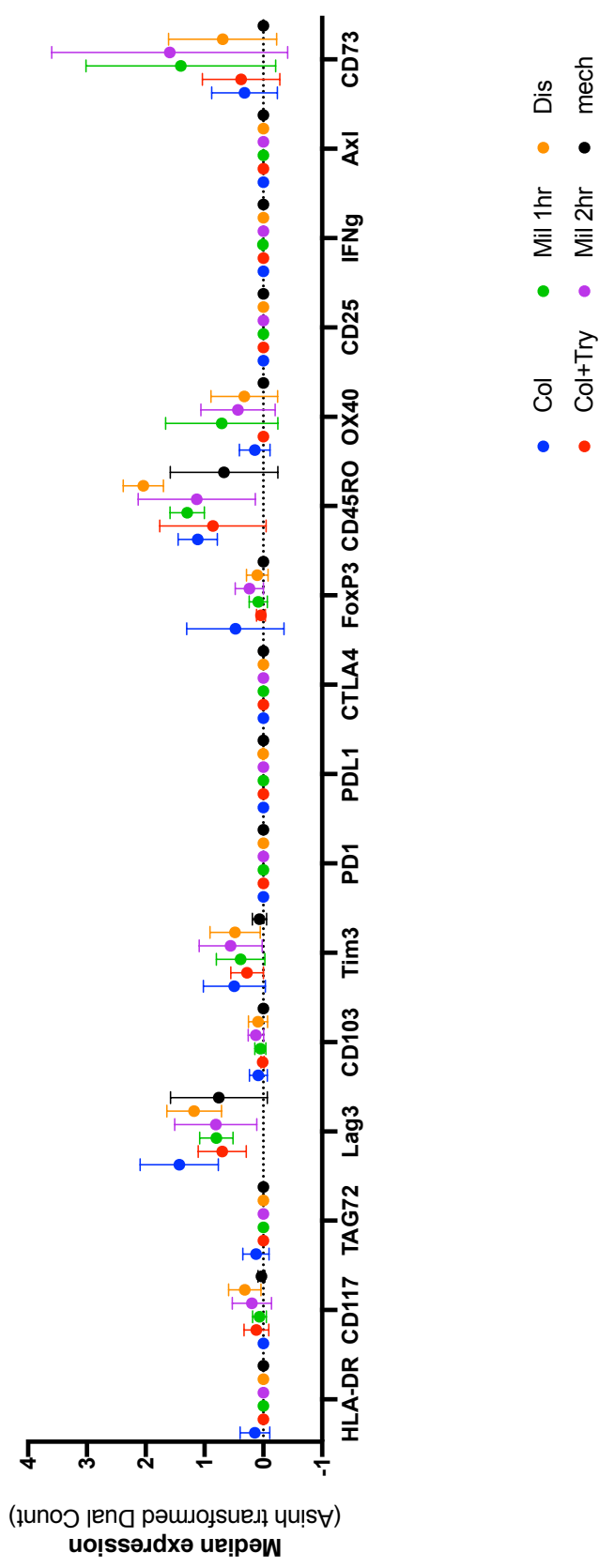
CD45CD3CD4 phenotype (Mean with SD, n=3)



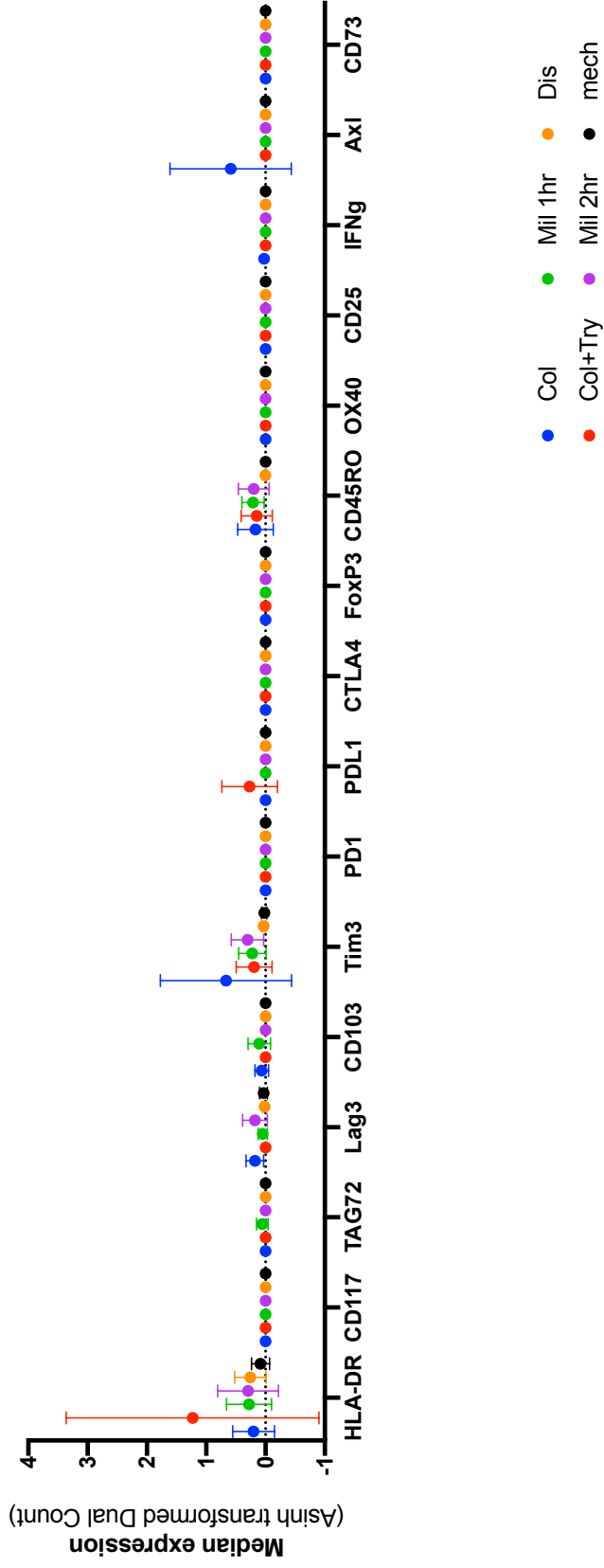
CD56 phenotype (Mean with SD, n=3)



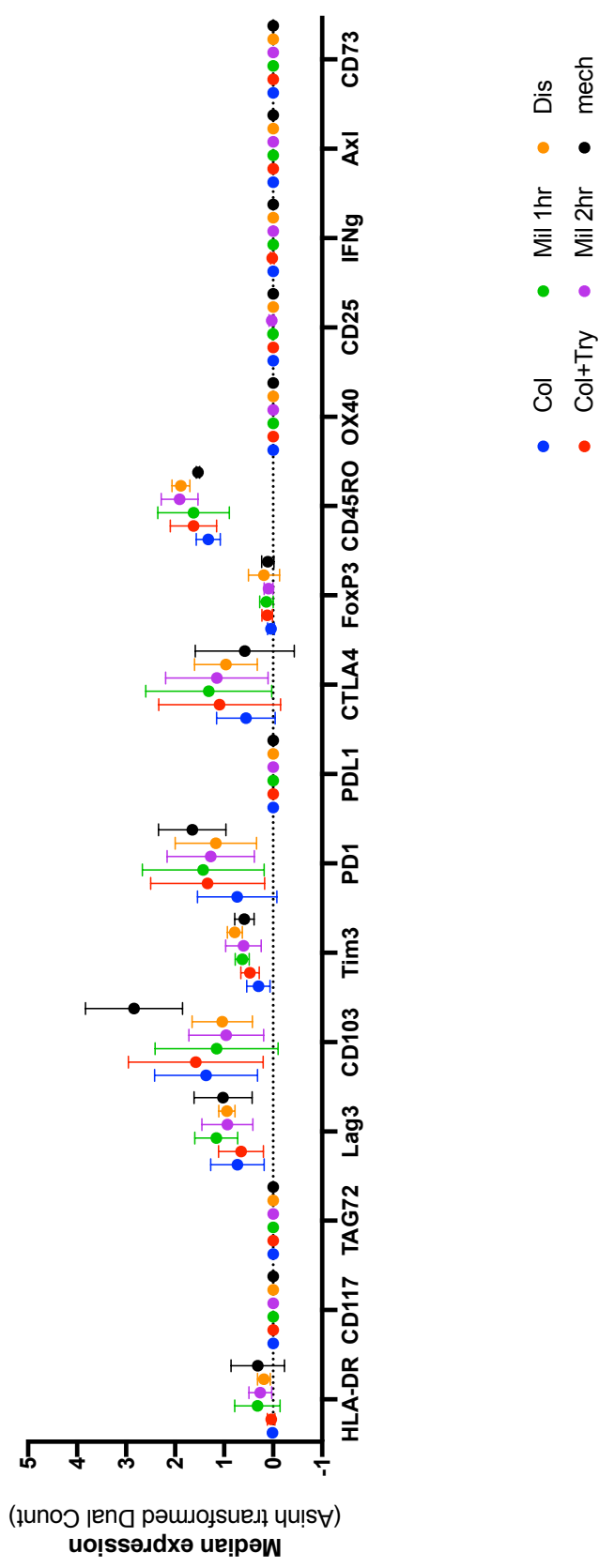
CD34 phenotype (Mean with SD, n=3)



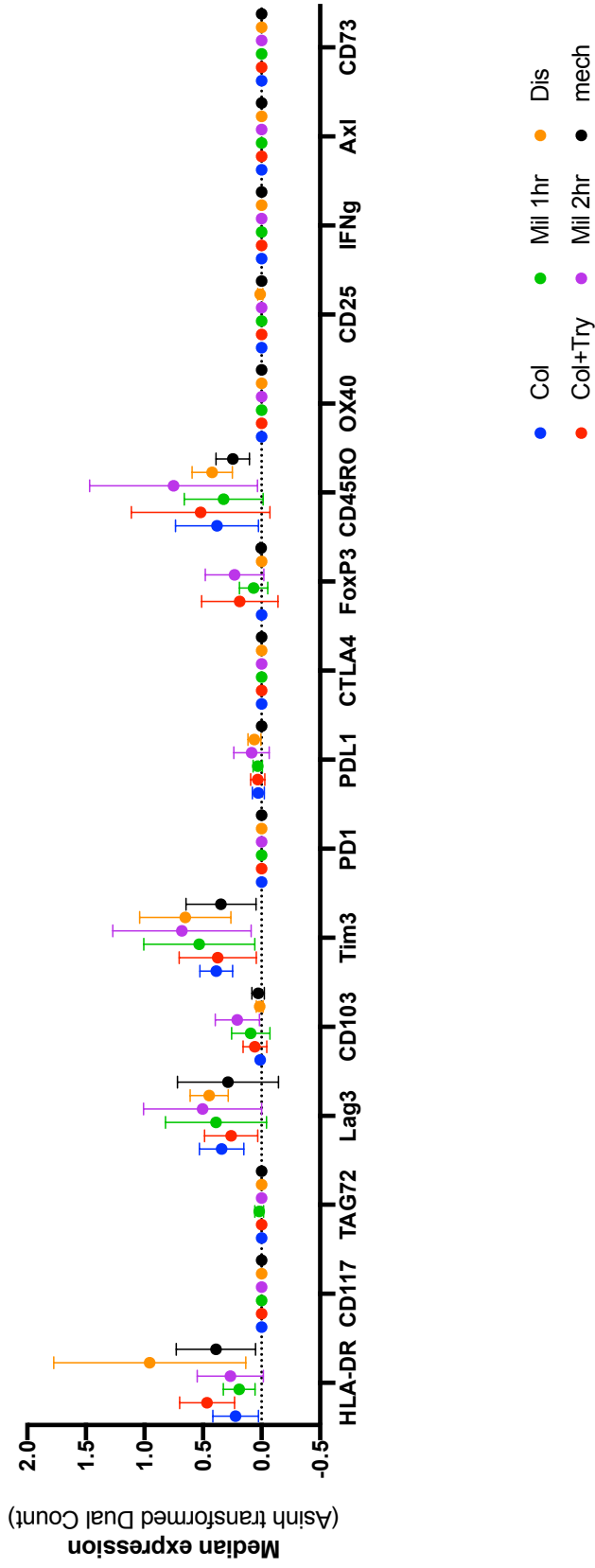
CD47CD56 phenotype (Mean with SD, n=3)



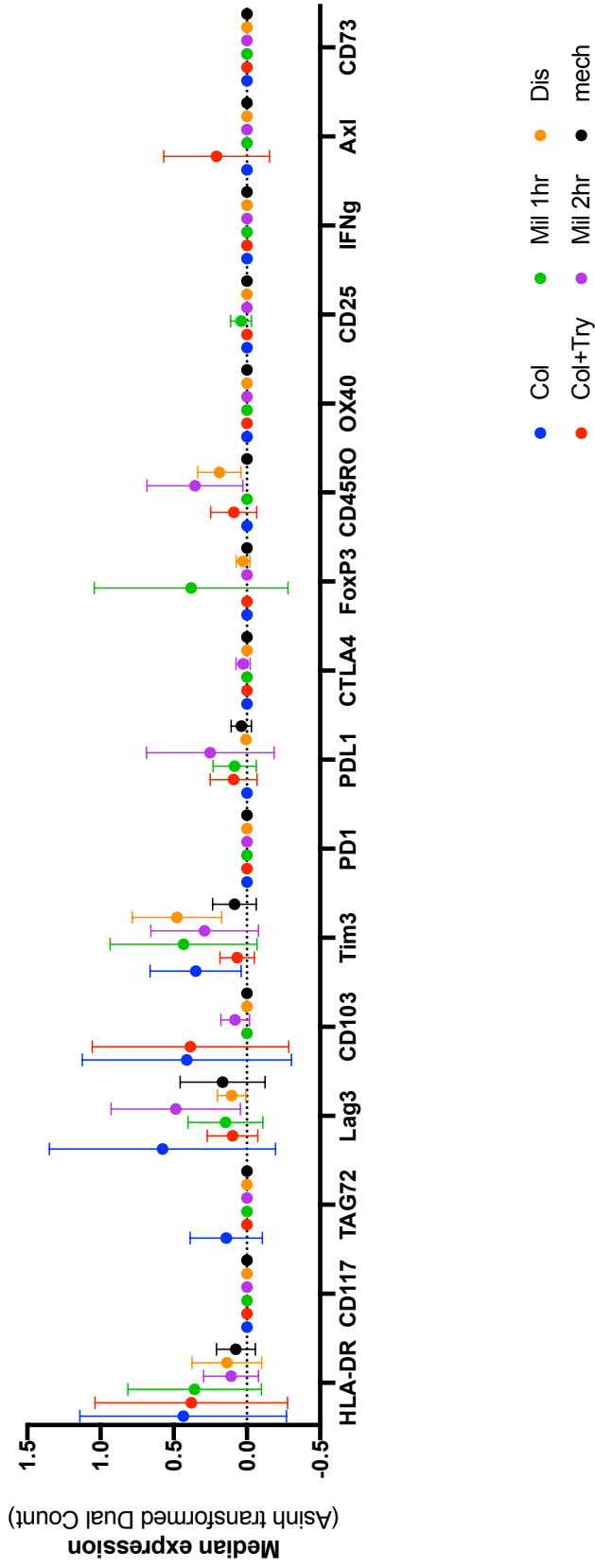
CD45CD3CD8 phenotype (Mean with SD, n=3)



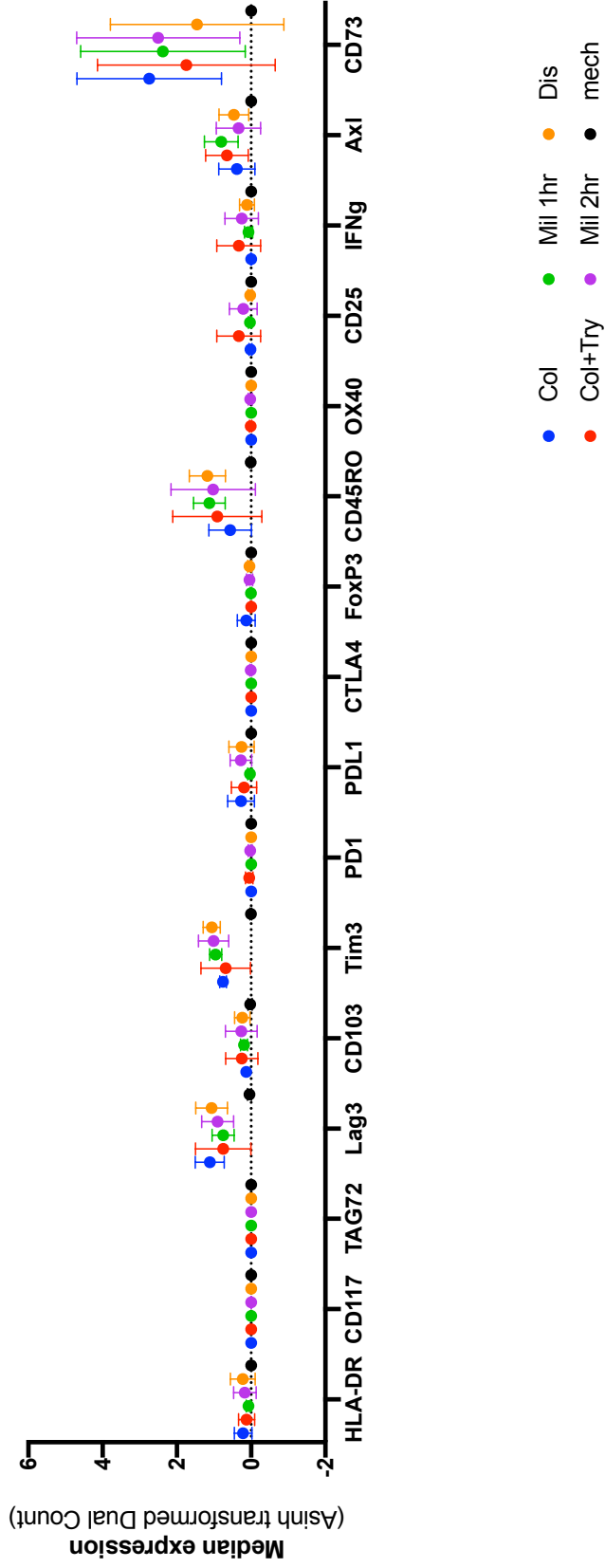
EpCAMCD47FOLR1CD56 phenotype (Mean with SD, n=3)



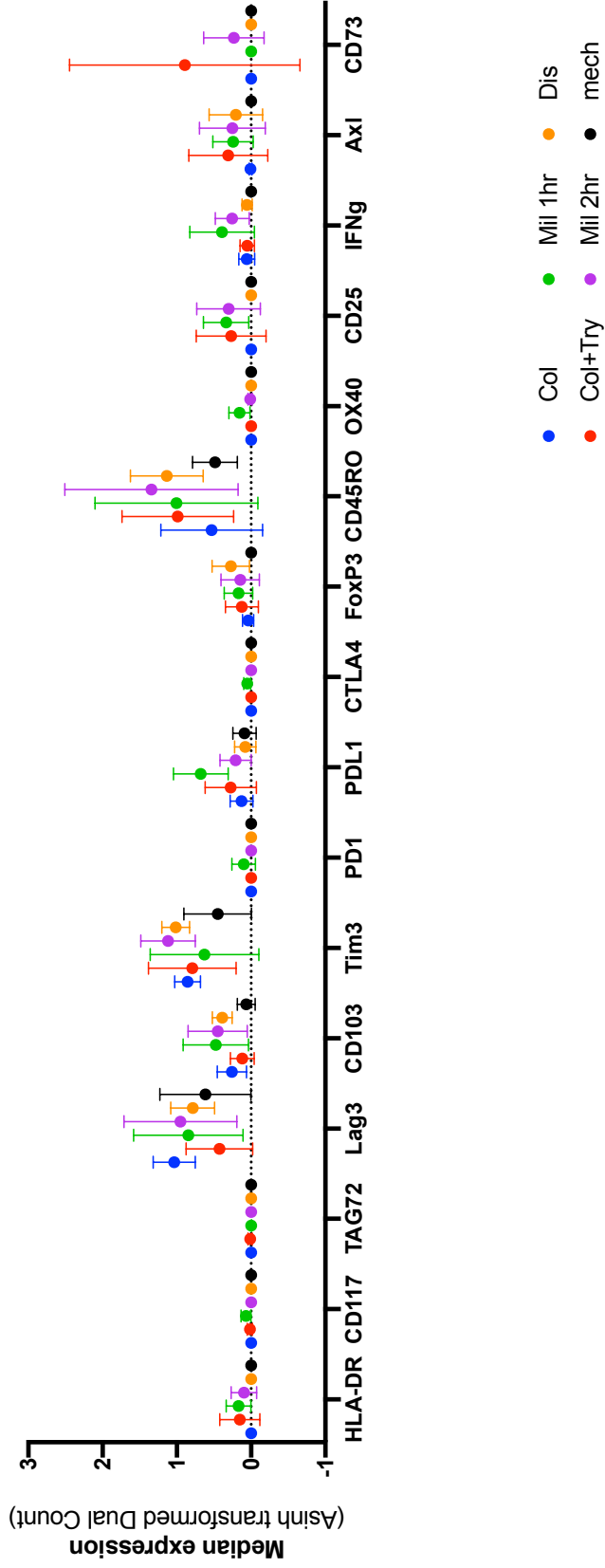
CD47FOLR1CD56 phenotype (Mean with SD, n=3)



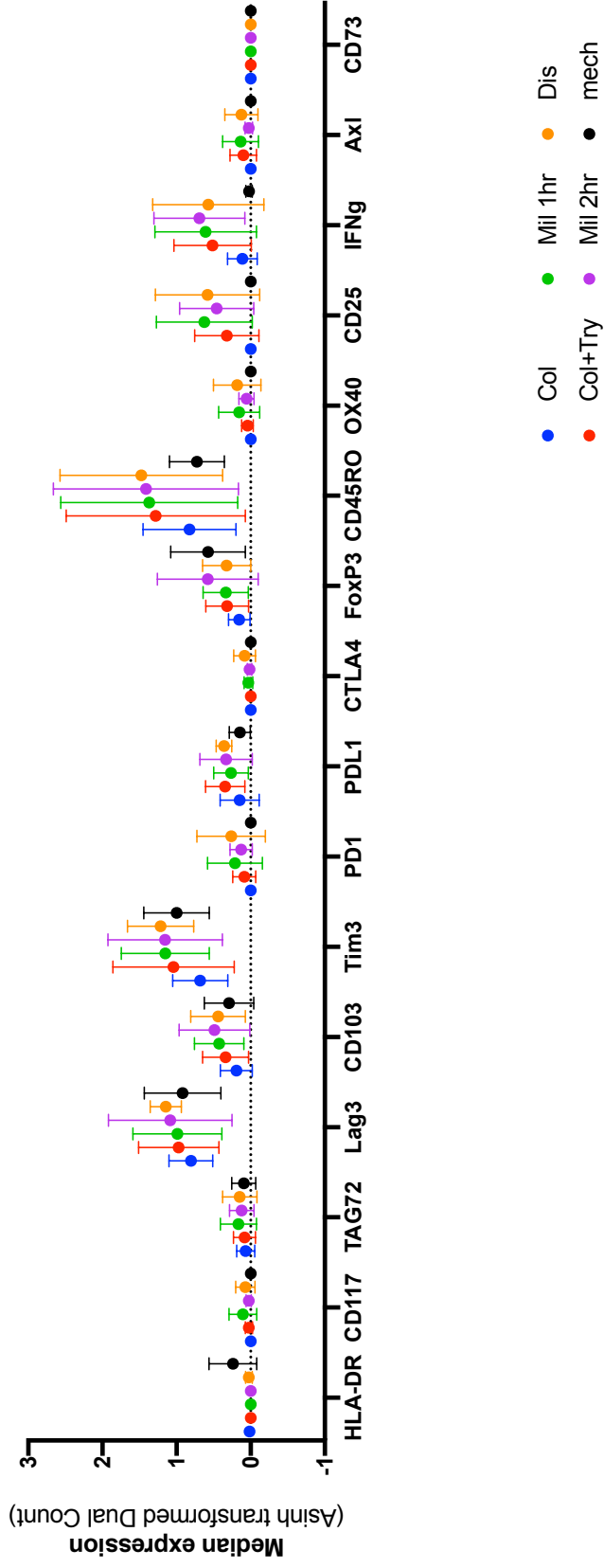
aSMAFAPa phenotype (Mean with SD, n=3)



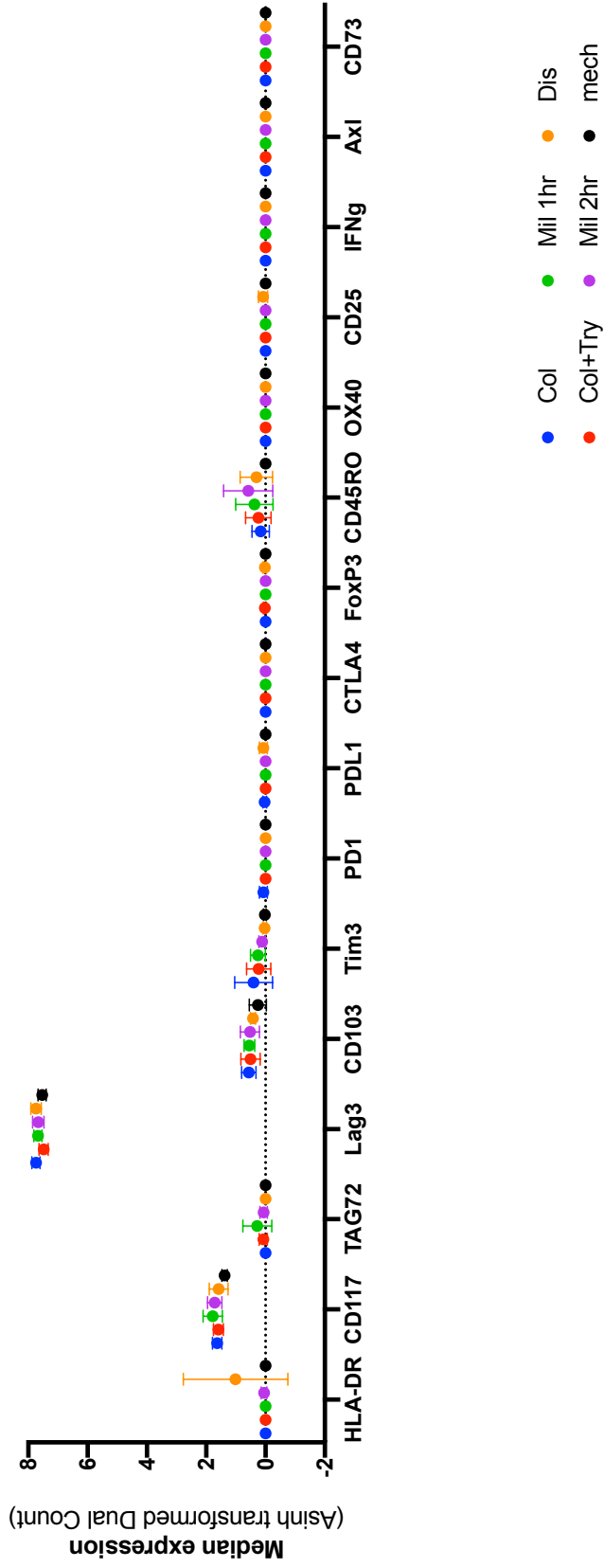
aSMAFAPa phenotype (Mean with SD, n=3)



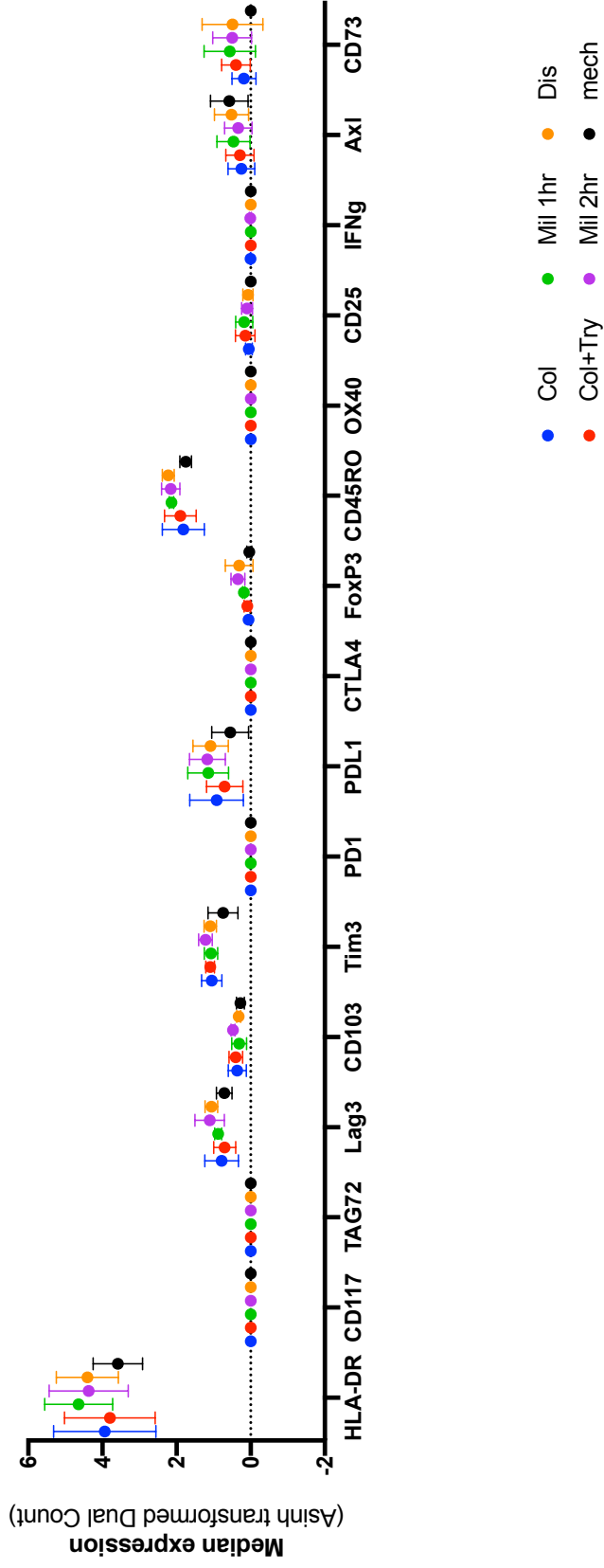
EpCAMCD47PDGFRFOLR1CD56CD24 phenotype (Mean with SD, n=3)



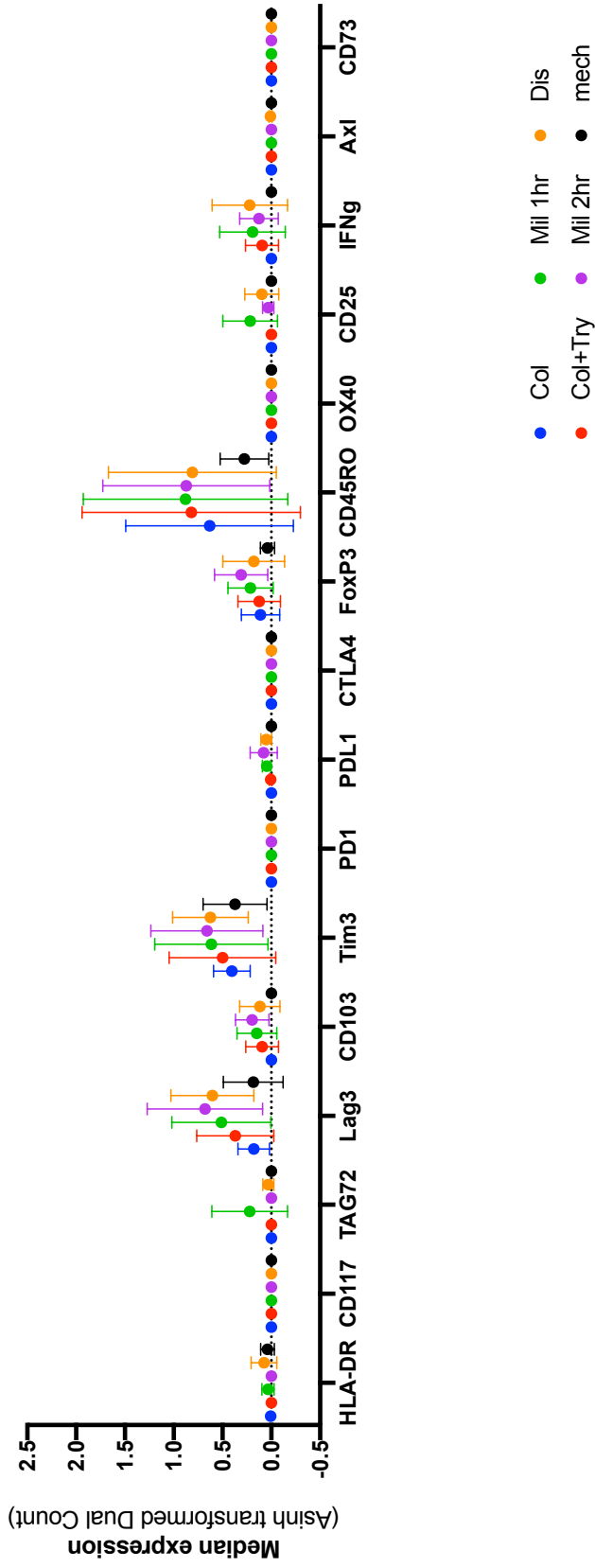
CD133CD34CD24 phenotype (Mean with SD, n=3)



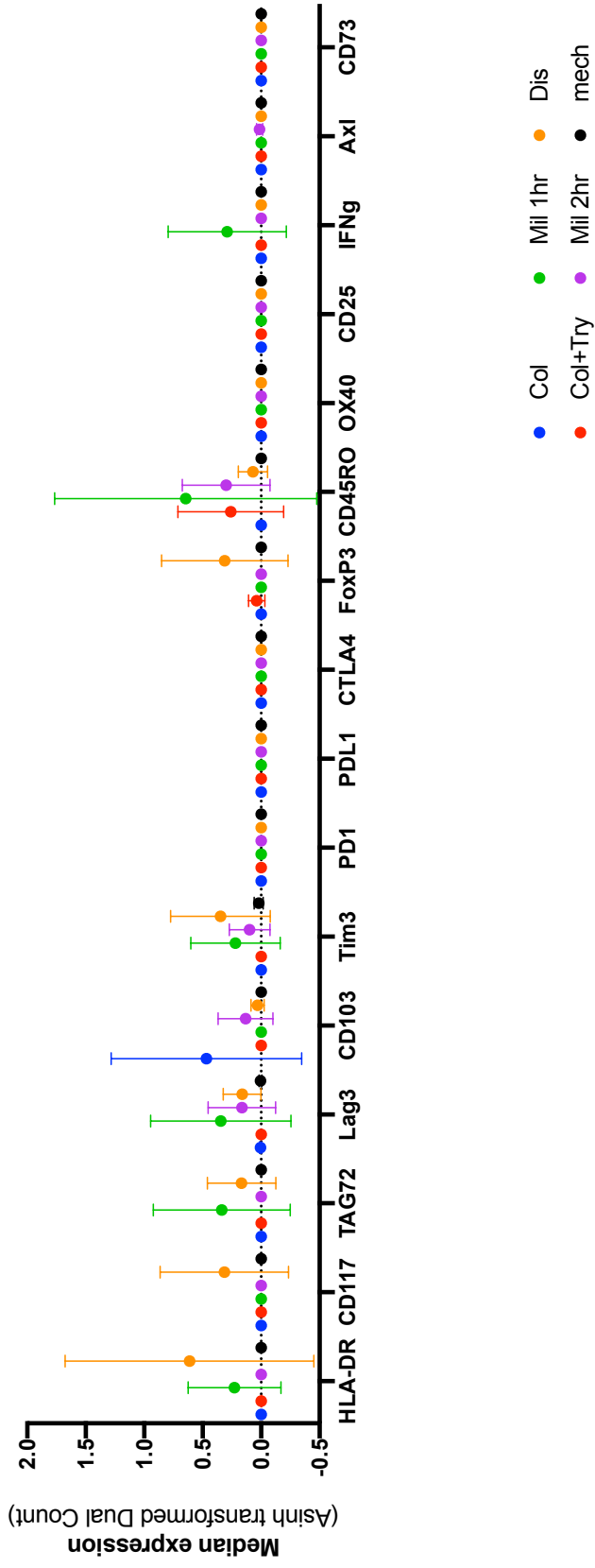
CD45CD4CD44CD47PDGFRHLADR phenotype (Mean with SD, n=3)



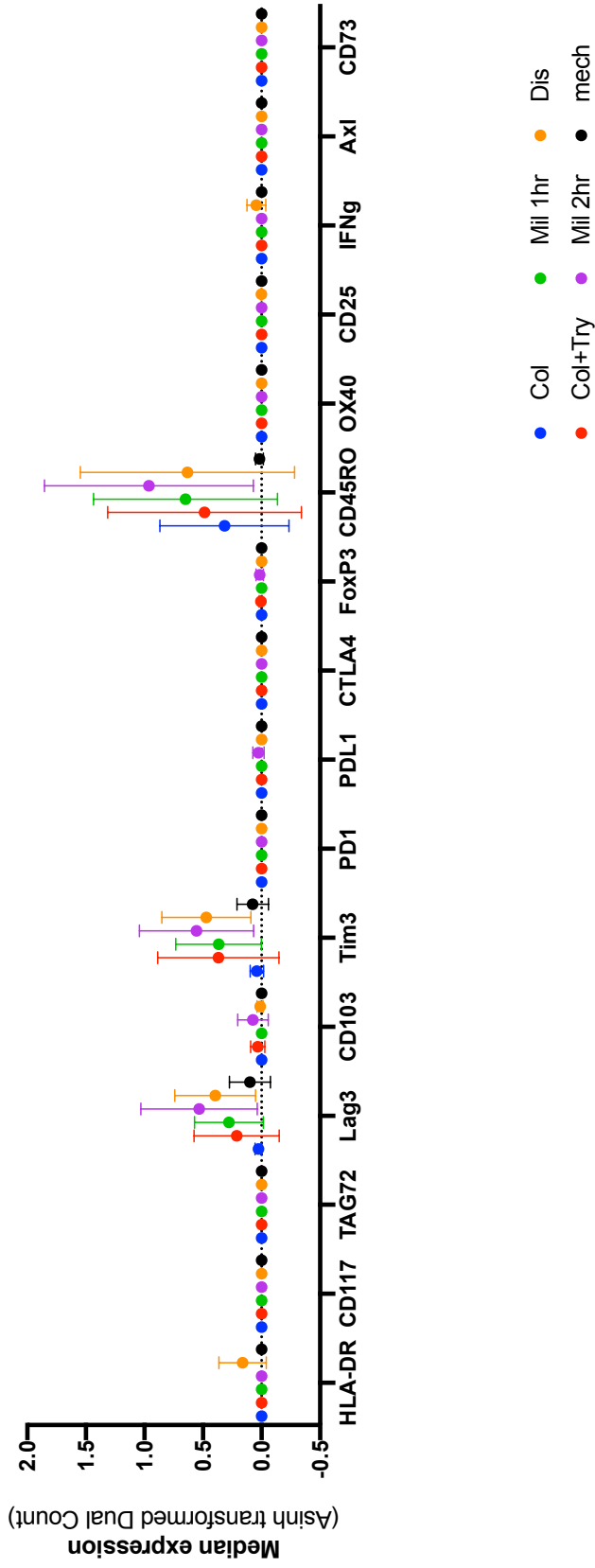
EpCAMCD47CD56 phenotype (Mean with SD, n=3)



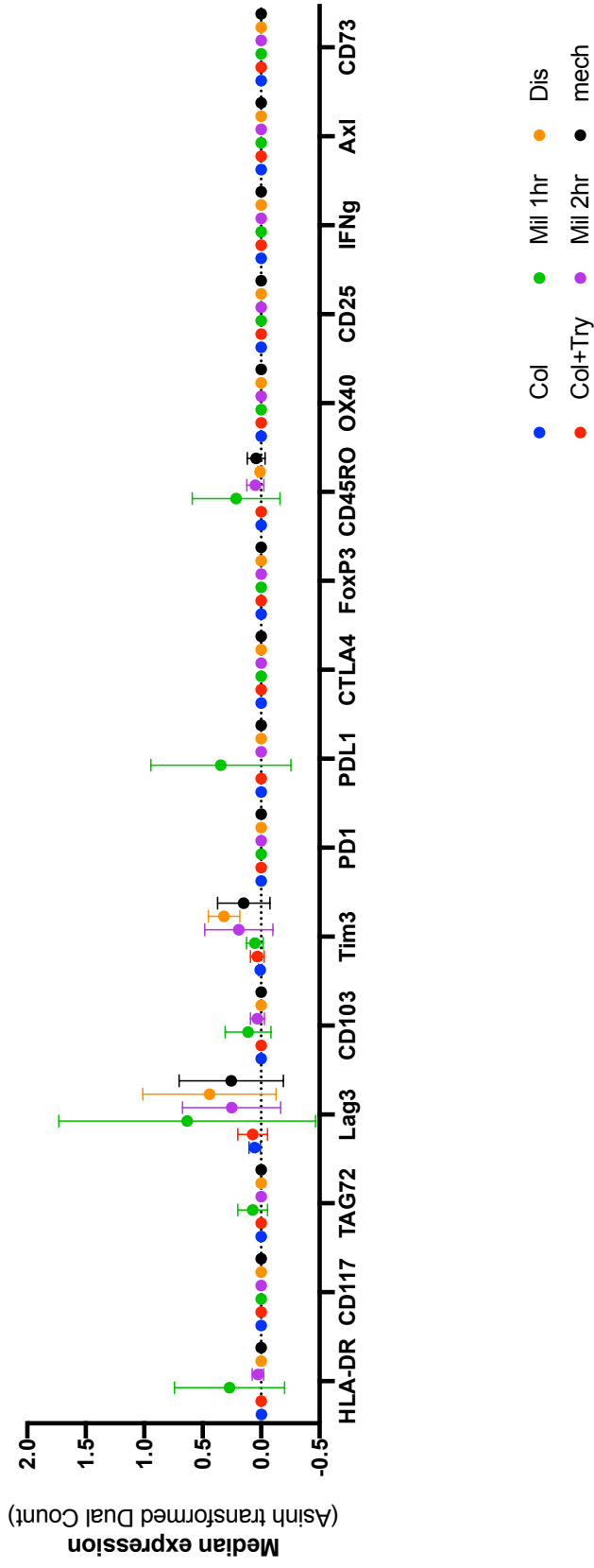
EpCAMCD47 phenotype (Mean with SD, n=3)



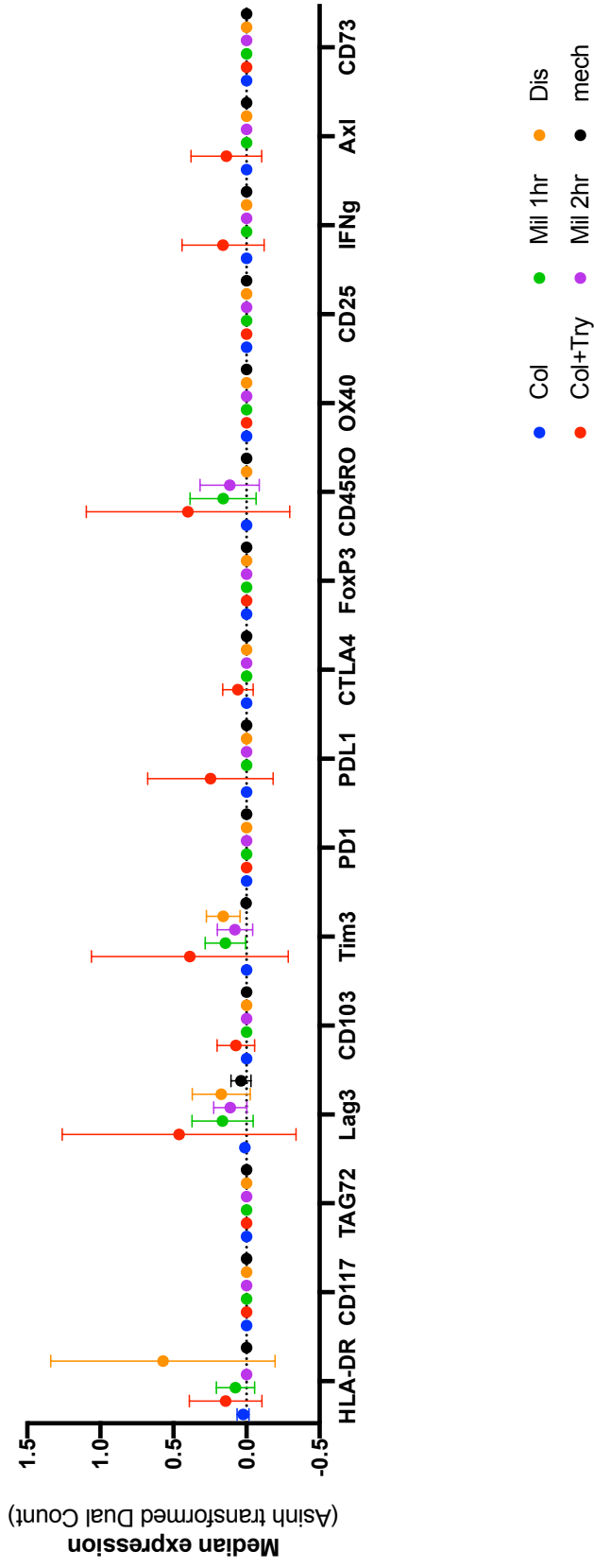
X phenotype (Mean with SD, n=3)



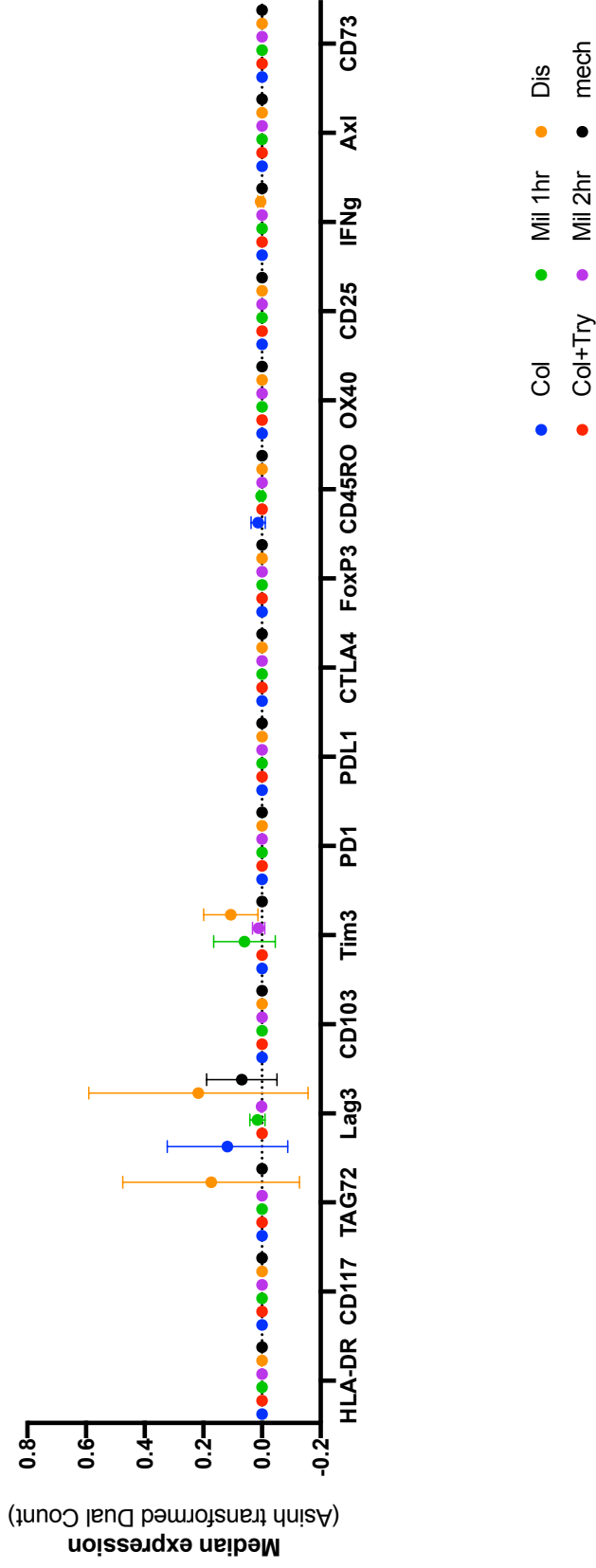
EpCAMFOLR1 phenotype (Mean with SD, n=3)



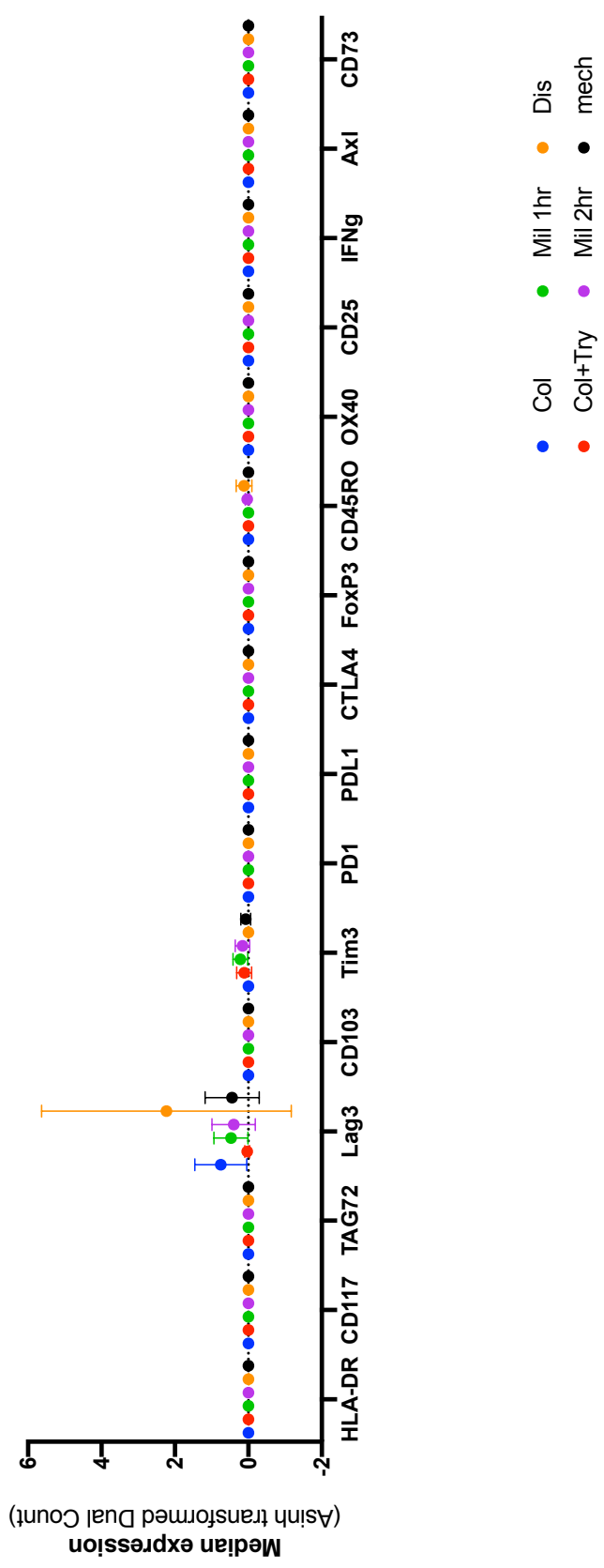
CD47 phenotype (Mean with SD, n=3)



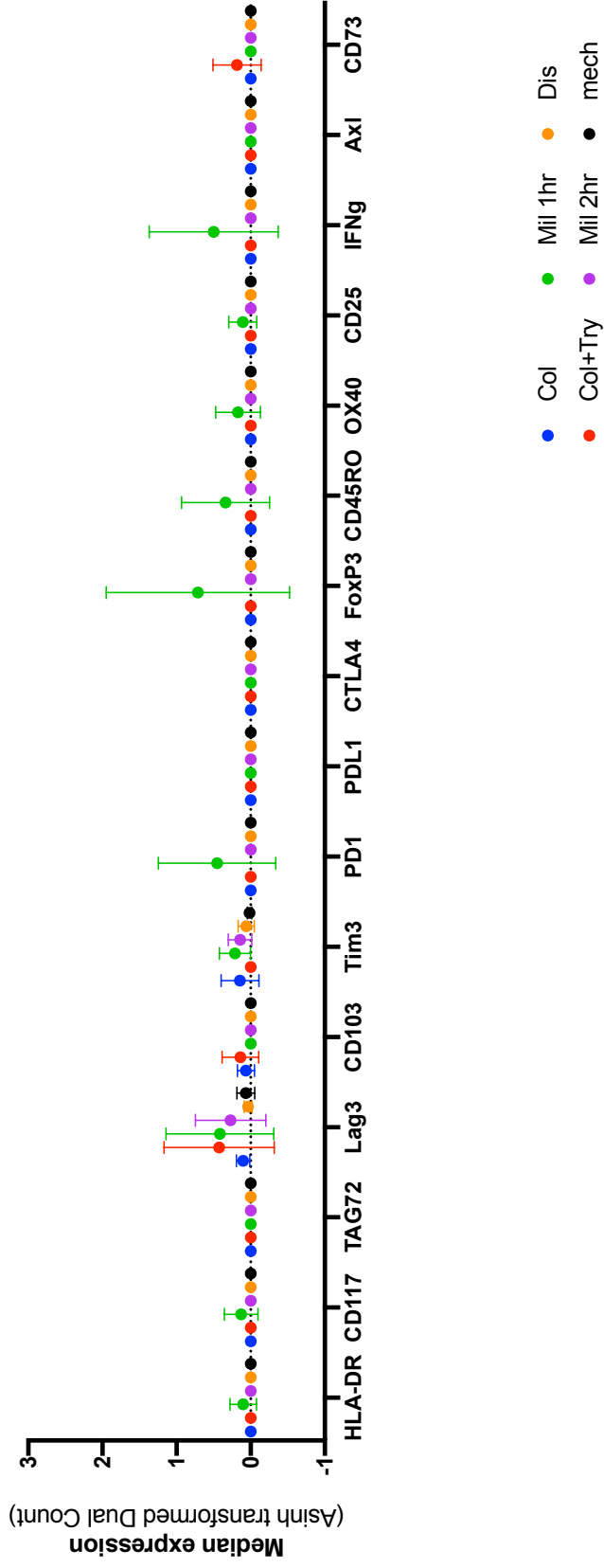
EpCAMdim phenotype (Mean with SD, n=3)



CD24 phenotype (Mean with SD, n=3)



FOLR1 phenotype (Mean with SD, n=3)



III



Graphic design: Communication Division, UIB / Print: Skjipes Kommunikasjon AS



uib.no

ISBN: 9788230858851 (print)
9788230869086 (PDF)